Response to reviewers' comments on the paper "Secondary Organic Aerosol Production from Local Emissions Dominates the Organic Aerosol Budget over Seoul, South Korea, during KORUS-AQ"

We would like to thank both reviewers for their time and for their useful comments, that have helped us improve and clarify our paper. For ease, comments from reviewers are in black, responses in blue, and new text added to paper in **bold blue**.

Reviewer #1

This paper presents airborne observations of organic aerosol (OA) made over and near Seoul, Korea and investigates the local urban contributions to the formation of secondary organic aerosol (SOA). The upwind transport of OA and SOA precursors coming into the Seoul region from China are evaluated to isolate the impact of transport versus local emissions and SOA production. The formation of SOA was determined to be mostly locally produced through evaluation using FLEXPART source analysis and factor analysis of OA and their correlation with other short-lived photochemically produced species. In addition, results using an OFR indicated greater potential SOA formation in air sampled over Seoul compared with air sampled upwind. Box model calculations reproduced SOA within 15% and showed that short-lived aromatic hydrocarbons are the main SOA precursors.

This is a relevant paper for ACP and would be of interest to ACP readers. The paper is very comprehensive, well written with clear study objectives, logically presented and articulated conclusions.

I recommend acceptance to ACP after addressing some minor comments.

R1.1: L184: not sure what is meant by 'also" encountered? In addition to what? Same thing with 'also' in the next line.

In line 184, we were referring to the three jet ways encountering pollution similar to Seoul. We have clarified line 184 to say:

"Many of the 3 lower elevation sampling legs around South Korea encountered significant pollution, similar to the flight segments over Seoul."

In line 185, we were referring to the coordinates for the three legs, similar to Seoul, being located in Table S2. We have updated line 185 to say:

"Similar to Seoul, the approximate coordinates defining these regions are included in Table S2."

R1.2: L192: highly customized, high-resolution time-of-flight mass spectrometer?? What is customized as it seems pretty standard.

How the CU-AMS is highly customized is discussed throughout Section 2.2 and highlighted here: (1) use of a customized pressure control inlet (PCI, line 211 - 212); (2) operation of CU-AMS in Fast Mass Spectrum (line 222 - 225); rapid particle filtering (line 228 - 230); and, use of a cryogenic pump to improve limits-of-detection for many species (line 252 - 257). There are also additional updates that are not described in detail, such as automatic inlet flow control vs. altitude, improvements to the supplementary data acquisition hardware and software, etc. These items are not part of a standard Aerodyne HR-ToF-AMS and have required an extensive amount of work and testing and improvement over many campaigns. These updates allow this instrument to measure NR-PM_1 on aircraft with fast time response (1 s), low detection limits, and improved accuracy, which is necessary to measure NR-PM_1 with high sensitivity at high altitude (including the customized PCI) and remote regions.

R1.3: L211: Are there any particle losses through the pressure controlled inlet, and if so, how were they accounted for?

The particle transmission (both ammonium nitrate and ammonium sulfate) and ionization efficiency (IE) were calibrated through the entire plumbing and pressure-control inlet. As was already shown in SI Figure 4, there were minimal losses of ammonium nitrate and sulfate through the pressure-controlled inlet compared to an instrument without a pressure-controlled inlet (the Hu et al. (2017) line in the figure).

We added the following statement to L213:
"The lens transmission calibration (SI Sect. 2 and Fig. S4) was conducted through the entire plumbing, including the pressure-controlled inlet. There were minimal losses of ammonium nitrate and sulfate through the pressure-controlled inlet during these calibrations."

R1.4: L230: ensure quality control . . . this oversimplifies the need for particle filter measurements. Suggest a brief explanation.

We have added the following explanation to L234 (updated text):

"The filters provide data quality checks throughout the flight by checking for leaks as the cabin changes pressure, to determine the response time of the different species (typically less than 2 seconds), and to validate the real-time continuous detection limits calculated by the Drewnick et al. (2009) method."

R1.5: L240: should state range of CE determined

We added the following text (L248 updated text):

"The collection efficiency (CE) for the CU-AMS was estimated per Middlebrook et al. (2012), and ranged from 0.5 – 1 (Fig. S28), with most of the values occurring around 0.5."

R1.6: L245: Was the contribution from organic nitrates estimated in this study (and stated anywhere)?

We added the following text to L254 (updated text):

"On average, during the campaign, organic nitrates were ~8% of the total CU-AMS NO_3 signal, and were only an important contribution to the NO_3 signal when NO_3 was less than 0.50 µg sm^{-3} (Figure S38)."

And the following supplemental figure has been added to the paper:

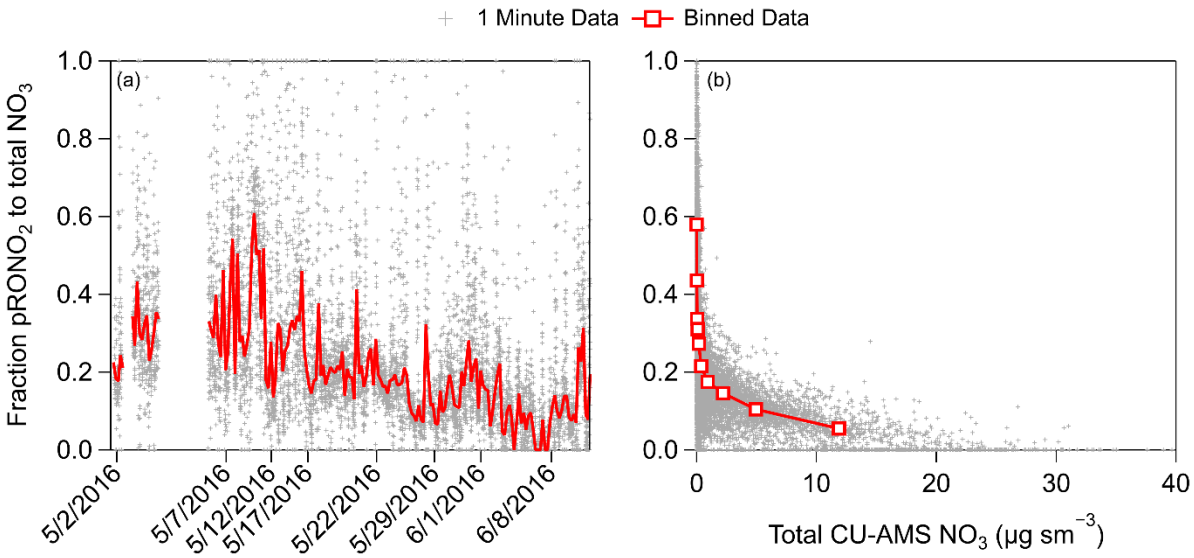

Figure 1. (a) Time series of the fractional contribution of organic nitrates ($pRONO_2$) to the total pNO_3 signal during KORUS-AQ. (b) Fractional contribution of organic nitrates versus pNO_3 during KORUS-AQ.

R1.7: L249: What was scaled? The detection limits? Why were they scaled?

The detection limits were scaled because the filters takes into account all ions for the different NR-PM_1 whereas Drewnick et al. (2009) only uses some ions to determine the detection limit.
We changed the sentence (L259 updated text) to say:

"The detection limits were scaled by ~×0.8, based on comparisons with periodic filter blanks, since the Drewnick et al. (2009) method only uses some ions to determine the detection limits, while filters take all ions into account, and thus the latter provide a more accurate estimate."

R1.8: L252-257: Should provide brief context behind statement ie. 24 hour power was not available and the AMS needed to be restarted each day (flight) etc. Otherwise confusing.

We added the following text (L269 in new text):

"The cryogenic pump is necessary since the airplane had power only 3 hours prior to take-off until 2 hours after landing; therefore, the CU-AMS was not constantly being pumped. This leads to high backgrounds each time the instrument is started."

R1.9: L257: Why reference another paper for the accuracy of your measurements? What are the estimated uncertainties related to subtracting an appropriate background (chopper closed) when sampling in/out of plumes? How wide are the regional plumes? More than 1 minute? How does this affect accuracies?

The reviewer may be confusing precision versus accuracy. Precision can be evaluated with changes in background, especially for sampling in and out of plumes, sampling through a particle filter (R1.4), and calibrations. We already report the limits of detection, which is related to precision, in line 241 - 243.

Accuracy is controlled by the uncertainties in ionization efficiency of nitrate (IE), relative ionization efficiencies of the different species (RIE), and collection efficiency (CE), of which, only a few can be regularly calibrated (IE and RIE for ammonium, sulfate, and chloride). The accuracy due to all three effects needs to be propagated in the quantification equation to determine the full accuracy of the AMS. Bahreini et al. (2009, their Supp. Info) performed this detailed analysis to determine what the overall accuracy (which typically dominates uncertainty, as precision tends to be much better) of the AMS. Due to this, the accuracy Bahreini et al. (2009) determined is regularly used and cited for the AMS.

R1.10: L323-325: I presume the pNO3 and OA measurements are also affected for those data taken not from the OFR?

We have shown through numerous studies that the short residence time to sample the measurements (~0.4 s in boundary layer and ~1.0 s at 7500 m) does not lead to any evaporation of OA and pNO_3 (Guo et al., 2016, 2017; Shingler et al., 2016).

We have added the following text in line 340 (new text):
" . . . and longer residence times (~150 s). However, for ambient measurements, the residence time was less than 1 s (Sect 2.2), which is rapid enough to prevent volatilization of OA and pNO_3, as discussed in prior work (Guo et al., 2016, 2017; Shingler et al., 2016)."

R1.11: L611-612: Awkward wording.

Please see response to R1.13.

R1.12: L621-622: maximum Chinese outflow stated at 40 µg/m3/ppmv, but this is only based on one flight….? I would think there could be substantial variation in this.

As we discussed in Lines 619 - 622, dilution-corrected OA concentration of 40 µg/m3/ppmv was observed in China (Beijing, Hu et al. (2016)) and downwind of China (Hu et al., 2013). This is in agreement with the value observed over the West Sea during the "transport/polluted" event. We have updated the text (L647 - 650 new text) to say:

"**Since 40 µg m^{-3} $ppmv^{-1}$ has been observed in and downwind of China (Hu et al., 2013, 2016), and observed over the West Sea during the "transport/polluted" event, this dilution-**

corrected OA concentration is taken to be representative of transport events from China to South Korea."

R1.13: L611-616: The results do seem to depend on assumed CO background. This is apparent in Fig. S34 where ΔOA/ ΔCO is different with different CO backgrounds especially in more aged air masses. What I think the authors mean is that there is still significant and rapid SOA formation greater than many megacities compared in the Figure, and therefore doesn't change the interpretation of this comparison. Also in SI Fig 35, confused about what is being shown here – I presume this is for Seoul data, but it's also not clear what CO background is being used here because the text in the paragraph indicates a CO background of 140ppgv, but the Figure 4 captions indicates for the Seoul data a background CO=200ppbv was applied (140ppb was for the WS).

We have rephrased lines 636 (updated text) to say:

"Finally, though the absolute ΔOA/ΔCO value changes depending on background CO used, assuming a lower CO background does not change the general result that Seoul has higher and more rapid SOA production than has been observed in prior megacities."

We have made the caption for SI Figure 35 more explicit to say:

"Same as Figure 4. ΔOA/ΔCO, using CO background of 200 ppbv, versus photochemical age, for observations collected over Seoul. The main difference is that the ΔOA/ΔCO versus different photochemical ages (NO_x clock in green, m+p-xylene/ethylbenzene in blue, and o-xylene/ethylbenzene in black) are plotted to show minimal differences in the final results of ΔOA/ΔCO versus photochemical age."

R1.14: L606-607: Seems to me that SOA formation is actually much higher than LA and Mexico City, rather than similar to.

We have changed L629 – 631 (updated text) to say:

"Qualitatively, the time scale for the production and plateauing of dilution-corrected OA is similar for Seoul, Los Angeles, and Mexico City; however, the amount of OA produced per CO is larger for Seoul compared to Los Angeles and Mexico City."

R1.15: L623: Do you mean finding SOA greater than POA concentrations…? And confused as to where this is shown in Figure 4 with the current data set?

We have rephrased this text (L653 updated text) as:

"The fact that OA concentrations are greater than POA concentrations at the youngest photochemical ages…"

R1.16: Fig 7g,h: Figh is discussed, but it is interesting why in the more polluted air masses over the West Sea, the CH2O and PAN ratios to CO are lower and constant compared to the West Sea clean.

We agree this an interesting feature; however, we do not know why this feature occurred. As we are using those species as general tracers of photochemically-produced pollution and not investigating their sources and sinks quantitatively, we prefer to not speculate about the causes of this observation.

R1.17: Supplemental, L57: What is meant by 'built-in' DMA?

We have replaced the text "sized with a built-in differential mobility analyzer" with the following text for clarity:

"sized with a differential mobility analyzer, TSI model 3080, that was installed in the same rack as the AMS"

R1.18: Supplemental, L65: Do you mean mobility diameter as identified on L57?

Corrected to **"mobility diameter"**.

R1.18 Supplemental, L72: Was the organic NO3 contribution determined? Didn't see this in the main text.

We have included text and a figure on this. See response to comment R1.6 above.

R1.19: Supplemental, Fig 2: Figure indicates eptof 3-5 sec and text indicates 8s…? I'd like to see the figure caption explain the ambient closed data in that there is a line connecting the 6s of data and the ambient open-closed are corrected through an interpolated background.

Corrected the caption to say:

"Though the final 8 s of each minute are dedicated to ePToF, some of the time is used by the computer in saving the 6 s of closed and 46 s of open signal and ePToF signal.; therefore, only 3 – 5 s of ePToF signal is actually recorded. The approximate saving times are shown as white spaces."

Figure has been updated and shown below:

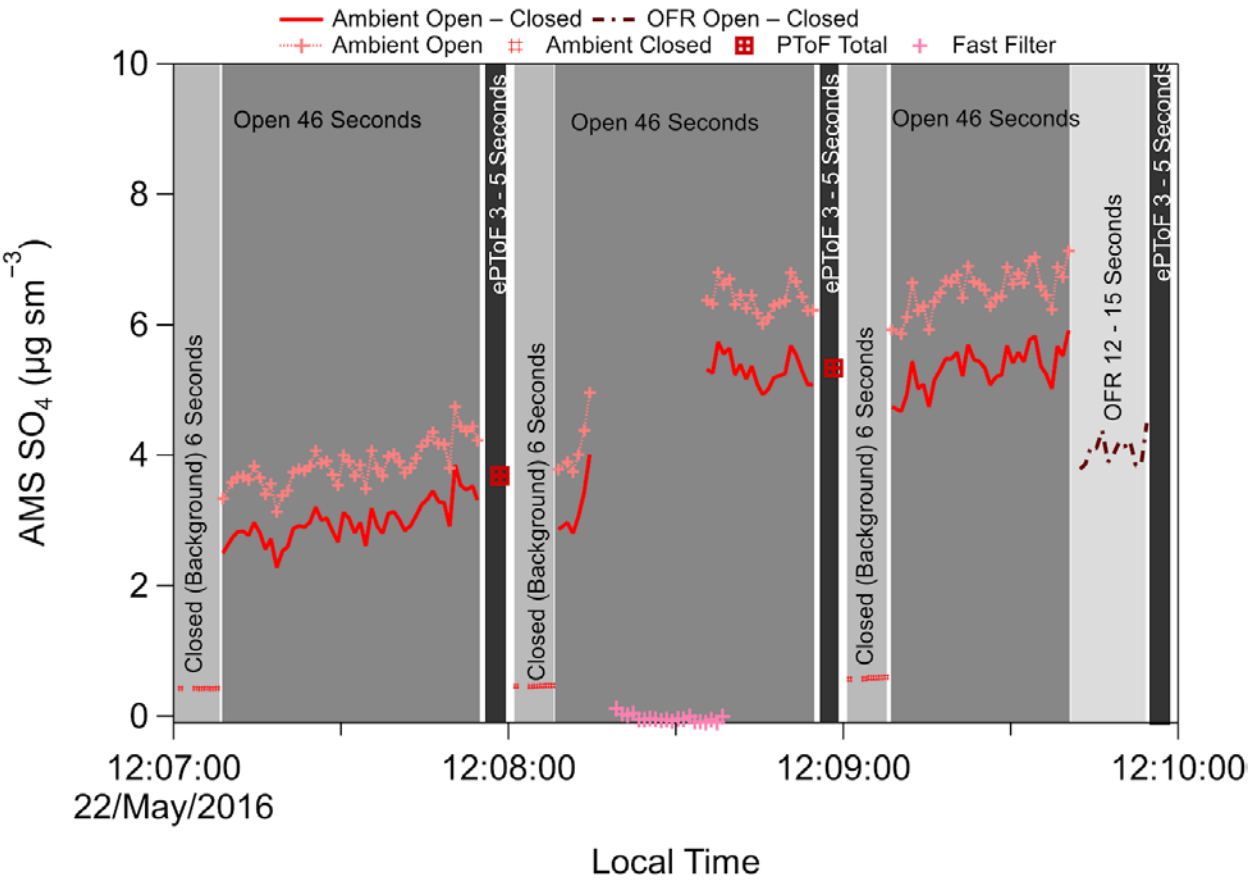

R1.20: Supplemental, SI Fig 37: Light pink and dark pink squares look almost identical; please change colour of one. Not sure where the light red crosses are shown for the binned values.

Updated the figure to make it more readable as:

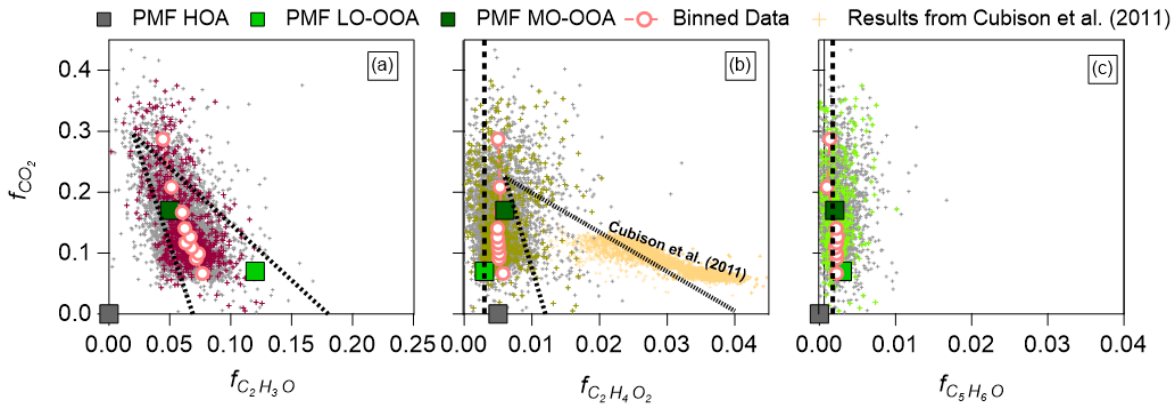

Updated the caption to read:

". . . . The quantile average values (averaged the x variables according to quantiles of the y variables) for each comparison are shown in light red circles."

Typos:
R1.21: L102: should be ‘suggest to be major’ ie Remove ‘a’

Corrected

R1.22: L155: should be instruments not instrument

Corrected

R1.23: L177: the wind ‘was’ instead of ‘is’

Corrected

R1.24: L251: periodic not period

Corrected

R1.25: Fig 10: olefins, not olefins

Corrected

R1.26: L933: units needed

Corrected

R1.27: L207: ram should be RAM as it is an acronym

Corrected

R1.28: Fig 10(b): lighter color, not lighter colored

Corrected

Reviewer #2

Nault et al. present the findings of organic aerosol measurements collected during the KORUS-AQ field campaign. The work finds that the secondary organic aerosols (SOA) formed in Seoul are predominantly formed from SOA precursors emitted locally. This conclusion is supported by back trajectory modeling, measurements of other secondary species (e.g., formaldehyde), airborne oxidation flow reactor measurements, and box model simulations. The paper is generally well written and the work provides valuable insights into SOA. I recommend the paper to be accepted with a few minor revisions detailed below.

R2.1: General question: Perhaps this is beyond the scope of this work, by do you have insight into why more SOA is formed from Seoul compared to other cities presented in Fig. 4? Is it just more reactive since other rapidly oxidized species follow a similar trend (Fig. 7) or are there more SOA precursors in Seoul or perhaps something else entirely which is unique to Seoul?

We agree that this is interesting. We are currently investigating the possible causes for higher SOA formation in Seoul compared to other megacities. This is a very complex topic, whose results may be reported in a future paper.

R2.2: Line 137: Add "is" after "aerosol load"

Corrected

R2.3: Line 256: Remove "much" and change "for several hours" to "after several hours"

Corrected

R2.4: Line 264: Change "allows the measurement of" to "measures"

Corrected

R2.5: Line 511: It's unclear how the dilution rate is used to calculate the 60 ppbv of $CO_{foreign}$. Perhaps this is covered in one of the other studies referenced?

We took the equation $C(t)=C(0)\times exp(-k_{dil}\times t)$, where t = ~1 day, $-k_{dil}$ = ~0.7 day^{-1}, and C(0) = 125 ppbv, which leads to ~60 ppbv of foreign CO. If we take a more complicated equation listed in McKeen et al. (1996), which takes the background CO (140 ppbv) into account, we get the exact same answer.

We have added the following text (L528 updated text) for clarification:
"$CO_{foreign}$ over Seoul was determined by Eq. (3), where t = ~1 day, $-k_{dil}$ = ~0.7 day^{-1}, and C(0) = 125 ppbv. Using the full equation from McKeen et al. (1996), a similar value of 60 ppbv $CO_{foreign}$ is derived.

$C(t)=C(0)\times exp(-k_{dil}\times t)$ (3)"

R2.6: Line 520: Hemispheric background not being included in the figure is a bit misleading since it is included in 2b and 2c. Presumably, the exclusion applies only to 2a and 2d but this is not apparent in Line 520.

We have changed the caption to say:

"Also, note that FLEXPART does not include hemispheric background; therefore, it is not included in (a) and (d); however, it is included for the actual observations in (b) and (c)."

R2.7: Line 526: Is "background subtracted CO" not the same so "$CO_{South\ Korea}$"?

We have changed "background subtracted CO" to the **"hemispheric background-subtracted CO"**, as this is for observations over the West Sea and not over Seoul, yet.

R2.8: Line 529: I may be misinterpreting this, but because $CO_{foreign}$ is both in the numerator and the denominator, $OA_{background}$ would simply equal OA, which doesn't seem right.

To avoid this point of confusion, we have changed the equation from $OA_{background} = CO_{foreign} \times (OA/CO)_{foreign}$ to:

$$\mathbf{OA_{background}(t) = CO_{foreign}(t) \times (OA/CO)_{foreign}(0)}$$

where t is for any observations after the initial OA/CO observation.

R2.9: Line 530: How were the fractions of HOA, LO-OOA, and MO-OOA determined?

HOA, LO-OOA, and MO-OOA were determined by positive matrix factorization, and the background values were determined similarly to OA, as described comment R2.8.

R2.10: Line 539: I had a hard time following this part of the sentence. I believe what's plotted is the FLEXPART NO_2 but the "sampled from aircraft position for contributions to" part is unclear.

We have removed the "sampled from aircraft position" for clarity.

Other Edits

While working on the comments, we noticed an error in Fig. 11. The HOA was low by 7 μg sm^{-3} $ppmv^{-1}$. We have updated the plot (see below). It did not change the conclusions, but it changed the average percent difference from 15% to 11%.

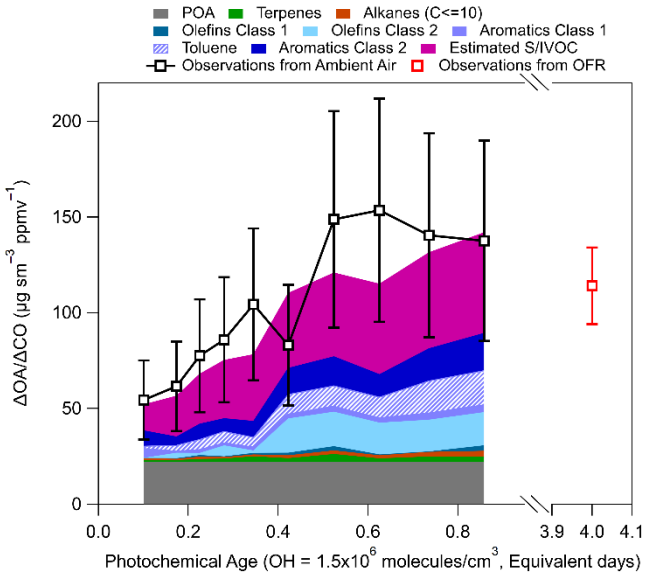

References

Bahreini, R., Ervens, B., Middlebrook, A. M., Warneke, C., de Gouw, J. A., DeCarlo, P. F., Jimenez, J. L., Brock, C. A., Neuman, J. A., Ryerson, T. B., Stark, H., Atlas, E., Brioude, J., Fried, A., Holloway, J. S., Peischl, J., Richter, D., Walega, J., Weibring, P., Wollny, A. G. and Fehsenfeid, F. C.: Organic aerosol formation in urban and industrial plumes near Houston and Dallas, Texas, J. Geophys. Res., 114(16), D00F16, doi:10.1029/2008JD011493, 2009.

Drewnick, F., Hings, S. S., Alfarra, M. R., Prevot, A. S. H. and Borrmann, S.: Aerosol quantification with the Aerodyne Aerosol Mass Spectrometer: detection limits and ionizer background effects, Atmos. Meas. Tech., 2(1), 33–46, doi:10.5194/amt-2-33-2009, 2009.

Guo, H., Sullivan, A. P., Campuzano-Jost, P., Schroder, J. C., Lopez-Hilfiker, F. D., Dibb, J. E., Jimenez, J. L., Thornton, J. A., Brown, S. S., Nenes, A. and Weber, R. J.: Fine particle pH and the partitioning of nitric acid during winter in the northeastern United States, J. Geophys. Res. Atmos., 121(17), 10,355-10,376, doi:10.1002/2016JD025311, 2016.

Guo, H., Liu, J., Froyd, K. D., Roberts, J. M., Veres, P. R., Hayes, P. L., Jimenez, J. L., Nenes, A. and Weber, R. J.: Fine particle pH and gas–particle phase partitioning of inorganic species in Pasadena, California, during the 2010 CalNex campaign, Atmos. Chem. Phys., 17(9), 5703–5719, doi:10.5194/acp-17-5703-2017, 2017.

Hu, W., Hu, M., Hu, W., Jimenez, J. L., Yuan, B., Chen, W., Wang, M., Wu, Y., Chen, C., Wang, Z., Peng, J., Zeng, L. and Shao, M.: Chemical composition, sources and aging process of sub-micron aerosols in Beijing: contrast between summer and winter, J. Geophys. Res. Atmos., doi:10.1002/2015JD024020, 2016.

Hu, W., Campuzano-Jost, P., Day, D. A., Croteau, P., Canagaratna, M. R., Jayne, J. T., Worsnop, D. R. and Jimenez, J. L.: Evaluation of the new capture vapourizer for aerosol mass spectrometers (AMS) through laboratory studies of inorganic species, Atmos. Meas. Tech., 10(6), 2897–2921, doi:10.5194/amt-10-2897-2017, 2017.

Hu, W. W., Hu, M., Yuan, B., Jimenez, J. L., Tang, Q., Peng, J. F., Hu, W., Shao, M., Wang, M., Zeng, L. M., Wu, Y. S., Gong, Z. H., Huang, X. F. and He, L. Y.: Insights on organic aerosol aging and the influence of coal combustion at a regional receptor site of central eastern China, Atmos. Chem. Phys., 13(19), 10095–10112, doi:10.5194/acp-13-10095-2013, 2013.

McKeen, S. A., Liu, S. C., Hsie, E.-Y., Lin, X., Bradshaw, J. D., Smyth, S., Gregory, G. L. and Blake, D. R.: Hydrocarbon ratios during PEM-WEST A: A model perspective, J. Geophys. Res. Atmos., 101(D1), 2087–2109, doi:10.1029/95JD02733, 1996.

Middlebrook, A. M., Bahreini, R., Jimenez, J. L. and Canagaratna, M. R.: Evaluation of Composition-Dependent Collection Efficiencies for the Aerodyne Aerosol Mass Spectrometer using Field Data, Aerosol Sci. Technol., 46(3), 258–271, doi:10.1080/02786826.2011.620041, 2012.

Shingler, T., Crosbie, E., Ortega, A., Shiraiwa, M., Zuend, A., Beyersdorf, A., Ziemba, L., Anderson, B., Thornhill, L., Perring, A. E., Schwarz, J. P., Campazano-Jost, P., Day, D. A., Jimenez, J. L., Hair, J. W., Mikoviny, T., Wisthaler, A. and Sorooshian, A.: Airborne characterization of subsaturated aerosol hygroscopicity and dry refractive index from the surface to 6.5km during the SEAC4RS campaign, J. Geophys. Res., 121(8), 4188–4210,

425 doi:10.1002/2015JD024498, 2016.

426
427

Secondary Organic Aerosol Production from Local Emissions Dominates the Organic Aerosol Budget over Seoul, South Korea, during KORUS-AQ

Benjamin A. Nault[1,2], Pedro Campuzano-Jost[1,2], Douglas A. Day[1,2], Jason C. Schroder[1,2], Bruce Anderson[3], Andreas J. Beyersdorf[3,*], Donald R. Blake[4], William H. Brune[5], , Yonghoon Choi[3,6], Chelsea A. Corr[3,**], Joost A. de Gouw[1,2], Jack Dibb[7], Joshua P. DiGangi[3], Glenn S. Diskin[3], Alan Fried[8], L. Gregory Huey[9], Michelle J. Kim[10], Christoph J. Knote[11], Kara D. Lamb[2,12], Taehyoung Lee[13], Taehyun Park[13], Sally E. Pusede[14], Eric Scheuer[7], Kenneth L. Thornhill[3,6], Jung-Hun Woo[15], and Jose L. Jimenez[1,2]

Affiliations

1. Department of Chemistry, University of Colorado, Boulder, CO, USA
2. Cooperative Institute for Research in Environmental Sciences, University of Colorado, Boulder, CO, USA
3. NASA Langley Research Center, Hampton, Virginia, USA
4. Department of Chemistry, University of California, Irvine, Irvine, CA, USA
5. Department of Meteorology and Atmospheric Science, Pennsylvania State University, University Park, Pennsylvania, USA
6. Science Systems and Applications, Inc., Hampton, Virginia, USA
7. Earth Systems Research Center, Institute for the Study of Earth, Oceans, and Space, University of New Hampshire, Durham, New Hampshire, USA
8. Institute of Arctic and Alpine Research, University of Colorado, Boulder, CO, USA
9. School of Earth and Atmospheric Sciences, Georgia Institute of Technology, Atlanta, Georgia, USA
10. Division of Geological and Planetary Sciences, California Institute of Technology, Pasadena, CA, USA
11. Meteorologisches Institut, Ludwig-Maximilians-Universität München, München, Germany
12. Chemical Sciences Division, Earth System Research Laboratory, National Oceanic and Atmospheric Administration, Boulder, CO, USA
13. Department of Environmental Science, Hankuk University of Foreign Studies, Republic of Korea
14. Department of Environmental Sciences, University of Virginia, Charlottesville, VA, USA
15. Department of Advanced Technology Fusion, Konkuk University, Seoul, Republic of Korea

* Now at: Department of Chemistry and Biochemistry, California State University, San Bernardino, California

** Now at: USDA UV-B Monitoring and Research Program, Natural Resource Ecology Laboratory, Colorado State University, Fort Collins, CO, USA

Correspondence to: J. L. Jimenez (jose.jimenez@colorado.edu)

Abstract

Organic aerosol (OA) is an important fraction of submicron aerosols. However, it is challenging to predict and attribute the specific organic compounds and sources that lead to observed OA loadings, largely due to contributions from secondary production. This is especially true for megacities surrounded by numerous regional sources that create an OA background. Here, we utilize *in-situ* gas and aerosol observations collected on-board the NASA DC-8 during the NASA/NIER KORUS-AQ (KORea United States-Air Quality) campaign to investigate the sources and hydrocarbon precursors that led to the secondary OA (SOA) production observed over Seoul. First, we investigate the contribution of transported OA to total loadings observed over Seoul, by using observations over the West Sea coupled to FLEXPART Lagrangian simulations. During KORUS-AQ, the average OA loading advected into Seoul was ~1 – 3 μg sm^{-3}. Second, taking this background into account, the dilution-corrected SOA concentration observed over Seoul was ~140 μg sm^{-3} $ppmv^{-1}$ at 0.5 equivalent photochemical days. This value is at the high end of what has been observed in other megacities around the world (20–70 μg sm^{-3} $ppmv^{-1}$ at 0.5 equivalent days). For the average OA concentration observed over Seoul (13 μg sm^{-3}), it is clear that production of SOA from locally emitted precursors is the major source in the region. The importance of local SOA production was supported by the following observations: (1) FLEXPART source contribution calculations indicate any hydrocarbons with a lifetime less than 1 day, which are shown to dominate the observed SOA production, mainly originate from South Korea. (2) SOA correlated strongly with other secondary photochemical species, including short-lived species (formaldehyde, peroxy acetyl nitrate, sum of acyl peroxy nitrates, dihydroxy toluene, and nitrate aerosol). (3) Results from an airborne oxidation flow reactor (OFR), flown for the first time, show a factor of 4.5 increase in potential SOA concentrations over Seoul versus over the West Sea, a region where background air masses that are advected into Seoul can be measured. (4) Box model simulations reproduce SOA observed over Seoul within 15% on average, and suggest that short-lived hydrocarbons (i.e., xylenes, trimethylbenzenes, semi- and intermediate volatility compounds) were the main SOA precursors over Seoul. Toluene, alone, contributes 9% of the modeled SOA over Seoul. Finally, along with these results, we use the metric $\Delta OA/\Delta CO_2$ to examine the amount of OA produced per fuel consumed in a megacity, which shows less variability across the world than $\Delta OA/\Delta CO$.

1. Introduction

Prior to 1950, 30% of the human population resided in urban areas (UNDESA, 2015). In 2007, the human population living in urban areas had increased to over 50% (making it the first time in human history that more people reside in urban than rural areas), and it is predicted that nearly 2/3 of the human population will be living in urban areas by 2050 (Monks et al., 2009; UNDESA, 2015; Baklanov et al., 2016). Urban areas are large sources of anthropogenic emissions to the atmosphere (from sources including transportation, industry, cooking, personal care products, and power produced from fossil fuels), and these emissions have important impacts on local, regional, and global air pollution, climate, and human and ecological health (Hallquist et al., 2009; Monks et al., 2009; Myhre et al., 2013; Baklanov et al., 2016; WHO, 2016; Cohen et al., 2017; Landrigan et al., 2018; McDonald et al., 2018). Effects from urban emissions are strongly modulated by the chemical evolution of the primary emissions (e.g., nitrogen oxides, hydrocarbons, and primary organic aerosols) to secondary pollutants, including secondary organic aerosols (SOA, produced from atmospheric reactions) and other aerosol (Monks et al., 2009). These emissions and their chemical by-products significantly influence hemispheric climate and air quality. They increase mortality in polluted urban areas, leading to over 3 million premature deaths annually (Lelieveld et al., 2015; Baklanov et al., 2016; WHO, 2016). Finally, the emissions and production of anthropogenic aerosol may strongly regulate cloud nucleation (Peng et al., 2014), which impacts the aerosols' direct and indirect effects on climate (Myhre et al., 2013).

Production of SOA is poorly understood (Hallquist et al., 2009; Shrivastava et al., 2017; Tsimpidi et al., 2017), including in large urban environments (Volkamer et al., 2006; de Gouw et al., 2008, 2009; Hayes et al., 2015; Woody et al., 2016; Janssen et al., 2017; Ma et al., 2017). It has been shown that a large fraction (35 – 85%) of urban fine aerosol is composed of OA (Zhang

et al., 2007; Jimenez et al., 2009), and a substantial fraction of this OA is typically SOA produced through the chemical processing of urban hydrocarbon emissions (Kleinman et al., 2016, 2007, 2008, 2009, Dzepina et al., 2009, 2011; DeCarlo et al., 2010; Hodzic et al., 2010; Hersey et al., 2013; Zhao et al., 2014, 2016; Freney et al., 2014; Hayes et al., 2015; Ma et al., 2017). Also, observations indicate the majority of urban SOA production is rapid and is nearly completed within 24 equivalent photochemical hours (a measure of OH exposure, assuming interactions in a volume with 1.5×10^6 molecules/cm^3 OH throughout a 24 h period; equivalent age enables comparison of chemistry rates across different events or studies) (DeCarlo et al., 2010; Hayes et al., 2013; Freney et al., 2014; Hu et al., 2016; Ortega et al., 2016; Ma et al., 2017), even during winter (Schroder et al., 2018). This consistently rapid SOA production over urban areas around the world may be due to the short lifetime (less than one day) of urban semi- and intermediate-volatile organic compounds (S/IVOCs), that numerous studies suggest to be ~~a~~ major SOA precursors, along with aromatics (Robinson et al., 2007; Zhao et al., 2014, 2016; Hayes et al., 2015; Ma et al., 2017; McDonald et al., 2018). S/IVOCs and low volatility organic compounds (LVOCs—compounds produced from the photooxidation of hydrocarbons (Robinson et al., 2007; Kroll and Seinfeld, 2008; Murphy et al., 2011; Palm et al., 2016)) are challenging to measure due to strong interaction with inlet and instrument surfaces (e.g., Pagonis et al., 2017), limiting our knowledge of the emission rates and concentrations of these species in the atmosphere (Zhao et al., 2014; Hunter et al., 2017). It has also been recently shown that historical chamber SOA yields are biased low due to unaccounted-for partitioning of S/IVOCs to walls (Matsunaga and Ziemann, 2010; Zhang et al., 2014; Krechmer et al., 2016, 2017). These missing or under-represented compounds and low-biased yields, along with uncertain emission inventories for SOA precursors (Shrivastava et al., 2008; Woody et al., 2016; Murphy et al., 2017), led SOA modeling efforts over urban areas using

pre-2007 models to under-predict observed SOA concentrations (de Gouw et al., 2005, 2009; Volkamer et al., 2006; Dzepina et al., 2009; Freney et al., 2014; Woody et al., 2016). More recent modeling efforts have achieved closure (and sometimes over-prediction) of the observed SOA, but with some controversy about the real causes of the increased modeled SOA (Dzepina et al., 2009; Hodzic et al., 2010; Tsimpidi et al., 2010; Hayes et al., 2015; Cappa et al., 2016; Ma et al., 2017; McDonald et al., 2018).

Another complexity in understanding SOA production over urban areas is addressing the contributions of transport of SOA and its gas-phase precursors. Airborne observations of SOA and SOA precursors upwind, over, and downwind of megacities around the world (Kleinman et al., 2007, 2008, 2009, 2016, DeCarlo et al., 2008, 2010; Bahreini et al., 2009; McMeeking et al., 2012; Craven et al., 2013; Freney et al., 2014; Schroder et al., 2018) have constrained the role of regional transport versus megacity emissions. In general, these studies show that there is often regional background SOA, often due to biogenic compounds and regional pollution, transported into megacities, but that rapid SOA production is always observed and is generally dominated by the anthropogenic emissions from the urban area being studied.

The Seoul Metropolitan Area (SMA), as considered here, is a densely populated megacity, extending beyond Seoul proper into the large Incheon and Gyeonggi cities. SMA has ~24 million people, or ~50% of the South Korean population, living on ~12,000 km^2 of land (Park et al., 2017). SMA has large anthropogenic emissions but is also often downwind of China, presenting the challenge of separating local emissions and production of SOA versus transport of SOA and its precursors from regions upwind (H. S. Kim et al., 2007; Heo et al., 2009; Kim et al., 2009, 2016; Jeong et al., 2017; H. Kim et al., 2017; H. C. Kim et al., 2017; Lee et al., 2017; Seo et al., 2017; Kim et al., 2018). Most of the studies in this region have used ground-based observations and/or

3D models to characterize the amount of aerosol, and aerosol precursors, transported to SMA and South Korea, finding 50 to 80% of the aerosol load is due to international transport in the seasons with favorable synoptic conditions (winter and spring). Though satellites are starting to be used to investigate transport of aerosols into SMA and South Korea (Lee et al., 2013; Park et al., 2014; Jeong et al., 2017), retrievals typically do not provide any chemical characterization or vertical location of the aerosol (boundary layer versus free troposphere), and are typically strongly influenced by larger aerosols (e.g., mineral dust). Airborne observations of the upwind transport and local production of aerosol and aerosol precursors have the potential to directly assess the impact of transport versus local emissions in this region.

In this study, we use observations collected on board the NASA DC-8 research aircraft during the NASA/NIER (South Korean National Institute of Environmental Research) KORean United States Air Quality (KORUS-AQ) field campaign. These data provided the opportunity to investigate SOA production; as well as, the role of OA and SOA precursor transport on the OA concentration and SOA production over Seoul during the campaign. We evaluate the observed SOA production over the SMA with source analysis models, correlation of secondary gas-phase species with SOA, an oxidation flow reactor, and box modeling to constrain local versus transport contributions. These results are discussed and placed into context of improving our knowledge about SOA production and sources in urban environments.

2. Methods

Here, we introduce the KORUS-AQ campaign (Sect. 2.1), the key instruments for this study (2.2), additional measurements used in the analyses (2.3), and the airborne oxidation flow reactor (2.4). All linear fits, unless otherwise noted, use the least orthogonal distance regression fitting method (ODR).

2.1 KORUS-AQ brief overview

KORUS-AQ was conducted over South Korea and the West Sea during May – June, 2016. This study focuses on the NASA DC-8 (Aknan and Chen, 2018) observations; however, there were numerous other measurement platforms in operation (Al-Saadi et al., 2015). The DC-8 was stationed in the Songtan area of Pyeongtaek, South Korea, approximately 60 km south of Seoul. The DC-8 flew 20 research flights (RF) (Figure 1; Table S1). For each RF, the DC-8 would take-off from near Seoul, typically at 8:00 local time (LT), which is Korean Standard Time, and perform a missed approach over Seoul Air Base, which is less than 15 km from the Seoul city center. This pattern was typically conducted 2 more times during each flight, around 12:00 LT and prior to landing (~15:00 LT), leading to 55 missed approaches over Seoul during the campaign. Each missed approach involved flying near Seoul below 1000 m (above ground) for 15 – 45 minutes, providing a large number of observations of the Seoul boundary layer. The observations collected during this pattern, along with any other flights conducted within the coordinates defined as Seoul (Table S2, Fig. S1) are referred to as "Seoul" below.

Briefly, the SMA is bordered by the West Sea (i.e., the Yellow Sea) and Gyeonggi Bay to the west and forests and mountainous regions to the north, south, and east (Park et al., 2017). Within this region, nearly 30% of the land is used for human activities, ~21% is used for cropland, pasture, and grassland, and ~36% is forested (Park et al., 2017). During the time period of KORUS-AQ, the wind was~~is~~ typically from the west to northwest, meaning that observations over the West Sea represent typical background (inflow) air mass observations for Seoul (H. C. Kim et al., 2017). May and June are typically characterized by low precipitation and rising temperatures prior to the summer monsoon (Hong and Hong, 2016; H. C. Kim et al., 2017).

Besides the Seoul missed approaches, the DC-8 would fly either over the West Sea, the Jeju jetway, or the Busan jetway at four different altitudes (nominally ~300 m, ~1000 m, ~1500 m, and ~7500 m above ground, depending on the height of the boundary layer, clouds, and chemical forecasts). Many of the 3 lower elevation sampling legs around South Korea ~~also~~ encountered significant pollution, similar to the flight segments over Seoul ~~in all regions~~. Similar to Seoul, ~~T~~the approximate coordinates defining ~~for~~ these regions are also included in Table S2. For this study, the observations over the West Sea have been split into 2 categories: "clean," referring to the typical conditions observed during KORUS-AQ, and "transport/polluted," referring to one RF (RF12, 24/May/2016) that had direct transport of pollution from the Shanghai region over the West Sea. Also, RF11 (21/May/2016) is not included in the West Sea category, as this flight was sampling outflow from the SMA (prevailing winds from the east).

2.2 CU-AMS sampling and analysis

A highly customized, high-resolution time-of-flight aerosol mass spectrometer (HR-ToF-AMS, Aerodyne Research, Inc.) was flown on the NASA DC-8 during KORUS-AQ. Hereafter, this instrument will be referred to as CU-AMS since there were two high-resolution AMSs on the DC-8 during KORUS-AQ (see Sect. 2.4). Both AMSs measured non-refractory composition of PM_1 (particulate matter with aerodynamic diameters less than 1 μm) (DeCarlo et al., 2006; Canagaratna et al., 2007). The key differences between the two AMSs was the type of vaporizer (standard for CU-AMS versus capture for the other AMS), which has been described in prior publications (Jayne and Worsnop, 2015; Hu et al., 2017a, 2017b, 2018a, 2018b; Xu et al., 2017) and below and in Sect. 2.4. The basic concept, and operation, of the CU-AMS for aircraft sampling has been described elsewhere (DeCarlo et al., 2006, 2008, 2010; Dunlea et al., 2009; Cubison et al., 2011; Kimmel et al., 2011; Schroder et al., 2018), and a brief description of other important

details follow. For detailed information on field AMS calibrations, positive matrix factorization, photochemical clock calculations, and model setups, see Supplemental Sect. S2 – S7.

Ambient particles were drawn into the airplane through an NCAR High-Performance Instrumented Airborne Platform for Environmental Research Modular Inlet (HIMIL; Stith et al., 2009) at a constant standard (T = 273 K and P = 1013 hPa) flow rate of 9 L min^{-1}. The ~~ram~~ RAM heating of the inlet dried the aerosol prior to entering the airplane, and the temperature of the cabin (typically ~10°C higher than ambient) maintained the sampling line RH to less than 40%, ensuring the aerosol remained dry prior to entering the AMS. The sample was introduced into the AMS aerodynamic focusing lens (Zhang et al., 2002, 2004), operated at 1.5 Torr, through a pressure-controlled inlet, which was operated at 433 hPa (325 Torr) (Bahreini et al., 2008). The lens transmission calibrations (SI Sect. 2 and Fig. S4) was conducted through the entire plumbing, including the pressure-controlled inlet. There were minimal losses of ammonium nitrate and sulfate through the pressure-controlled inlet during these calibrations. The focused particles were then introduced after several differential pumping stages into a detection chamber, where they impacted on an inverted cone porous tungsten vaporizer ("standard" vaporizer) held at 600°C. The non-refractory species were flash-vaporized and the vapors were ionized by 70 eV electron ionization. Finally, the ions were extracted, and analyzed by a high-resolution time-of-flight mass spectrometer (HTOF, Tofwerk AG). The residence time from outside the inlet to the vaporizer was ~0.4 s in the boundary layer and ~1.0 s at 7500 m during KORUS-AQ. Unless otherwise noted, all aerosol data reported here is at standard temperature (273 K) and pressure (1013 hPa) (STP), leading to the notation μg sm^{-3} (sm^{-3} is the standard volume, in m^3, at STP). Notation in scm^{-3} is also at STP.

For KORUS-AQ, the CU-AMS was operated in the Fast Mass Spectrum (FMS) mode (Kimmel et al., 2011), in order to obtain high-time resolution measurements (1 Hz) continuously. Each FMS 1 s "run" is either collected as chopper closed (background with particle beam blocked) or chopper open (background plus ambient particles and air) position. For KORUS-AQ, the CU-AMS sampled with chopper closed for 6 s and chopper open for 46 s. For the remaining 8 s of the 1 min cycle, it sampled with the efficient particle time-of-flight (ePToF) mode which provides particle sizing but with reduced sensitivity (Fig. S2). Also, once every 20 – 30 min, rapid sampling (20 s) of outside air through a particle filter was used to ensure quality control of the instrument background and detection limits. The filters provide data quality checks throughout the flight by checking for leaks as the cabin changes pressure, to determine the response time of the different species (typically less than 2 seconds), and to validate the real-time continuous detection limits calculated by the Drewnick et al. (2009) method. The average of the two background signal periods (chopper closed) before and after the open signal was subtracted from each 1 s open measurement. In addition to the 1 s data, we reported a 1 min data product, in which we averaged raw mass spectra prior to fitting the high-resolution ions, leading to improved signal-to-noise (SNR) from reduced nonlinear fitting noise (beyond the expected increased SNR from averaging in an ion-counting noise regime). For this study, the 1 min data product is used since the additional spatial resolution provided by the 1 s product was not required for the analysis of regional plumes. The software packages Squirrel V1.60 and PIKA V1.20 within Igor Pro 7 (Wavemetrics) (DeCarlo et al., 2006; Sueper, 2018) were used to analyze all AMS data.

The CU-AMS always used the "V-mode" ion path (DeCarlo et al., 2006), with a spectral resolution ($m/\Delta m$) of 2500 at *m/z* 44 and 2800 at *m/z* 184. The collection efficiency (CE) for the CU-AMS was estimated per Middlebrook et al. (2012), and ranged from 0.5 – 1 (Fig. S28), with

most of the values occurring around 0.5. Calibrations of the CU-AMS are discussed in the supplement (Sect. S2), and detections limits for the 1 min data were 26, 12, 4, 10, and 115 ng sm^{-3} for SO_4 (sulfate), NO_3 (nitrate), NH_4 (ammonium), Chl (chloride), and OA, respectively (Note that the charge symbol is not included for the nominally inorganic species, as organic compounds may make (typically small) contributions to these species (e.g., organonitrates, organosulfates, and reduced organic nitrogen species) (Huffman et al., 2009; Farmer et al., 2010). On average, during the campaign, organic nitrates were ~8% of the total CU-AMS NO_3 signal, and were only an important contribution to the NO_3 signal when NO_3 was less than 0.50 µg sm^{-3} (Fig. S38). pNO_3 will be used throughout the rest of the paper to represent aerosol NO_3 and to ensure it is not confused with radical NO_3. These detection limits are estimated for every data point per Drewnick et al. (2009) and remained nearly constant during each flight and throughout the campaign. The detection limits were ~~It was~~ scaled by ~×0.8, based on comparison with periodic filter blanks (Campuzano-Jost et al., 2016), since the Drewnick et al. (2009) method only uses some ions to determine the detection limits, while filters take all ions into account, and thus the latter provide a more accurate estimate. It was found that the scaling with the periodic blanks from the filters were not impacted by the length of sampling outside air through the filter. The low limit of detection for these species remained nearly constant during the flight by using a cryogenic pump that lowered the temperature of a surface surrounding the vaporizer region to 90 K. This freezes out most background gases, and provided consistently low detection limits during the flight, when other AMSs may suffer from ~~much~~ increased detection limits after~~for~~ several hours into a flight due to pumping out of large initial backgrounds. The cryogenic pump is necessary since the airplane had power only 3 hours prior to take-off until 2 hours after landing; therefore, the CU-AMS was not constantly being pumped. This leads to high backgrounds each time the instrument is started. The

2σ accuracy for the CU-AMS of inorganic and organic species is estimated to be 35% and 38%, respectively (Bahreini et al., 2009). The O/C and H/C ratios were determined using the improved-ambient method (Canagaratna et al., 2015). The CU-AMS was fully operational during KORUS-AQ, except for 2 hours in RF01, leading to nearly 99% data collection coverage. Additional information on AMS data interpretation can be found in Jimenez et al. (2018) as well as the datafile headers for the KORUS-AQ AMS data (Aknan and Chen, 2018).

2.3 Oxidation flow reactor sampling and analysis

The Potential Aerosol Mass (PAM) oxidation flow reactor (OFR) ~~allows the measurement of~~measures the aerosol mass that can be formed from the precursors that are present in ambient or laboratory air (Kang et al., 2007; Lambe et al., 2011). The OFR has been successfully deployed in multiple urban and forested locations to quantify potential SOA (Ortega et al., 2016; Palm et al., 2016, 2017, 2018; Kang et al., 2018). The chemical regimes and comparability to ambient results of the OFR have been characterized extensively by modeling, which indicate that SOA formation proceeds by chemistry similar to the atmosphere, dominated by OH oxidation under low-NO conditions (Li et al., 2015; Peng et al., 2015, 2016). The sampling schematic of the OFR during KORUS-AQ is shown in Fig. S12. Briefly, it is a 13 L (45.7 cm length OD × 19.7 cm ID) cylindrical aluminum tubular vessel that uses two low-pressure mercury 185 and 254 nm lamps (BHK, Inc., model no. 82-904-03) to produce OH radical through the photolysis of ambient H_2O, O_2, and O_3 (R1 – R5). This mode of operation is referred to as "OFR185."

$$H_2O + h\nu\ (185\ nm) \rightarrow OH + H \quad \text{(R1)}$$

$$O_2 + h\nu\ (185\ nm) \rightarrow 2\ O(^3P) \quad \text{(R2)}$$

$$O_2 + O(^3P) \rightarrow O_3 \quad \text{(R3)}$$

$$O_3 + h\nu\ (254\ nm) \rightarrow O_2 + O(^1D) \quad \text{(R4)}$$

722 $O(^1D) + H_2O \rightarrow 2\ OH$ (R5)

723 The KORUS-AQ study represents the first airborne operation of an OFR to our knowledge.
724 Unlike prior ground-based field studies (Ortega et al., 2016; Palm et al., 2016, 2017, 2018), the
725 UV lamps were typically maintained at one constant light setting since the OFR was sampling
726 more rapidly varying air masses. Since external OH reactivity (OHR) and water vapor
727 concentrations changed with air mass, a range of OH exposures (OH_{exp}) were reached inside the
728 OFR despite the constant photolytic flux (Peng et al., 2015). The OFR OH_{exp} was calibrated using
729 two different methods: (1) Using the removal of ambient CO in the OFR during flight (on-line
730 calibration in Fig. S14a). (2) While on the ground, injecting known amounts of humidified
731 (multichannel Nafion drier) CO from a zero air cylinder spiked with ~2 ppmv of CO (Scott
732 Marrin), and varying the light intensity to produce different amounts of OH (off-line calibration in
733 Fig. S14b) and thus CO reactive removal. Both the off- and on-line approach yielded a calibration
734 factor of ×0.4 for the OH_{exp}, calculated using the parameterization of Peng et al. (2015), similar to
735 Palm et al. (2016). The OH_{exp} calculated with the calibrated equation is used for periods in which
736 the Picarro was not sampling the OFR output. A histogram of the other key parameters used to
737 calculate OH_{exp} with the Peng et al. (2015) equation—H_2O(g) (measured by DLH) and ambient
738 OH reactivity (measured by ATHOS)—are shown in Fig. S15. The OFR operating conditions were
739 in the "Safe" zone (Peng et al., 2015, 2016), meaning that they were consistent with tropospheric
740 chemistry.

741 A key difference between the operation of this OFR during KORUS-AQ and previous field
742 studies (which did not use any inlet (Ortega et al., 2016; Palm et al., 2016, 2017, 2018)) was that
743 the gas and aerosol passed through ~1.8 m of ~4.6 mm ID stainless steel tubing at 5 vlpm
744 (residence time ~1.4 s through tubing). The residence time in the OFR was ~150 s. The gas and

745 aerosol sample entered the OFR through a ½" press fitted stainless steel inlet that was coated in
746 SilcoNert (SilcoTek Co, Bellefonte, PA) and had 18 evenly spaced holes (Fig. S13), to promote
747 more even injection of the sample into the OFR flow cross-section (Ortega et al., 2016; Palm et
748 al., 2017; Mitroo et al., 2018). The gas-phase output of the OFR was sampled by an 8.25 cm
749 diameter Teflon ring inside the OFR connected to 1/8" Teflon tubing, and sampled by two gas
750 analyzers for O_3 (Model 205, 2B Technologies, Boulder, CO, USA) and CO (Picarro, see above).
751 The aerosol was sampled by a 2 mm ID stainless steel tube. A constant flow through the OFR at
752 all times was maintained with a bypass flow (when the CU-AMS or CO instrument were not
753 sampling from the OFR) to always maintain a constant residence time in the OFR. The CU-AMS
754 sampled from the OFR for 12 – 15 seconds every three minutes (Fig. S2). This sampling scheme
755 was chosen to ensure the CU-AMS had a high sampling frequency for ambient aerosol, while also
756 sampling the OFR once each time the air inside it was replaced (given its residence time of ~150
757 s).

758 In prior ground-based studies the OFR was placed outside, leading to the ambient and OFR
759 temperature being within 1 – 2°C (Ortega et al., 2016; Palm et al., 2016, 2017, 2018). During
760 KORUS-AQ the OFR was housed inside the DC-8 cabin, which was typically ~10°C (range 0 –
761 20°C) warmer than ambient air (Fig. S16). Since $(NH_4)_2SO_4$ is nonvolatile, there was little impact
762 on the amount of SO_4 entering and exiting the OFR (as confirmed when the UV lights were off
763 and OH_{exp} was zero) (Fig. S17). For OA, which is typically a mixture of semivolatile and
764 nonvolatile compounds, and for pNO_3, which can be quite semivolatile (Huffman et al., 2009;
765 Cappa and Jimenez, 2010), the mass concentration exiting the OFR was significantly lower than
766 when entering, with lights off. This is due to evaporation of OA and pNO_3 at the warmer cabin
767 temperatures and longer residence times (~150 s). However, for ambient measurements, the

residence time was less than 1 s (Sect 2.2), which is rapid enough to prevent volatilization of OA and pNO_3, as discussed in prior work (Guo et al., 2016, 2017; Shingler et al., 2016). Thus, the average ratio of OA transmitted through the OFR versus bypassing the OFR with lights off is used (slope in Fig. S17) as an approximate correction for the amount of OA that should have exited the OFR without chemistry when the OFR was in oxidation mode. These values were highly correlated (R^2 = 0.94) and did not vary for the entire campaign, leading to confidence in the correction. This corrects for the semi-volatile nature of ambient OA, but it does not correct for any temperature dependence of SOA formation.

The average aerosol condensation sink (CS) inside the OFR is needed for the LVOC fate model described in Palm et al. (2016) to compute the amount of condensable vapors that do not form SOA in the OFR (due to residence-time limitations and surface losses), but that would be expected to form SOA in the atmosphere. Since there were no particle sizers available to estimate the changes in the aerosol surface area after the OFR (Palm et al., 2016), we used Eq. (1) to estimate the average aerosol surface area in the OFR and estimated condensational sink (CS_{est}).

$$CS_{est} = CS_{amb} \times \left(\frac{\text{AMS Tot Mass Out} + \text{AMS Tot Mass In}}{2 \times \text{AMS Tot Mass In}} \right)^{2/3} \times 2 \quad (1)$$

The CS_{amb} (ambient condensational sink) is calculated using the LAS and SMPS measurements. The second term is a scaling factor to account for the observed increase in mass in OFR (with a power of 2/3 for approximate conversion to relative surface area). The third term is a scaling factor for relative increase in surface area due to strong nanoparticle formation in the OFR, as observed in Los Angeles during CalNex (Ortega et al., 2016). A hygroscopic growth factor is not included in the CS_{est} (Palm et al., 2016) as the aerosol in the OFR was dry (Sect. 2.1).

One simple way to confirm the validity of the OH exposures derived from the in-field calibrations and measurements, is to compare the observed versus modeled sulfate enhancements

in the OFR while traversing SO_2 plumes (Palm et al., 2016) (Fig. S18 and S19). Albeit the point-to-point comparison is noisy as expected, we find good agreement on average between the modeled and measured SO_4 enhancement (slope = 0.94), validating the quantification of the OFR for this study. We obtained results from the OFR for all flights except RF12 (24/May/2016), when a valve malfunction prevented measurements of O_3 and thus the ability to quantify OFR OH_{exp}. During this flight, the Picarro was also not sampling from the OFR.

2.4 Co-located supporting measurements used in this study

In addition, the CU-AMS measurements, this study utilizes several co-located gas- and aerosol-phase measurements collected on-board the DC-8.

2.4.1 Gas-phase measurements

NO, NO_2, NO_y, and O_3 were measured by the NCAR chemiluminescence instrument (Weinheimer et al., 1994). For CO, the ambient measurements were made with the NASA Langley tunable diode laser absorption spectroscopy (DACOM) (Sachse et al., 1987) while the measurements for CO exiting the oxidation flow reactor (Sect. 2.3) were made with a Picarro G2401-m. The Picarro was calibrated in flight with a WMO traceable gas standard. Gas-phase H_2O was measured with the NASA Langley open-path tunable diode laser hygrometer (DLH) (Diskin et al., 2002). The Pennsylvania State University Airborne Tropospheric Hydrogen Oxides Sensor (ATHOS), based on laser-induced fluorescence, measured OH, HO_2, and OH reactivity (Faloona et al., 2004; Mao et al., 2009). Hydrocarbons were measured by the University of California-Irvine whole air sampler (WAS), followed by analysis with a gas-chromatography followed by either a flame ionization detector or mass spectrometer (Blake et al., 2003), and also by the University of Oslo proton transfer reaction time-of-flight mass spectrometer (PTR-MS) (Wisthaler et al., 2002; Müller et al., 2014). SO_2 and speciated acyl peroxy nitrates (e.g., PAN and

PPN) were measured by the Georgia Institute of Technology chemical ionization mass spectrometer (GT-CIMS) (Huey et al., 2004; Slusher et al., 2004; S. Kim et al., 2007) The sum of the total peroxy nitrates ($\Sigma ROONO_2$) and total alkyl and multifunctional nitrates ($\Sigma RONO_2$) were measured by the University of California-Berkeley thermal-dissociation laser-induced fluorescence (TD-LIF) technique (Day et al., 2002; Wooldridge et al., 2010). Formaldehyde was measured with the University of Colorado-Boulder difference frequency absorption spectrometer (CAMS, or Compact Atmospheric Multi-species Spectrometer) (Weibring et al., 2010; Richter et al., 2015). Finally, HCN, HNO_3, and dihydroxy-toluene were measured by the California Institute of Technology chemical ionization mass spectrometer (CIT-CIMS) (Crounse et al., 2006; Schwantes et al., 2017).

2.4.2 Supporting aerosol measurements

Refractory Black carbon (BC) mass concentrations in the accumulation mode size range measured by the NOAA Single Particle Soot Photometer (SP2) (Schwarz et al., 2013). SO_4^{2-} was measured both by the University of New Hampshire mist-chamber ion-chromatograph (MC/IC, fine mode only) (Talbot et al., 1997) and total particulate filters, analyzed off-line with ion chromatography (fine and coarse mode with an estimated size cut of 4 μm) (Dibb et al., 2003; McNaughton et al., 2007; Heim et al., 2018). Besides the CU-AMS, the Hankuk University of Foreign Studies operated an AMS onboard as well (hereinafter referred to as K-AMS); however, using a “capture vaporizer” (see Sect. 2.2 above). Briefly, the geometry and material of the vaporizer has been modified to reduce the amount of particle bounce, and this leads to a CE of ~1 for all ambient species, albeit with more thermal decomposition (Jayne and Worsnop, 2015; Hu et al., 2017a, 2017b, 2018a, 2018b; Xu et al., 2017).

Finally, the physical concentration and properties of the aerosol were measured by the NASA Langley Aerosol Research Group (LARGE). These included: (1) Size-resolved particle number concentrations (values used to estimate surface area and volume) were measured by a TSI Laser Aerosol Spectrometer (LAS, model 3340; TSI Inc., St. Paul, MN; calibrated with a range of NIST traceable polystyrene latex spheres (PSL), size range 100 – 5000 nm PSL mobility diameter), a scanning mobility particle sizer (SMPS, composed of a differential mobility analyzer, TSI model 3081 long column with custom flow system and SMPS operated using TSI software) and a CPC (TSI model 3010, size range 10 – 200 nm PSL mobility diameter). (2) Scattering coefficients at 450, 550 and 700 nm were measured with an integrating nephelometer (TSI, Inc. model 3563) and corrected for truncation errors per Anderson and Ogren (1998). (3) Absorption coefficients at 470, 532 and 660 nm were measured with a Particle Soot Absorption Photometer (PSAP, Radiance Research) and corrected for filter scattering per Virkkula (2010). In order to calculate extinction, which is used in this study, the measured Angstrom exponent was used to adjust the scattering at 550 nm to 532 nm (Ziemba et al., 2013).

3. PM_1 comparisons, composition, and transport during KORUS-AQ

3.1 Intercomparisons of airborne PM_1 during KORUS-AQ

The intercomparison of aerosol measurements less than 1 μm are summarized here and shown in Table 1, and the full detailed intercomparison is found in SI 8. The AMS and the other aerosol measurements agree within their combined uncertainties, similar to prior studies (DeCarlo et al., 2008; Dunlea et al., 2009; Hayes et al., 2013; Liu et al., 2017; Schroder et al., 2018).

Table 1. Overview of intercomparisons for KORUS-AQ CU-AMS versus other PM_1 measurements. Uncertainties listed are 1σ.

Instrument Comparison	*What is being Compared*	*Slope*	R^2	*Combined Uncertainty of Instruments*	*Uncertainty of Regression Slope*
MC//IC	SO_4 Mass	0.95	0.76	±20%	±1%
Filters	SO_4 Mass	0.80	0.86	±24%	±2%

AMS Scatter Plot (Total Campaign)	Total PM_1 Mass/CE	0.95		±27%	±1%
AMS Scatter Plot (Lower PM_1 Sizes)[a]	Mass/CE/ Transmission	1.02	0.91	±27%	±1%
AMS Scatter Plot (Higher PM_1 Sizes)[b]	Mass/ Transmission	0.84	0.82	±27%	±1%
Extinction	Total PM_1 Mass to 532 nm Extinction	6.00	0.87	±31%	±3%
LAS (all data)	PM_1 Volume	1.56	0.86	±43%	±1%
LAS (Conc. Filter)[c]	PM_1 Volume	1.19	0.91	±43%	±1%
LAS (Mass Filter)[c]	PM_1 Volume	1.00	0.79	±43%	±1%

[a]Comparison of K-AMS and CU-AMS for RFs 1 – 9, 11, 15, 19. [b]Comparison of K-AMS and CU-AMS for RFs 10, 12 – 14, 16 – 18, 20. [c]Using the lower concentration and mass filter. See SI 8 and Fig. S27.

There are two comparisons that show lower agreement. The slope between AMS SO_4 versus filter SO_4 is 20% lower than unity. As previously mentioned, the filters collect aerosols with diameters up to 4 µm, and Heim et al. (2018) concluded that the difference was due to supermicron SO_4^{2-} throughout the campaign from the transport of dust from continental Asia to South Korea. Thus, the differences in the diameter cut-off between the AMS and filters and observations of supermicron SO_4^{2-} are the likely cause of the lower slope. The comparison of calculated volume from AMS plus BC versus calculated volume from LAS indicate that the AMS and BC calculated volume is higher. Part of the reason could be that LAS vaporizes BC (Kupc et al., 2018); however, as shown in Figure 1, BC accounts for a small fraction of PM_1. As discussed in SI 8, the LAS detector saturated at high particle number concentrations/high mass concentrations. This has also been observed by Liu et al. (2017) in a prior airborne campaign with the same instruments. Comparing the LAS and AMS plus BC volume at lower total mass concentrations/particle number concentrations, the difference is reduced to ~10%, which is well within the combined uncertainties.

3.2 PM_1 concentration and composition over South Korea during KORUS-AQ

We briefly describe the PM_1 composition observed over South Korea during the campaign and compare it to prior observations in the same region and for other large urban areas around the world. First, the comparison of PM_1 in the boundary layer (estimated to be ~600 m from temperature profiles measured on the DC-8 during the entire campaign, as shown in Figure 1) in the KORUS-AQ domain is discussed. As shown in Figure 1, the highest average PM_1 during KORUS-AQ were observed over the West Sea during the "transport/polluted" research flight (RF12, 24/May/2016), at 39 μg sm^{-3}, and over Seoul, at 31 μg sm^{-3} (average of all flights over Seoul). However, during the latter half of the mission, PM_1 was regularly greater than 60 μg sm^{-3}, and as high as 100 μg sm^{-3}, over Seoul. During the rest of the flights, the average mass concentration over the West Sea was a factor of 3 lower (13 μg sm^{-3}). Also, the Seoul and West Sea PM_1 composition was different, where SO_4 and more-oxidized oxidized organic aerosol (MO-OOA) dominated the West Sea PM_1 budget, indicative of transported, aged chemistry (Dunlea et al., 2009; Lee et al., 2015). Also, the O/C ratio for the West Sea was 0.84 (WS Clean) to 0.88 (WS polluted). Seoul showed higher fractions of less-oxidized OOA (LO-OOA) than MO-OOA, and higher pNO_3 than SO_4, which is more typical of fresher, urban chemistry, with an average O/C ratio of 0.70 (DeCarlo et al., 2008; Hennigan et al., 2008; Hayes et al., 2013; H. Kim et al., 2017; Kim et al., 2018). The eastern side of South Korea had lower average PM_1 than observed over Seoul. This region of South Korea is not as highly populated as around Seoul, reducing the sources and production of PM_1 and is more representative of PM_1 background pollution/transport across the country. The average PM_1 observed over the Jeju jetway was similar to what was observed over Seoul. Also, this area had similar contributions from hydrocarbon-like organic aerosol (HOA) and pNO_3 as Seoul, indicating local emissions, including industry, along with transport/background, are impacting the PM_1 composition (e.g., Hayes et al., 2013). This part of

South Korea has some large population centers (e.g., Gwangju and Jeonju) and power plants (e.g., Boryeong Power Station), which are consistent with the observed impact.

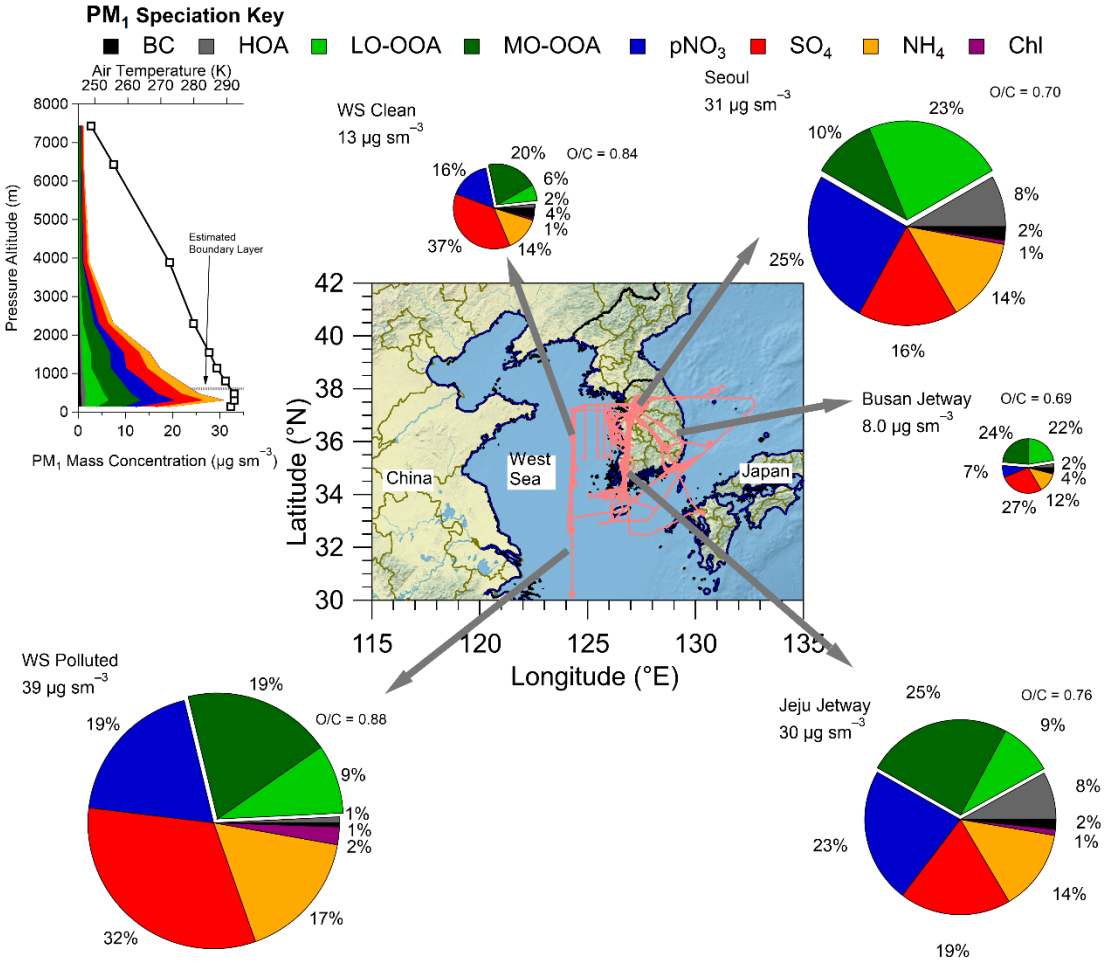

Figure 1. Pie charts of the average boundary layer PM_1 composition by the different regions (defined in Table S2) sampled over South Korea during the campaign. The flight paths are shown in light red. The Busan jetway had no measurable Chl; therefore, Chl is not included in the pie chart. The pie charts area is proportional to PM_1 in each region. The average O/C for the OA is shown by each OA section in the pie charts. The map shows the DC-8 flight paths throughout KORUS-AQ. The average vertical profile of PM_1 species (along with temperature and continental PBL height) over all of South Korea is shown in the upper left.

The average PM_1 observed over Seoul during KORUS-AQ was similar to the mass concentration measured in Seoul in previous years (37, 38, 37, 27, and 22 μg m^{-3} for Choi et al., 2012, Kim et al., 2007, H. C. Kim et al., 2016, Park et al., 2012, and Kim and Zhang, 2017,

913 respectively). Also, the average PM_1 over the West Sea during clean conditions (13 μg sm^{-3}) is in
914 line with what has been reported over Baengnyeong Island (Lee et al., 2015), located west of South
915 Korea in the West Sea (37°58'00" N, 124°37'04" S). Finally, the $PM_{2.5}$ mass concentrations have
916 remained nearly constant for the last ~20 years (OECD, 2018).

917 The PM_1 composition over Seoul is dominated by pNO_3 and SOA, similar to what was
918 observed on the ground during the same time period (Kim et al., 2018). The composition over
919 Seoul is more similar to what has been observed over Mexico City during MILAGRO (DeCarlo
920 et al., 2008), and in Los Angeles during CalNex (Hayes et al., 2013) than observed over large
921 urban areas in Asia (Hu et al., 2016).

922 As the differences in PM_1 composition for the different regions mostly occurred in the
923 boundary layer, we show the average PM_1 profile observed during all of KORUS-AQ in the inset
924 of Figure 1, and the fractional contribution to the profile in Fig. S32. At low altitudes, the PM_1
925 mass is dominated by secondary PM_1 species that compose the largest fractions in the pie charts
926 in Figure 1 (LO-OOA, MO-OOA, pNO_3, and SO_4). The fractional contributions of SO_4 and MO-
927 OOA to PM_1 mass increase with altitude and become dominant above ~4 km, representative of
928 more aged aerosol, away from sources (e.g., Dunlea et al., 2009).

3.3 Analysis of background and transport influence on PM_1

Transport of aerosols and aerosol precursors from distant sources creates a larger-scale background that needs to be quantified in order to understand the impact of local emissions on aerosol production. Prior studies have shown the potential impact of long-distance transport in creating a background aerosol mass over Seoul (H. S. Kim et al., 2007; Heo et al., 2009; Kim et al., 2009, 2016, 2018; H. C. Kim et al., 2017; H. Kim et al., 2017; Jeong et al., 2017; Lee et al., 2017; Seo et al., 2017). To investigate the influence of background and transported air to Seoul, the FLEXPART Lagrangian model with WRF winds and meteorology is used. The application of FLEXPART to this study is described in SI 7. Briefly, the model uses back trajectories from the point where the DC-8 was sampling and calculates the amount of CO and NO_2 contributed by different emission regions for each sampled air parcel.

The CO concentration measured during KORUS-AQ can be described by Eq. (2). The average CO mixing ratios observed during the campaign are used.

$$CO_{ambient}=CO_{hem.\ bckg.}+CO_{foreign}+CO_{South\ Korean} \quad (2)$$

Here, $CO_{hem.\ bckg.}$ is the hemispheric background of CO. In FLEXPART, the foreign emissions are from China, Hong Kong, Japan, Laos, Macau, Myanmar, Mongolia, North Korea, Russia, Taiwan and Vietnam. FLEXPART does not include the CO hemispheric background; therefore, that term is estimated from upwind sites (Mt. Waliguan, China and Ulann Uul, Mongolia) (Novelli et al., 2017) to be 140 ppbv CO. The West Sea is the simplest case, as FLEXPART predicted that all the CO originated from the foreign sources listed above (Figure 2a). Thus, $CO_{ambient}$ in the West Sea can be attributed to 140 ppbv $CO_{hem.\ bckg.}$ and 125 ppbv $CO_{foreign}$ (Figure 2b). The advection of CO from the West Sea to Seoul will lead to dilution and mixing of the $CO_{foreign}$ with air containing only the $CO_{hem.\ bckg.}$. With an average wind speed of 4 m/s over the West Sea, and a distance of

~300 km, the air takes ~1 actual day to move from where the DC-8 sampled over the West Sea to Seoul. The results from FLEXPART are used to estimate the dilution rate, ~0.7 day^{-1}, comparable to the values determined in prior studies (McKeen et al., 1996; Price et al., 2004; Arnold et al., 2007; Dzepina et al., 2011; Fried et al., 2011). $CO_{foregin}$ over Seoul was determined by Eq. (3), where t = ~1 day, $-k_{dil}$ = ~0.7 day^{-1}, and C(0) = 125 ppbv. Using the full equation from McKeen et al. (1996), a similar value of 60 ppbv $CO_{foreign}$ is derived.

$$C(0)=C(t)\times exp^{(-k_{dil}\times t)} \quad (3)$$

~~Thus, after 1 day of advection, ~60 ppbv $CO_{foreign}$ is expected over Seoul (Figure 2c); thus, w~~With Eq. (2), the total CO background ($CO_{foreign}$ + $CO_{hem.\ bckg.}$) is 200 ppbv, and the remainder of the observed ambient CO is attributed to local South Korean emissions (on average, 165 ppbv CO). Finally, results from FLEXPART show that the $CO_{foreign}$ contribution (Figure 2d) remained nearly constant throughout the campaign at all observed photochemical ages. Therefore, 200 ppbv CO background for observations over Seoul will be used throughout this study.

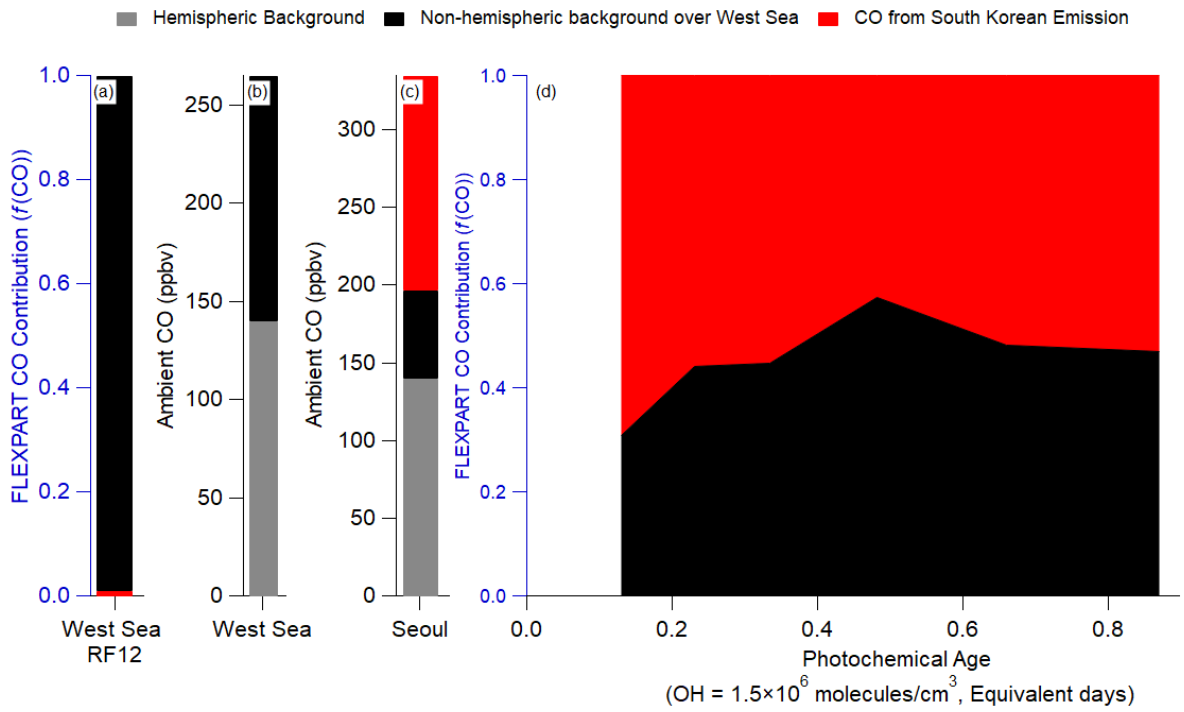

965

966 **Figure 2.** Note differences in labels and values for each y-axis. Also, note that FLEXPART does
967 not include hemispheric background; therefore, it is not included in ~~the figure~~(a) and (d); however,
968 it is included for the actual observations in (b) and (c). (a) Fractional contribution of foreign versus
969 South Korean CO emission over the West Sea from FLEXPART. (b) Estimated measured
970 partitioning of the average CO observed over the West Sea. (c) Same as (b), but for over Seoul.
971 (d) Same as (a), but for over Seoul. For all panels, CO does not include any chemical losses or
972 production.

973 From the observed dilution-corrected OA concentrations (OA concentration divided by the
974 hemispheric background subtracted CO mixing ratios) over the West Sea (13 and 40 μg sm^{-3}
975 $ppmv^{-1}$ for clean West Sea and RF12 West Sea, respectively), the $CO_{foreign}$ over Seoul would
976 correspond to 1 – 3 μg sm^{-3} OA background (Eq. (~~3~~4)).

977 $$OA_{background}(t)=CO_{foreign}(t)\times\left(\frac{OA}{CO}\right)_{foreign}(0) \quad (~~3~~4)$$

978

979 The upper limit will be used for the remainder of the study. The corresponding observed
980 background values for HOA, LO-OOA, and MO-OOA are 0, 1±1, and 2±2 μg sm^{-3}, respectively.
981 Finally, the background for key gas-phase and aerosol species (which are discussed below) are

1.05±0.28 (CH_2O), 69±5 (O_x), 0.25±0.06 (PAN), and 0.30±0.10 ($\Sigma ROONO_2$) ppbv, 0.44±0.34 (Dihydroxy toluene) pptv, and 2±2 μg sm^{-3} (pNO_3). Thus, the increase in OA mass concentration from the background values (3 μg sm^{-3}) to average Seoul values (13 μg sm^{-3}) must be due to South Korean emissions of POA and production of SOA.

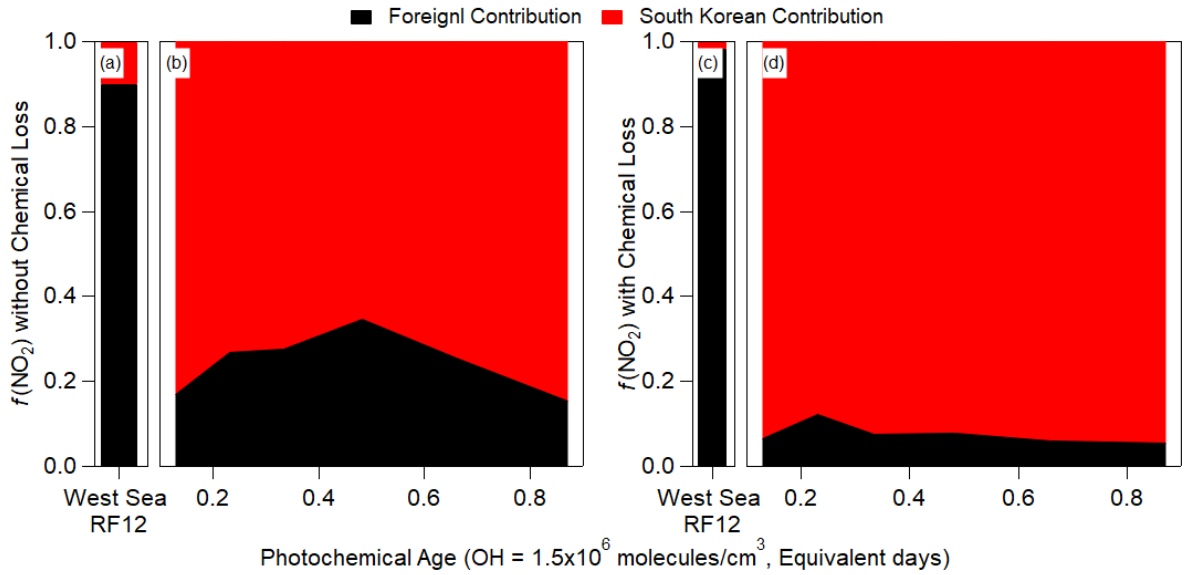

Figure 3. Binned fractional contribution (South Korea/(South Korea + Foreign)) of the FLEXPART~~, sampled from aircraft position for~~ contributions to (a and b) NO_2 (without any chemical losses) and (c and d) NO_2 (with chemical losses (τ = 1 day)) versus the observed (aircraft) photochemical age. For (a) and (c), the West Sea bars are the average fractional contributions for RF12.

The contribution of foreign versus South Korean emissions of NO_2 from FLEXPART over Seoul and West Sea (Figure 3) is analyzed next. NO_2 is investigated since it has a photochemical lifetime of ~1 day (at OH ≈ 1.5×10^6 molecules/cm^3). This lifetime is similar to short-lived hydrocarbons (e.g., xylene, S/IVOC, etc.) that are thought to dominate urban SOA production in this campaign and other megacities (de Gouw et al., 2005; Kleinman et al., 2007, 2008; DeCarlo et al., 2010; Wood et al., 2010; Hayes et al., 2013, 2015, Hu et al., 2013, 2016; Ortega et al., 2016; Ma et al., 2017; Schroder et al., 2018). In general, $f(NO_2)_{foreign}$ and $f(NO_2)_{local}$ (with and without photochemical loss included in the FLEXPART model runs) is quite constant with photochemical

age (Figure 3), like CO. Unlike CO, the contribution of local NO_2 is ~70% (if photochemical removal is not included) and ~90% (if photochemical removal is included). This strongly suggests that most short-lived hydrocarbons over Seoul, which are believed to dominate urban SOA production, are dominated by South Korean emissions and not transport from foreign sources.

4. SOA production over the Seoul Metropolitan Area

4.1 SOA production over Seoul during KORUS-AQ

The conceptual model for analysis of photochemical SOA production over and downwind of megacities has been discussed in detail in de Gouw (2005) and DeCarlo et al. (2010) and subsequent studies (Hayes et al., 2013; Hu et al., 2013, 2016; Freney et al., 2014; Schroder et al., 2018). An air mass with "background" values of OA and CO is advected over a megacity area, where fresh emissions of POA, SOA precursors, and CO are emitted into the air mass. The SOA precursors will oxidize to produce SOA and undergo dilution with the surrounding background air masses. To correct for this dilution effect, the change of OA over background OA (ΔOA = OA – background OA) is divided by the change of CO over background CO (ΔCO = CO – background CO), and this term is the dilution-corrected concentration. CO has been used in prior studies as a surrogate for primary pollution emissions as this compound has high signal-to-noise between urban plumes and background and a long photochemical lifetime (meaning minimal CO is lost due to chemistry or produced from VOC oxidation over a ~1 day timescale (Griffin et al., 2007)) (de Gouw et al., 2005; DeCarlo et al., 2010). Finally, ΔOA/ΔCO is plotted versus estimated photochemical age. The photochemical age approximately accounts for the chemical evolution of precursors either into products which can be estimated from the time evolution of NO_x/NO_y, or the differences in removal rates of two hydrocarbons (o-xylene or m+p-xylene to ethylbenzene). See

SI 5 for more information about the calculation of the photochemical age. The potential impact of SOA precursors being advected into Seoul is addressed in Sect. 4.4.

Throughout the paper, the estimated photochemical age from NO_x/NO_y will be used as this measurement has higher temporal coverage, and an emissions ratio is not needed to calculate the photochemical age (SI 5), but note that ages estimated from hydrocarbon-based clocks are consistent. For photochemical ages greater than 1 day (measurements over the West Sea), the aromatic photochemical clock is used (SI 5) as the NO_x/NO_y clock does not work well past 1 equivalent day (SI 5). As discussed in Parrish et al. (2007), compounds used to calculate photochemical ages should have lifetimes on the order of the range in ages to be quantified. For example, photochemical age over Seoul is less than 1 equivalent day, which is equivalent to the NO_x lifetime; whereas, the photochemical age over the West Sea is expected to be a few equivalent days, which is bracketed by the lifetimes of benzene and toluene.

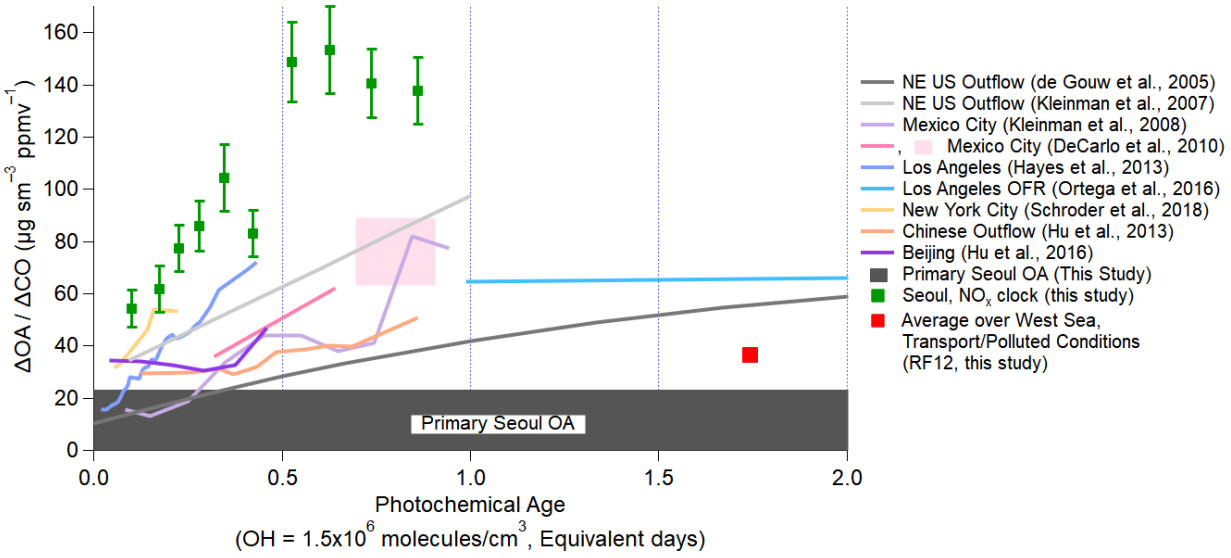

Figure 4. Evolution of dilution-corrected OA versus equivalent photochemical age (days), where ΔOA = OA – background OA and ΔCO = CO – background CO, during KORUS-AQ. Over Seoul and the West Sea, the CO background is 200 (hemispheric plus foreign) and 140 ppbv (hemispheric only), respectively. The vertical error bars for the observations during KORUS-AQ are the standard error of ΔOA/ΔCO for each bin. Photochemical age is determined by the NO_x/NO_y. The dark grey bar at the bottom (22 μg sm^{-3} ppmv^{-1}) is the observed POA over Seoul during the

campaign. Observations from other megacities (de Gouw et al., 2005; Kleinman et al., 2007, 2008; DeCarlo et al., 2010; Hayes et al., 2013; Hu et al., 2013, 2016; Ortega et al., 2016; Schroder et al., 2018) are also shown, as lines, for comparison, and have been updated, as described in Schroder et al. (2018).

Similar to prior studies, OA over Seoul increased rapidly within the first photochemical equivalent day from the emission source (Figure 4). The dilution-corrected SOA production is very rapid for photochemical ages less than 0.7 equivalent days (note that this would be only 4 actual hours of exposure for average OH concentration of 6×10^6 molecules/cm^3 observed during this campaign). After that time, the dilution-corrected OA plateaus and remains nearly constant. George et al. (2008) and Ortega et al. (2016) found that after ~4 – 5 equivalent days, OH heterogeneous reactions start fragmenting the compounds in SOA, leading to a reduction in the dilution-corrected OA mass with age. Compared to prior megacity studies, the dilution-corrected OA produced over Seoul is between 40 – 80 μg sm^{-3} ppmv^{-1} higher at ~0.5 equivalent days of photochemical aging and ~70 μg sm^{-3} ppmv^{-1} higher than in Chinese megacities (Hu et al., 2013, 2016). ~~The strong SOA production over Seoul is similar to that observed in other relatively isolated megacities (e.g., Los Angeles and Mexico City)~~Qualitatively, the time scale for the production and plateauing of dilution-corrected OA is similar for Seoul, Los Angeles, and Mexico City; however, the amount of OA produced per CO is larger for Seoul compared to Los Angeles and Seoul. It also appears not to be significantly influenced by the outflow of upwind Chinese megacities, since Seoul SOA formation is very rapid and occurs much faster than air mass transport from those megacities, and since the dilution-corrected production is much larger in Seoul than in Chinese megacities.

Finally, though the absolute ΔOA/ΔCO value changes depending on background CO used, assuming a lower CO background does not change the general results that Seoul has higher and more rapid SOA production than has been observed in prior megacities.~~these results do not depend~~

~~on the assumed CO background.~~ As shown in Fig. S34, the OA mass concentration increases versus CO mixing ratios as photochemical age increase, and in Fig. S35, even assuming a lower CO background (140 ppbv), the dilution-corrected OA concentration is still ~100 μg sm^{-3} $ppmv^{-1}$. This value is still higher than what has been observed in prior cities (Figure 4). If the CO background is higher than assumed here (200 pbbv), the OA production would be even higher.

To further investigate the potential influence from upwind megacities, we compare ΔOA/ΔCO over the West Sea versus that over Seoul (Figure 4). The average ΔOA/ΔCO over the West Sea during the "transport/polluted" conditions (RF12, 24/May/2016) is ~40 μg sm^{-3} $ppmv^{-1}$. Since 40 μg sm^{-3} $ppmv^{-1}$ has been observed in and downwind of China ~~This value is similar to the upper limit values observed in Beijing (Hu et al., 2016) and Changdao (Chinese outflow)~~ (Hu et al., 2013, 2016)~~(Hu et al., 2013).~~, and observed over the West Sea during the "transport/polluted" event, this diluation-corrected OA concentration is taken to be representative of transport events from China to South Korea ~~This suggests that for Chinese outflow, the maximum dilution-corrected OA concentration is ~40 μg sm^{-3} $ppmv^{-1}$~~. This value has already been subtracted from the observations over Seoul. The fact that OA concentrations are greater than ~~Finding OA concentrations greater than~~ POA concentrations at the youngest photochemical ages may be due to (1) very rapid SOA production; (2) sunrise occurring 3 – 4 hours (sunrise between 5:10 – 5:30 LT) prior to sampling air over Seoul in the morning; and, (3) the imperfect characterization provided by the average photochemical age when fresh emissions have been recently injected into an air parcel.

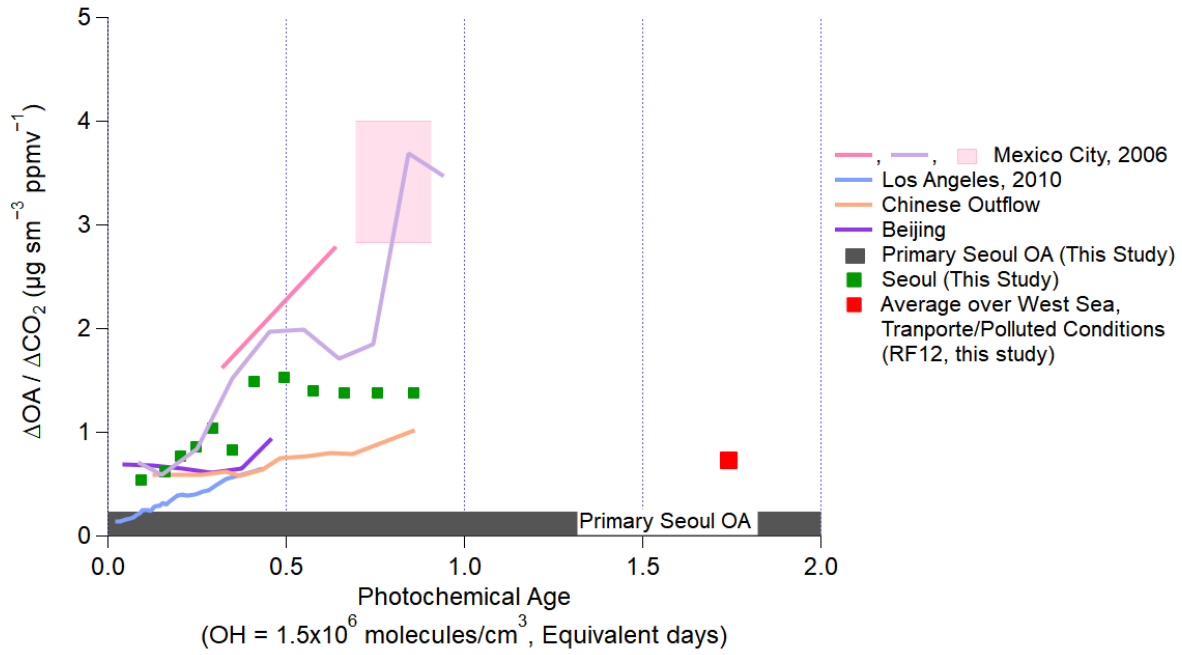

Figure 5. Same as Figure 4, but normalized by ΔCO_2. The ratios to CO_2 are calculated using $\Delta CO/\Delta CO_2$ emissions ratios from prior studies in each megacity that occur during the same campaign or for the same time of year, since direct measurements of the CO_2 enhancements above background during the aircraft studies of each megacity are very challenging. (Table S4).

Here, we introduce another dilution-correction method to investigate SOA production over a megacity—$\Delta OA/\Delta CO_2$ (Figure 5). $\Delta OA/\Delta CO_2$ is a way to investigate the amount of OA produced per unit mass of fuel burned in each megacity. Note that although some SOA precursors are not emitted from combustion sources, such as volatile consumer products (McDonald et al., 2018), one can still define this ratio in an average sense for each megacity. It has been used previously for laboratory experiments (e.g., Gordon et al., 2013; Platt et al., 2013, 2017) and biomass burning (e.g., Akagi et al., 2012; Collier et al., 2016); however, to the best of the authors' knowledge, it has not been used for SOA production over a megacity. As noted above, CO has been typically used instead, given that it is always measured in pollution studies, and it typically has a higher signal-to-background ratio than CO_2 in urban areas. Also, during spring and summer, CO_2 is taken up by plants, which can reduce its signal-to-background ratio. However, the ratio of

other gases to CO can vary between urban areas depending on the average combustion efficiency of the dominant sources (Silva et al., 2013). CO_2 better accounts for fuel consumption in an urban area (Vay et al., 2009; Tang et al., 2018). Multiple recent studies have reported average emissions ratios for different megacities based on high precision measurements of $\Delta CO/\Delta CO_2$ (Vay et al., 2009; Wang et al., 2010; Peischl et al., 2013; Silva et al., 2013; Tohjima et al., 2014; Tang et al., 2018). These results provide an ability to convert the $\Delta OA/\Delta CO$ determined in prior studies to $\Delta OA/\Delta CO_2$ (Table S4). We find that for most of the megacities studied, $\Delta OA/\Delta CO_2$ is very similar, though Mexico City and Seoul show higher values (approximately factor of 2). The range of observed $\Delta OA/\Delta CO_2$ versus photochemical age is narrower, compared to the spread for all megacities observed for $\Delta OA/\Delta CO$. Both analyses suggest that Seoul has larger relative emissions of SOA precursors compared to other megacities, which could be targeted for air quality improvement. However, more observations across other megacities and additional comparative analyses would be beneficial.

4.2 Composition-based analysis of the foreign versus South Korean contribution to SOA precursors and SOA over Seoul

4.2.1 Evolution of oxygenated organic aerosol over Seoul

Here, we focus on the positive matrix factorization (PMF) (Ulbrich et al., 2009) factors for OA resolved during KORUS-AQ, whose evolution over Seoul is shown in Figure 6. Total OOA (LO-OOA plus MO-OOA) is used as a surrogate of total SOA. The fractional contribution of these two factors can be found in Fig. S36. Rapid production of OOA is observed, accounting for all of the observed growth in total OA over Seoul. LO-OOA, overall, is slightly more abundant than MO-OOA (Fig. S36). LO-OOA has lower O/C compared to MO-OOA (Fig. S10); thus, the faster production of LO-OOA likely represents the less oxidized OOA produced from the photooxidation

of SOA precursors (Hayes et al., 2013; Freney et al., 2014; Hu et al., 2016; Kim et al., 2018), while MO-OOA may represent the more oxidized species or those formed from later generations of oxidation (Robinson et al., 2007; Miracolo et al., 2010; Tritscher et al., 2011; Ortega et al., 2016; Sato et al., 2017; Schwantes et al., 2017).

The PMF factors have very different dilution-corrected concentrations over the West Sea during the "transport/polluted" event (Figure 6a). All ΔPMF factors/ΔCO show much lower values than for aged air over Seoul. The discontinuity between the three factors between Seoul and West Sea indicate that transported OA, and transported SOA production, has limited impact on the OA over Seoul.

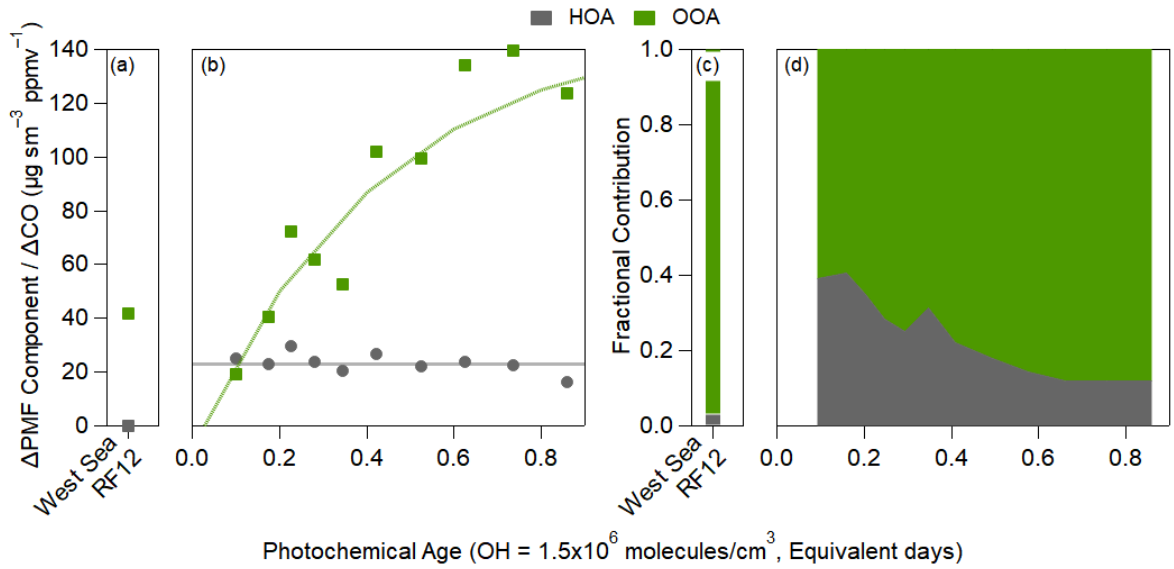

Figure 6. Same as Figure 4, but for the PMF results of the OA evolution over (a) West Sea during the polluted event (West Sea RF12 at ~1.75 equivalent days) and (b) over Seoul. For (b), fit to HOA and OOA are 23 μg sm^{-3} ppmv^{-1} and 150×(1–exp(–2.3×eq. day), respectively. For the OOA equation, 150 equals the max SOA. Fractional contribution of the PMF factors over (c) West Sea (RF12) and (d) over Seoul.

The slope of ΔHOA/ΔCO versus age was nearly zero μg sm^{-3} ppmv^{-1} equivalent day^{-1}, indicating minimal evolution within these timescales. There are mixed results on whether HOA changes with photochemical age (DeCarlo et al., 2010; Hayes et al., 2013; Hu et al., 2013, 2016;

Freney et al., 2014; Schroder et al., 2018); however, due to the uncertainty that comes from the CO background, it is difficult to determine whether these changes are real or not.

At the lowest photochemical ages, HOA is ~35% of the total ΔOA/ΔCO (Figure 6d). Since HOA remains approximately constant with age while OOA rapidly increases (Figure 6b), the HOA contribution to total ΔOA/ΔCO decreases to ~10% after ~1 equivalent day. It has been observed in prior urban campaigns that HOA contributes 10 – 50% and total POA (HOA + other primary OA factors in AMS) contributes 30 – 60% (Aiken et al., 2009; DeCarlo et al., 2010; Hayes et al., 2013; Crippa et al., 2014; Hu et al., 2016; H. Kim et al., 2017; Kim et al., 2018). The fractional contribution of HOA in Seoul is within this range.

A more detailed discussion of the behavior of AMS OA source tracers can be found in SI 11. In general, the AMS OA source tracers behave similarly to other urban campaigns (e.g., Hayes et al., 2013; Freney et al., 2014). Some dilute biomass burning OA was evident, but this source was not major most of the KORUS-AQ. Similarly, isoprene oxidation chemistry was not a major contributor to SOA during this campaign.

4.2.2 Correlation of SOA versus other fast photochemical products

Results above support that a major fraction of the SOA observed over Seoul is rapidly produced through photooxidation of South Korean SOA precursors. To further evaluate this result, we analyze the correlation of OOA with other secondary species known to be rapidly produced through photooxidation of organic precursors.

The other secondary species used in this study are odd oxygen (O_x), formaldehyde (CH_2O), peroxy acetyl nitrate (PAN), the sum of all acyl peroxy nitrates ($\Sigma ROONO_2$), and pNO_3. O_x (approximated as $NO_2 + O_3$) is used instead of O_3 to account for titration of O_3 in the presence of fresh NO emissions. Prior studies have used O_x to provide insights into SOA production (Herndon

et al., 2008; Wood et al., 2010; Hayes et al., 2013; Morino et al., 2014; Zhang et al., 2015; Hu et al., 2016) since O_x has a similar lifetime to SOA (~1 week) (Jacob, 2000; Goldberg et al., 2015; Hodzic et al., 2015; Ortega et al., 2016), and O_x is also produced through the photooxidation of organic compounds. However, since both O_x and SOA have longer lifetimes, the correlation observed between these two species may have a contribution from transport of polluted air masses. To reduce the influence of transport on this analysis, the correlation of OOA with CH_2O, PAN, and $\Sigma ROONO_2$ is also investigated. The benefit of these species is that they have estimated lifetimes of less than 3 hours during daytime in KORUS-AQ (typical temperature for transported air 17°C). Also, it has been shown that dilution-corrected pNO_3 decreases rapidly from urban centers, possibly due to dilution with surrounding air low in HNO_3 and NH_3 and irreversible uptake of HNO_3 onto coarser particles (e.g., DeCarlo et al., 2008).

Example time series of OOA with O_x, CH_2O, PAN, $\Sigma ROONO_2$, and pNO_3 during three different afternoon Seoul overpasses are shown in Figure 7a. All gas and aerosol species exhibit similar behavior, indicating that these species are undergoing photochemical production during these afternoon passes, similar to what has been observed in other urban environments during the afternoon (Perring et al., 2010; Fried et al., 2011; Parrish et al., 2012; Hayes et al., 2013; Zhang et al., 2015). OOA also tracks the evolution of these species, consistent with OOA also being a secondary product from hydrocarbon photooxidation.

Analyzing the entire KORUS-AQ campaign, correlations with $R^2 > 0.50$ are observed between OOA and O_x, CH_2O, PAN, $\Sigma ROONO_2$, and pNO_3 for the overpass observations after 12:00 LT (Figure 7b-f). These correlations for these secondary species produced through the oxidation of hydrocarbons, in the afternoon, when photochemical production dominates over

mixing and losses, further supports that the OOA production observed in Figure 4 and 6 is dominated by the photochemistry of locally emitted hydrocarbons.

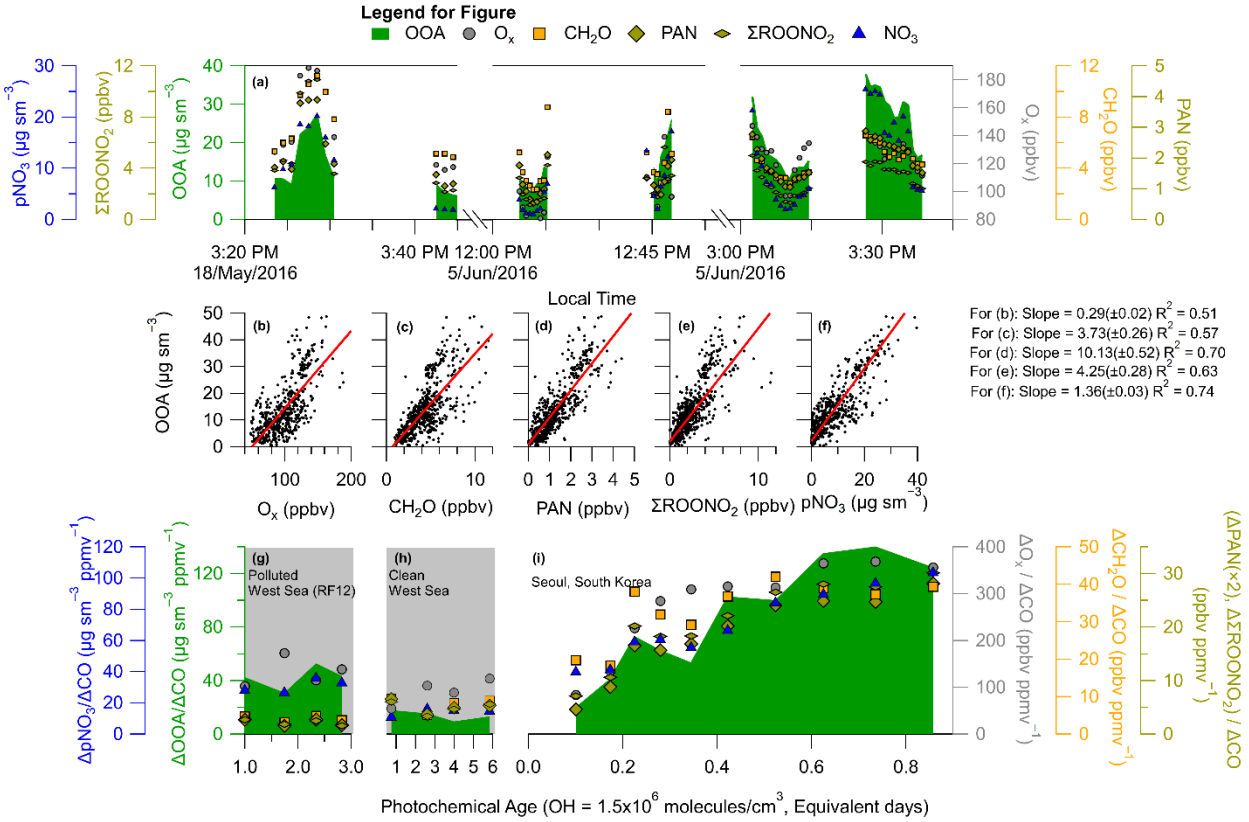

Figure 7. (a) Time series of OOA (OOA = LO-OOA + MO-OOA), O_x, CH_2O, PAN, $\Sigma ROONO_2$, and pNO_3 during RF09 (18/May/2016), and RF18 (05/June/2016) noon and afternoon overpasses. Gaps in time series correspond to climbing out of the boundary layer. OOA versus (b) O_x (O_x = O_3 + NO_2), (c) CH_2O, (d) PAN, (e) $\Sigma ROONO_2$, and (f) pNO_3 over Seoul, South Korea, during KORUS-AQ. For panels (b) – (f), the observations are after 12:00 local time (03:00 UTC), the black dots are all data, and the slopes (red line) is an ODR fit to the data. (g – i) Same as Figure 6 for $\Delta OOA/\Delta CO$ versus photochemical age, and including the dilution-corrected production of O_x, CH_2O, PAN, $\Sigma ROONO_2$, and pNO_3. (g) is over the West Sea (RF12), (h) is over the West Sea (normal conditions) and (i) is over Seoul. Similar to Figure 4, the Δ corresponds to subtracting the background values for the respective species.

O_x, CH_2O, PAN, $\Sigma ROONO_2$, and pNO_3, when dilution-corrected with ΔCO, show a similar trend as OOA (Figure 7i). From the lowest observed photochemical age (~0.1 equivalent day) to the highest (~0.85 equivalent day), O_x, CH_2O, PAN, $\Sigma ROONO_2$, and pNO_3 increase by factors of 4, 2, 7, 4, and 2, respectively. Over Mexico City, increases of factors of ~2 (CH_2O) (Fried et al.,

2011) and ~3 ($\Sigma ROONO_2$) (Perring et al., 2010) were observed, which are comparable to the Seoul observations. These rapid increases can only be explained by photooxidation of South Korean primary emissions (hydrocarbons and NO_x).

The influence of the upwind, background air masses over the West Sea are investigated and shown in Figure 7g and h. Over the West Sea, the dilution-corrected concentration of SOA, O_x, CH_2O, PAN, $\Sigma ROONO_2$, and pNO_3 were all nearly constant. This indicates that the secondary short-lived gas-phase species have reached steady state. Also, since dilution-corrected SOA concentration is flat, this suggests that the SOA precursors have been depleted, and the SOA production has ended, with SOA concentration reaching the plateau that is typically observed after ~1 equivalent day (Ortega et al., 2016). The low PAN concentration and influence from transport over the West Sea was also observed by Lee et al. (2012) over Baengyeoung Island, a regional background monitoring location for Seoul and South Korea, during August 2010 and March – April 2011. This further indicates low amounts of PAN are transported due to its thermal decomposition and very short lifetime, and any production, and correlation, of PAN with OOA would suggest local, photochemical production.

Besides the ubiquitous (but less specific) secondary species from organic compound oxidation, OOA shows a robust correlation with dihydroxy toluene (DHT) (Figure 8), a known SOA precursor from toluene photooxidation (Schwantes et al., 2017). DHT is very short lived, with a photochemical lifetime of less than 1 hour, and it is formed under both low and high NO conditions (Schwantes et al., 2017). The lower correlation, compared to the ubiquitous secondary species, is possibly due to DHT forming from one precursor (toluene) instead of the broad range of precursors that form OOA and O_x, PAN, and CH_2O. The correlation of OOA with a known SOA precursor, that is very short-lived, again supports that OOA production is dominated by

photooxidation of locally emitted hydrocarbons, including toluene. The increasing ratio of OOA to DHT also suggests that SOA production is fastest at low equivalent ages and is starting to plateau at higher ages.

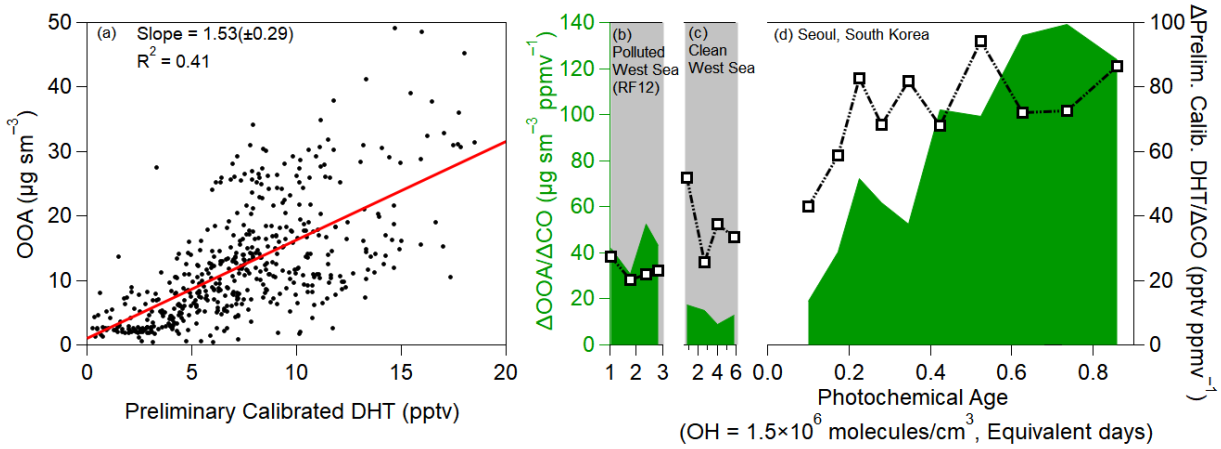

Figure 8. (a) Scatter plot of OOA versus DHT over Seoul, South Korea, during KORUS-AQ, after 12:00 local time (03:00 UTC). (b) Same as Figure 7f, but for DHT over the West Sea (RF12). (c) Same as Figure 7g, but for DHT over the West Sea. (d) Same as Figure 7i, but for DHT over Seoul. As an important note, concentrations of DHT are based on a preliminary calibration; however, any further calibrations are not expected to impact the relative trend and general correlation.

The correlation between OOA and secondary species that have very short lifetimes further suggest that the observed OOA is dominantly due to photooxidation of local emissions to produce SOA and the other secondary species and not transport. This is due to the fact that the short photochemical lifetimes of PAN, CH_2O, DHT, and $\Sigma ROONO_2$ would cause the secondary species to be in steady state. The observations over the West Sea, which is mainly upwind of Seoul and thus background air, show much lower ratios. These two observations further suggest that local SMA emissions are the precursors that undergo the rapid photooxidation to produce SOA, pNO_3, and the other secondary species.

4.2.3 Oxidation state of SOA

We investigate the oxidation state of the observed OA with the van Krevelen diagram (Heald et al., 2010) in Figure 9a. The slope over Seoul (−0.69) is close to the average slope for numerous studies summarized by Chen et al. (2015) (−0.60) and similar to the range of slopes (−0.7 to −1.0) for studies impacted by urban pollution (Aiken et al., 2009; Docherty et al., 2011; Ge et al., 2012), including Los Angeles during CalNex (ranges from −0.64 to −0.68 from Hayes et al. (2013) and Ortega et al. (2016)) or chamber studies investigating the photooxidation of combustion exhausts (Heald et al., 2010; Lambe et al., 2012; Jathar et al., 2013; Presto et al., 2014; Tkacik et al., 2014; Liu et al., 2015). This generally indicates that the photochemistry controlling the production of SOA is similar in urban areas, including photooxidation of diesel and gasoline emissions, evaporative diesel and gasoline, and cooking emissions (Hayes et al., 2015; Woody et al., 2016; Janssen et al., 2017; Ma et al., 2017; Kim et al., 2018).

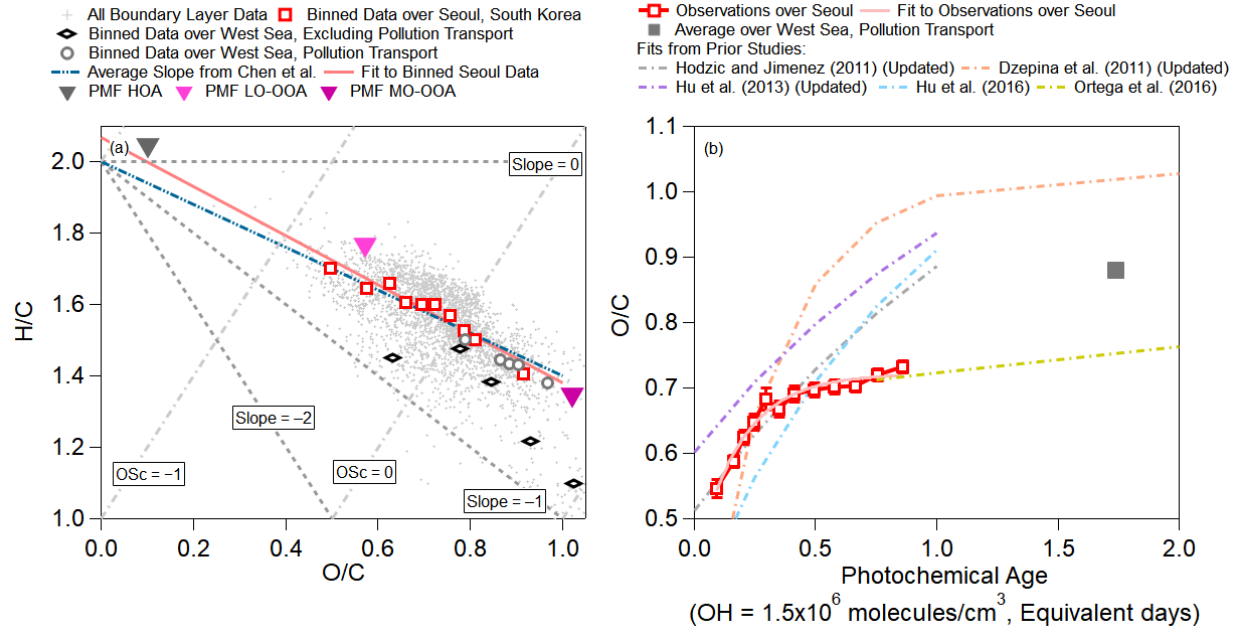

Figure 9. (a) Van Krevelen diagram for all of KORUS-AQ. OSc = (O/C – 2×H/C) (Kroll et al., 2011). The observations are binned, into deciles, for observations over Seoul, South Korea, and binned, into 5 bins, for clean West Sea, and polluted West Sea. The teal line represents the average slope reported in Chen et al. (2015) of −0.60, and the light red line represents the slope (slope =

−0.69(±0.15), y-intercept=2.07(±0.11)) observed over Seoul, South Korea, during the campaign. (b) Binned O/C from observations versus photochemical age, over Seoul, South Korea, and averaged O/C versus photochemical clock over polluted West Sea. The light red line is the fit to the observations over Seoul during KORUS-AQ. The values of O/C versus photochemical age from Hodzic and Jimenez (2011), Dzepina et al. (2011), Hu et al. (2013), are updated with calibrations of Canagaratna et al. (2015); whereas, Hu et al. (2016), and Ortega et al. (2016) did not need updates.

The "transport/polluted" evolution of H/C versus O/C falls on the same slope as the observations over Seoul; however, the values lie at higher O/C ratios, indicative of more aged OOA. O/C versus H/C during the "transported/polluted" event over the West Sea is also comparable to the H/C versus O/C slope (−0.63) observed in Chinese outflow at Changdao (Hu et al., 2013). On the other hand, O/C versus H/C over the West Sea during "clean" events show distinctly lower values and a steeper evolution (slope = −1.1).

The evolution of O/C with photochemical age over Seoul and over the West Sea is shown in Figure 9b, along with results from prior studies (Dzepina et al., 2011; Hodzic and Jimenez, 2011; Hu et al., 2013, 2016; Ortega et al., 2016). Note that older studies have been updated with the calibration of Canagaratna et al. (2015). For the first 0.5 equivalent days, O/C is nearly identical to the Mexico City observations (Hodzic and Jimenez, 2011); however, after 0.5 equivalent days, the O/C ratio growth slows down. The O/C evolution then becomes more similar to that observed when processing Los Angeles air in an OFR (Ortega et al., 2016). The evolution of O/C over Seoul is at the low end of the range of values observed from prior megacities. The average O/C value observed over the West Sea during RF12 is more similar to the values observed after 1 equivalent day in two sites in China (Hu et al., 2013, 2016).

4.4 Influence of local versus transported SOA precursors to SOA production over Seoul

OFR results can be used to investigate the role of SOA production from South Korean and Seoul emissions versus long-distance transported SOA precursors. As shown in prior studies (Ortega et al., 2016; Palm et al., 2016, 2017, 2018), the SOA potential decreases drastically in the

daytime, as the most reactive compounds to OH have already oxidized and formed SOA. Thus, these results will not directly capture the full emitted SOA potential for Seoul, South Korea. Also, recent studies indicate that lower volatility species (e.g., S/IVOCs) can be lost to tubing walls, or their transfer can be greatly delayed (Pagonis et al., 2017; Deming et al., 2018). Thus, it is likely that the OFR inlet line on the DC-8 acted at least as a partial sink of S/IVOCs and thus reduced the measured potential SOA. As a reminder, a correction is included for the condensational sink (CS) of LVOC in the OFR based on Eq. (1).

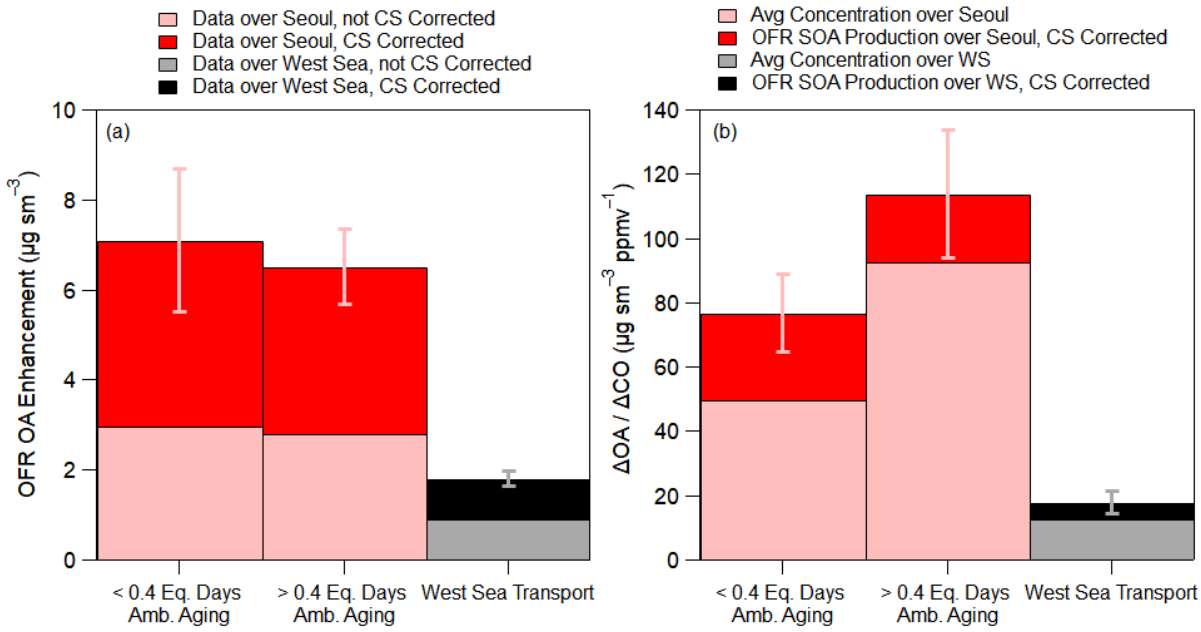

Figure 10. (a) Comparison of OFR OA enhancement (OFR OA enhancement = OA exiting OFR – ambient OA) over Seoul, South Korea, and the West Sea, corrected for evaporation losses. The difference between the two stacked shaded bars is that the lighter (bottom) shade has no CS correction whereas the darker shade does. (b) The lighter color~~ed~~ represents the average dilution-corrected observed ambient OA preexisting concentration corresponding to the OFR observations of the same air mass. The darker color represents the dilution-corrected SOA production in the OFR. The average additional photochemical age added in the OFR is ~4 days (OH_{exp} ~ 5.4×10^{11} molecules/cm^3×s) for both over Seoul and West Sea. Also, the observations for the West Sea are for all flights, not including RF12, where the average ΔOA/ΔCO was 13 µg sm^{-3} ppmv^{-1}. For both (a) and (b), the OFR observations over Seoul are split between lower and higher equivalent ages (see x-axis). The average ambient ages for the two bars are 0.17 and 0.63 equivalent days. Error bars are the standard errors of the observations.

The average OA enhancement in the OFR (OA Enhancement = OA in OFR – Ambient OA) in Seoul is slightly greater for the less aged ambient air (7.1±1.6 versus 6.5±0.8 μg sm^{-3}) but both values lie within the range of the measurements (Figure 10a). The less aged ambient air show slightly higher OA enhancement suggests that more SOA precursors might have been present and available to form SOA mass (Ortega et al., 2016; Palm et al., 2016, 2017, 2018). The OA enhancement observed over Seoul was a factor of 3.5 greater than observed over the West Sea (~7 μg sm^{-3} over Seoul versus ~2 μg sm^{-3} over the West Sea). The much higher SOA formation potential observed over Seoul versus the West Sea indicates that the majority of the precursors that led to the observed SOA and SOA production over Seoul originated from local emissions, consistent with results above.

Plotting the OA enhancements as ΔOA/ΔCO, similar to Figure 4, the amount of ambient SOA production, not including pre-existing OA, for ambient air that has aged less than 0.4 equivalent days is 27(±12) μg sm^{-3} $ppmv^{-1}$, a 50% increase compared to the average ΔOA/ΔCO observed over Seoul at the same ambient photochemical age (Figure 10b). For air older than 0.4 equivalent days, the increase is slightly smaller (21(±20) μg sm^{-3} $ppmv^{-1}$ above ambient pre-existing OA) since a large fraction of the most reactive, high aerosol producing compounds have already been depleted and produced ambient SOA (Ortega et al., 2016; Palm et al., 2016, 2017, 2018).

Finally, there is still a small amount of SOA production potential in the air transported over the West Sea to Seoul. The average potential, not including pre-existing OA, is 5(±4) μg sm^{-3} $ppmv^{-1}$. This is a factor of 4 – 5 less than the potential SOA production observed in the OFR for Seoul. Including the pre-existing dilution-corrected OA for the West Sea observation (18 μg sm^{-3} $ppmv^{-1}$), the concentration is approximately a factor of 8.5 less than the maximum ambient

dilution-corrected OA concentration and a factor of 6 – 8 less than the total dilution corrected OA concentration exiting the OFR. Some of this remaining production would have been further consumed during transport between the West Sea and Seoul (typically 1 day); therefore, it is not expected to significantly impact the SOA production over Seoul. This further indicates that, during this campaign, the transported SOA precursors to Seoul from foreign sources did not contribute significantly to the overall observed SOA production.

4.5 Calculated precursor contributions to the SOA production over Seoul

We use a simple SOA model (Dzepina et al., 2009; Zhao et al., 2014) to calculate the contribution of various precursors to SOA over Seoul (Figure 11, details in Sect. SI 6). Observed hydrocarbons (Table 2), from WAS, along with estimated S/IVOC (Robinson et al., 2007; Dzepina et al., 2009; Hayes et al., 2015) and SOA yields updated to account for vapor wall losses (Ma et al., 2017) were used to estimate (SI Eq. (S3) and (S4)) the contribution of various precursors to SOA production observed over Seoul. Dzepina et al. (2009) and Hayes et al. (2015) both found that the "Robinson" parameterization of SOA from S/IVOC was consistent with SOA production in Mexico City and Los Angeles for observations at 1 equivalent day or less; thus, the same parameterizations are used here.

The percent difference between the modeled and measured total OA ranged between –24 to 3~~4~~2% with an average value of the observations being 1~~1~~5% higher. This provides confidence that the calculation described in SI 6 captures the chemical production of SOA over Seoul. Also, the difference between the estimated and measured OA is comparable to, or better than, found in other studies that utilized a similar modeling approaches (Dzepina et al., 2009; Zhao et al., 2014, 2016; Hayes et al., 2015; Huang et al., 2015; Ma et al., 2017), and within the uncertainty of the measured OA (38%, 2σ).

This box model does not explicitly consider volatile consumer products (VCPs) (Khare and Gentner, 2018; McDonald et al., 2018), S/IVOC from cooking emissions (e.g., Hayes et al., 2013; Ots et al., 2016), or glyoxal (Volkamer et al., 2006; Knote et al., 2014), although contributions from these components may be partially included in the empirical estimation of S/IVOC. Modeled SOA in Los Angeles, using estimates of S/IVOC from ΔHOA/ΔCO, including ~2/3 of VCPs and not including glyoxal, were able to capture the observed SOA in the first 0.5 equivalent days (Hayes et al., 2015; McDonald et al., 2018), similar to the results here.

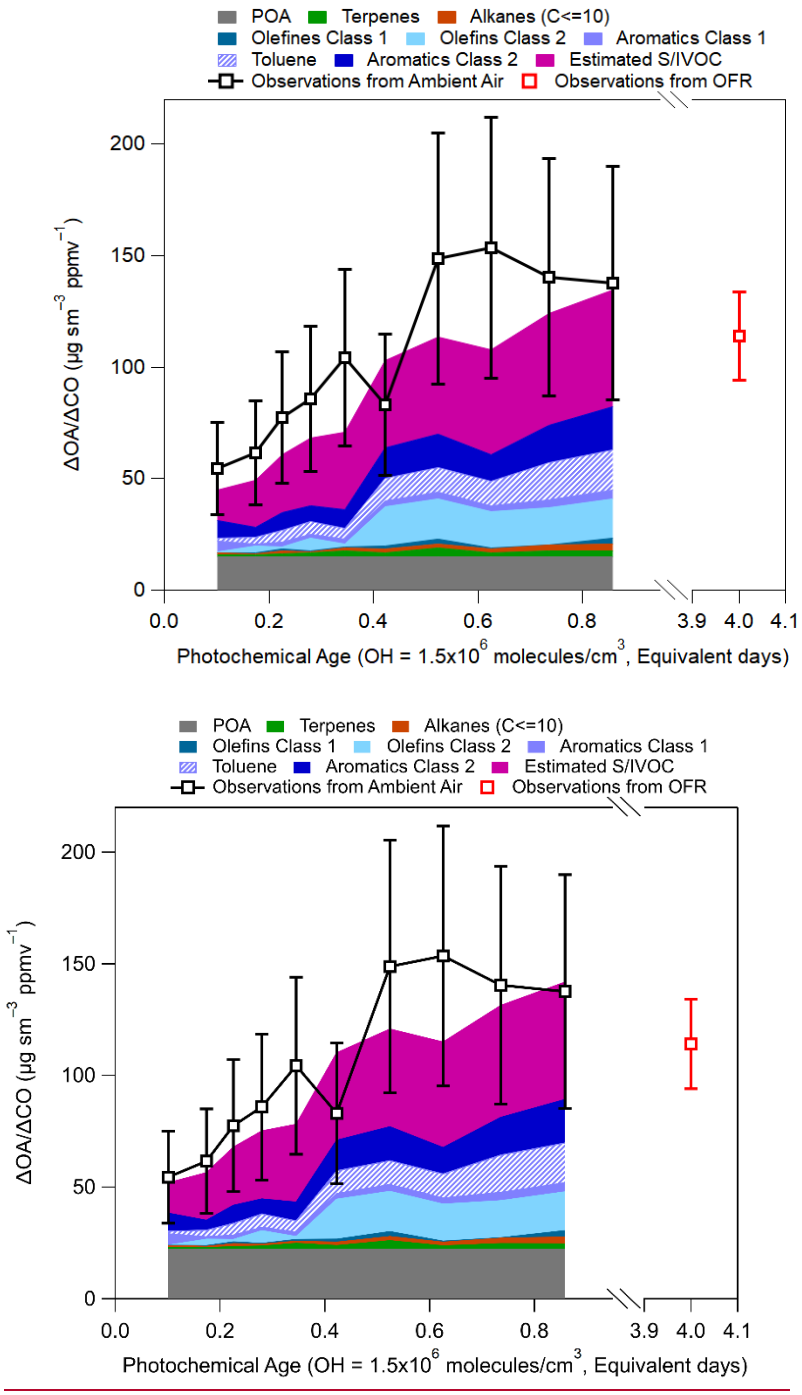

Figure 11. Calculated SOA production for KORUS-AQ. POA is from observations shown in Figure 6, and the observations of ΔOA/ΔCO are from Figure 4. The SOA precursor classes are defined in Table 2. Note, Toluene is part of Aromatics Class 1 (light purple), but it is shown separately for discussion. The error bars represent the uncertainty in OA (±38%). The OFR observations, and error bars, are from Figure 10.

Table 2. Definition of classes used in Figure 11. The VOCs listed in the table were all measured by WAS.

Class	*Included Compounds or Parameterization*
Terpenes	alpha-pinene, beta-pinene
Alkanes (C≤10)	methyl-cyclopentane, cyclohexane, methyl-cyclohexane, n-hetpane, n-octane, n-nonane, n-decane,
Olefins Class 1	1-butene, i-butene, cis-butene, trans-butene
Olefins Class 2	Styrene, 1,3-butadiene
Aromatics Class 1	benzene, toluene, isopropylbenzene, n-propylbenzene, ethylbenzene,
Aromatics Class 2	m+p-xylene, o-xylene, 3-ethyltoluene, 4-ethyltoluene, 1,2,3-trimethylbenzene, 1,2,4-trimethylbenzene, 1,3,5-trimethylbenzene
Estimated S/IVOC	6.7[a]×ΔHOA/ΔCO (ΔHOA/ΔCO = 22 μg sm^{-3} $ppmv^{-1}$ from Figure 6)

[a] This value is taken from Dzepina et al. (2009), which is based on partitioning calculations.

The most important calculated SOA precursors are S/IVOC and the most reactive aromatics (Table 2). These two classes of compounds comprise ~70% of the total modeled SOA over Seoul. The calculation further supports the conclusions from multiple previous studies (Dzepina et al., 2009, 2011; Hodzic et al., 2010; Chen et al., 2015; Hayes et al., 2015; Ma et al., 2017) that aromatics and primary S/IVOC dominate SOA formation over different urban environments. A consistent feature across most species in both classes of compounds is that they all have photochemical lifetimes of less than 1 equivalent day and less than 4 actual hours for the average observed daytime OH (6×10^6 molecules/cm^3) over Seoul. With the typical wind speeds during KORUS-AQ (~4 m/s), the lifetime of these species would limit their transport approximately 60 km during daytime. Since these compounds have short photochemical lifetimes, and they compose the majority of the calculated SOA budget, our conclusion that the SOA production over Seoul originates from local emissions is further supported.

Numerous prior studies have shown the importance of S/IVOC in order to explain the observed SOA production (Robinson et al., 2007; Dzepina et al., 2009, 2011; Grieshop et al., 2009; Pye and Seinfeld, 2010; Hodzic et al., 2010; Zhao et al., 2014; Jathar et al., 2014; Chen et al., 2015; Hayes et al., 2015; Palm et al., 2016, 2017, 2018; Ortega et al., 2016; Janssen et al., 2017;

Ma et al., 2017). Until recently, it has been analytically challenging to measure these compounds (Ait-Helal et al., 2014; Zhao et al., 2014; Hunter et al., 2017), and they can make up a small fraction of the total measured, and speciated, hydrocarbons in an urban location (Ait-Helal et al., 2014; Zhao et al., 2014). However, due to the higher initial molecular weight, S/IVOC already have a low saturation concentration ($C^* \sim 1 - 1000$ μg m^{-3} for SVOC and $\sim 1\times10^4 - 1\times10^6$ μg m^{-3} for IVOC), especially compared to aromatic compounds ($C^* \sim 10^7$ μg m^{-3}); thus, any addition of functional groups will more easily lead to the partitioning of oxidized S/IVOC to the particle phase (Robinson et al., 2007; Hayes et al., 2015; Ma et al., 2017). In urban environments, S/IVOC emissions come from numerous sources, including transportation, cooking, and VCPs (Robinson et al., 2007; Hayes et al., 2015; Woody et al., 2016; Janssen et al., 2017; Ma et al., 2017; McDonald et al., 2018).

The next most important compound is toluene, composing 9(±3)% of the estimated SOA production. Though this single compound is as important as the rest of Aromatics Class 1, Olefins Class 1 and 2, alkanes, and terpenes (Table 2) combined, it does not contribute the majority of the calculated SOA budget, as was recently suggested in another study (Wu et al., 2016). The average aerosol yield for toluene used in this study ($Y \approx 0.30$) is similar to the value used in Wu et al. (2016) and recommended by Hildebrandt et al. (2015). The aerosol yield is similar for all aromatics; however, the more reactive aromatics will contribute more SOA per unit precursor at shorter photochemical ages. The longer photochemical lifetime (factor of 2) for toluene decreases the overall amount of SOA produced compared to the very reactive aromatics.

4.6 Conceptual model representing rapid photochemical production

A conceptual model representing rapid photochemical production of SOA, pNO_3, O_x, and CH_2O is presented here. For the model, the flow is simplified to be from the west to the east. The

lateral and vertical dilution have been represented as the equivalent first order rate, constrained by observations (~0.7 day^{-1}). Also, the hemispheric and foreign transport is accurate on average based on observations, and is discussed in Sect. 3.3. For the production over Seoul, it is represented by photochemical aging, constrained by observations (Figure 7i), as a first order rate. Thus, the important processes are represented with realistic quantitative constraints, but in a simple enough system to demonstrate the impact of the secondary chemistry from Seoul.

The results are shown in Figure 12. The figure summarizes and demonstrates the results discussed throughout the paper. First, as discussed in Sect. 3.2 and 4.2, there is no clear net production of the pollutants over the West Sea. Instead, they undergo dilution as the air travels across the West Sea. Then, as the air enters SMA area, there are fresh injections of primary emissions (CO, HOA, hydrocarbons, and NO_x). These primary emissions undergo rapid photooxidation to produce SOA, pNO_3, O_x, and CH_2O, as detailed in Sect. 4.2. As demonstrated in Figure 12, most of the production occurs with SMA prior to dilution taking over. This demonstrates that the emissions and subsequent chemistry from SMA are directly impacting the residents of SMA. Thus, control of the primary pollutants, including the SOA precursors discussed in Sect. 4.5 (aromatics and S/IVOC), and NO_x, would substantially reduce concentration of the secondary photochemical products impacting SMA, even during period of higher foreign transport than observed during KORUS-AQ.

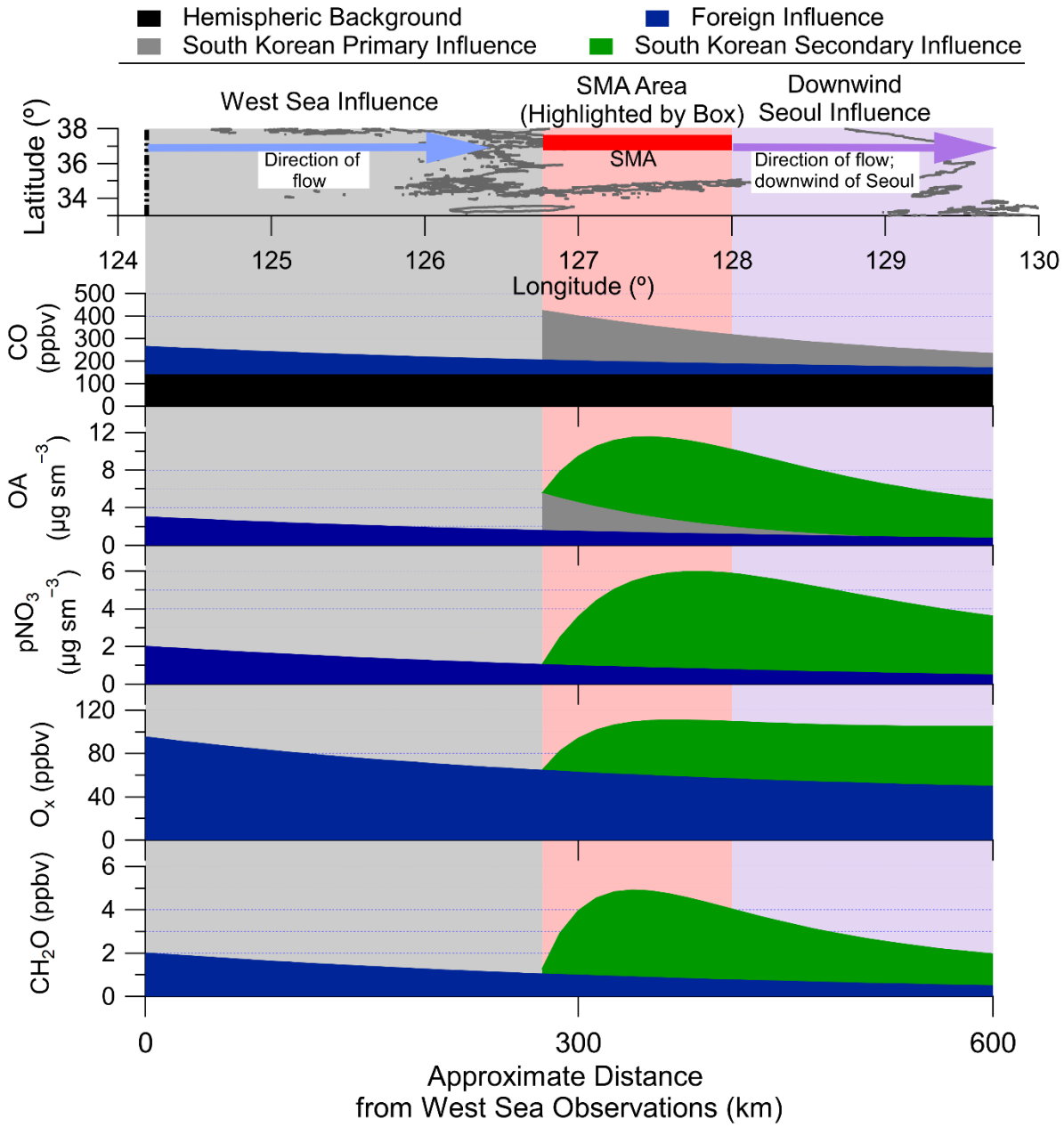

1430

1431 **Figure 12.** Conceptual model representing the transport of background into Seoul, and the
1432 emissions of primary species (CO and HOA) and photochemical production of secondary species
1433 (SOA, pNO_3, O_x, and CH_2O) impacting Seoul.

5. Summary

A suite of aerosol- and gas-phase measurements were made over Seoul and the West Sea during May and June, 2016, as part of the KORUS-AQ campaign. The results from this study are summarized below.

(1) Using a combination of a Lagrangian backtrajectory model (FLEXPART) and observations, the hemispheric CO background was estimated to be 140 ppbv, the CO foreign background over Seoul was estimated to be 60 ppbv, and the remainder of the CO over Seoul was due to South Korean emissions. The CO background analysis allows estimating background values for other species used throughout this study. In particular, the OA background was estimated to be between 1 – 3 μg sm^{-3}.

(2) FLEXPART was also used for source analysis of NO_2, as a surrogate for SOA precursors. NO_2 has a photochemical lifetime of less than 1 day (similar to the dominant urban SOA precursors). Results from FLEXPART indicate that greater than 90% of NO_2 originates from South Korea, consistent with most of the important SOA and pNO_3 precursors also originating there.

(3) Factor analysis of OA showed that the OA growth over Seoul was dominated by OOA (surrogate for SOA). This OOA (background subtracted) was low at low photochemical ages and rapidly increased throughout the day as photochemistry occurred. This points to local emissions controlling SOA production over Seoul.

(4) OOA was correlated with secondary gas-phase species, including O_x (O_3 + NO_2), formaldehyde, peroxy acetyl nitrates, sum of acyl peroxy nitrates, dihydroxy toluene, and pNO_3. Correlation with these species indicates that the SOA was produced from local emissions and

photochemistry since some of these compounds (CH_2O and PAN) had photochemical lifetimes of less than three daytime hours during KORUS-AQ.

(5) Using an airborne OFR for the first time, the amount of potential SOA produced from air sampled over Seoul was a factor of three higher than for air sampled over the West Sea (a background inflow location). This points to local SOA precursor emissions from Seoul, and subsequent rapid photochemistry, causing the increase in SOA observed over Seoul. The air sampled over West Sea did not have enough SOA precursors to cause the SOA production observed over Seoul.

(6) A simple box model showed good agreement with the measured SOA growth. This allows an estimation of the contribution of various precursors to SOA over Seoul. Hydrocarbons with a photochemical lifetime of less than one day dominate the production of SOA. Specifically, short lived aromatic compounds (i.e., ethyltoluenes, xylenes, trimethylbenzenes) and S/IVOC are the main precursors to SOA, accounting for 70% of the calculated SOA. Toluene was found to contribute 9% of the calculated SOA.

(7) Over Seoul, a large megacity with numerous sources of emissions, local emissions and their photochemical products overwhelm the foreign influence during KORUS-AQ. However, for smaller cities or more rural areas in South Korea that are not downwind of Seoul or other large sources, the foreign influence can more easily overwhelm the smaller local emissions. Thus, outside of the Seoul Metropolitan Area, the foreign influence has a greater impact on the air quality. During periods in which the foreign influence is larger than during KORUS-AQ (due to more favorable transport conditions), it will be more comparable to the importance of the Seoul emissions. However, given the apparently stronger emissions of SOA precursors than in other megacities, reducing South Korean emissions should improve air quality under all conditions.

Author Contribution

BAN, PCJ, DAD, JCS, and JLJ collected the AMS data; BA, AJB, CAC, and KLT collected the data from LARGE; DRB collected the WAS data; WHB collected the OH, HO_2, and OHR data; YC and JPD collected the CO measurements from Picarro; JD and ES collected MC/IC and filter measurements; GD and SEP collected H_2O and ambient CO measurements; AF collected CH_2O measurements; LGH collected PAN, PPN, and SO_2 measurements; MJK collected HNO_3, DHT, and HCN measurements; CK ran the FLEXPART analysis; KDL collected the BC measurements; TL and TP collected the KAMS data; and, JHW provided the emissions for the FLEXPART analysis. JAdG assisted in the analysis of the photochemical clocks and SOA production. BAN and JLJ prepared the original manuscript, and all authors contributed to the review and editing of the manuscript.

Acknowledgements

This study was supported by NASA grants NNX15AT96G & 80NSSC18K0630, and EPA STAR 83587701-0. It has not been formally reviewed by EPA. The views expressed in this document are solely those of the authors and do not necessarily reflect those of EPA. EPA does not endorse any products or commercial services mentioned in this publication. MJK was funded by NSF award number 1524860. Joost de Gouw worked as a part-time consultant for Aerodyne Research Inc during the preparation phase of this manuscript. The authors acknowledge Joshua Schwarz and Anne Perring for the use of their black carbon data, Ronald Cohen, Paul Wooldridge, and Paul Romer for use of their $\Sigma RONO_2$ and $\Sigma ROONO_2$ data, Paul Wennberg and John Crounse for the use of their HCN, DHT, and HNO_3 data, Armin Wisthaler for the use of their PTR-MS data, and Andrew Weinheimer and Denise Montzka for the use of their O_3, NO_x, and NO_y data. Finally, the authors acknowledge the NOAA ESRL GMD CCGG for the use of the CO measurements in Mongolia and China for the background measurements.

Data Availability

Measurements and FLEXPART results from the KORUS-AQ campaign are available at https://www-air.larc.nasa.gov/cgi-bin/ArcView/korusaq. Measurements for the CO background are available at ftp://aftp.cmdl.noaa.gov/data/trace_gases/co/flask/surface/.

Competing Interests

The authors declare that they have no conflict of interest.

References

Aiken, A. C., Salcedo, D., Cubison, M. J., Huffman, J. A., DeCarlo, P. F., Ulbrich, I. M., Docherty, K. S., Sueper, D., Kimmel, J. R., Worsnop, D. R., Trimborn, A., Northway, M., Stone, E. A., Schauer, J. J., Volkamer, R. M., Fortner, E., de Foy, B., Wang, J., Laskin, A., Shutthanandan, V., Zheng, J., Zhang, R., Gaffney, J., Marley, N. A., Paredes-Miranda, G., Arnott, W. P., Molina, L. T., Sosa, G. and Jimenez, J. L.: Mexico City aerosol analysis during MILAGRO using high resolution aerosol mass spectrometry at the urban supersite (T0) – Part 1: Fine particle composition and organic source apportionment, Atmos. Chem. Phys, 9(9), 6633–6653, doi:10.5194/acpd-9-8377-2009, 2009.

Ait-Helal, W., Borbon, A., Sauvage, S., De Gouw, J. A., Colomb, A., Gros, V., Freutel, F., Crippa, M., Afif, C., Baltensperger, U., Beekmann, M., Doussin, J.-F. F., Durand-Jolibois, R., Fronval, I., Grand, N., Leonardis, T., Lopez, M., Michoud, V., Miet, K., Perrier, S., Prévôt, A. S. H., Schneider, J., Siour, G., Zapf, P. and Locoge, N.: Volatile and intermediate volatility organic compounds in suburban Paris: Variability, origin and importance for SOA formation, Atmos. Chem. Phys., 14(19), 10439–10464, doi:10.5194/acp-14-10439-2014, 2014.

Akagi, S. K., Craven, J. S., Taylor, J. W., Mcmeeking, G. R., Yokelson, R. J., Burling, I. R., Urbanski, S. P., Wold, C. E., Seinfeld, J. H., Coe, H., Alvarado, M. J. and Weise, D. R.: Evolution of trace gases and particles emitted by a chaparral fire in California, Atmos. Chem. Phys., 12, 1397–1421, doi:10.5194/acp-12-1397-2012, 2012.

Aknan, A. and Chen, G.: KORUS-AQ DC-8 Aircraft Dataset, [online] Available from: https://www-air.larc.nasa.gov/cgi-bin/ArcView/korusaq (Accessed 6 December 2018), 2018.

Al-Saadi, J., Carmichael, G., Crawford, J., Emmons, L., Korean, S. K., Group, S., Song, C.-K., Chang, L.-S., Lee, G., Kim, J. and Park, R.: NASA Contributions to KORUS-AQ: An International Cooperative Air Quality Field Study in Korea, 2015.

Anderson, T. L. and Ogren, J. A.: Determining Aerosol Radiative Properties Using the TSI 3563 Integrating Nephelometer, Aerosol Sci. Technol., 29(1), 57–69, doi:10.1080/02786829808965551, 1998.

Arnold, S. R., Methven, J., Evans, M. J., Chipperfield, M. P., Lewis, A. C., Hopkins, J. R., Mcquaid, J. B., Watson, N., Purvis, R. M., Lee, J. D., Atlas, E. L., Blake, D. R. and Rappenglück, B.: Statistical inference of OH concentrations and air mass dilution rates from successive observations of nonmethane hydrocarbons in single air masses, J. Geophys. Res. Atmos., 112, D10S40, doi:10.1029/2006JD007594, 2007.

Bahreini, R., Dunlea, E. J., Matthew, B. M., Simons, C., Docherty, K. S., DeCarlo, P. F., Jimenez, J. L., Brock, C. A. and Middlebrook, A. M.: Design and Operation of a Pressure-Controlled Inlet for Airborne Sampling with an Aerodynamic Aerosol Lens, Aerosol Sci. Technol., 42(6), 465–471, doi:10.1080/02786820802178514, 2008.

Bahreini, R., Ervens, B., Middlebrook, A. M., Warneke, C., de Gouw, J. A., DeCarlo, P. F., Jimenez, J. L., Brock, C. A., Neuman, J. A., Ryerson, T. B., Stark, H., Atlas, E., Brioude, J., Fried, A., Holloway, J. S., Peischl, J., Richter, D., Walega, J., Weibring, P., Wollny, A. G. and Fehsenfeid, F. C.: Organic aerosol formation in urban and industrial plumes near Houston and Dallas, Texas, J. Geophys. Res., 114(16), D00F16, doi:10.1029/2008JD011493, 2009.

Baklanov, A., Molina, L. T. and Gauss, M.: Megacities, Air Quality and Climate, Atmos. Environ., 126, 235–249, doi:10.1016/j.atmosenv.2015.11.059, 2016.

Blake, N. J., Blake, D. R., Sive, B. C., Katzenstein, A. S., Meinardi, S., Wingenter, O. W., Atlas, E. L., Flocke, F., Ridley, B. A. and Rowland, F. S.: The seasonal evolution of NMHC's and light alkyl nitrates at middle to northern latitudes during TOPSE, J. Geophys. Res., 108(D4), 8359, 2003.

Campuzano-Jost, P., Day, D. A., Nault, B. A., Schroder, J. C. and Jimenez, J. L.: Temporal Variability of the Pieber Effect and Some Notes on AMS Dection Limits, in 17th AMS Users' Meeting, Portland. [online] Available from: http://cires1.colorado.edu/jimenez-group/UsrMtgs/UsersMtg17/10-14-2016_PCJ_AMSUsersMtg_Prez.pdf (Accessed 5 April 2018), 2016.

Canagaratna, M. R., Jayne, J. T., Jimenez, J. L., Allan, J. D., Alfarra, M. R., Zhang, Q., Onasch, T. B., Drewnick, F., Coe, H., Middlebrook, A. M., Delia, A., Williams, L. R., Trimborn, A. M., Northway, M. J., DeCarlo, P. F., Kolb, C. E., Davidovits, P. and Worsnop, D. R.: Chemical and microphysical characterization of ambient aerosols with the Aerodyne Aerosol Mass Spectrometer, Mass Spectrom. Rev., 26(2), 185–222, doi:10.1002/mas, 2007.

Canagaratna, M. R., Jimenez, J. L., Kroll, J. H., Chen, Q., Kessler, S. H., Massoli, P., Hildebrandt Ruiz, L., Fortner, E., Williams, L. R., Wilson, K. R., Surratt, J. D., Donahue, N. M., Jayne, J. T. and Worsnop, D. R.: Elemental ratio measurements of organic compounds using aerosol mass spectrometry: characterization, improved calibration, and implications, Atmos. Chem. Phys., 15(1), 253–272, doi:10.5194/acp-15-253-2015, 2015.

Cappa, C. D. and Jimenez, J. L.: Quantitative estimates of the volatility of ambient organic aerosol, Atmos. Chem. Phys., 10(12), 5409–5424, doi:10.5194/acp-10-5409-2010, 2010.

Cappa, C. D., Jathar, S. H., Kleeman, M. J., Docherty, K. S., Jimenez, J. L., Seinfeld, J. H. and Wexler, A. S.: Simulating secondary organic aerosol in a regional air quality model using the statistical oxidation model – Part 2: Assessing the influence of vapor wall losses, Atmos. Chem. Phys., 16(5), 3041–3059, doi:10.5194/acp-16-3041-2016, 2016.

Chen, Q., Heald, C. L., Jimenez, J. L., Canagaratna, M. R., He, L., Huang, X.-F., Campuzano-Jost, P., Palm, B. B., Poulain, L., Kuwata, M., Martin, S. T., Abbatt, J. P. D., Lee, A. K. Y., Liggio, J., Zhang, Q., He, L. and Huang, X.-F.: Elemental composition of organic aerosol: The gap between ambient and laboratory measurements, Geophys. Res. Lett., 42(10), 4182–4189, doi:10.1002/2015GL063693, 2015.

Choi, J. K., Heo, J. B., Ban, S. J., Yi, S. M. and Zoh, K. D.: Chemical characteristics of PM2.5 aerosol in Incheon, Korea, Atmos. Environ., 60, 583–592, doi:10.1016/j.atmosenv.2012.06.078, 2012.

Cohen, A. J., Brauer, M., Burnett, R., Anderson, H. R., Frostad, J., Estep, K., Balakrishnan, K., Brunekreef, B., Dandona, L., Dandona, R., Feigin, V., Freedman, G., Hubbell, B., Jobling, A., Kan, H., Knibbs, L., Liu, Y., Martin, R., Morawska, L., Pope, C. A., Shin, H., Straif, K., Shaddick, G., Thomas, M., van Dingenen, R., van Donkelaar, A., Vos, T., Murray, C. J. L. and Forouzanfar, M. H.: Estimates and 25-year trends of the global burden of disease attributable to ambient air pollution: an analysis of data from the Global Burden of Diseases Study 2015., Lancet (London, England), 389(10082), 1907–1918, doi:10.1016/S0140-6736(17)30505-6, 2017.

Collier, S., Zhou, S., Onasch, T. B., Jaffe, D. A., Kleinman, L., Sedlacek, A. J., Briggs, N. L., Hee, J., Fortner, E., Shilling, J. E., Worsnop, D., Yokelson, R. J., Parworth, C., Ge, X., Xu, J., Butterfield, Z., Chand, D., Dubey, M. K., Pekour, M. S., Springston, S. and Zhang, Q.: Regional

Influence of Aerosol Emissions from Wildfires Driven by Combustion Efficiency: Insights from the BBOP Campaign, Environ. Sci. Technol., 50(16), 8613–8622, doi:10.1021/acs.est.6b01617, 2016.

Craven, J. S., Metcalf, A. R., Bahreini, R., Middlebrook, A., Hayes, P. L., Duong, H. T., Sorooshian, A., Jimenez, J. L., Flagan, R. C. and Seinfeld, J. H.: Los Angeles Basin airborne organic aerosol characterization during CalNex, J. Geophys. Res. Atmos., 118(19), 11,453-11,467, doi:10.1002/jgrd.50853, 2013.

Crippa, M., Canonaco, F., Lanz, V. A., Äijälä, M., Allan, J. D., Carbone, S., Capes, G., Ceburnis, D., Dall'Osto, M., Day, D. A., DeCarlo, P. F., Ehn, M., Eriksson, A., Freney, E., Hildebrandt Ruiz, L. H., Hillamo, R., Jimenez, J. L., Junninen, H., Kiendler-Scharr, A., Kortelainen, A.-M., Kulmala, M., Laaksonen, A., Mensah, A. A., Mohr, C., Nemitz, E., O'Dowd, C., Ovadnevaite, J., Pandis, S. N., Petäjä, T., Poulain, L., Saarikoski, S., Sellegri, K., Swietlicki, E., Tiitta, P., Worsnop, D. R., Baltensperger, U. and Prévôt, A. S. H.: Organic aerosol components derived from 25 AMS data sets across Europe using a consistent ME-2 based source apportionment approach, Atmos. Chem. Phys., 14(12), 6159–6176, doi:10.5194/acp-14-6159-2014, 2014.

Crounse, J., McKinney, K. A., Kwan, A. J. and Wennberg, P. O.: Measurement of gas-phase hydroperoxides by chemical ionization mass spectrometry, Anal. Chem., 78(19), 6726–6732, doi:doi:10.1021/ac0604235, 2006.

Cubison, M. J., Ortega, A. M., Hayes, P. L., Farmer, D. K., Day, D. A., Lechner, M. J., Brune, W. H., Apel, E., Diskin, G. S., Fisher, J. A., Fuelberg, H. E., Hecobian, A., Knapp, D. J., Mikoviny, T., Riemer, D., Sachse, G. W., Sessions, W., Weber, R. J., Weinheimer, A. J., Wisthaler, A. and Jimenez, J. L.: Effects of aging on organic aerosol from open biomass burning smoke in aircraft and laboratory studies, Atmos. Chem. Phys., 11(23), 12049–12064, doi:10.5194/acp-11-12049-2011, 2011.

Day, D. A., Wooldridge, P. J., Dillon, M. B., Thornton, J. A. and Cohen, R. C.: A thermal dissociation laser-induced fluorescence instrument for in situ detection of NO_2, peroxy nitrates, alkyl nitrates, and HNO_3, J. Geophys. Res., 107(D5-6), 4046, doi:10.1029/2001JD000779, 2002.

DeCarlo, P. F., Kimmel, J. R., Trimborn, A., Northway, M. J., Jayne, J. T., Aiken, A. C., Gonin, M., Fuhrer, K., Horvath, T., Docherty, K. S., Worsnop, D. R. and Jimenez, J. L.: Field-Deployable, High-Resolution, Time-of-Flight Aerosol Mass Spectrometer, Anal. Chem., 78(24), 8281–8289, doi:10.1021/ac061249n, 2006.

DeCarlo, P. F., Dunlea, E. J., Kimmel, J. R., Aiken, A. C., Sueper, D., Crounse, J., Wennberg, P. O., Emmons, L., Shinozuka, Y., Clarke, A., Zhou, J., Tomlinson, J., Collins, D. R., Knapp, D., Weinheimer, A. J., Montzka, D. D., Campos, T. and Jimenez, J. L.: Fast airborne aerosol size and chemistry measurements above Mexico City and Central Mexico during the MILAGRO campaign, Atmos. Chem. Phys., 8(14), 4027–4048, doi:10.5194/acp-8-4027-2008, 2008.

DeCarlo, P. F., Ulbrich, I. M., Crounse, J., de Foy, B., Dunlea, E. J., Aiken, A. C., Knapp, D., Weinheimer, A. J., Campos, T., Wennberg, P. O. and Jimenez, J. L.: Investigation of the sources and processing of organic aerosol over the Central Mexican Plateau from aircraft measurements during MILAGRO, Atmos. Chem. Phys., 10(12), 5257–5280, doi:10.5194/acp-10-5257-2010, 2010.

Deming, B., Pagonis, D., Liu, X., Talukdar, R. K., Roberts, J. M., Veres, P. R., Krechmer, J. E., de Gouw, J. A., Jimenez, J. L. and Zieman, P. J.: Measurements of Delays of Gas-Phase

Compounds in a Wide Variety of Tubing Materials due to Gas-Wall Partitioning, Atmos. Meas. Tech., In Prep., 2018.

Dibb, J. E., Talbot, R. W., Scheuer, E. M., Seid, G., Avery, M. A. and Singh, H. B.: Aerosol chemical composition in Asian continental outflow during the TRACE-P campaign: Comparison with PEM-West B, J. Geophys. Res., 108(D21), 8815, doi:10.1029/2002JD003111, 2003.

Diskin, G. S., Podolske, J. R., Sachse, G. W. and Slate, T. A.: Open-path airborne tunable diode laser hygrometer, vol. 4817, edited by A. Fried, p. 196, International Society for Optics and Photonics., 2002.

Docherty, K. S., Aiken, A. C., Huffman, J. A., Ulbrich, I. M., DeCarlo, P. F., Sueper, D., Worsnop, D. R., Snyder, D. C., Peltier, R. E., Weber, R. J., Grover, B. D., Eatough, D. J., Williams, B. J., Goldstein, A. H., Ziemann, P. J. and Jimenez, J. L.: The 2005 Study of Organic Aerosols at Riverside (SOAR-1): instrumental intercomparisons and fine particle composition, Atmos. Chem. Phys., 11(23), 12387–12420, doi:DOI 10.5194/acp-11-12387-2011, 2011.

Drewnick, F., Hings, S. S., Alfarra, M. R., Prevot, A. S. H. and Borrmann, S.: Aerosol quantification with the Aerodyne Aerosol Mass Spectrometer: detection limits and ionizer background effects, Atmos. Meas. Tech., 2(1), 33–46, doi:10.5194/amt-2-33-2009, 2009.

Dunlea, E. J., DeCarlo, P. F., Aiken, A. C., Kimmel, J. R., Peltier, R. E., Weber, R. J., Tomlison, J., Collins, D. R., Shinozuka, Y., McNaugthon, C. S., Howell, S. G., Clarke, A. D., Emmons, L. K., Apel, E. C., Pfister, G. G., van Donkelaar, A., Martin, R. V., Millett, D. B., Heald, C. L. and Jimenez, J. L.: Evolution of Asian aerosols during transpacific transport in INTEX-B, Atmos. Chem. Phys., 9(19), 7257–7287, doi:10.5194/acp-9-7257-2009, 2009.

Dzepina, K., Volkamer, R. M. R., Madronich, S., Tulet, P., Ulbrich, I. M., Zhang, Q., Cappa, C. D., Ziemann, P. J. and Jimenez, J. L.: Evaluation of recently-proposed secondary organic aerosol models for a case study in Mexico City, Atmos. Chem. Phys., 9(15), 5681–5709, doi:10.5194/acp-9-5681-2009, 2009.

Dzepina, K., Cappa, C. D., Volkamer, R. M., Madronich, S., DeCarlo, P. F., Zaveri, R. A. and Jimenez, J. L.: Modeling the Multiday Evolution and Aging of Secondary Organic Aerosol During MILAGRO 2006, Environ. Sci. Technol., 45(8), 3496–3503, doi:10.1021/es103186, 2011.

Faloona, I. C., Tan, D., Lesher, R. L., Hazen, N. L., Frame, C. L., Simpas, J. B., Harder, H., Martinez, M., Di Carlo, P., Ren, X. and Brune, W. H.: A Laser-induced Fluorescence Instrument for Detecting Tropospheric OH and HO_2 : Characteristics and Calibration, J. Atmos. Chem., 47(2), 139–167, doi:10.1023/B:JOCH.0000021036.53185.0e, 2004.

Farmer, D. K., Matsunaga, A., Docherty, K. S., Surratt, J. D., Seinfeld, J. H., Ziemann, P. J. and Jimenez, J. L.: Response of an aerosol mass spectrometer to organonitrates and organosulfates and implications for atmospheric chemistry, Proc. Natl. Acad. Sci. U. S. A., 107(15), 6670–6675, doi:10.1073/pnas.0912340107, 2010.

Freney, E. J., Sellegri, K., Canonaco, F., Colomb, A., Borbon, A., Michoud, V., Doussin, J.-F., Crumeyrolle, S., Amarouche, N., Pichon, J.-M., Bourianne, T., Gomes, L., Prevot, A. S. H., Beekmann, M. and Schwarzenböeck, A.: Characterizing the impact of urban emissions on regional aerosol particles: airborne measurements during the MEGAPOLI experiment, Atmos. Chem. Phys., 14(3), 1397–1412, doi:10.5194/acp-14-1397-2014, 2014.

Fried, A., Cantrell, C., Olson, J., Crawford, J. H., Weibring, P., Walega, J., Richter, D.,

Junkermann, W., Volkamer, R., Sinreich, R., Heikes, B. G., O'Sullivan, D., Blake, D. R., Blake, N., Meinardi, S., Apel, E., Weinheimer, A., Knapp, D., Perring, A., Cohen, R. C., Fuelberg, H., Shetter, R. E., Hall, S. R., Ullmann, K., Brune, W. H., Mao, J., Ren, X., Huey, L. G., Singh, H. B., Hair, J. W., Riemer, D., Diskin, G. and Sachse, G.: Detailed comparisons of airborne formaldehyde measurements with box models during the 2006 INTEX-B and MILAGRO campaigns: Potential evidence for significant impacts of unmeasured and multi-generation volatile organic carbon compounds, Atmos. Chem. Phys., 11(22), 11867–11894, doi:10.5194/acp-11-11867-2011, 2011.

Ge, X., Setyan, A., Sun, Y. and Zhang, Q.: Primary and secondary organic aerosols in Fresno, California during wintertime: Results from high resolution aerosol mass spectrometry, J. Geophys. Res. Atmos., 117(D19), n/a-n/a, doi:10.1029/2012JD018026, 2012.

George, I. J., Slowik, J. and Abbatt, J. P. D.: Chemical aging of ambient organic aerosol from heterogeneous reaction with hydroxyl radicals, Geophys. Res. Lett., 35(13), L13811, doi:10.1029/2008GL033884, 2008.

Goldberg, D. L., Vinciguerra, T. P., Hosley, K. M., Loughner, C. P., Canty, T. C., Salawitch, R. . and Dickerson, R. R.: Evidence for an increase in the ozone photochemical lifetime in the eastern United States using a regional air quality model, J. Geophys. Res. Atmos., 120, 12,778-12,793, doi:10.1002/2015JD02390, 2015.

Gordon, T. D., Tkacik, D. S., Presto, A. A., Zhang, M., Jathar, S. H., Nguyen, N. T., Massetti, J., Truong, T., Cicero-Fernandez, P., Maddox, C., Rieger, P., Chattopadhyay, S., Maldonado, H., Maricq, M. M. and Robinson, A. L.: Primary Gas- and Particle-Phase Emissions and Secondary Organic Aerosol Production from Gasoline and Diesel Off-Road Engines, Environ. Sci. Technol., 47(24), 14137–14146, doi:10.1021/es403556e, 2013.

de Gouw, J. A., Middlebrook, A. M., Warneke, C., Goldan, P. D., Kuster, W. C., Roberts, J. M., Fehsenfeld, F. C., Worsnop, D. R., Canagaratna, M. R., Pszenny, A. A. P., Keene, W. C., Marchewka, M. L., Bertman, S. B. and Bates, T. S.: Budget of organic carbon in a polluted atmosphere: Results from the New England Air Quality Study in 2002, J. Geophys. Res., 110(16), D16305, doi:10.1029/2004JD005623, 2005.

de Gouw, J. A., Brock, C. A., Atlas, E. L., Bates, T. S., Fehsenfeld, F. C., Goldan, P. D., Holloway, J. S., Kuster, W. C., Lerner, B. M., Matthew, B. M., Middlebrook, A. M., Onasch, T. B., Peltier, R. E., Quinn, P. K., Senff, C. J., Stohl, A., Sullivan, A. P., Trainer, M., Warneke, C., Weber, R. J. and Williams, E. J.: Sources of particulate matter in the northeastern United States in summer: 1. Direct emissions and secondary formation of organic matter in urban plumes, J. Geophys. Res., 113(8), D08301, doi:10.1029/2007JD009243, 2008.

de Gouw, J. A., Welsh-Bon, D., Warneke, C., Kuster, W. C., Alexander, L., Baker, A. K., Beyersdorf, A. J., Blake, D. R., Canagaratna, M., Celada, a. T., Huey, L. G., Junkermann, W., Onasch, T. B., Salcido, A., Sjostedt, S. J., Sullivan, A. P., Tanner, D. J., Vargas, O., Weber, R. J., Worsnop, D. R., Yu, X. Y. and Zaveri, R.: Emission and chemistry of organic carbon in the gas and aerosol phase at a sub-urban site near Mexico City in March 2006 during the MILAGRO study, Atmos. Chem. Phys., 9(10), 3425–3442, doi:10.5194/acp-9-3425-2009, 2009.

Grieshop, A. P., Miracolo, M. A., Donahue, N. M. and Robinson, A. L.: Constraining the Volatility Distribution and Gas-Particle Partitioning of Combustion Aerosols Using Isothermal Dilution and Thermodenuder Measurements, Environ. Sci. Technol., 43(13), 4750–4756, doi:10.1021/Es8032378, 2009.

Griffin, R. J., Chen, J., Carmody, K., Vutukuru, S. and Dabdub, D.: Contribution of gas phase oxidation of volatile organic compounds to atmospheric carbon monoxide levels in two areas of the United States, J. Geophys. Res. Atmos., 112(D10), doi:10.1029/2006JD007602, 2007.

Guo, H., Sullivan, A. P., Campuzano-Jost, P., Schroder, J. C., Lopez-Hilfiker, F. D., Dibb, J. E., Jimenez, J. L., Thornton, J. A., Brown, S. S., Nenes, A. and Weber, R. J.: Fine particle pH and the partitioning of nitric acid during winter in the northeastern United States, J. Geophys. Res. Atmos., 121(17), 10,355-10,376, doi:10.1002/2016JD025311, 2016.

Guo, H., Liu, J., Froyd, K. D., Roberts, J. M., Veres, P. R., Hayes, P. L., Jimenez, J. L., Nenes, A. and Weber, R. J.: Fine particle pH and gas–particle phase partitioning of inorganic species in Pasadena, California, during the 2010 CalNex campaign, Atmos. Chem. Phys., 17(9), 5703–5719, doi:10.5194/acp-17-5703-2017, 2017.

Hallquist, M., Wenger, J. C., Baltensperger, U., Rudich, Y., Simpson, D., Claeys, M., Dommen, J., Donahue, N. M., George, C., Goldstein, A. H., Hamilton, J. F., Herrmann, H., Hoffmann, T., Iinuma, Y., Jang, M., Jenkin, M. E., Jimenez, J. L., Kiendler-Scharr, A., Maenhaut, W., McFiggans, G., Mentel, T. F., Monod, A., Prévôt, A. S. H., Seinfeld, J. H., Surratt, J. D., Szmigielski, R. and Wildt, J.: The formation, properties and impact of secondary organic aerosol: current and emerging issues, Atmos. Chem. Phys., 9(14), 5155–5236, doi:10.5194/acp-9-5155-2009, 2009.

Hayes, P. L., Ortega, A. M., Cubison, M. J., Froyd, K. D., Zhao, Y., Cliff, S. S., Hu, W. W., Toohey, D. W., Flynn, J. H., Lefer, B. L., Grossberg, N., Alvarez, S., Rappenglück, B., Taylor, J. W., Allan, J. D., Holloway, J. S., Gilman, J. B., Kuster, W. C., de Gouw, J. A., Massoli, P., Zhang, X., Liu, J., Weber, R. J., Corrigan, A. L., Russell, L. M., Isaacman, G., Worton, D. R., Kreisberg, N. M., Goldstein, A. H., Thalman, R., Waxman, E. M., Volkamer, R., Lin, Y. H., Surratt, J. D., Kleindienst, T. E., Offenberg, J. H., Dusanter, S., Griffith, S., Stevens, P. S., Brioude, J., Angevine, W. M. and Jimenez, J. L.: Organic aerosol composition and sources in Pasadena, California, during the 2010 CalNex campaign, J. Geophys. Res., 118(16), 9233–9257, doi:10.1002/jgrd.50530, 2013.

Hayes, P. L., Carlton, A. G., Baker, K. R., Ahmadov, R., Washenfelder, R. A., Alvarez, S., Rappenglück, B., Gilman, J. B., Kuster, W. C., de Gouw, J. A., Zotter, P., Prévôt, A. S. H., Szidat, S., Kleindienst, T. E., Ma, P. K. and Jimenez, J. L.: Modeling the formation and aging of secondary organic aerosols in Los Angeles during CalNex 2010, Atmos. Chem. Phys., 15(10), 5773–5801, doi:10.5194/acp-15-5773-2015, 2015.

Heald, C. L., Kroll, J. H., Jimenez, J. L., Docherty, K. S., Decarlo, P. F., Aiken, A. C., Chen, Q., Martin, S. T., Farmer, D. K. and Artaxo, P.: A simplified description of the evolution of organic aerosol composition in the atmosphere, Geophys. Res. Lett., 37(8), L08803, doi:10.1029/2010GL042737, 2010.

Heim, E., Dibb, J., Scheuer, E., Campuzano-Jost, P., Nault, B. A., Jimenez, J. L., Peterson, D., Knote, C., Fenn, M., Hair, J., Beyersdorf, A. J. and Anderson, B. E.: Asian Dust Observed during KORUS-AQ Facilitates the Uptake and Incorporation of Soluble Pollutants during Transport to South Korea: The Hwangsa Anthropogenic Model, J. Geophys. Res. Atmos., submitted, 2018.

Hennigan, C. J., Sullivan, A. P., Fountoukis, C. I., Nenes, A., Hecobian, A., Vargas, O., Peltier, R. E., Hanks, A. T. C., Huey, L. G., Lefer, B. L., Russell, A. G. and Weber, R. J.: On the volatility and production mechanisms of newly formed nitrate and water soluble organic aerosol in Mexico City, Atmos. Chem. Phys., 8(14), 3761–3768, doi:10.5194/acp-8-3761-2008, 2008.

Heo, J.-B., Hopke, P. K. and Yi, S.-M.: Source apportionment of PM2.5 in Seoul, Korea, Atmos. Chem. Phys., 9(14), 4957–4971, doi:10.5194/acp-9-4957-2009, 2009.

Herndon, S. C., Onasch, T. B., Wood, E. C., Kroll, J. H., Canagaratna, M. R., Jayne, J. T., Zavala, M. A., Knighton, W. B., Mazzoleni, C., Dubey, M. K., Ulbrich, I. M., Jimenez, J. L., Seila, R., de Gouw, J. A., de Foy, B., Fast, J., Molina, L. T., Kolb, C. E. and Worsnop, D. R.: Correlation of secondary organic aerosol with odd oxygen in Mexico City, Geophys. Res. Lett., 35(15), doi:10.1029/2008GL034058, 2008.

Hersey, S. P., Craven, J. S., Metcalf, A. R., Lin, J., Lathem, T., Suski, K. J., Cahill, J. F., Duong, H. T., Sorooshian, A., Jonsson, H. H., Shiraiwa, M., Zuend, A., Nenes, A., Prather, K. A., Flagan, R. C. and Seinfeld, J. H.: Composition and hygroscopicity of the Los Angeles Aerosol: CalNex, J. Geophys. Res. Atmos., 118(7), 3016–3036, doi:10.1002/jgrd.50307, 2013.

Hildebrandt Ruiz, L., Paciga, A. L., Cerully, K. M., Nenes, A., Donahue, N. M. and Pandis, S. N.: Formation and aging of secondary organic aerosol from toluene: changes in chemical composition, volatility, and hygroscopicity, Atmos. Chem. Phys., 15(14), 8301–8313, doi:10.5194/acp-15-8301-2015, 2015.

Hodzic, A. and Jimenez, J. L.: Modeling anthropogenically controlled secondary organic aerosols in a megacity: A simplified framework for global and climate models, Geosci. Model Dev., 4(4), 901–917, doi:10.5194/gmd-4-901-2011, 2011.

Hodzic, A., Jimenez, J. L., Madronich, S., Canagaratna, M. R., DeCarlo, P. F., Kleinman, L. and Fast, J.: Modeling organic aerosols in a megacity: Potential contribution of semi-volatile and intermediate volatility primary organic compounds to secondary organic aerosol formation, Atmos. Chem. Phys., 10(12), 5491–5514, doi:10.5194/acp-10-5491-2010, 2010.

Hodzic, A., Madronich, S., Kasibhatla, P. S., Tyndall, G., Aumont, B., Jimenez, J. L., Lee-Taylor, J. and Orlando, J.: Organic photolysis reactions in tropospheric aerosols: effect on secondary organic aerosol formation and lifetime, Atmos. Chem. Phys., 15(16), 9253–9269, doi:10.5194/acp-15-9253-2015, 2015.

Hong, J.-W. and Hong, J.: Changes in the Seoul Metropolitan Area Urban Heat Environment with Residential Redevelopment, J. Appl. Meteorol. Climatol., 55, 1091–1106, doi:10.1175/JAMC-D-15-0321.1, 2016.

Hu, W., Hu, M., Hu, W., Jimenez, J. L., Yuan, B., Chen, W., Wang, M., Wu, Y., Chen, C., Wang, Z., Peng, J., Zeng, L. and Shao, M.: Chemical composition, sources and aging process of sub-micron aerosols in Beijing: contrast between summer and winter, J. Geophys. Res. Atmos., doi:10.1002/2015JD024020, 2016.

Hu, W., Campuzano-Jost, P., Day, D. A., Croteau, P., Canagaratna, M. R., Jayne, J. T., Worsnop, D. R. and Jimenez, J. L.: Evaluation of the new capture vaporizer for aerosol mass spectrometers (AMS) through field studies of inorganic species, Aerosol Sci. Technol., 51(6), 735–754, doi:10.1080/02786826.2017.1296104, 2017a.

Hu, W., Campuzano-Jost, P., Day, D. A., Croteau, P., Canagaratna, M. R., Jayne, J. T., Worsnop, D. R. and Jimenez, J. L.: Evaluation of the new capture vapourizer for aerosol mass spectrometers (AMS) through laboratory studies of inorganic species, Atmos. Meas. Tech., 10(6), 2897–2921, doi:10.5194/amt-10-2897-2017, 2017b.

Hu, W., Day, D. A., Campuzano-Jost, P., Nault, B. A., Park, T., Lee, T., Croteau, P., Canagaratna,

M. R., Jayne, J. T., Worsnop, D. R. and Jimenez, J. L.: Evaluation of the new capture vaporizer for Aerosol Mass Spectrometers: Characterization of organic aerosol mass spectra, Aerosol Sci. Technol., 52(7), 752–739, doi:10.1080/02786826.2018.1454584, 2018a.

Hu, W., Day, D. A., Campuzano-Jost, P., Nault, B. A., Park, T., Lee, T., Croteau, P., Canagaratna, M. R., Jayne, J. T., Worsnop, D. R. and Jimenez, J. L.: Evaluation of the New Capture Vaporizer for Aerosol Mass Spectrometers (AMS): Elemental Composition and Source Apportionment of Organic Aerosols (OA), ACS Earth Sp. Chem., 2(4), 410–421, doi:10.1021/acsearthspacechem.8b00002, 2018b.

Hu, W. W., Hu, M., Yuan, B., Jimenez, J. L., Tang, Q., Peng, J. F., Hu, W., Shao, M., Wang, M., Zeng, L. M., Wu, Y. S., Gong, Z. H., Huang, X. F. and He, L. Y.: Insights on organic aerosol aging and the influence of coal combustion at a regional receptor site of central eastern China, Atmos. Chem. Phys., 13(19), 10095–10112, doi:10.5194/acp-13-10095-2013, 2013.

Huang, C., Wang, H. L., Li, L., Wang, Q., Lu, Q., de Gouw, J. A., Zhou, M., Jing, S. A., Lu, J. and Chen, C. H.: VOC species and emission inventory from vehicles and their SOA formation potentials estimation in Shanghai, China, Atmos. Chem. Phys., 15(19), 11081–11096, doi:10.5194/acp-15-11081-2015, 2015.

Huey, L. G., Tanner, D. J., Slusher, D. L., Dibb, J. E., Arimoto, R., Chen, G., Davis, D., Buhr, M. P., Nowak, J. B., Mauldin III, R. L., Eisele, F. L. and Kosciuch, E.: CIMS measurements of HNO_3 and SO_2 at the South Pole during ISCAT 2000, Atmos. Environ., 38(32), 5411–5421, doi:10.1016/J.ATMOSENV.2004.04.037, 2004.

Huffman, J. A., Docherty, K. S., Aiken, A. C., Cubison, M. J., Ulbrich, I. M., DeCarlo, P. F., Sueper, D., Jayne, J. T., Worsnop, D. R., Ziemann, P. J. and Jimenez, J. L.: Chemically-resolved aerosol volatility measurements from two megacity field studies, Atmos. Chem. Phys., 9(1), 7161–7182, doi:doi:10.5194/acp-9-7161-2009, 2009.

Hunter, J. F., Day, D. A., Palm, B. B., Yatavelli, R. L. N., Chan, A. W. H., Kaser, L., Cappellin, L., Hayes, P. L., Cross, E. S., Carrasquillo, A. J., Campuzano-Jost, P., Stark, H., Zhao, Y., Hohaus, T., Smith, J. N., Hansel, A., Karl, T., Goldstein, A. H., Guenther, A., Worsnop, D. R., Thornton, J. A., Heald, C. L., Jimenez, J. L. and Kroll, J. H.: Comprehensive characterization of atmospheric organic carbon at a forested site, Nat. Geosci., 10(10), 748–753, doi:10.1038/ngeo3018, 2017.

Jacob, D. J.: Heterogeneous chemistry and tropospheric ozone, Atmos. Environ., 34, 2131–2159, doi:10.1016/S1352-2310(99)00462-8, 2000.

Janssen, R. H. H., Tsimpidi, A. P., Karydis, V. A., Pozzer, A., Lelieveld, J., Crippa, M., Prévôt, A. S. H., Ait-Helal, W., Borbon, A., Sauvage, S. and Locoge, N.: Influence of local production and vertical transport on the organic aerosol budget over Paris, J. Geophys. Res. Atmos., 1–21, doi:10.1002/2016JD026402, 2017.

Jathar, S. H., Miracolo, M. A., Tkacik, D. S., Donahue, N. M., Adams, P. J. and Robinson, A. L.: Secondary Organic Aerosol Formation from Photo-Oxidation of Unburned Fuel: Experimental Results and Implications for Aerosol Formation from Combustion Emissions, Environ. Sci. Technol., 47(22), 12886–12893, doi:10.1021/es403445q, 2013.

Jathar, S. H., Gordon, T. D., Hennigan, C. J., Pye, H. O. T., Pouliot, G., Adams, P. J., Donahue, N. M. and Robinson, A. L.: Unspeciated organic emissions from combustion sources and their influence on the secondary organic aerosol budget in the United States., Proc. Natl. Acad. Sci. U.

S. A., 111(29), 10473–10478, doi:10.1073/pnas.1323740111, 2014.

Jayne, J. T. and Worsnop, D. R.: Particle Capture Device Aerodyne Research, 2015.

Jeong, U., Kim, J., Lee, H. and Lee, Y. G.: Assessing the effect of long-range pollutant transportation on air quality in Seoul using the conditional potential source contribution function method, Atmos. Environ., 150, 33–44, doi:10.1016/j.atmosenv.2016.11.017, 2017.

Jimenez, J. L., Canagaratna, M. R., Donahue, N. M., Prévôt, A. S. H., Zhang, Q., Kroll, J. H., DeCarlo, P. F., Allan, J. D., Coe, H., Ng, N. L., Aiken, A. C., Docherty, K. S., Ulbrich, I. M., Grieshop, A. P., Robinson, A. L., Duplissy, J., Smith, J. D., Wilson, K. R., Lanz, V. A., Hueglin, C., Sun, Y. L., Tian, J., Laaksonen, A., Raatikainen, T., Rautiainen, J., Vaattovaara, P., Ehn, M., Kulmala, M., Tomlinson, J. M., Collins, D. R., Cubison, M. J., Dunlea, E. J., Huffman, J. A., Onasch, T. B., Alfarra, M. R., Williams, P. I., Bower, K., Kondo, Y., Schneider, J., Drewnick, F., Borrmann, S., Weimer, S., Demerjian, K., Salcedo, D., Cottrell, L., Griffin, R., Takami, A., Miyoshi, T., Hatakeyama, S., Shimono, A., Sun, J. Y., Zhang, Y. M., Dzepina, K., Kimmel, J. R., Sueper, D., Jayne, J. T., Herndon, S. C., Trimborn, A. M., Williams, L. R., Wood, E. C., Middlebrook, A. M., Kolb, C. E., Baltensperger, U. and Worsnop, D. R.: Evolution of Organic Aerosols in the Atmosphere, Science (80-.)., 326(5959), 1525–1529, doi:10.1126/science.1180353, 2009.

Jimenez, J. L., Campuzano-Jost, P., Day, D. A., Nault, B. A., Schroder, J. C. and Cubison, M. J.: Frequently AMS Questions for AMS Data Users, [online] Available from: http://cires.colorado.edu/jimenez-group/wiki/index.php?title=FAQ_for_AMS_Data_Users, accessed month-year (Accessed 6 December 2018), 2018.

Kang, E., Root, M. J., Toohey, D. W. and Brune, W. H.: Introducing the concept of Potential Aerosol Mass (PAM), Atmos. Chem. Phys., 7(22), 5727–5744, doi:10.5194/acp-7-5727-2007, 2007.

Kang, E., Lee, M., Brune, W. H., Lee, T., Park, T., Ahn, J. and Shang, X.: Photochemical aging of aerosol particles in different air masses arriving at Baengnyeong Island, Korea, Atmos. Chem. Phys., 18(9), 6661–6677, doi:10.5194/acp-18-6661-2018, 2018.

Khare, P. and Gentner, D. R.: Considering the future of anthropogenic gas-phase organic compound emissions and the increasing influence of non-combustion sources on urban air quality, Atmos. Chem. Phys., 18(8), 5391–5413, doi:10.5194/acp-18-5391-2018, 2018.

Kim, B. M., Seo, J., Kim, J. Y., Lee, J. Y. and Kim, Y.: Transported vs. local contributions from secondary and biomass burning sources to PM2.5, Atmos. Environ., 144, 24–36, doi:10.1016/j.atmosenv.2016.08.072, 2016.

Kim, H., Zhang, Q., Bae, G.-N., Kim, J. Y. and Lee, S. B.: Sources and atmospheric processing of wintertime aerosols in Seoul, Korea: Insights from real-time measurements using a high-resolution aerosol mass spectrometer, Atmos. Chem. Phys. Discuss., 17(3), 2009–2003, doi:10.5194/acp-17-2009-2017, 2017.

Kim, H., Zhang, Q. and Heo, J.: Influence of Intense secondary aerosol formation and long-range transport on aerosol chemistry and properties in the Seoul Metropolitan Area during spring time : Results from KORUS-AQ, Atmos. Chem. Phys., 18, 7149–7168, doi:10.51944/acp-2017-947, 2018.

Kim, H. C., Kim, E. H., Kim, B. U. and Kim, S.: Regional Contributions to the Particulate Matter

Concentration in the Seoul Metropolitan Area, Korea: Seasonal Variation and Sensitivity to Meteorology, Atmos. Chem. Phys, 17(17), 10315–10332, doi:10.5194/acp-17-10315-2017, 2017.

Kim, H. S., Huh, J. B., Hopke, P. K., Holsen, T. M. and Yi, S. M.: Characteristics of the major chemical constituents of PM2.5 and smog events in Seoul, Korea in 2003 and 2004, Atmos. Environ., 41(32), 6762–6770, doi:10.1016/j.atmosenv.2007.04.060, 2007.

Kim, S., Huey, L. G., Stickel, R. E., Tanner, D. J., Crawford, J. H., Olson, J. R., Chen, G., Brune, W. H., Ren, X., Lesher, R., Wooldridge, P. J., Bertram, T. H., Perring, A., Cohen, R. C., Lefer, B. L., Shetter, R. E., Avery, M., Diskin, G. and Sokolik, I.: Measurement of HO_2 NO_2 in the free troposphere during the Intercontinental Chemical Transport Experiment–North America 2004, J. Geophys. Res., 112, D12S01, doi:10.1029/2006JD007676, 2007.

Kim, Y. J., Woo, J. H., Ma, Y. Il, Kim, S., Nam, J. S., Sung, H., Choi, K. C., Seo, J., Kim, J. S., Kang, C. H., Lee, G., Ro, C. U., Chang, D. and Sunwoo, Y.: Chemical characteristics of long-range transport aerosol at background sites in Korea, Atmos. Environ., 43(34), 5556–5566, doi:10.1016/j.atmosenv.2009.03.062, 2009.

Kimmel, J. R., Farmer, D. K., Cubison, M. J., Sueper, D., Tanner, C., Nemitz, E., Worsnop, D. R., Gonin, M. and Jimenez, J. L.: Real-time aerosol mass spectrometry with millisecond resolution, Int. J. Mass Spectrom., 303(1), 15–26, doi:10.1016/j.ijms.2010.12.004, 2011.

Kleinman, L., Kuang, C., Sedlacek, A., Senum, G., Springston, S., Wang, J., Zhang, Q., Jayne, J., Fast, J., Hubbe, J., Shilling, J. and Zaveri, R.: What do correlations tell us about anthropogenic-biogenic interactions and SOA formation in the Sacramento plume during CARES?, Atmos. Chem. Phys., 16(3), 1729–1746, doi:10.5194/acp-16-1729-2016, 2016.

Kleinman, L. I., Daum, P. H., Lee, Y.-N., Senum, G. I., Springston, S. R., Wang, J., Berkowitz, C., Hubbe, J., Zaveri, R. A., Brechtel, F. J., Jayne, J., Onasch, T. B. and Worsnop, D.: Aircraft observations of aerosol composition and ageing in New England and Mid-Atlantic States during the summer 2002 New England Air Quality Study field campaign, J. Geophys. Res., 112(D9), D09310, doi:10.1029/2006JD007786, 2007.

Kleinman, L. I., Springston, S. R., Daum, P. H., Lee, Y.-N., Nunnermacker, L. J., Senum, G. I., Wang, J., Weinstein-Lloyd, J., Alexander, M. L., Hubbe, J., Ortega, J., Canagaratna, M. R. and Jayne, J.: The time evolution of aerosol composition over the Mexico City plateau, Atmos. Chem. Phys., 8(6), 1559–1575, doi:10.5194/acp-8-1559-2008, 2008.

Kleinman, L. I., Springston, S. R., Wang, J., Daum, P. H., Lee, Y.-N. N., Nunnermacker, L. J., Senum, G. I., Weinstein-Lloyd, J., Alexander, M. L., Hubbe, J., Ortega, J., Zaveri, R. A., Canagaratna, M. R. and Jayne, J.: The time evolution of aerosol size distribution over the Mexico City plateau, Atmos. Chem. Phys., 9(13), 4261–4278, doi:10.5194/acpd-9-1621-2009, 2009.

Knote, C., Hodzic, A., Jimenez, J. L., Volkamer, R., Orlando, J. J., Baidar, S., Brioude, J., Fast, J., Gentner, D. R., Goldstein, A. H., Hayes, P. L., Knighton, W. B., Oetjen, H., Setyan, A., Stark, H., Thalman, R., Tyndall, G., Washenfelder, R., Waxman, E. and Zhang, Q.: Simulation of semi-explicit mechanisms of SOA formation from glyoxal in aerosol in a 3-D model, Atmos. Chem. Phys., 14(12), 6213–6239, doi:10.5194/acp-14-6213-2014, 2014.

Krechmer, J. E., Pagonis, D., Ziemann, P. J. and Jimenez, J. L.: Quantification of Gas-Wall Partitioning in Teflon Environmental Chambers Using Rapid Bursts of Low-Volatility Oxidized Species Generated in Situ, Environ. Sci. Technol., 50(11), 5757–5765,

doi:10.1021/acs.est.6b00606, 2016.

Krechmer, J. E., Day, D. A., Ziemann, P. J. and Jimenez, J. L.: Direct Measurements of Gas/Particle Partitioning and Mass Accommodation Coefficients in Environmental Chambers, Environ. Sci. Technol., 51(20), 11867–11875, doi:10.1021/acs.est.7b02144, 2017.

Kroll, J. H. and Seinfeld, J. H.: Chemistry of secondary organic aerosol: Formation and evolution of low-volatility organics in the atmosphere, Atmos. Environ., 42(16), 3593–3624, doi:10.1016/J.ATMOSENV.2008.01.003, 2008.

Kroll, J. H., Donahue, N. M., Jimenez, J. L., Kessler, S. H., Canagaratna, M. R., Wilson, K. R., Altieri, K. E., Mazzoleni, L. R., Wozniak, A. S., Bluhm, H., Mysak, E. R., Smith, J. D., Kolb, C. E. and Worsnop, D. R.: Carbon oxidation state as a metric for describing the chemistry of atmospheric organic aerosol., Nat. Chem., 3(2), 133–139, doi:10.1038/nchem.948, 2011.

Kupc, A., Williamson, C., Wagner, N. L., Richardson, M. and Brock, C. A.: Modification, calibration, and performance of the Ultra-High Sensitivity Aerosol Spectrometer for particle size distribution and volatility measurements during the Atmospheric Tomography Mission (ATom) airborne campaign, Atmos. Meas. Tech., 11(1), 369–383, doi:10.5194/amt-11-369-2018, 2018.

Lambe, A. T., Ahern, A. T., Williams, L. R., Slowik, J. G., Wong, J. P. S., Abbatt, J. P. D., Brune, W. H., Ng, N. L., Wright, J. P., Croasdale, D. R., Worsnop, D. R., Davidovits, P. and Onasch, T. B.: Characterization of aerosol photooxidation flow reactors: heterogeneous oxidation, secondary organic aerosol formation and cloud condensation nuclei activity measurements, Atmos. Meas. Tech., 4(3), 445–461, doi:10.5194/amt-4-445-2011, 2011.

Lambe, A. T., Onasch, T. B., Croasdale, D. R., Wright, J. P., Martin, A. T., Franklin, J. P., Massoli, P., Kroll, J. H., Canagaratna, M. R., Brune, W. H., Worsnop, D. R. and Davidovits, P.: Transitions from Functionalization to Fragmentation Reactions of Laboratory Secondary Organic Aerosol (SOA) Generated from the OH Oxidation of Alkane Precursors, Environ. Sci. Technol., 46(10), 5430–5437, doi:10.1021/Es300274t, 2012.

Landrigan, P. J., Fuller, R., Acosta, N. J. R., Adeyi, O., Arnold, R., Basu, N., Baldé, A. B., Bertollini, R., Bose-O'Reilly, S., Boufford, J. I., Breysse, P. N., Chiles, T., Mahidol, C., Coll-Seck, A. M., Cropper, M. L., Fobil, J., Fuster, V., Greenstone, M., Haines, A., Hanrahan, D., Hunter, D., Khare, M., Krupnick, A., Lanphear, B., Lohani, B., Martin, K., Mathiasen, K. V, McTeer, M. A., Murray, C. J. L., Ndahimananjara, J. D., Perera, F., Potočnik, J., Preker, A. S., Ramesh, J., Rockström, J., Salinas, C., Samson, L. D., Sandilya, K., Sly, P. D., Smith, K. R., Steiner, A., Stewart, R. B., Suk, W. A., van Schayck, O. C. P., Yadama, G. N., Yumkella, K. and Zhong, M.: The Lancet Commission on pollution and health, Lancet, 391(10119), 462–512, doi:10.1016/S0140-6736(17)32345-0, 2018.

Lee, G., Choi, H. S., Lee, T., Choi, J., Park, J. S. and Ahn, J. Y.: Variations of regional background peroxyacetyl nitrate in marine boundary layer over Baengyeong Island, South Korea, Atmos. Environ., 61, 533–541, doi:10.1016/j.atmosenv.2012.07.075, 2012.

Lee, H. M., Park, R. J., Henze, D. K., Lee, S., Shim, C., Shin, H. J., Moon, K. J. and Woo, J. H.: PM2.5 source attribution for Seoul in May from 2009 to 2013 using GEOS-Chem and its adjoint model, Environ. Pollut., 221, 377–384, doi:10.1016/j.envpol.2016.11.088, 2017.

Lee, S., Ho, C.-H., Lee, Y. G., Choi, H.-J. and Song, C.-K.: Influence of transboundary air pollutants from China on the high-PM10 episode in Seoul, Korea for the period October 16–20,

2008, Atmos. Environ., 77, 430–439, doi:10.1016/J.ATMOSENV.2013.05.006, 2013.

Lee, T., Choi, J., Lee, G., Ahn, J., Park, J. S., Atwood, S. A., Schurman, M., Choi, Y., Chung, Y. and Collett, J. L.: Characterization of aerosol composition, concentrations, and sources at Baengnyeong Island, Korea using an aerosol mass spectrometer, Atmos. Environ., 120, 297–306, doi:10.1016/j.atmosenv.2015.08.038, 2015.

Lelieveld, J., Evans, J. S., Fnais, M., Giannadaki, D. and Pozzer, A.: The contribution of outdoor air pollution sources to premature mortality on a global scale, Nature, 525(7569), 367–371, doi:10.1038/nature15371, 2015.

Li, R., Palm, B. B., Ortega, A. M., Hlywiak, J., Hu, W., Peng, Z., Day, D. A., Knote, C., Brune, W. H., de Gouw, J. A. and Jimenez, J. L.: Modeling the radical chemistry in an oxidation flow reactor: radical formation and recycling, sensitivities, and the OH exposure estimation equation., J. Phys. Chem. A, 119(19), 4418–4432, doi:10.1021/jp509534k, 2015.

Liu, T., Wang, X., Deng, W., Hu, Q., Ding, X., Zhang, Y., He, Q., Zhang, Z., Lü, S., Bi, X., Chen, J. and Yu, J.: Secondary organic aerosol formation from photochemical aging of light-duty gasoline vehicle exhausts in a smog chamber, Atmos. Chem. Phys., 15(15), 9049–9062, doi:10.5194/acp-15-9049-2015, 2015.

Liu, X., Huey, L. G., Yokelson, R. J., Selimovic, V., Simpson, I. J., Müller, M., Jimenez, J. L., Campuzano-Jost, P., Beyersdorf, A. J., Blake, D. R., Butterfield, Z., Choi, Y., Crounse, J. D., Day, D. A., Diskin, G. S., Dubey, M. K., Fortner, E., Hanisco, T. F., Hu, W., King, L. E., Kleinman, L., Meinardi, S., Mikoviny, T., Onasch, T. B., Palm, B. B., Peischl, J., Pollack, I. B., Ryerson, T. B., Sachse, G. W., Sedlacek, A. J., Shilling, J. E., Springston, S., St. Clair, J. M., Tanner, D. J., Teng, A. P., Wennberg, P. O., Wisthaler, A. and Wolfe, G. M.: Airborne measurements of western U.S. wildfire emissions: Comparison with prescribed burning and air quality implications, J. Geophys. Res., 122(11), 6108–6129, doi:10.1002/2016JD026315, 2017.

Ma, P. K., Zhao, Y., Robinson, A. L., Worton, D. R., Goldstein, A. H., Ortega, A. M., Jimenez, J.-L., Zotter, P., Prévôt, A. S. H., Szidat, S. and Hayes, P. L.: Evaluating the impact of new observational constraints on P-S/IVOC emissions, multi-generation oxidation, and chamber wall losses on SOA modeling for Los Angeles, CA, Atmos. Chem. Phys., 17(15), 9237–9259, doi:10.5194/acp-17-9237-2017, 2017.

Mao, J., Ren, X., Brune, W. H., Olson, J. R., Crawford, J. H., Fried, a., Huey, L. G., Cohen, R. C., Heikes, B., Singh, H. B., Blake, D. R., Sachse, G. W., Diskin, G. S., Hall, S. R. and Shetter, R. E.: Airborne measurement of OH reactivity during INTEX-B, Atmos. Chem. Phys., 9(1), 163–173, doi:10.5194/acp-9-163-2009, 2009.

Matsunaga, A. and Ziemann, P. J.: Gas-Wall Partitioning of Organic Compounds in a Teflon Film Chamber and Potential Effects on Reaction Product and Aerosol Yield Measurements, Aerosol Sci. Technol., 44(10), 881–892, doi:10.1080/02786826.2010.501044, 2010.

McDonald, B. C., de Gouw, J. A., Gilman, J. B., Jathar, S. H., Akherati, A., Cappa, C. D., Jimenez, J. L., Lee-Taylor, J., Hayes, P. L., McKeen, S. A., Cui, Y. Y., Kim, S.-W., Gentner, D. R., Isaacman-VanWertz, G., Goldstein, A. H., Harley, R. A., Frost, G. J., Roberts, J. M., Ryerson, T. B. and Trainer, M.: Volatile chemical products emerging as largest petrochemical source of urban organic emissions., Science, 359(6377), 760–764, doi:10.1126/science.aaq0524, 2018.

McKeen, S. A., Liu, S. C., Hsie, E.-Y., Lin, X., Bradshaw, J. D., Smyth, S., Gregory, G. L. and

Blake, D. R.: Hydrocarbon ratios during PEM-WEST A: A model perspective, J. Geophys. Res. Atmos., 101(D1), 2087–2109, doi:10.1029/95JD02733, 1996.

McMeeking, G. R., Bart, M., Chazette, P., Haywood, J. M., Hopkins, J. R., McQuaid, J. B., Morgan, W. T., Raut, J.-C., Ryder, C. L., Savage, N., Turnbull, K. and Coe, H.: Airborne measurements of trace gases and aerosols over the London metropolitan region, Atmos. Chem. Phys., 12(11), 5163–5187, doi:10.5194/acp-12-5163-2012, 2012.

McNaughton, C. S., Clarke, A. D., Howell, S. G., Pinkerton, M., Anderson, B., Thornhill, L., Hudgins, C., Winstead, E., Dibb, J. E., Scheuer, E. and Maring, H.: Results from the DC-8 Inlet Characterization Experiment (DICE): Airborne versus surface sampling of mineral dust and sea salt aerosols, Aerosol Sci. Technol., 41(2), 136–159, doi:10.1080/02786820601118406, 2007.

Middlebrook, A. M., Bahreini, R., Jimenez, J. L. and Canagaratna, M. R.: Evaluation of Composition-Dependent Collection Efficiencies for the Aerodyne Aerosol Mass Spectrometer using Field Data, Aerosol Sci. Technol., 46(3), 258–271, doi:10.1080/02786826.2011.620041, 2012.

Miracolo, M. A., Presto, A. A., Lambe, A. T., Hennigan, C. J., Donahue, N. M., Kroll, J. H., Worsnop, D. R. and Robinson, A. L.: Photo-Oxidation of Low-Volatility Organics Found in Motor Vehicle Emissions: Production and Chemical Evolution of Organic Aerosol Mass, Environ. Sci. Technol., 44(5), 1638–1643, doi:10.1021/es902635c, 2010.

Mitroo, D., Sun, Y., Combest, D. P., Kumar, P. and Williams, B. J.: Assessing the degree of plug flow in oxidation flow reactors (OFRs): a study on a potential aerosol mass (PAM) reactor, Atmos. Meas. Tech, 11, 1741–1756, doi:10.5194/amt-11-1741-2018, 2018.

Monks, P. S., Granier, C., Fuzzi, S., Stohl, A., Williams, M. L., Akimoto, H., Amann, M., Baklanov, A., Baltensperger, U., Bey, I., Blake, N., Blake, R. S., Carslaw, K., Cooper, O. R., Dentener, F., Fowler, D., Fragkou, E., Frost, G. J., Generoso, S., Ginoux, P., Grewe, V., Guenther, A., Hansson, H. C., Henne, S., Hjorth, J., Hofzumahaus, A., Huntrieser, H., Isaksen, I. S. A., Jenkin, M. E., Kaiser, J., Kanakidou, M., Klimont, Z., Kulmala, M., Laj, P., Lawrence, M. G., Lee, J. D., Liousse, C., Maione, M., McFiggans, G., Metzger, A., Mieville, A., Moussiopoulos, N., Orlando, J. J., O'Dowd, C. D., Palmer, P. I. I., Parrish, D. D., Petzold, A., Platt, U., Pöschl, U., Prévôt, A. S. H., Reeves, C. E., Reimann, S., Rudich, Y., Sellegri, K., Steinbrecher, R., Simpson, D., ten Brink, H., Theloke, J., van der Werf, G. R., Vautard, R., Vestreng, V., Vlachokostas, C. and von Glasow, R.: Atmospheric composition change - global and regional air quality, Atmos. Environ., 43(33), 5268–5350, doi:10.1016/j.atmosenv.2009.08.021, 2009.

Morino, Y., Tanabe, K., Sato, K. and Ohara, T.: Secondary organic aerosol model intercomparison based on secondary organic aerosol to odd oxygen ratio in Tokyo, J. Geophys. Res. Atmos., 119(23), 13,489-13,505, doi:10.1002/2014JD021937, 2014.

Müller, M., Mikoviny, T., Feil, S., Haidacher, S., Hanel, G., Hartungen, E., Jordan, A., Märk, L., Mutschlechner, P., Schottkowsky, R., Sulzer, P., Crawford, J. H. and Wisthaler, A.: A compact PTR-ToF-MS instrument for airborne measurements of volatile organic compounds at high spatiotemporal resolution, Atmos. Meas. Tech., 7(11), 3763–3772, doi:10.5194/amt-7-3763-2014, 2014.

Murphy, B. N., Donahue, N. M., Fountoukis, C. and Pandis, S. N.: Simulating the oxygen content of ambient organic aerosol with the 2D volatility basis set, Atmos. Chem. Phys., 11(15), 7859–7873, doi:10.5194/acp-11-7859-2011, 2011.

Murphy, B. N., Woody, M. C., Jimenez, J. L., Carlton, A. M. G., Hayes, P. L., Liu, S., Ng, N. L., Russell, L. M., Setyan, A., Xu, L., Young, J., Zaveri, R. A., Zhang, Q. and Pye, H. O. T.: Semivolatile POA and parameterized total combustion SOA in CMAQv5.2: impacts on source strength and partitioning, Atmos. Chem. Phys., 17(18), 11107–11133, doi:10.5194/acp-17-11107-2017, 2017.

Myhre, G., Shindell, D., Bréon, F.-M., Collins, W., Fuglestvedt, J., Huang, J., Koch, D., Lamarque, J.-F., Lee, D., Mendoza, B., Nakajima, T., Robock, A., Stephens, G., Takemura, T. and Zhang, H.: Anthropogenic and Natural Radiative Forcing, in Climate Change 2013: The Physical Science Basis. Contribution of Working Group I to the Fifth Assessment Report of the Intergovernmental Panel on Climate Change, edited by T. F. Stocker, D. Qin, G.-K. Plattner, M. Tignor, S. K. Allen, J. Boschung, A. Nauels, Y. Xia, V. Bex, and P. M. Midgley, p. 659, Cambridge University Press, Cambridge, United Kingdom and New York, NY, USA, United Kingdom and New York, NY, USA. [online] Available from: https://www.ipcc.ch/report/ar5/wg1/, 2013.

Novelli, P. C., Crotwell, A., Lang, P. M. and Mund, J.: Atmospheric Carbon Monoxide Dry Air Mole Fractions from the NOAA ESRL Carbon Cycle Cooperative Global Air Sampling Network, 1988-2016, Version: 2017-07-28, [online] Available from: ftp://aftp.cmdl.noaa.gov/data/trace_gases/co/flask/surface/, 2017.

OECD: Exposure to PM2.5 in countries and regions : Exposure to PM2.5 in macroregions, [online] Available from: https://stats.oecd.org/index.aspx?queryid=72722 (Accessed 1 August 2018), 2018.

Ortega, A. M., Hayes, P. L., Peng, Z., Palm, B. B., Hu, W., Day, D. A., Li, R., Cubison, M. J., Brune, W. H., Graus, M., Warneke, C., Gilman, J. B., Kuster, W. C., de Gouw, J. A., Gutiérrez-Montes, C. and Jimenez, J. L.: Real-time measurements of secondary organic aerosol formation and aging from ambient air in an oxidation flow reactor in the Los Angeles area, Atmos. Chem. Phys., 16(11), 7411–7433, doi:10.5194/acp-16-7411-2016, 2016.

Ots, R., Vieno, M., Allan, J. D., Reis, S., Nemitz, E., Young, D. E., Coe, H., Di Marco, C., Detournay, A., Mackenzie, I. A., Green, D. C. and Heal, M. R.: Model simulations of cooking organic aerosol (COA) over the UK using estimates of emissions based on measurements at two sites in London, Atmos. Chem. Phys., 16(21), 13773–13789, doi:10.5194/acp-16-13773-2016, 2016.

Pagonis, D., Krechmer, J. E., de Gouw, J., Jimenez, J. L. and Ziemann, P. J.: Effects of gas–wall partitioning in Teflon tubing and instrumentation on time-resolved measurements of gas-phase organic compounds, Atmos. Meas. Tech., 10(12), 4687–4696, doi:10.5194/amt-10-4687-2017, 2017.

Palm, B. B., Campuzano-Jost, P., Ortega, A. M., Day, D. A., Kaser, L., Jud, W., Karl, T., Hansel, A., Hunter, J. F., Cross, E. S., Kroll, J. H., Peng, Z., Brune, W. H. and Jimenez, J. L.: In situ secondary organic aerosol formation from ambient pine forest air using an oxidation flow reactor, Atmos. Chem. Phys., 16(5), 2943–2970, doi:10.5194/acp-16-2943-2016, 2016.

Palm, B. B., Campuzano-Jost, P., Day, D. A., Ortega, A. M., Fry, J. L., Brown, S. S., Zarzana, K. J., Dube, W., Wagner, N. L., Draper, D. C., Kaser, L., Jud, W., Karl, T., Hansel, A., Gutiérrez-Montes, C. and Jimenez, J. L.: Secondary organic aerosol formation from in situ OH, O3, and NO3 oxidation of ambient forest air in an oxidation flow reactor, Atmos. Chem. Phys., 17(8), 5331–5354, doi:10.5194/acp-17-5331-2017, 2017.

Palm, B. B., de Sá, S. S., Day, D. A., Campuzano-Jost, P., Hu, W., Seco, R., Sjostedt, S. J., Park, J.-H., Guenther, A. B., Kim, S., Brito, J., Wurm, F., Artaxo, P., Thalman, R., Wang, J., Yee, L. D., Wernis, R., Isaacman-VanWertz, G., Goldstein, A. H., Liu, Y., Springston, S. R., Souza, R., Newburn, M. K., Alexander, M. L., Martin, S. T. and Jimenez, J. L.: Secondary organic aerosol formation from ambient air in an oxidation flow reactor in central Amazonia, Atmos. Chem. Phys., 18(1), 467–493, doi:10.5194/acp-18-467-2018, 2018.

Park, M.-S., Park, S.-H., Chae, J.-H., Choi, M.-H., Song, Y., Kang, M. and Roh, J.-W.: High-resolution urban observation network for user-specific meteorological information service in the Seoul Metropolitan Area, South Korea, Atmos. Meas. Tech, 10, 1575–1594, doi:10.5194/amt-10-1575-2017, 2017.

Park, M. E., Song, C. H., Park, R. S., Lee, J., Kim, J., Lee, S., Woo, J.-H., Carmichael, G. R., Eck, T. F., Holben, B. N., Lee, S.-S., Song, C. K. and Hong, Y. D.: New approach to monitor transboundary particulate pollution over Northeast Asia, Atmos. Chem. Phys, 14, 659–674, doi:10.5194/acp-14-659-2014, 2014.

Park, S. S., Kim, J.-H. and Jeong, J.-U.: Abundance and sources of hydrophilic and hydrophobic water-soluble organic carbon at an urban site in Korea in summer., J. Environ. Monit., 14(1), 224–32, doi:10.1039/c1em10617a, 2012.

Parrish, D. D., Stohl, A., Forster, C., Atlas, E. L., Blake, D. R., Goldan, P. D., Kuster, W. C. and de Gouw, J. A.: Effects of mixing on evolution of hydrocarbon ratios in the troposphere, J. Geophys. Res., 112(D10), D10S34, doi:10.1029/2006JD007583, 2007.

Parrish, D. D., Ryerson, T. B., Mellqvist, J., Johansson, J., Fried, A., Richter, D., Walega, J. G., Washenfelder, R. A., de Gouw, J. A., Peischl, J., Aikin, K. C., McKeen, S. A., Frost, G. J., Fehsenfeld, F. C. and Herndon, S. C.: Primary and secondary sources of formaldehyde in urban atmospheres: Houston Texas region, Atmos. Chem. Phys., 12(7), 3273–3288, doi:10.5194/acp-12-3273-2012, 2012.

Peischl, J., Ryerson, T. B., Brioude, J., Aikin, K. C., Andrews, A. E., Atlas, E., Blake, D., Daube, B. C., de Gouw, J. A., Dlugokencky, E., Frost, G. J., Gentner, D. R., Gilman, J. B., Goldstein, A. H., Harley, R. A., Holloway, J. S., Kofler, J., Kuster, W. C., Lang, P. M., Novelli, P. C., Santoni, G. W., Trainer, M., Wofsy, S. C. and Parrish, D. D.: Quantifying sources of methane using light alkanes in the Los Angeles basin, California, J. Geophys. Res. Atmos., 118(10), 4974–4990, doi:10.1002/jgrd.50413, 2013.

Peng, J. F., Hu, M., Wang, Z. B., Huang, X. F., Kumar, P., Wu, Z. J., Guo, S., Yue, D. L., Shang, D. J., Zheng, Z. and He, L. Y.: Submicron aerosols at thirteen diversified sites in China: size distribution, new particle formation and corresponding contribution to cloud condensation nuclei production, Atmos. Chem. Phys., 14(18), 10249–10265, doi:10.5194/acp-14-10249-2014, 2014.

Peng, Z., Day, D. A., Stark, H., Li, R., Lee-Taylor, J., Palm, B. B., Brune, W. H. and Jimenez, J. L.: HO_x radical chemistry in oxidation flow reactors with low-pressure mercury lamps systematically examined by modeling, Atmos. Meas. Tech., 8(11), 4863–4890, doi:10.5194/amt-8-4863-2015, 2015.

Peng, Z., Day, D. A., Ortega, A. M., Palm, B. B., Hu, W., Stark, H., Li, R., Tsigaridis, K., Brune, W. H. and Jimenez, J. L.: Non-OH chemistry in oxidation flow reactors for the study of atmospheric chemistry systematically examined by modeling, Atmos. Chem. Phys., 16(7), 4283–4305, doi:10.5194/acp-16-4283-2016, 2016.

Perring, A. E., Bertram, T. H., Farmer, D. K., Wooldridge, P. J., Dibb, J., Blake, N. J., Blake, D. R., Singh, H. B., Fuelberg, H., Diskin, G., Sachse, G. and Cohen, R. C.: The production and persistence of $\Sigma RONO_2$ in the Mexico City plume, Atmos. Chem. Phys., 10(15), 7215–7229, doi:10.5194/acp-10-7215-2010, 2010.

Platt, S. M., El Haddad, I., Zardini, A. A., Clairotte, M., Astorga, C., Wolf, R., Slowik, J. G., Temime-Roussel, B., Marchand, N., Ježek, I., Drinovec, L., Močnik, G., Möhler, O., Richter, R., Barmet, P., Bianchi, F., Baltensperger, U. and Prévôt, A. S. H.: Secondary organic aerosol formation from gasoline vehicle emissions in a new mobile environmental reaction chamber, Atmos. Chem. Phys., 13(18), 9141–9158, doi:10.5194/acp-13-9141-2013, 2013.

Platt, S. M., El Haddad, I., Pieber, S. M., Zardini, A. A., Suarez-Bertoa, R., Clairotte, M., Daellenbach, K. R., Huang, R.-J., Slowik, J. G., Hellebust, S., Temime-Roussel, B., Marchand, N., de Gouw, J., Jimenez, J. L., Hayes, P. L., Robinson, A. L., Baltensperger, U., Astorga, C. and Prévôt, A. S. H.: Gasoline cars produce more carbonaceous particulate matter than modern filter-equipped diesel cars, Sci. Rep., 7(1), 4926, doi:10.1038/s41598-017-03714-9, 2017.

Presto, A. A., Gordon, T. D. and Robinson, A. L.: Primary to secondary organic aerosol: Evolution of organic emissions from mobile combustion sources, Atmos. Chem. Phys., 14(10), 5015–5036, doi:10.5194/acp-14-5015-2014, 2014.

Price, H. U., Jaffe, D. A., Cooper, O. R. and Doskey, P. V: Photochemistry, ozone production, and dilution during long-range transport episodes from Eurasia to the northwest United States, J. Geophys. Res. Atmos., 109, D23S13, doi:10.1029/2003JD004400, 2004.

Pye, H. O. T. and Seinfeld, J. H.: A global perspective on aerosol from low-volatility organic compounds, Atmos. Chem. Phys. Atmos. Chem. Phys., 10(9), 4377–4401, doi:10.5194/acp-10-4377-2010, 2010.

Richter, D., Weibring, P., Walega, J. G., Fried, A., Spuler, S. M. and Taubman, M. S.: Compact highly sensitive multi-species airborne mid-IR spectrometer, Appl. Phys. B, 119(1), 119–131, doi:10.1007/s00340-015-6038-8, 2015.

Robinson, A. L., Donahue, N. M., Shrivastava, M. K., Weitkamp, E. A., Sage, A. M., Grieshop, A. P., Lane, T. E., Pierce, J. R. and Pandis, S. N.: Rethinking Organic Aerosols: Semivolatile Emissions and Photochemical Aging, Science (80-.)., 315(5816), 1259–1262, doi:10.1126/science.1133061, 2007.

Sachse, G. W., Hill, G. F., Wade, L. O. and Perry, M. G.: Fast-Response, High-Precision Carbon Monoxide Sensor using a Tunable Diode Laser Absorption Technique, J. Geophys. Res., 92(D2), 2071–2081, doi:doi:10.1029/JD092iD02p02071, 1987.

Sato, K., Nakashima, Y., Morino, Y., Imamura, T., Kurokawa, J. and Kajii, Y.: Total OH reactivity measurements for the OH-initiated oxidation of aromatic hydrocarbons in the presence of NO_x, Atmos. Environ., 171, 272–278, doi:10.1016/j.atmosenv.2017.10.036, 2017.

Schroder, J. C., Campuzano-Jost, P., Day, D. A., Shah, V., Larson, K., Sommers, J. M., Sullivan, A. P., Campos, T., Reeves, J. M., Hills, A., Hornbrook, R. S., Blake, N. J., Scheuer, E., Guo, H., Fibiger, D. L., McDuffie, E. E., Hayes, P. L., Weber, R. J., Dibb, J. E., Apel, E. C., Jaeglé, L., Brown, S. S., Thronton, J. A. and Jimenez, J. L.: Sources and Secondary Production of Organic Aerosols in the Northeastern US during WINTER, J. Geophys. Res. Atmos., doi:10.1029/2018JD028475, 2018.

Schwantes, R. H., Schilling, K. A., McVay, R. C., Lignell, H., Coggon, M. M., Zhang, X., Wennberg, P. O. and Seinfeld, J. H.: Formation of Highly Oxygenated Low-Volatility Products from Cresol Oxidation, Atmos. Chem. Phys., 7(5), 3453–3474, doi:10.5194/acp-17-3453-2017, 2017.

Schwarz, J. P., Samset, B. H., Perring, A. E., Spackman, J. R., Gao, R. S., Stier, P., Schulz, M., Moore, F. L., Ray, E. A. and Fahey, D. W.: Global-scale seasonally resolved black carbon vertical profiles over the Pacific, Geophys. Res. Lett., 40(20), 5542–5547, doi:10.1002/2013GL057775, 2013.

Seo, J., Kim, J. Y., Youn, D., Lee, J. Y., Kim, H., Lim, Y. Bin, Kim, Y. and Jin, H. C.: On the multi-day haze in the Asian continental outflow: An important role of synoptic condition combined with regional and local sources, Atmos. Chem. Phys., 17(15), 9311–9332, doi:10.5194/acp-17-9311-2017, 2017.

Shingler, T., Crosbie, E., Ortega, A., Shiraiwa, M., Zuend, A., Beyersdorf, A., Ziemba, L., Anderson, B., Thornhill, L., Perring, A. E., Schwarz, J. P., Campazano-Jost, P., Day, D. A., Jimenez, J. L., Hair, J. W., Mikoviny, T., Wisthaler, A. and Sorooshian, A.: Airborne characterization of subsaturated aerosol hygroscopicity and dry refractive index from the surface to 6.5km during the SEAC4RS campaign, J. Geophys. Res., 121(8), 4188–4210, doi:10.1002/2015JD024498, 2016.

Shrivastava, M., Cappa, C. D., Fan, J., Goldstein, A. H., Guenther, A. B., Jimenez, J. L., Kuang, C., Laskin, A., Martin, S. T., Ng, N. L., Petaja, T., Pierce, J. R., Rasch, P. J., Roldin, P., Seinfeld, J. H., Shilling, J., Smith, J. N., Thornton, J. A., Volkamer, R., Wang, J., Worsnop, D. R., Zaveri, R. A., Zelenyuk, A. and Zhang, Q.: Recent advances in understanding secondary organic aerosol: Implications for global climate forcing, Rev. Geophys., 55(2), 509–559, doi:10.1002/2016RG000540, 2017.

Shrivastava, M. K., Lane, T. E., Donahue, N. M., Pandis, S. N. and Robinson, A. L.: Effects of gas particle partitioning and aging of primary emissions on urban and regional organic aerosol concentrations, J. Geophys. Res., 113(D18), D18301, doi:10.1029/2007JD009735, 2008.

Silva, S. J., Arellano, A. F. and Worden, H. M.: Toward anthropogenic combustion emission constraints from space-based analysis of urban CO_2/CO sensitivity, Geophys. Res. Lett., 40(18), 4971–4976, doi:10.1002/grl.50954, 2013.

Slusher, D. L., Huey, L. G., Tanner, D. J., Flocke, F. M. and Roberts, J. M.: A thermal dissociation–chemical ionization mass spectrometry (TD-CIMS) technique for the simultaneous measurement of peroxyacyl nitrates and dinitrogen pentoxide, J. Geophys. Res., 109(D19), D19315, doi:10.1029/2004JD004670, 2004.

Stith, J. L., Ramanathan, V., Cooper, W. A., Roberts, G. C., DeMott, P. J., Carmichael, G., Hatch, C. D., Adhikary, B., Twohy, C. H., Rogers, D. C., Baumgardner, D., Prenni, A. J., Campos, T., Gao, R., Anderson, J. and Feng, Y.: An overview of aircraft observations from the Pacific Dust Experiment campaign, J. Geophys. Res., 114(D5), D05207, doi:10.1029/2008JD010924, 2009.

Sueper, D.: ToF-AMS Data Analysis Software Webpage, [online] Available from: http://cires1.colorado.edu/jimenez-group/wiki/index.php/ToF-AMS_Analysis_Software (Accessed 4 January 2017), 2018.

Talbot, R. W., Dibb, J. E., Lefer, B. L., Scheuer, E. M., Bradshaw, J. D., Sandholm, S. T., Smyth,

S., Blake, D. R., Blake, N. J., Sachse, G. W., Collins, J. E. and Gregory, G. L.: Large-scale distributions of tropospheric nitric, formic, and acetic acids over the western Pacific basin during wintertime, J. Geophys. Res., 102(D23), 28303–28313, 1997.

Tang, W., Arellano, A. F., DiGangi, J. P., Choi, Y., Diskin, G. S., Agustí-Panareda, A., Parrington, M., Massart, S., Gaubert, B., Lee, Y., Kim, D., Jung, J., Hong, J., Hong, J.-W., Kanaya, Y., Lee, M., Stauffer, R. M., Thompson, A. M., Flynn, J. H. and Woo, J.-H.: Evaluating High-Resolution Forecasts of Atmospheric CO and CO_2 from a Global Prediction System during KORUS-AQ Field Campaign, Atmos. Chem. Phys. Discuss., 1–41, doi:10.5194/acp-2018-71, 2018.

Tkacik, D. S., Lambe, A. T., Jathar, S., Li, X., Presto, A. A., Zhao, Y., Blake, D., Meinardi, S., Jayne, J. T., Croteau, P. L. and Robinson, A. L.: Secondary Organic Aerosol Formation from in-Use Motor Vehicle Emissions Using a Potential Aerosol Mass Reactor., Environ. Sci. Technol., 48(19), 11235–42, doi:10.1021/es502239v, 2014.

Tohjima, Y., Kubo, M., Minejima, C., Mukai, H., Tanimoto, H., Ganshin, A., Maksyutov, S., Katsumata, K., Machida, T. and Kita, K.: Temporal changes in the emissions of CH4 and CO from China estimated from CH4 / CO2 and CO / CO2 correlations observed at Hateruma Island, Atmos. Chem. Phys., 14(3), 1663–1677, doi:10.5194/acp-14-1663-2014, 2014.

Tritscher, T., Dommen, J., DeCarlo, P. F., Gysel, M., Barmet, P. B., Praplan, A. P., Weingartner, E., Prévôt, A. S. H., Riipinen, I., Donahue, N. M. and Baltensperger, U.: Volatility and hygroscopicity of aging secondary organic aerosol in a smog chamber, Atmos. Chem. Phys., 11(22), 11477–11496, doi:10.5194/acp-11-11477-2011, 2011.

Tsimpidi, A. P., Karydis, V. A., Zavala, M., Lei, W., Molina, L., Ulbrich, I. M., Jimenez, J. L. and Pandis, S. N.: Evaluation of the volatility basis-set approach for the simulation of organic aerosol formation in the Mexico City metropolitan area, Atmos. Chem. Phys., 10(2), 525–546, doi:10.5194/acp-10-525-2010, 2010.

Tsimpidi, A. P., Karydis, V. A., Pandis, S. N. and Lelieveld, J.: Global-scale combustion sources of organic aerosols: sensitivity to formation and removal mechanisms, Atmos. Chem. Phys., 17(12), 7345–7364, doi:10.5194/acp-17-7345-2017, 2017.

Ulbrich, I. M., Canagaratna, M. R., Zhang, Q., Worsnop, D. R. and Jimenez, J. L.: Interpretation of organic components from Positive Matrix Factorization of aerosol mass spectrometric data, Atmos. Chem. Phys., 9(9), 2891–2918, doi:10.5194/acp-9-2891-2009, 2009.

UNDESA, P. D.: World Urbanization Prospects: The 2014 Revision., 2015.

Vay, S. A., Tyler, S. C., Choi, Y., Blake, D. R., Blake, N. J., Sachse, G. W., Diskin, G. S. and Singh, H. B.: Sources and transport of Δ14C in CO 2 within the Mexico City Basin and vicinity, Atmos. Chem. Phys., 9, 4973–4985, doi:10.159/acp-9-4973-2009, 2009.

Virkkula, A.: Correction of the Calibration of the 3-wavelength Particle Soot Absorption Photometer (3λ PSAP), Aerosol Sci. Technol., 44, 706–712, doi:10.1080/02786826.2010.482110, 2010.

Volkamer, R., Jimenez, J. L., San Martini, F., Dzepina, K., Zhang, Q., Salcedo, D., Molina, L. T., Worsnop, D. R. and Molina, M. J.: Secondary organic aerosol formation from anthropogenic air pollution: Rapid and higher than expected, Geophys. Res. Lett., 33(17), L17811, doi:10.1029/2006GL026899, 2006.

Wang, Y., Munger, J. W., Xu, S., McElroy, M. B., Hao, J., Nielsen, C. P. and Ma, H.: CO_2 and its correlation with CO at a rural site near Beijing: implications for combustion efficiency in China, Atmos. Chem. Phys., 10(18), 8881–8897, doi:10.5194/acp-10-8881-2010, 2010.

Weibring, P., Richter, D., Walega, J. G., Rippe, L. and Fried, A.: Difference frequency generation spectrometer for simultaneous multispecies detection, Opt. Express, 18(26), 27670, doi:10.1364/OE.18.027670, 2010.

Weinheimer, A. J., Walega, J. G., Ridley, B. A., Gary, B. L., Blake, D. R., Blake, N. J., Rowland, F. S., Sachse, G. W., Anderson, B. E. and Collins, J. E.: Meridional distributions of NOx , NOy , and other species in the lower stratosphere and upper troposphere during AASE II, Geophys. Res. Lett., 21(23), 2583–2586, doi:10.1029/94GL01897, 1994.

WHO: Ambient air pollution: A global assessment of exposure and burden of disease, World Health Organization., 2016.

Wisthaler, A., Hansel, A., Dickerson, R. R. and Crutzen, P. J.: Organic trace gas measurements by PTR-MS during INDOEX 1999, J. Geophys. Res., 107(D19), 8024, doi:10.1029/2001JD000576, 2002.

Wood, E. C., Canagaratna, M. R., Herndon, S. C., Onasch, T. B., Kolb, C. E., Worsnop, D. R., Kroll, J. H., Knighton, W. B., Seila, R., Zavala, M., Molina, L. T., DeCarlo, P. F., Jimenez, J. L., Weinheimer, A. J., Knapp, D. J., Jobson, B. T., Stutz, J., Kuster, W. C. and Williams, E. J.: Investigation of the correlation between odd oxygen and secondary organic aerosol in Mexico City and Houston, Atmos. Chem. Phys., 10(18), 8947–8968, doi:DOI 10.5194/acp-10-8947-2010, 2010.

Woody, M. C., Baker, K. R., Hayes, P. L., Jimenez, J. L., Koo, B. and Pye, H. O. T.: Understanding sources of organic aerosol during CalNex-2010 using the CMAQ-VBS, Atmos. Chem. Phys., 16(6), 4081–4100, doi:10.5194/acp-16-4081-2016, 2016.

Wooldridge, P. J., Perring, A. E., Bertram, T. H., Flocke, F. M., Roberts, J. M., Singh, H. B., Huey, L. G., Thornton, J. A., Wolfe, G. M., Murphy, J. G., Fry, J. L., Rollins, A. W., LaFranchi, B. W. and Cohen, R. C.: Total Peroxy Nitrates (ΣPNs) in the atmosphere: the Thermal Dissociation-Laser Induced Fluorescence (TD-LIF) technique and comparisons to speciated PAN measurements, Atmos. Meas. Tech., 3(3), 593–607, doi:DOI 10.5194/amt-3-593-2010, 2010.

Wu, W., Zhao, B., Wang, S. and Hao, J.: Ozone and secondary organic aerosol formation potential from anthropogenic volatile organic compounds emissions in China, J. Environ. Sci., 53, doi:10.1016/j.jes.2016.03.025, 2016.

Xu, W., Croteau, P., Williams, L., Canagaratna, M., Onasch, T., Cross, E., Zhang, X., Robinson, W., Worsnop, D. and Jayne, J.: Laboratory characterization of an aerosol chemical speciation monitor with $PM_{2.5}$ measurement capability, Aerosol Sci. Technol., 51(1), 69–83, doi:10.1080/02786826.2016.1241859, 2017.

Zhang, Q., Jimenez, J. L., Canagaratna, M. R., Allan, J. D., Coe, H., Ulbrich, I., Alfarra, M. R., Takami, A., Middlebrook, A. M., Sun, Y. L., Dzepina, K., Dunlea, E., Docherty, K., DeCarlo, P. F., Salcedo, D., Onasch, T., Jayne, J. T., Miyoshi, T., Shimono, A., Hatakeyama, S., Takegawa, N., Kondo, Y., Schneider, J., Drewnick, F., Borrmann, S., Weimer, S., Demerjian, K., Williams, P., Bower, K., Bahreini, R., Cottrell, L., Griffin, R. J., Rautiainen, J., Sun, J. Y., Zhang, Y. M. and Worsnop, D. R.: Ubiquity and dominance of oxygenated species in organic aerosols in

anthropogenically-influenced Northern Hemisphere midlatitudes, Geophys. Res. Lett., 34(13), L13801, doi:10.1029/2007gl029979, 2007.

Zhang, Q. J., Beekmann, M., Freney, E., Sellegri, K., Pichon, J. M., Schwarzenboeck, A., Colomb, A., Bourrianne, T., Michoud, V. and Borbon, A.: Formation of secondary organic aerosol in the Paris pollution plume and its impact on surrounding regions, Atmos. Chem. Phys., 15(24), 13973–13992, doi:10.5194/acp-15-13973-2015, 2015.

Zhang, X., Smith, K. A., Worsnop, D. R., Jimenez, J., Jayne, J. T. and Kolb, C. E.: A Numerical Characterization of Particle Beam Collimation by an Aerodynamic Lens-Nozzle System: Part I. An Individual Lens or Nozzle, Aerosol Sci. Technol., 36, 617–631, doi:10.1080/02786820252883856, 2002.

Zhang, X., Smith, K. A., Worsnop, D. R., Jimenez, J. L., Jayne, J. T., Kolb, C. E., Morris, J. and Davidovits, P.: Numerical Characterization of Particle Beam Collimation: Part II Integrated Aerodynamic-Lens–Nozzle System, Aerosol Sci. Technol., 38, 619–638, doi:10.1080/02786820490479833, 2004.

Zhang, X., Cappa, C. D., Jathar, S. H., McVay, R. C., Ensberg, J. J., Kleeman, M. J., Seinfeld, J. H. and Christopher D. Cappa: Influence of vapor wall loss in laboratory chambers on yields of secondary organic aerosol., Proc. Natl. Acad. Sci. U. S. A., 111(16), 1–6, doi:10.1073/pnas.1404727111, 2014.

Zhao, Y., Hennigan, C. J., May, A. A., Tkacik, D. S., de Gouw, J. A., Gilman, J. B., Kuster, W. C., Borbon, A. and Robinson, A. L.: Intermediate-volatility organic compounds: a large source of secondary organic aerosol, Environ. Sci. Technol., 48(23), 13743–50, doi:10.1021/es5035188, 2014.

Zhao, Y., Nguyen, N. T., Presto, A. A., Hennigan, C. J., May, A. A. and Robinson, A. L.: Intermediate Volatility Organic Compound Emissions from On-Road Gasoline Vehicles and Small Off-Road Gasoline Engines, Environ. Sci. Technol., 50(8), 4554–4563, doi:10.1021/acs.est.5b06247, 2016.

Ziemba, L. D., Lee Thornhill, K., Ferrare, R., Barrick, J., Beyersdorf, A. J., Chen, G., Crumeyrolle, S. N., Hair, J., Hostetler, C., Hudgins, C., Obland, M., Rogers, R., Scarino, A. J., Winstead, E. L. and Anderson, B. E.: Airborne observations of aerosol extinction by in situ and remote-sensing techniques: Evaluation of particle hygroscopicity, Geophys. Res. Lett., 40(2), 417–422, doi:10.1029/2012GL054428, 2013.

Supplemental Material for Secondary Organic Aerosol Production from Local Emissions Dominates the Organic Aerosol Budget over Seoul, South Korea, during KORUS-AQ

B. A. Nault[1,2], P. Campuzano-Jost[1,2], D. A. Day[1,2], J. C. Schroder[1,2], B. Anderson[3], A. J. Beyersdorf[3,*], D. R. Blake[4], W. H. Brune[5], , Y. Choi[3,6], C. A. Corr[3,**], J. A. de Gouw[1,2], J. Dibb[7], J. P. DiGangi[3], G. S. Diskin[3], A. Fried[8], L. G. Huey[9], M. J. Kim[10], C. J. Knote[11], K. D. Lamb[2,12], T. Lee[13], T. Park[13], S. E. Pusede[14], E. Scheuer[7], K. L. Thornhill[3,6], J.-H. Woo[15], and J. L. Jimenez[1,2]

Affiliations
1. Department of Chemistry, University of Colorado, Boulder, CO, USA
2. Cooperative Institute for Research in Environmental Sciences, University of Colorado, Boulder, CO, USA
3. NASA Langley Research Center, Hampton, Virginia, USA
4. Department of Chemistry, University of California, Irvine, Irvine, CA, USA
5. Department of Meteorology and Atmospheric Science, Pennsylvania State University, University Park, Pennsylvania, USA
6.6. Science Systems and Applications, Inc., Hampton, Virginia, USA
7. Earth Systems Research Center, Institute for the Study of Earth, Oceans, and Space, University of New Hampshire, Durham, New Hampshire, USA
8. Institute of Arctic and Alpine Research, University of Colorado, Boulder, CO, USA
9. School of Earth and Atmospheric Sciences, Georgia Institute of Technology, Atlanta, Georgia, USA
10. Division of Geological and Planetary Sciences, California Institute of Technology, Pasadena, CA, USA
11. Meteorologisches Institut, Ludwig-Maximilians-Universität München, München, Germany
12. Chemical Sciences Division, Earth System Research Laboratory, National Oceanic and Atmospheric Administration, Boulder, CO, USA
13. Department of Environmental Science, Hankuk University of Foreign Studies, Republic of Korea
14. Department of Environmental Sciences, University of Virginia, Charlottesville, VA, USA
15. Department of Advanced Technology Fusion, Konkuk University, Seoul, Republic of Korea
* Now at: Department of Chemistry and Biochemistry, California State University, San Bernardino, San BernardinoBernardino, California
** Now at: USDA UV-B Monitoring and Research Program, Natural Resource Ecology Laboratory, Colorado State University, Fort Collins, CO, USA

Correspondence to: J. L. Jimenez (jose.jimenez@colorado.edu)

SI 1. KORUS-AQ Overview

SI Table 1. List of NASA DC-8 research flights and date of take-off. Unless noted, the take-off dates are different than the local dates since the data was recorded in UTC. We document the research flights with the UTC dates to correspond with the data repository (Aknan and Chen, 2018).

Research Flight Number	*Date of Take-off*	*Regions Sampled*	*Number of Seoul Missed Approaches*
01	01/May/2016	Jeju jetway (×2)	3
02	03/May/2016	West Sea, Jeju jetway	3
03	04/May/2016	Jeju jetway	2
04	06/May/2016	Busan jetway (×2)	3
05	10/May/2016	Jeju jetway, other[b]	2
06	11/May/2016	West Sea, other[c]	3
07	12/May/2016	West Sea, other[d]	0
08	16/May/2016	Jeju jetway, Busan jetway	3
09	17/May/2016	West Sea, Busan jetway	3
10	19/May/2016	Busan jetway (×2)	3
11	21/May/2016	West Sea	3
12	24/May/2016	West Sea	2
13	26/May/2016[a]	Jeju Jetway	2
14	29/May/2016	West Sea, Busan jetway	4
15	30/May/2016	West Sea, Jeju jetway	3
16	01/June/2016	Busan jetway, Jeju jetway	3
17	02/June/2016	Busan jetway, Jeju jetway	3
18	04/June/2016	West Sea, other[e]	5
19	08/June/2016	Busan jetway (×2)	3
20	09/June/2016	Jeju jetway, other[b]	2

[a]For RF13, the DC-8 took-off after 00:00 UTC, corresponding to the date in local time and UTC time being the same.
[b]The DC-8 sampled south of the Korean peninsula.
[c]The DC-8 sampled east of Seoul to the Sea of Japan.
[d]The DC-8 sampled the Sea of Japan.
[e]The DC-8 remained in the greater Seoul area to sample point sources.

SI Table 2. Description of the geographical locations used in Figure 1 and throughout the text, and shown in SI Figure 1..

Location	*Lat Min (°N)*	*Lat Max (°N)*	*Lon Min (°E)*	*Lon Max (°E)*
Seoul	36.8	37.6	124.6[a]	128.0
West Sea			124.0	126.0
Jeju jetway	34.2	36.8	126	127
Busan jetway	35.2	36.8	128.6	129.9

[a]This value was chosen to include the Seoul outflow observed during RF11 and RF18.

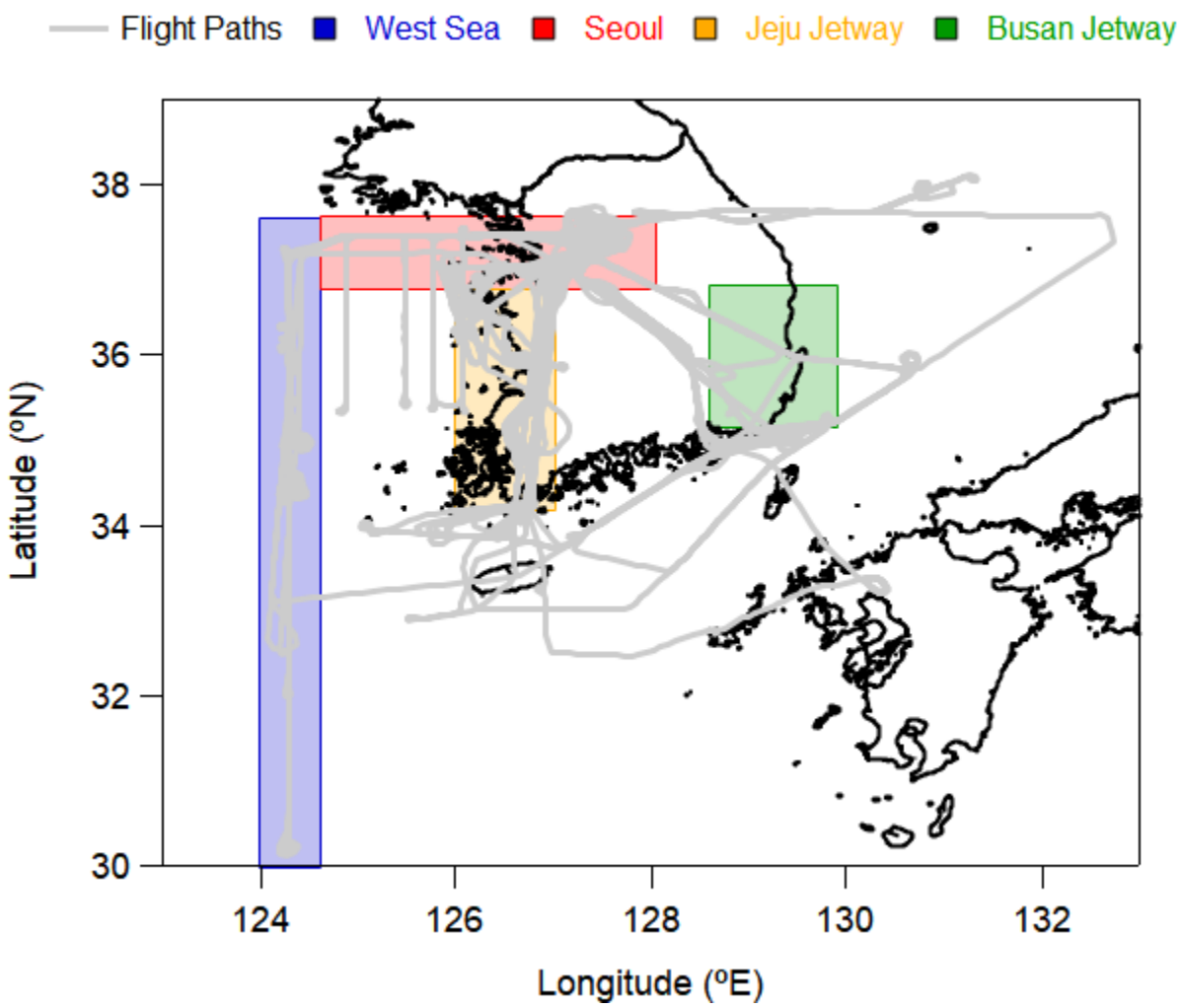

SI Figure 1. Geographical regions shown in SI Table 1. Note, the Seoul box is extended into the West Sea to capture the outflow of Seoul emissions for two flights (RF11 and RF18).

SI 2. CU-AMS Sampling and Calibration

After almost every flight, the ionization efficiency (IE) was calibrated (SI Figure 3) using the single particle technique. Briefly, air containing 150 – 250 particles/cm^3 of NH_4NO_3, of 400 nm (mobility diameter, sized ~~with a built-in differential mobility analyzer, DMA~~with a differential mobility analyzer, TSI model 3080, that was installed in the same rack as the CU-AMS) was sampled by the AMS. Thresholds of 4 (*m/z* 30) or 3 (*m/z* 46) ions per event were selected to produce a low, but detectable background (typically ~7 events/cm^3 background). An event would be recorded, after evaporation and ionization of NH_4NO_3 particle, if at least 4 (*m/z* 30) or 3 (*m/z* 46) ions were observed. These values were analyzed using the ToF AMS Ionization Efficiency Calibration Panel for ET, v1.0.5F (http://cires1.colorado.edu/jimenez-group/ToFAMSResources/ToFSoftware/index.html#ToF_IE_Cal), to process the data and calculate IE and IE/AB (AB is air beam). Typical values during KORUS-AQ, for 400 nm (mobility~~geometric~~ diameter) NH_4NO_3 calibrations were the following: 10 baseline segments and minimum and maximum ions per particle values of 1 and 200. During KORUS-AQ, the average IE/AB was $8.10(\pm0.64)\times10^{-13}$ ions/molecule of nitrate, which leads to an overall 10% variability for this value during the whole campaign. Further details about using single particle technique for IE/AB calibrations can be found in Nault et al. (2016).

These IE calibrations also provided relative ionization efficiency (RIE) calibrations of NH_4 after nearly every flight, as well (SI Figure 3), along with the NO^+ and NO_2^+ ratios of ammonium nitrate, which are useful to estimate particle organic nitrate concentrations, as detailed in Fry et al. (2013). The SO_4 and Chl RIEs were measured about once every week, and the interpolated values were used for the SO_4 and Chl concentrations. For the organic aerosol, we used an RIE of 1.4 (Jimenez et al., 2016; Xu et al., 2018). Finally, to test the effects of solution mixtures on RIE for

SO_4 and NH_4, we made calibration solutions ranging from 0 – 100% NH_4NO_3, with the balance coming from $(NH_4)_2SO_4$. We find no effects, both on the calculated NH_4 balance (SI Figure 6), when using the NH_4 and SO_4 RIE's from the pure calibration, and on the recalculated NH_4 (SO_4) RIE when keeping a constant SO_4 (NH_4) RIE from the pure calibrations (SI Figure 6). The consistency in the NH_4 balance, as observed in prior studies (Docherty et al., 2011; Jimenez et al., 2016), and the high precision (3% precision in all calculations) provides further confidence in the stability of the RIEs for the species in calculating their mass in mixed particles, and indicates that there are no effects on the RIE with changing composition, and, thus, CE (Jimenez et al., 2016).

Also, the IE calibrations performed after each flight provided an opportunity to calculate the effect of pNO_3 on producing a small artifact CO_2^+ signal, as detailed in Pieber et al. (2016), and of pNO_3 on producing small artifact HCl^+ and Cl^+ signal, as detailed in Hu et al. (2017a) (SI Figure 3). The CU-AMS data has been corrected for these small effects. The corrections were typically 1% of CO_2^+ and 0.8% Chl.

Three different lens transmission calibrations to characterize the high end of the AMS transmission curve were performed: (1) comparing the NH_4NO_3 mass measured with the CPC and the CU-AMS between 200 – 450 nm (mobility diameter, d_m); (2) comparing the number of particles measured with the CPC and the CU-AMS between 300 – 450 nm (d_m) using the single particle vaporization technique detailed above; and (3) comparing the $(NH_4)_2SO_4$ mass measured with the CPC and the CU-AMS between 250 – 450 nm (d_m), normalizing to the value at 250 nm. The NH_4NO_3 diameters were converted to vacuum aerodynamic diameters (d_{va}), as discussed in DeCarlo et al. (2004). As seen in SI Figure 4, both techniques show good agreement for the particle transmission, and this transmission is similar to the recommended transmission curve in the literature (Knote et al., 2011; Hu et al., 2017b). For this curve, it is assumed that the transmission

linearly increases from 0 – 100% between 40 – 100 nm (d_{va}) (Q. Zhang et al., 2004), remains 100% between 100 – 550 nm (aerodynamic diameter), and decreases linearly from 100 – 0% between 550 nm – 1500 nm (d_{va}). This leads to a 50% cut-off of ~900 nm (d_{va}) during KORUS-AQ.

The particle sizing in the AMS Particle Time-of-Flight (PToF) mode was calibrated with PSLs, ranging from 70 – 700 nm (geometric diameter) (SI Figure 5). This calibration was compared against the velocities calculated from data collected during the NH_4NO_3 lens transmission measurements. As seen in SI Figure 5, these two different methods to calibrate the PToF velocity show comparable results, falling within the 95% confidence interval of the PSL calibration. The fact that both PToF calibrations agree, and that the SMPS used for the AN calibrations showed less than 2 nm deviation from the nominal PSLs diameters at all sizes increases our confidence in accuracy of the IE calibration described above, and in particular on lack of evaporation of NH_4NO_3 after its size selection in the DMA.

Finally, the vaporizer power, and thus, temperature, was calibrated by using monodisperse $NaNO_3$ particles of d_m = 350 nm (SI Figure 8), as recommended by Williams (2010) and Hu et al. (2017b). This method is more accurate than relying on the temperature reported by the thermocouple on the AMS vaporizer, which can often be unreliable (Williams, 2010; Hu et al., 2017b). The general idea is to increase the vaporizer power between ~1 – 7 W and locate where the $NaNO_3$ full-width half maximum nearly remains constant, indicating that the vaporizer temperature is ~600°C and allowing for maximum peaks in OA, pNO_3, and SO_4 while minimizing the influence of refractory species (Williams, 2010; Hu et al., 2017b).

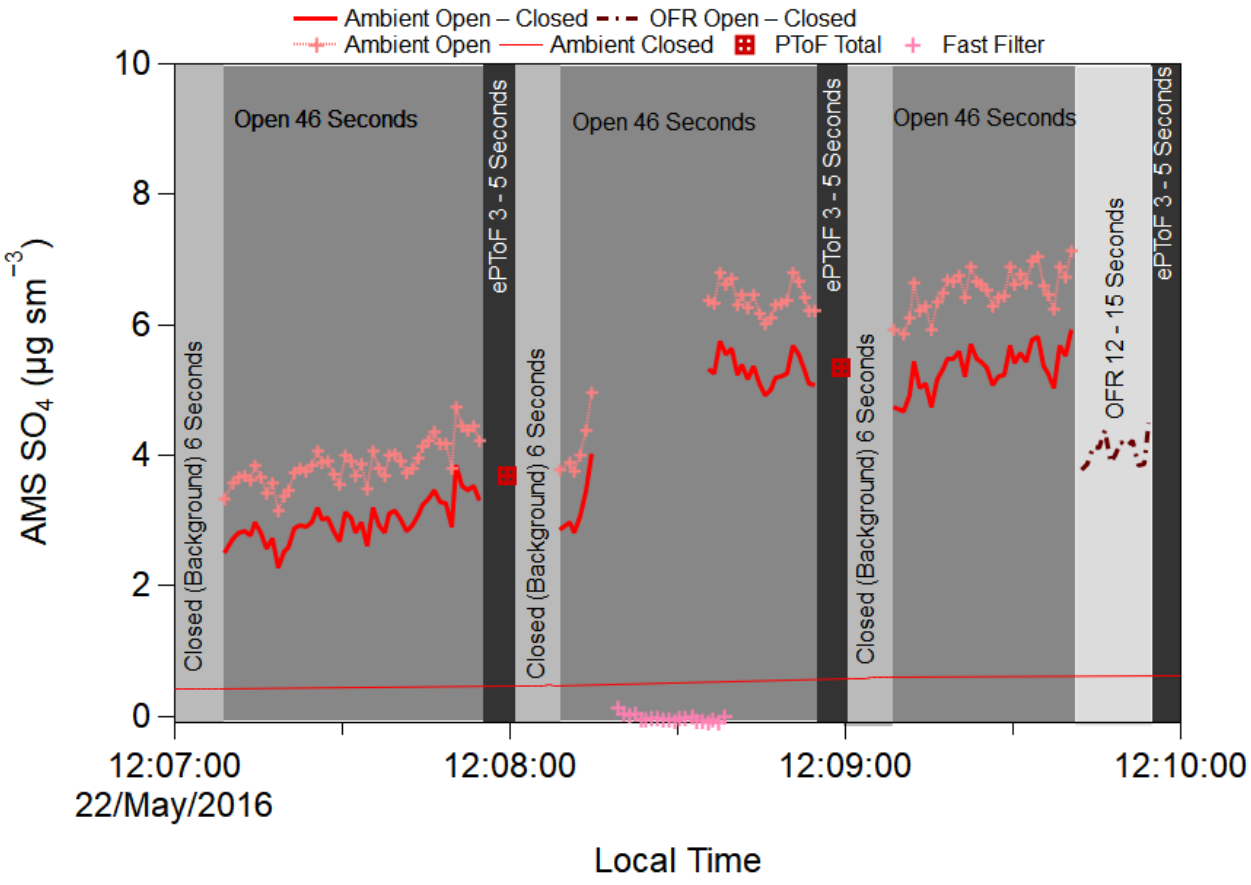
Ambient Open – Closed
OFR Open – Closed
Ambient Open
Ambient Closed
PToF Total
Fast Filter
Open 46 Seconds
Open 46 Seconds
Open 46 Seconds
Closed (Background) 6 Seconds
ePToF 3 - 5 Seconds
Closed (Background) 6 Seconds
ePToF 3 - 5 Seconds
Closed (Background) 6 Seconds
OFR 12 - 15 Seconds
ePToF 3 - 5 Seconds
AMS SO4 (µg sm-3)
10
8
6
4
2
0
12:07:00
22/May/2016
12:08:00
12:09:00
12:10:00
Local Time

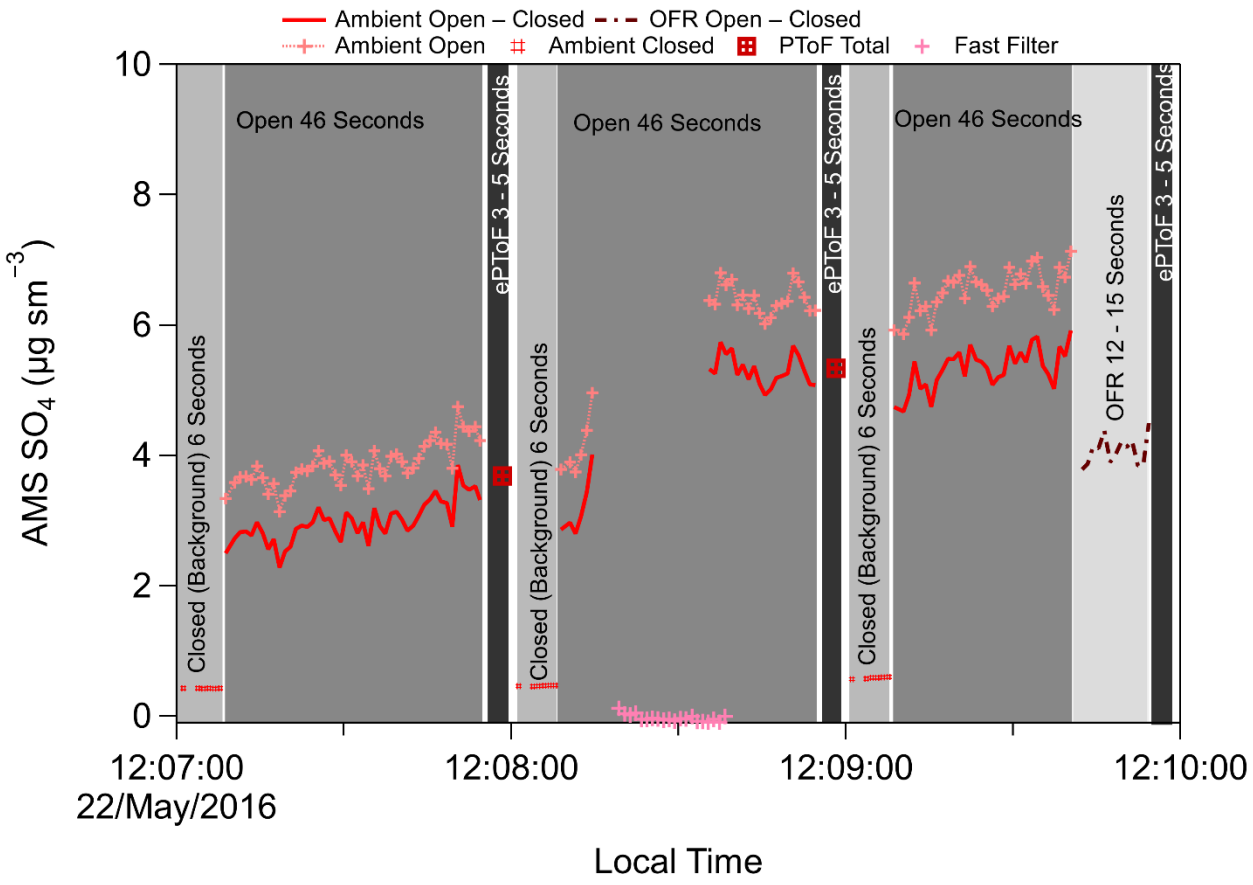

SI Figure 2. Example time series of the CU-AMS sampling scheme during KORUS-AQ. Though the final 8 s of each minute are dedicated to ePToF, some of the time is ued by the computer in saving the 6 s of closed and 46 s of open signal and ePToF signal; therefore, only 3 – 5 s of ePToF signal is actually recorded. The approximate saving time are shown as white spaces.

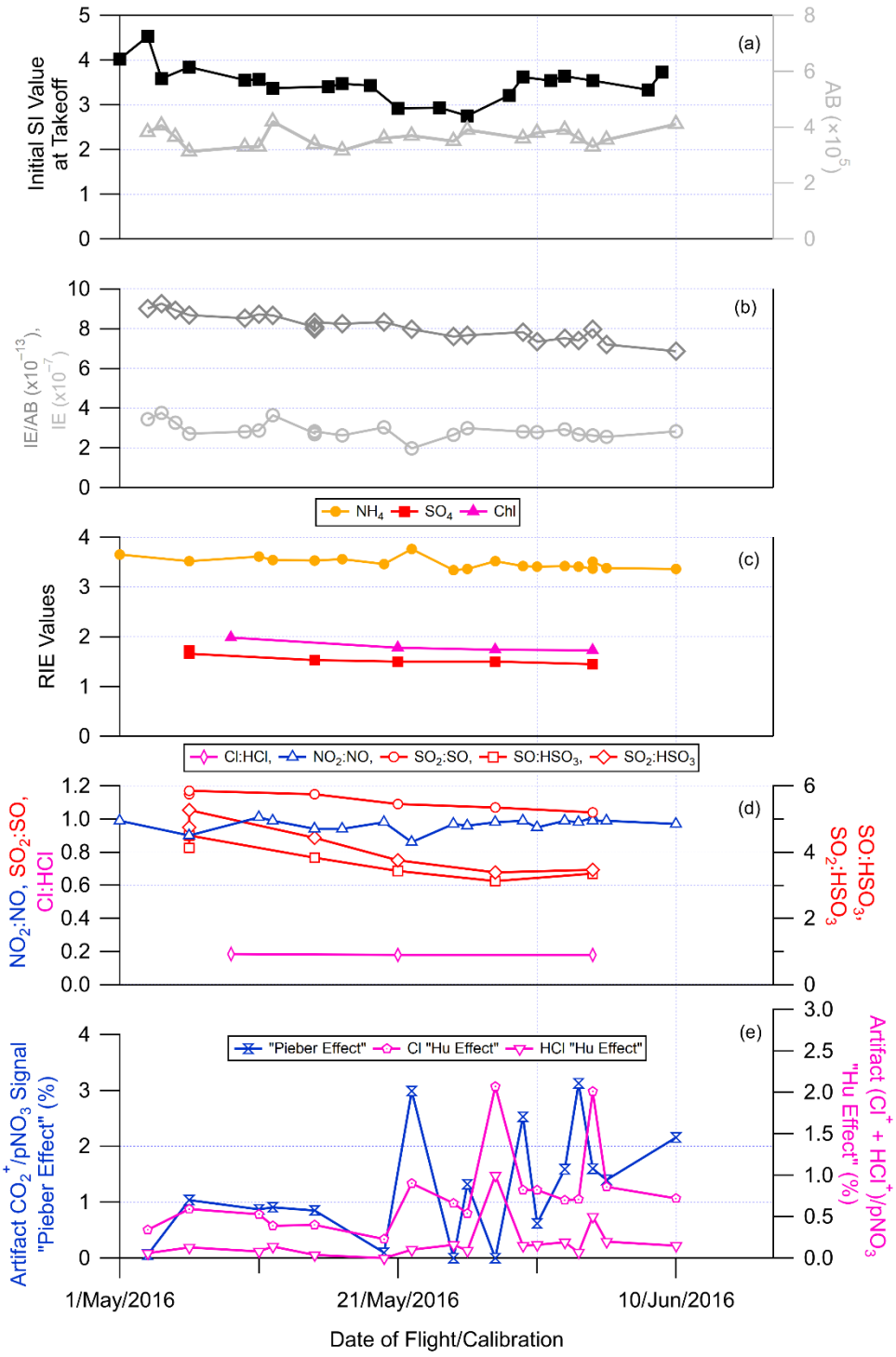

SI Figure 3. Time series of the (a) the Single Ion (SI) at take-off for each flight; (b) the air beam (AB, dark grey), ionization energy (IE, light grey), and IE/AB (middle grey) for each calibration; (c) the relative ionization energies (RIE) for ammonium (NH_4), sulfate (SO_4), and chloride (Chl) for each calibration; (d) the ratios of different ions for each calibration; and, (e) measured artifact signal ratios for CO_2^+/pNO_3 "Pieber effect" (Pieber et al., 2016) and $(Cl^+ + HCl^+)/pNO_3$ "Hu efffect" (Hu et al., 2017a) effects from each calibration.

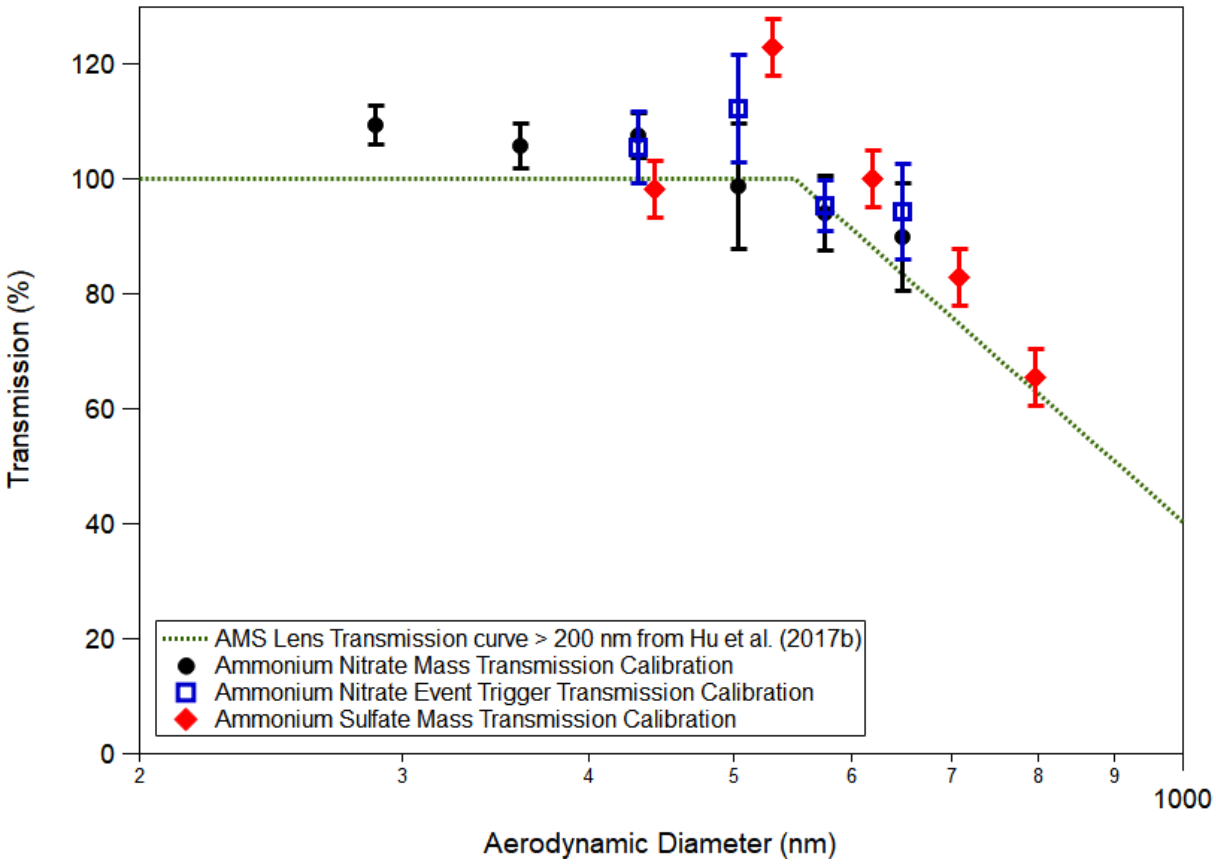

SI Figure 4. Measured transmission percentage of ammonium nitrate and ammonium sulfate versus vacuum aerodynamic diameters (nm) during KORUS-AQ. The green dashed-line is the expected transmission curve for the CU-AMS from the literature (Knote et al., 2011; Hu et al., 2017b). The black data represents the ammonium nitrate transmission curve using mass closure, from an experiment conducted on 09/May/2016. The blue data represents the ammonium nitrate transmission curve using single particle ("event trigger") number closure, from an experiment conducted on 17May/2016. The red data represents the ammonium sulfate transmission curve using mass, from an experiment conducted on 06/May/2016. Finally, the error bars represent 1σ variability for the transmission at each size.

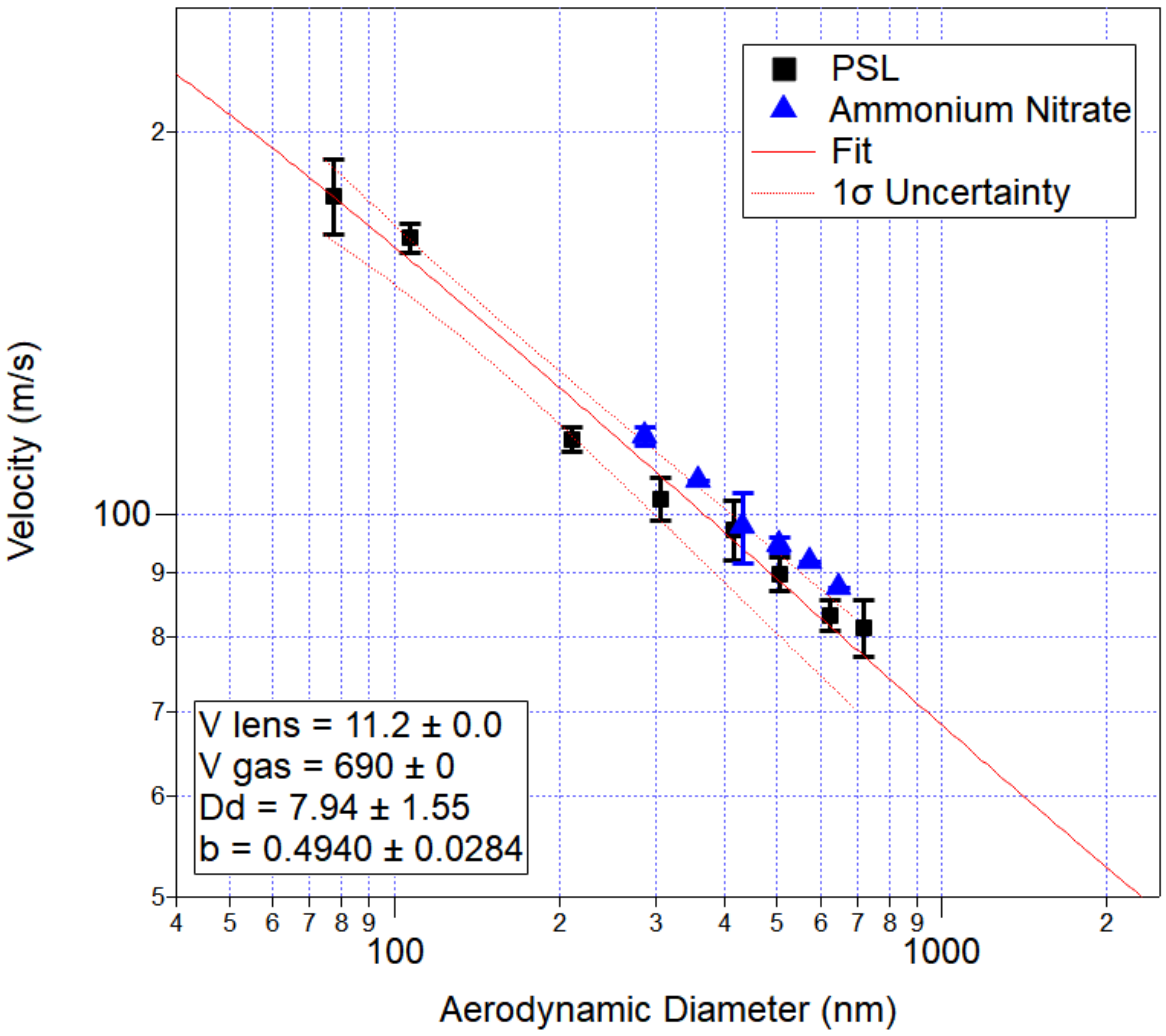

SI Figure 5. Particle velocity (m/s) inside the AMS vacuum chamber (after exiting the aerodynamic lens) versus vacuum aerodynamic diameter (nm) calibrations for the ePToF mode, using PSLs (black). Solid red line is the fit to the PSLs. The ammonium nitrate measured for the mass closure transmission curves (SI Figure 4) for comparison to the PSL values.

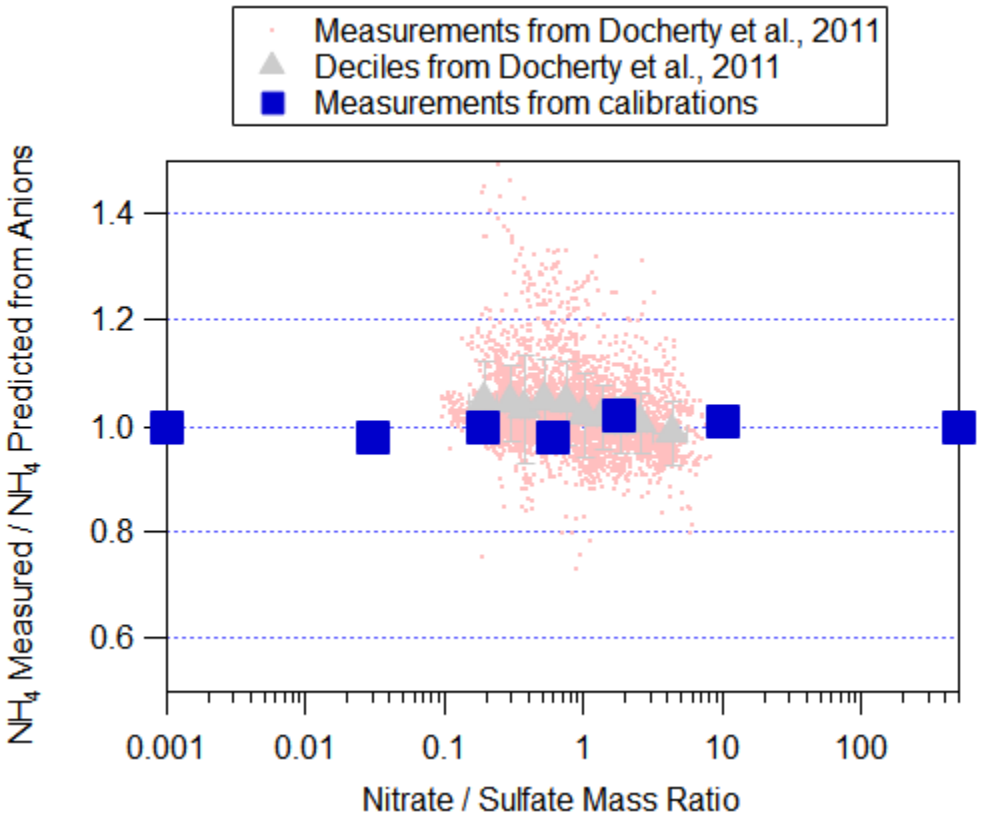

SI Figure 6. Ratio of measured and predicted NH_4 from anions versus ratio of nitrate to sulfate mass. Red points are from Docherty et al. (2011), grey triangles are deciles of the data from Docherty et al., and blue points are measurements from calibration solutions of varying mixtures of NH_4NO_3 and $(NH_4)_2SO_4$. Such consistency would be unexpected if a major fraction of the particle NH_4^+ evaporated as intact salts, as suggested by Murphy (2016) (Hu et al., 2017b) .

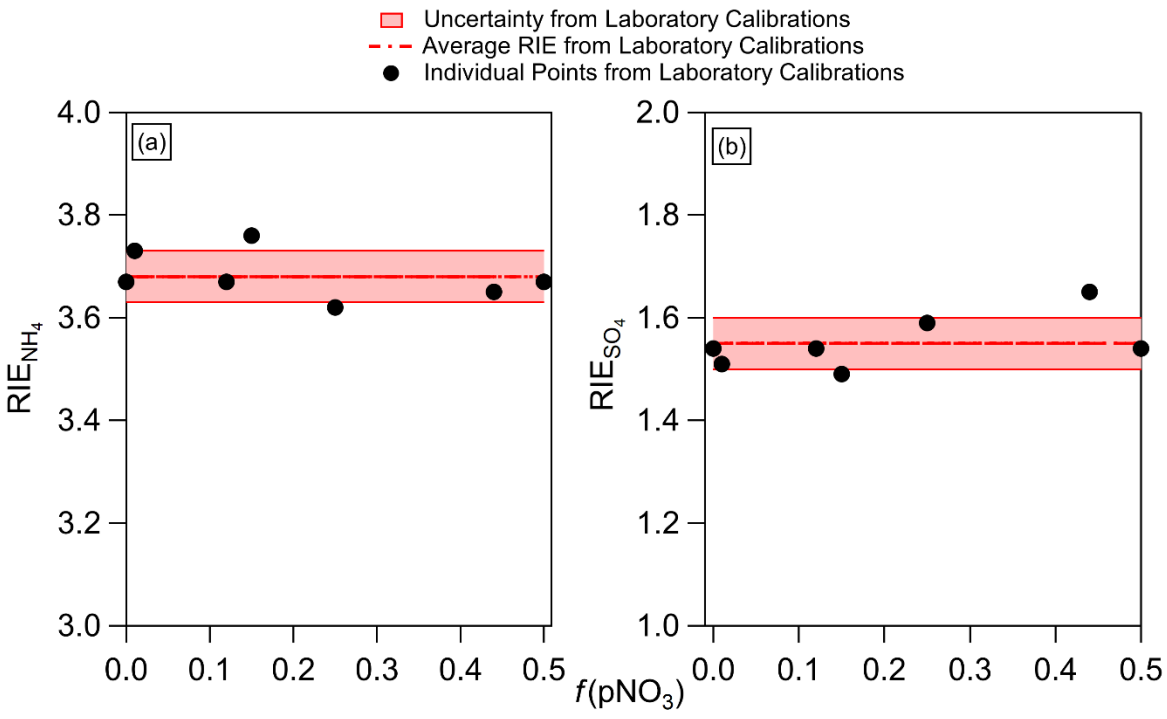

SI Figure 7. (a) Plot of NH_4 RIE, keeping SO_4 RIE constant, versus the molar fraction of pNO_3 measured in the solution, for calibration solutions of varying mixtures of NH_4NO_3 and $(NH_4)_2SO_4$. (b) Same as (a), but for SO_4 RIE and keeping NH_4 RIE constant. For both figures, the black dots are the values from the calibrations, the thick red line is the average of all the values, and the shaded red area is ±1σ.

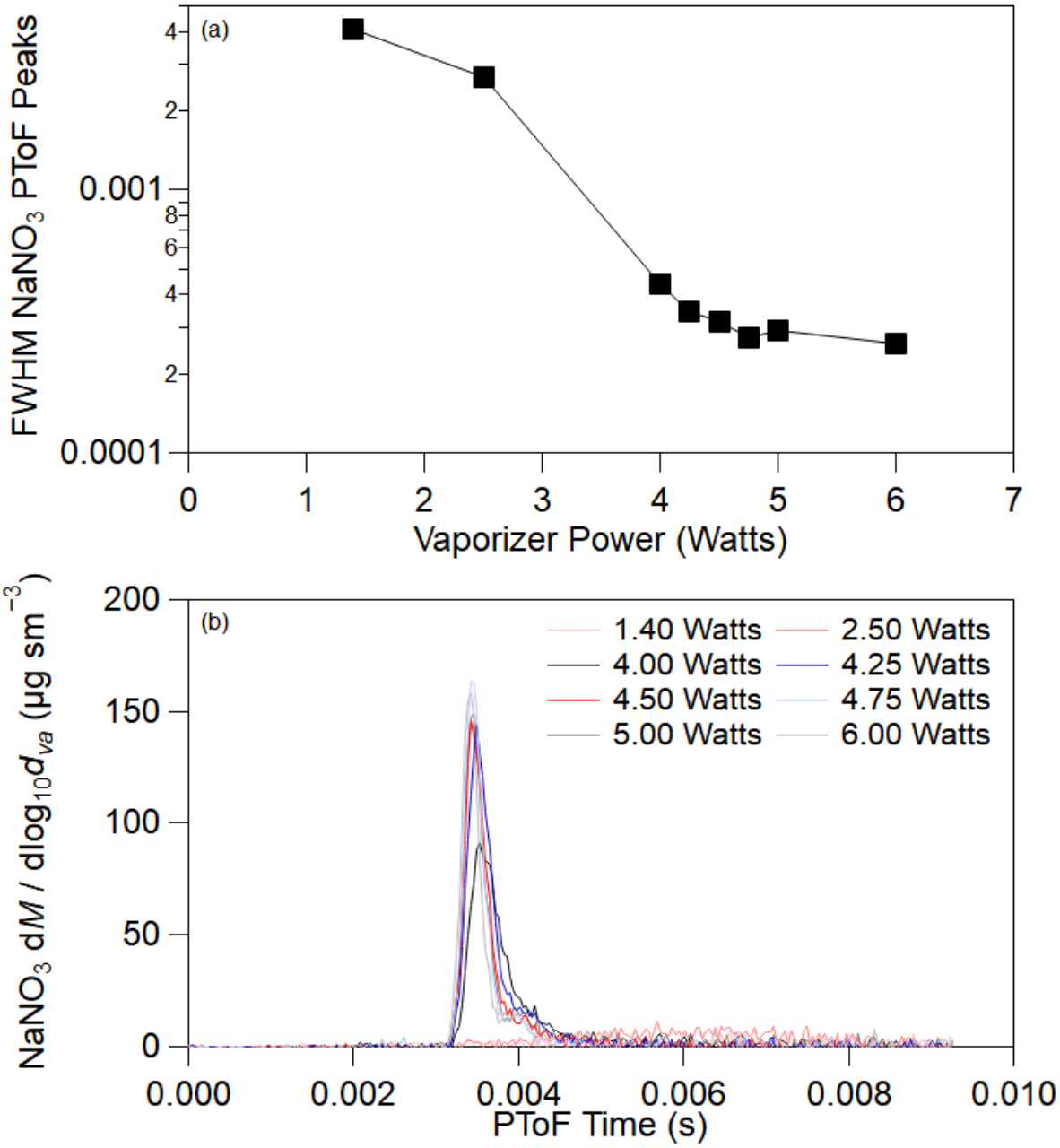

SI Figure 8. (a) Full-width half-maximum (FWHM) of $NaNO_3$ size distributions in PToF mode (b) vs. different vaporizer power inputs. See text for further details.

SI 3. Application of Positive Matrix Factorization (PMF)

Positive matrix factorization analysis (PMF, performed using the CU-Boulder PMF Evaluation Tool PET-Panel v3.00A, http://cires1.colorado.edu/jimenez-group/wiki/index.php/PMF-AMS_Analysis_Guide#PMF_Evaluation_Tool_Software) (Ulbrich et al., 2009) was used to apportion the total OA aerosol into several components. PMF was run on the combined CU-AMS 1 min organic ion matrix for all RFs together during KORUS-AQ. A 6-factor solution was derived with an FPEAK value of 0. Based on comparisons with reference mass spectra from the AMS high-resolution spectral database (http://cires1.colorado.edu/jimenez-group/HRAMSsd/#Ambient), comparisons of time series (SI Figure 9), and correlations with other trace species (SI Figure 11), the factors were recombined into more-oxidized, oxidized organic aerosol (MO-OOA), less-oxidized, oxidized aerosol (LO-OOA), and hydrocarbon-like organic aerosol (HOA) (SI Figure 10). HOA correlated with primary emissions (e.g., NO_x, various hydrocarbons) whereas LO-OOA and MO-OOA correlated with secondary photochemical products (e.g., CH_2O, PAN, pNO_3, SO_4). Here, primary OA is defined as the HOA factor and total oxidized OA (OOA) as the LO-OOA plus MO-OOA factors. OOA is assumed to be dominantly composed of secondary organic aerosol, which is supported by its strong correlation with other secondary photochemical products as documented in the paper, as well as by many prior studies (e.g., Jimenez et al., 2009; and references therein).

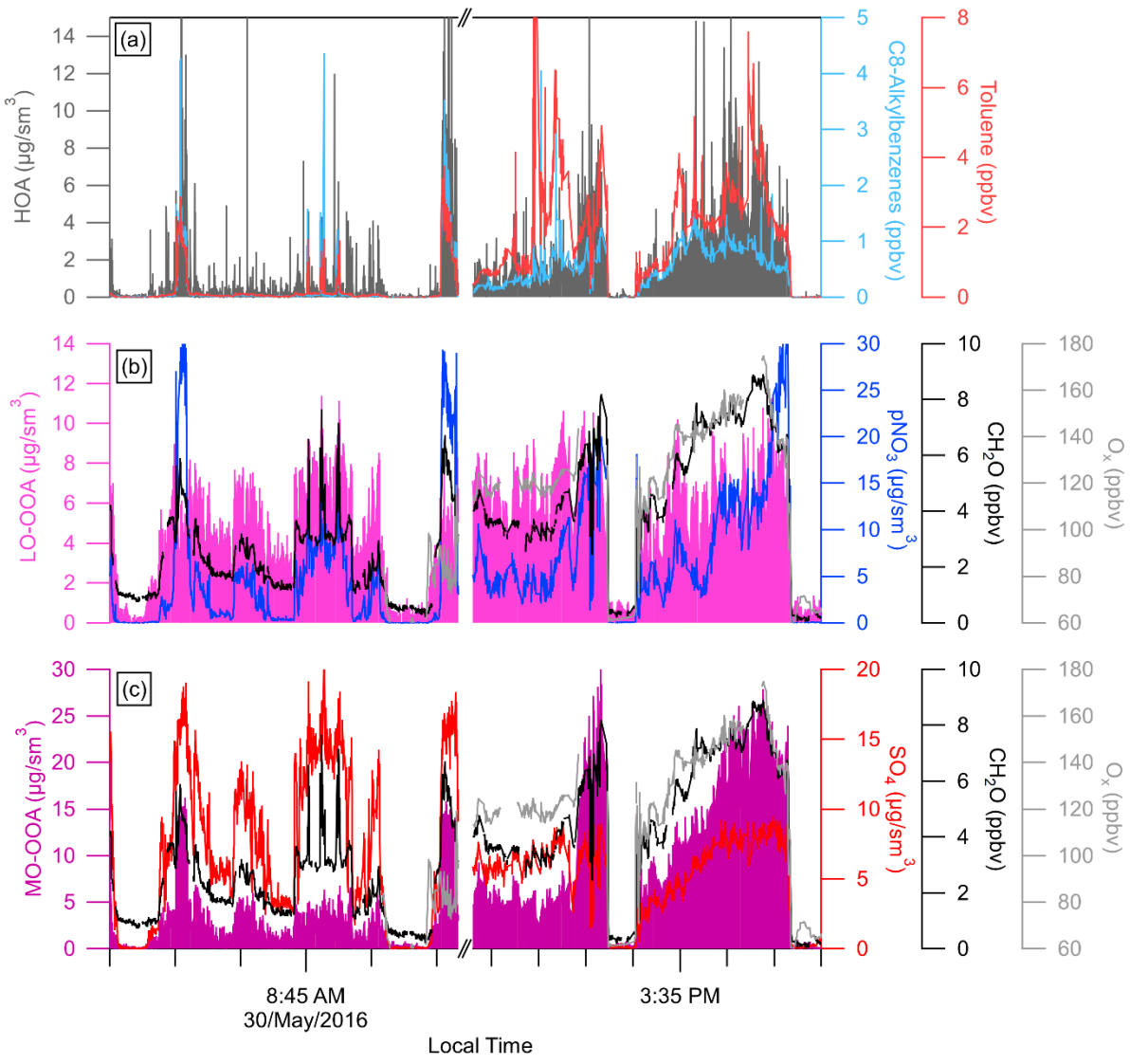

SI Figure 9. Example time series of the 3 PMF ((a) HOA, (b) LO-OOA, and (c) MO-OOA) results (left axes) and some species that correlate with the corresponding PMF results (right axes) from RF14. The morning and afternoon overpasses over Seoul, South Korea, are shown.

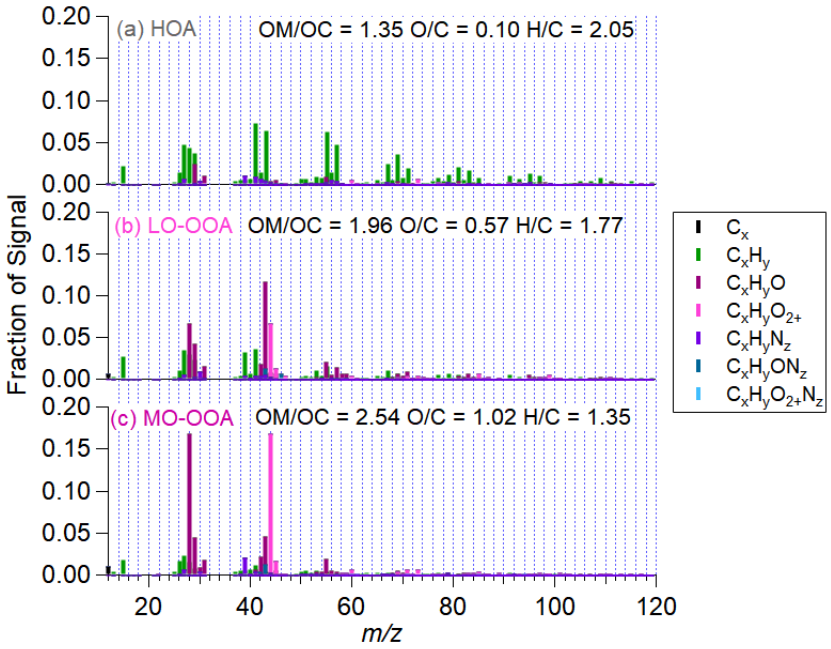

SI Figure 10. Mass spectra for PMF solution (a) HOA, (b) LO-OOA, and (c) MO-OOA for all of KORUS-AQ.

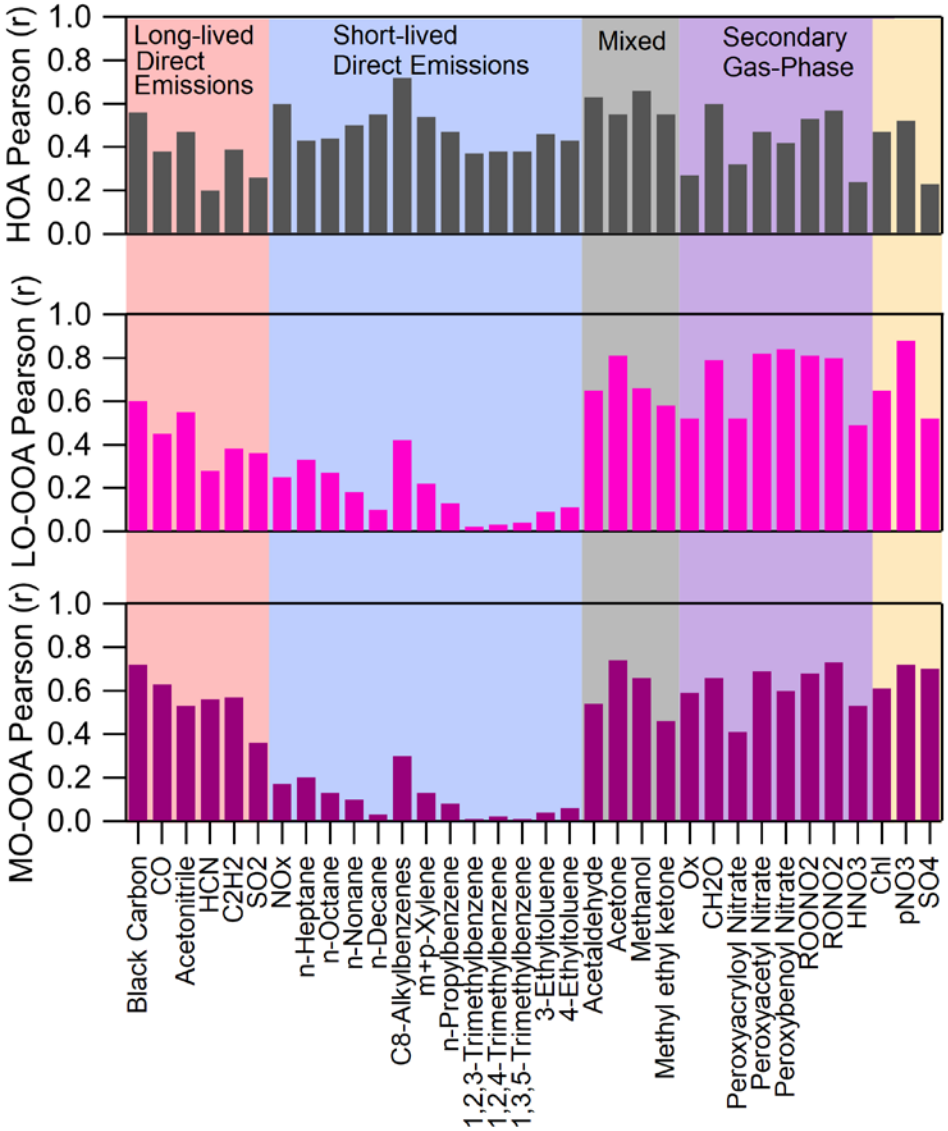

SI Figure 11. Pearson correlation coefficients for HOA (grey, top), LO-OOA (light pink, middle), and MO-OOA (dark pink, bottom) factors versus species listed in x-axis. The background colors represent the dominant group of sources of the correlating species. The yellow in the far right indicates other PM_1 components measured by the CU-AMS.

SI 4. Oxidation Flow Reactor (OFR) Sampling

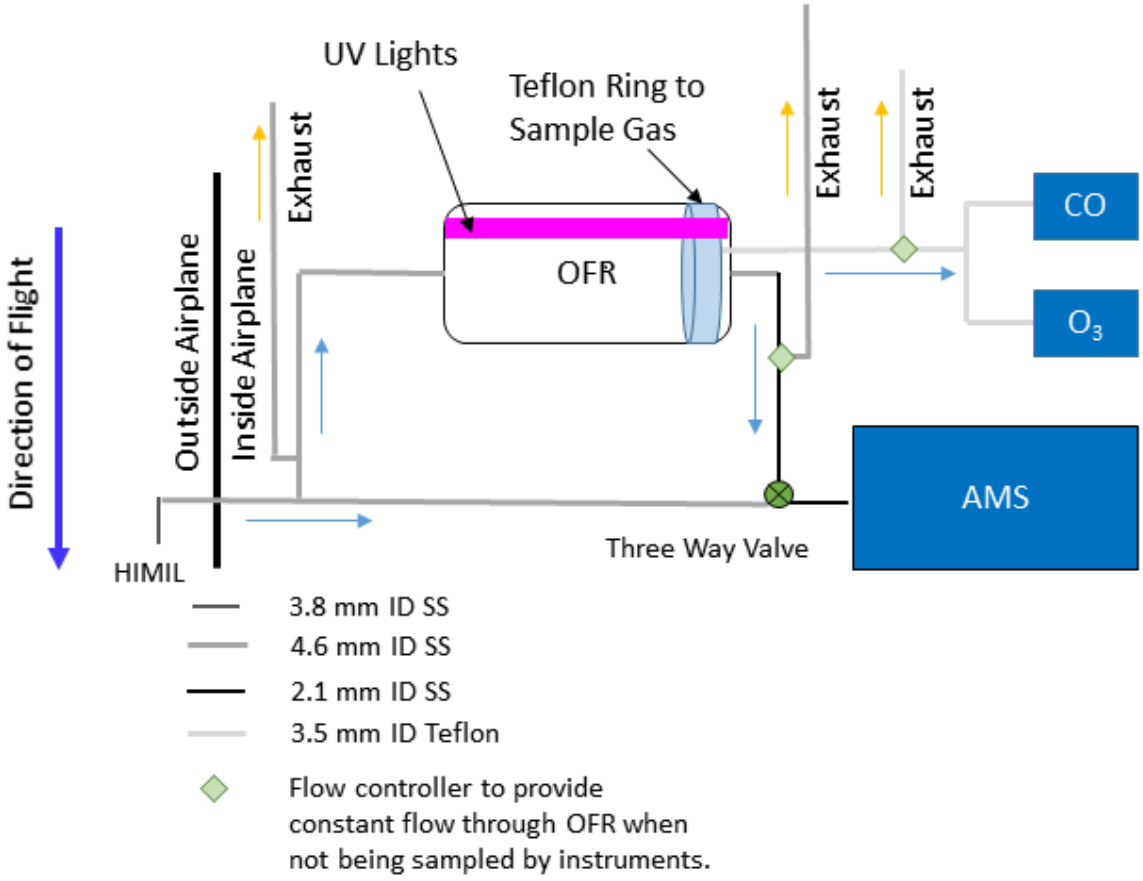

SI Figure 12. Schematic of the OFR sampling during KORUS-AQ. UV lamp is represented by the purple light in the OFR. Size and type of tubing is represented in figure, where ID is internal diameter and SS is stainless steel. Tubing distances were always as short as feasible and often shorter than represented, but they are stretched in this drawing for clarity

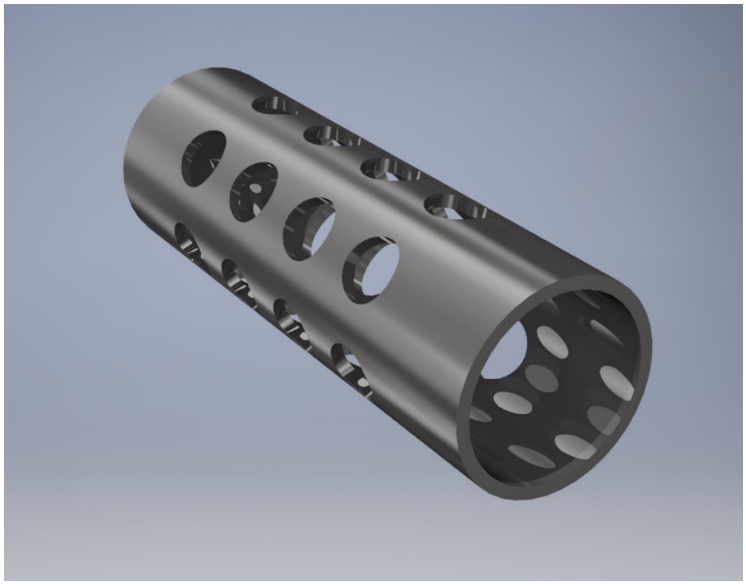

SI Figure 13. 3D rendition of the computer model of the ½" press fitted stainless steel inlet, coated in SilcoNert (SilcoTek Co, Bellefonte, PA), used in the inlet of the OFR during KORUS-AQ, to avoid "short-circuiting" between the inlet and outlet of the OFR.

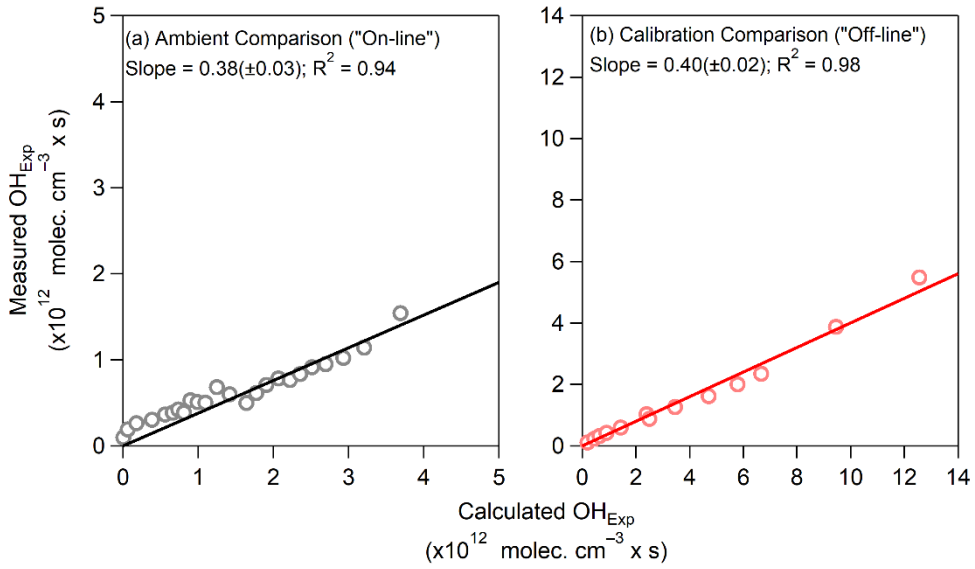

SI Figure 14. (left) Measured OH_{exp} from the decay of CO in ambient air (measured by the DACOM instrument, see text) and OFR output air (measured by the Picarro instrument) and (right) measured OH_{exp} from the decay of CO from a calibration cylinder versus calculated OH_{exp} using the predictive expression in Peng et al. (2015). The calibration factor determined by this analysis was similar to past studies (Palm et al., 2016) and was applied to all data shown in this paper.

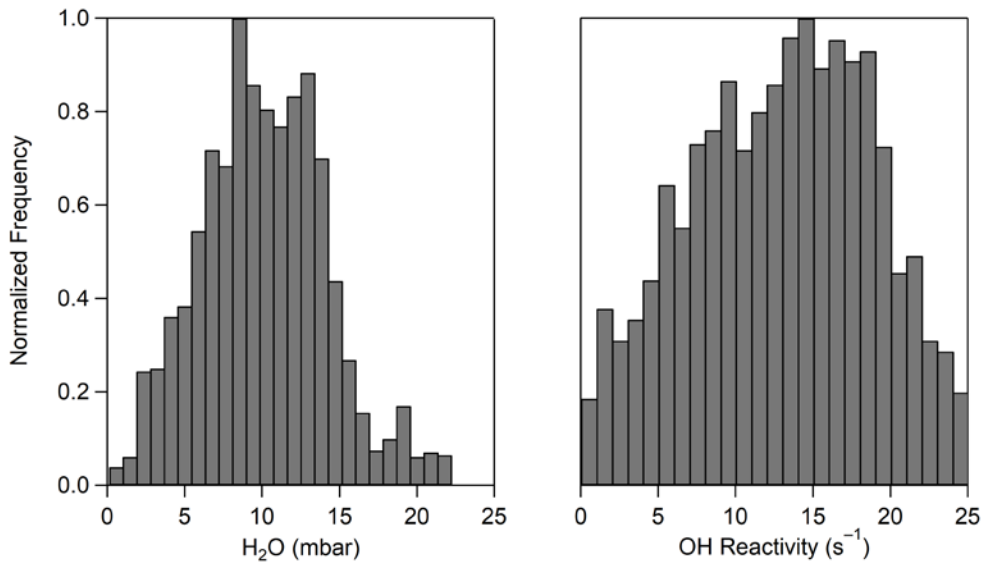

SI Figure 15. (left) Frequency distribution of water vapor below 2 km during KORUS-AQ. (right) Normalized histogram of measured OH reactivity (OHR) below 2 km during KORUS-AQ.

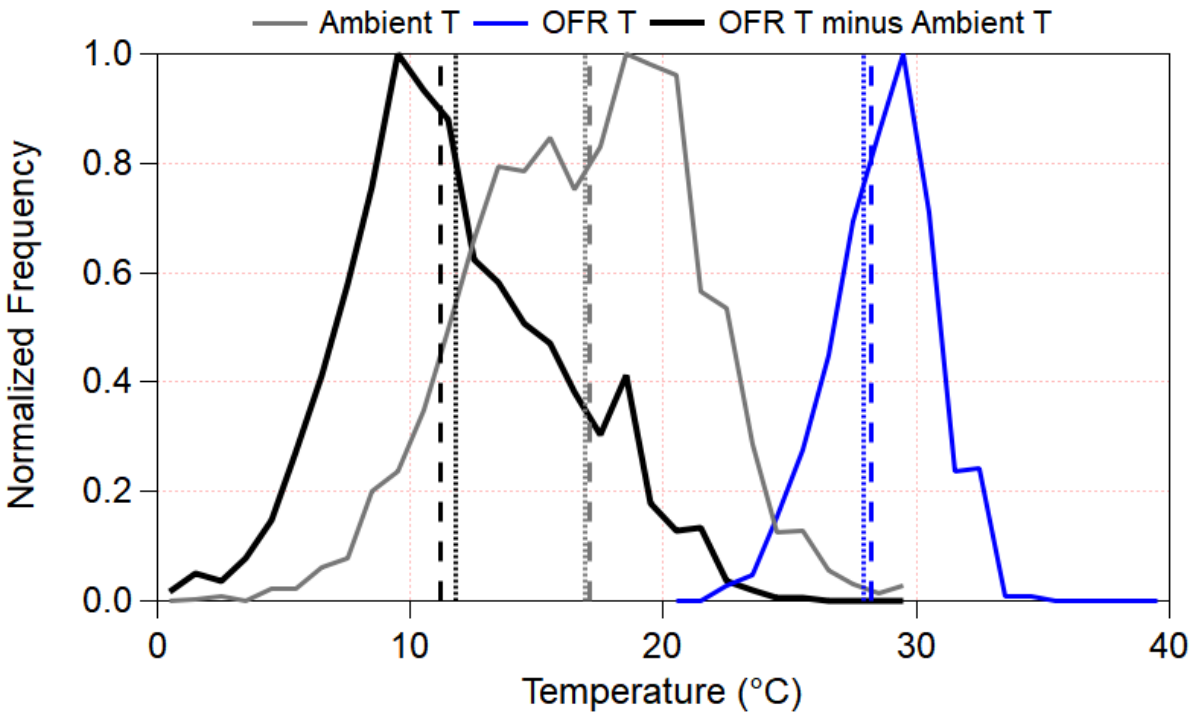

SI Figure 16. Frequency distribution of the ambient (black), OFR (blue), and difference between OFR and ambient temperature (grey) (°C). Vertical lines show the mean (long-dashed) and median (short-dashed) temperatures for the ambient, OFR, and difference between the two.

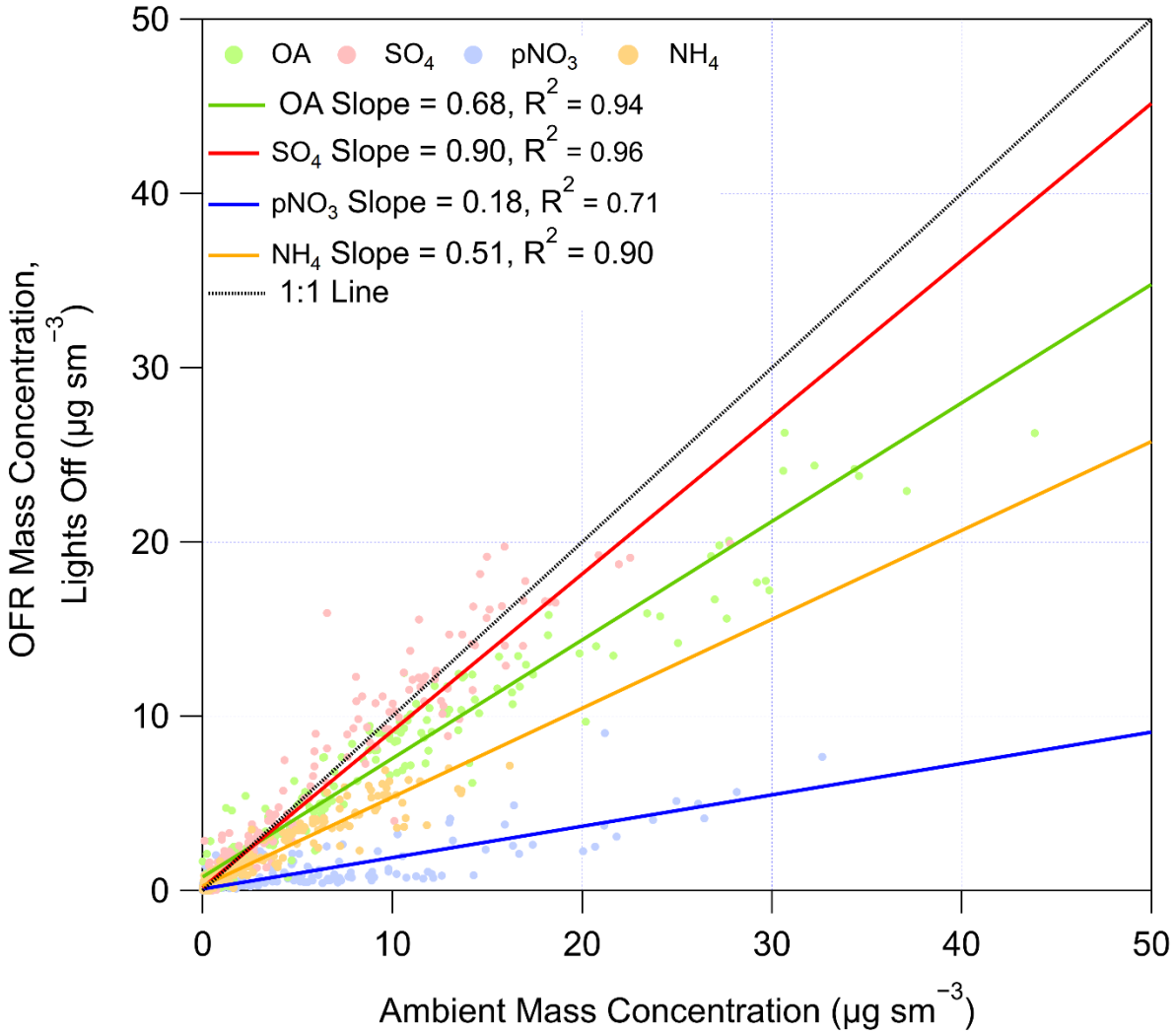

SI Figure 17. Comparison of organic (green), sulfate (red), nitrate (blue), and ammonium (orange) aerosol sampled through the OFR, with lights off, versus ambient aerosol. Under these conditions the OFR is just acting as a thermal denuder (e.g. Huffman et al., 2009), leading to evaporation of some aerosols due to increased temperature in the aircraft cabin vs. outside. In addition, small particle losses in lines and the OFR are observed for sulfate, which is generally non-volatile. Figure is adapted from Heim et al. (2018). See text for further details and discussion.

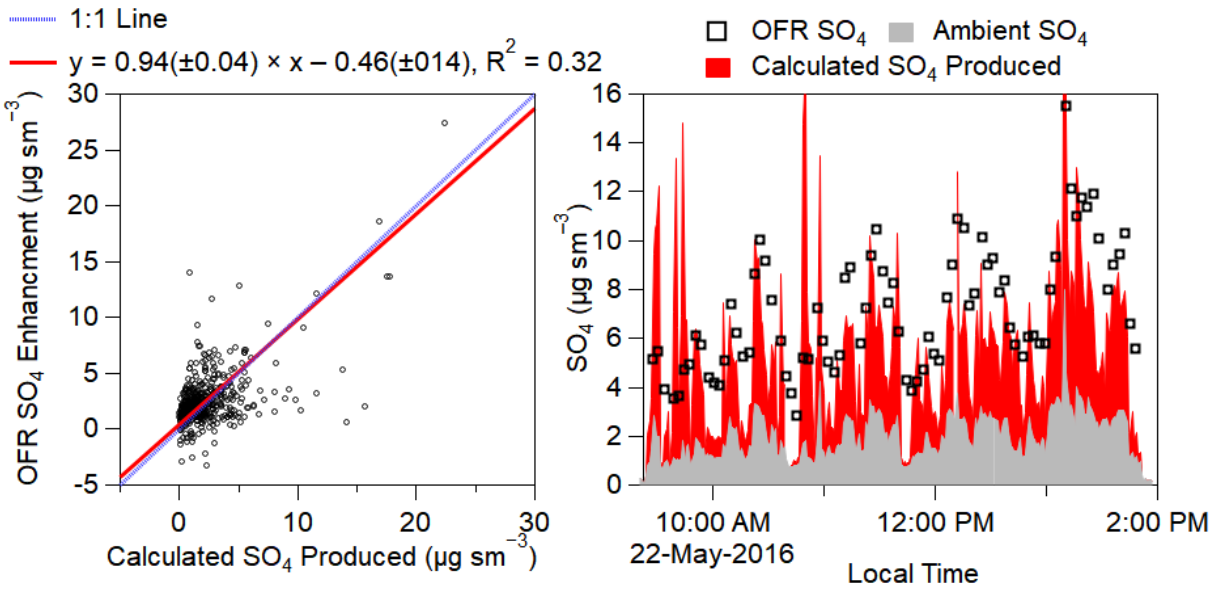

SI Figure 18. (a) Scatter plot of OFR SO_4 Enhancement (OFR – Ambient) versus calculated SO_4 produced, using SO_2 observations, estimated OH_{exp}, and condensation fate correction. (b) Time series of OFR SO_4 (black squares), ambient SO_4 (light grey), and calculated SO_4 (dark red) for the RF11 flight.

Analysis of CS Values for KORUS-AQ

If we used the condensational sink from just the ambient data, which neglects the added particle surface area formed in the OFR as described in Section 2.4 and Eq. 1 (Ortega et al., 2016; Palm et al., 2016, 2017, 2018), the agreement between calculated and measured SO_4 enhancement decreases to a slope of 0.74 (R^2 = 0.28), indicating that the condensational sink is likely too low. This suggests that, to first order, the aerosol surface area, estimated from observations and Eq. 1 (in the main paper), provides a reasonable estimate of the condensational sink within the OFR during KORUS-AQ. Thus, similar to other studies (Ortega et al., 2016; Palm et al., 2016, 2017, 2018), we find, at the typical OH_{exp} in the OFR, that 50 – 60% of the oxidized condensable organic gases are condensing onto aerosol, with 20 – 25% undergoing further reactions with OH leading to highly volatile compounds, 8 – 13% exiting the OFR prior to condensing on aerosol, and 12%

condensing to the wall (SI Figure 19). Note that the further reactions with OH are not relevant for H_2SO_4, and thus they have not been included in the analysis shown in in Fig. SI-18.

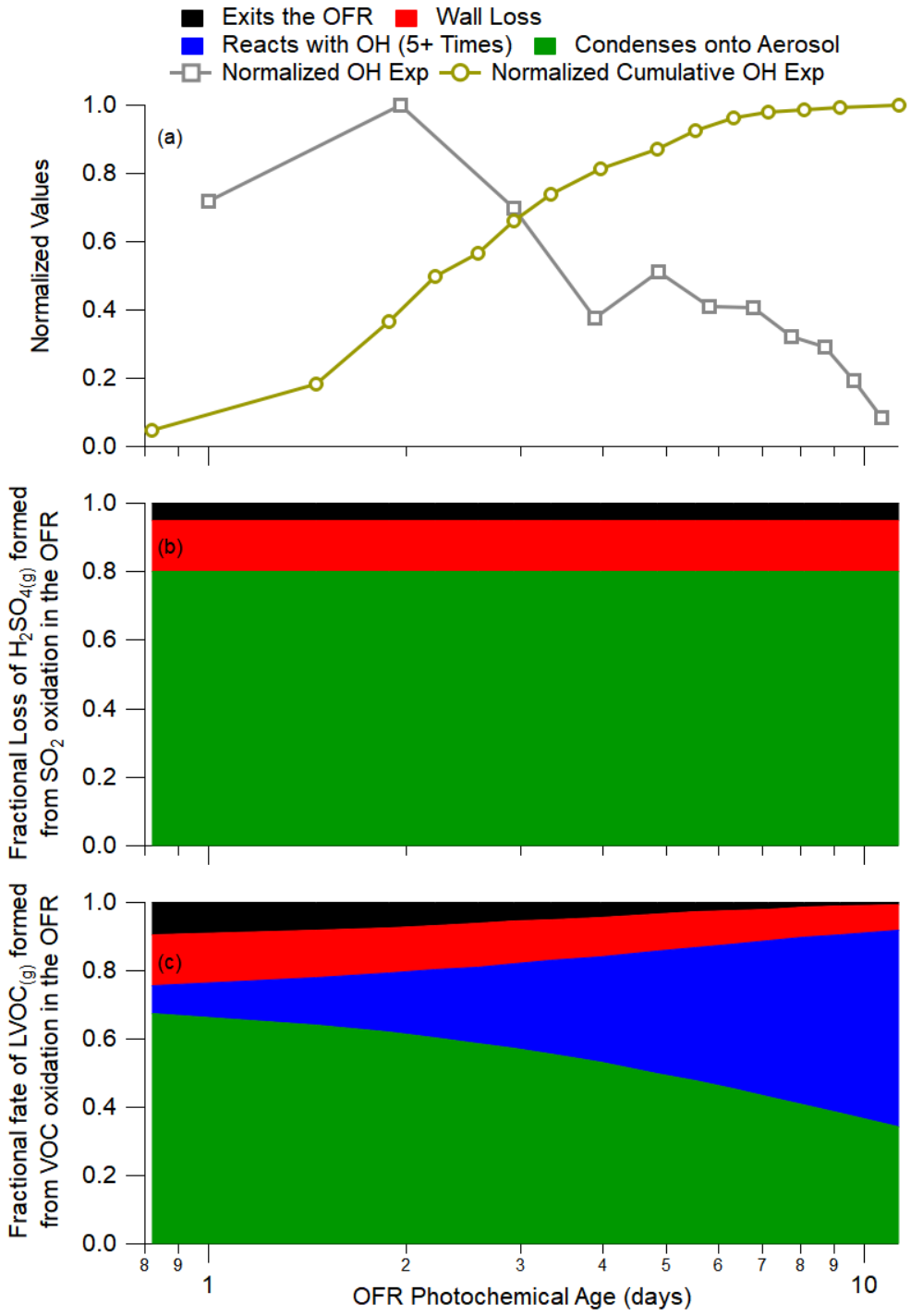

SI Figure 19. (a) Observed normalized frequency and cumulative frequency of OH Exposure observed during KORUS-AQ in the OFR. (b) Calculated fate of the SO_2 oxidized in the OFR

versus OFR OH Exposure. (c) Calculated fate of low-volatility condensable vapors (formed from VOC oxidation) versus OFR OH Exposure. For (b) and (c), the losses include flowing through the OFR without condensing onto aerosol (black), condensing onto the wall (red), condensing onto the aerosol (assuming a median value of 85.8 s, green), and reacting with OH enough to make it too volatile to condense onto aerosol (blue).

SI 5. Calculation of Photochemical Age over Seoul, South Korea

The photochemical clock calculations used throughout this work are described here. The rate constants used for these clocks are located in SI Table 3. For the NO_x/NO_y photochemical clock (e.g., Kleinman et al., 2007) (herein referred to as the NO_x photochemical clock), Eq. S1 is used, with the updated rate constant from Mollner et al. (2010).

$$t = \frac{ln\left(\frac{NO_x}{NO_y}\right)}{k_{OH+NO_2}[OH]} \quad \text{(S1)}$$

where *t* is the time, in days, [OH] is assumed to be 1.5×10^6 molecules/cm^3 (for standarization), and NO_x and NO_y are the chemiluminescence measurements. The NO_x clock is used for photochemical ages less than 1 day to (1) reduce the effect of loss of HNO_3 and other oxidized reservoirs due to deposition (lifetime ~6 hours) (Neuman et al., 2004; Nguyen et al., 2015; Romer et al., 2016) and (2) to ensure that t was still sensitive (and precise) to the NO_x and NO_y concentrations (~20% of NO_x still remaining at *t* = 1 day).

For the aromatic photochemical clock over Seoul, the more reactive aromatics (ethylbenzene in the denominator) are utilized, which should be more sensitive to the short photochemical aging observed over Seoul (Parrish et al., 2007), along with Eq. SS2.

$$t = -\frac{1}{[OH]\times\left(k_{aromatic_i}-k_{ethylbenzene}\right)} \times \left(ln\left(\frac{aromatic_i(t)}{ethylbenzene(t)}\right) - ln\left(\frac{aromatic_i(0)}{ethylbenzene(0)}\right)\right) \quad \text{(S2)}$$

where *t* is the time, in hours, the *k*'s are the corresponding OH rate constants for each aromatic compound (SI Table 3), and the third term ($\ln\left(\frac{\text{aromatic}_i(0)}{\text{ethylbenzene}(0)}\right)$) corresponds to the emission ratios for those two aromatic compounds. Similar to the NO_x clock, we assume [OH] = 1.5×10^6 molecules/cm^3 for standardization. The aromatics measurements used in this calculation are from WAS.

To evaluate which aromatic compounds to use in the clock, the behavior of the ratios of each aromatic compound with ethylbenzene versus the three missed approaches (morning, noon, and afternoon) over Seoul during KORUS-AQ (SI Figure 20) are compared. The idea is that if the 2 aromatic compounds are co-emitted, the ratios should be removed proportionally to their OH rate constants. E.g. for faster reacting compounds (e.g., o-xylene), the ratio to ethylbenzene should decrease with time as more o-xylene was consumed, compared to ethylbenzene, by OH (de Gouw et al., 2017). On the other hand, for slower reacting compounds (e.g., toluene), the ratio to ethylbenzene should increase with time as more ethylbenzene was consumed by OH. Also, this analysis provides an indication of which ratios would provide meaningful results throughout the entire day (de Gouw et al., 2017). Ideally, there should be a decrease with each later missed approach, and not a leveling off after two missed approaches (e.g., the trimethylbenzenes and ethyltoluenes). Only the m+p-xylene/ethylbenzene and o-xylene/ethylbenzene ratios meet this criterion. Finally, to determine the emission ratios, we calculated what the m+p-xylene/ethylbenzene and o-xylene/ethylbenzene ratio was for observations where the NO_x photochemical was less than 0.07 days (corresponding to less than 10% of either species being consumed). Comparing these two aromatic clocks to the NO_x photochemical clock (SI Figure 21), a similar agreement between the two aromatic clocks with the NO_x photochemical clock was observed, providing confidence in using all three clocks to calculate photochemical age to evaluate OA production over Seoul. For the remainder of the paper, we mainly use the NO_x photochemical clock to eliminate the uncertainty of the emission ratios, unless otherwise noted.

Finally, for observations over the West Sea, the aromatic clock (Eq. SS2) was used, but benzene and toluene were used since these air masses are more photochemically processed (Parrish et al., 2007). For the emission ratios, values reported by Yuan et al (2013) were used.

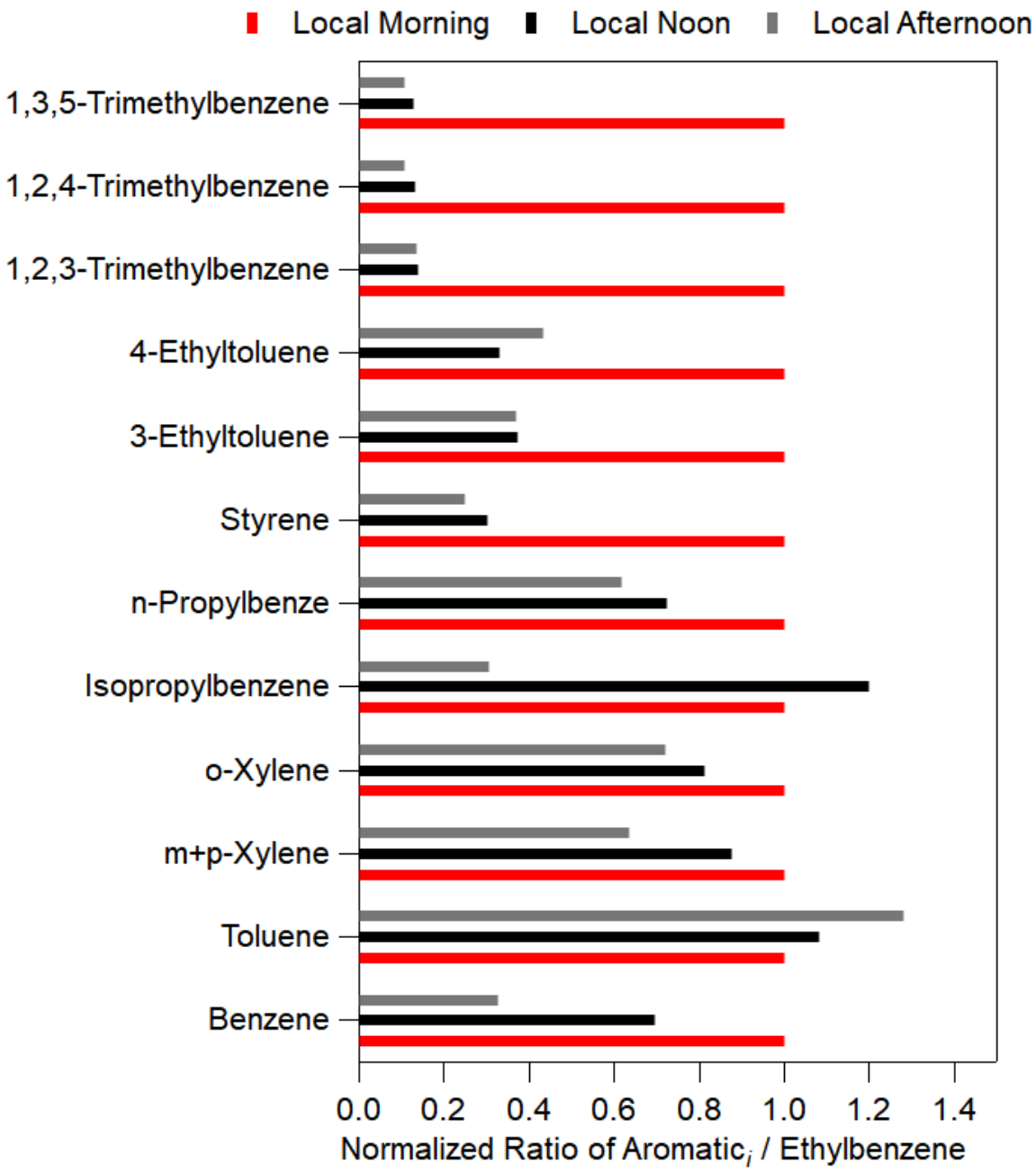

SI Figure 20. Comparison of various aromatic compounds/ethylbenzene ratios sampled over Seoul, South Korea, during KORUS-AQ. The ratios are normalized by the morning ratios.

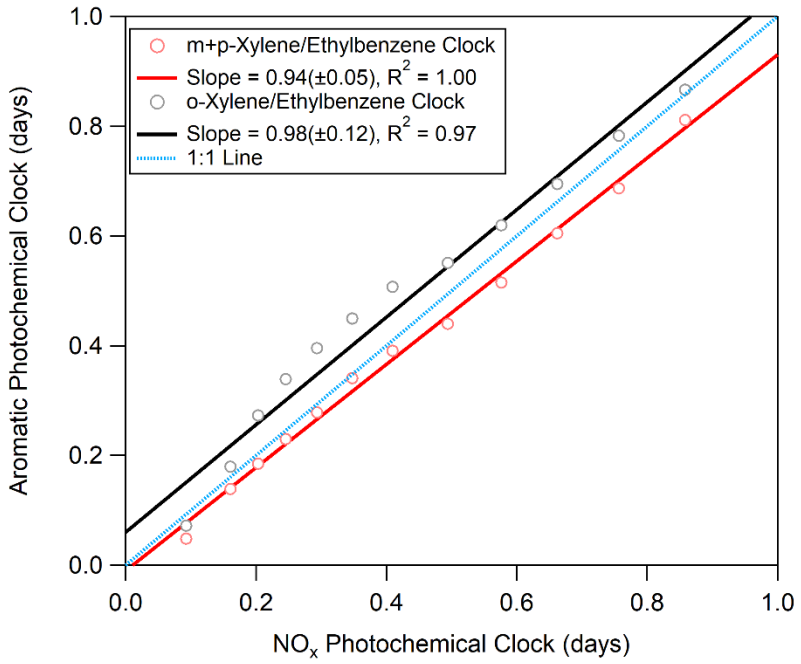

SI Figure 21. Binned scatter plot of the aromatic photochemical clock ages versus NO_x photochemical clock ages for all observations over Seoul. All ages are normalized to OH = 1.5×10^6 molecules/cm^3.

SI Table 3. Rate constants used throughout this study. Unless noted otherwise, rate constants without temperature dependence only have a value measured at 298 K.

Reaction	Rate Constant (cm^3/molecules/s)	Reference
Inorganic		
CO	$2.28\times10^{-13,a}$	Sander et al. (2011)
NO_2	$1.23\times10^{-11,a}$	Mollner et al. (2010)
SO_2	$8.94\times10^{-13,a}$	Atkinson et al. (2004)
Alkanes		
Ethane	$6.9\times10^{-12}\times\exp(-1000/T)$	Atkinson et al. (2006)
Propane	$7.6\times10^{-12}\times\exp(-585/T)$	Atkinson et al. (2006)
n-Butane	$9.8\times10^{-12}\times\exp(-425/T)$	Atkinson et al. (2006)
i-Butane	$1.17\times10^{-17}\times T^2\times\exp(213/T)$	Atkinson (2003)
n-Pentane	$2.52\times10^{-17}\times T^2\times\exp(158/T)$	Atkinson (2003)
i-Pentane	3.6×10^{-12}	Atkinson (2003)
n-Hexane	$2.54\times10^{-14}\times T\times\exp(-112/T)$	Atkinson (2003)
Methyl-cyclopentane	7.65×10^{-12}	Sprengnether et al. (2009)
Cyclohexane	$3.26\times10^{-17}\times T^2\times\exp(262/T)$	Atkinson (2003)
Methyl-cyclohexane	9.43×10^{-12}	Sprengnether et al. (2009)
n-Heptane	$1.95\times10^{-17}\times T^2\times\exp(406/T)$	Atkinson (2003)
n-Octane	$2.72\times10^{-17}\times T^2\times\exp(361/T)$	Atkinson (2003)
n-Nonane	$2.53\times10^{-17}\times T^2\times\exp(436/T)$	Atkinson (2003)
n-Decane	$3.17\times10^{-17}\times T^2\times\exp(406/T)$	Atkinson (2003)
Alkenes		
Ethylene	$7.84\times10^{-12,a}$	Atkinson et al. (2006)
Propene	$2.86\times10^{-11,a}$	Atkinson et al. (2006)
1-butene	$6.6\times10^{-12}\times\exp(465/T)$	Atkinson et al. (2006)
i-butene	$9.4\times10^{-12}\times\exp(505/T)$	Atkinson et al. (2006)
cis-butene	$1.1\times10^{-11}\times\exp(485/T)$	Atkinson et al. (2006)
trans-butene	$1.0\times10^{-11}\times\exp(553/T)$	Atkinson et al. (2006)
1,3-butadiene	$1.48\times10^{-11}\times\exp(448/T)$	Atkinson and Arey (2003)
Aromatics		
Benzene	$2.3\times10^{-12}\times\exp(-190/T)$	Atkinson et al. (2006)
Toluene	$1.8\times10^{-12}\times\exp(340/T)$	Atkinson et al. (2006)
Ethylbenzene	7×10^{-12}	Atkinson and Arey (2003)
Isopropylbenzene	6.3×10^{-12}	Atkinson and Arey (2003)
n-propylbenzene	5.8×10^{-12}	Atkinson and Arey (2003)
Styrene	5.8×10^{-11}	Atkinson and Arey (2003)
m+p-xylene	$1.87\times10^{-11,b}$	Atkinson and Arey (2003)
o-xylene	1.36×10^{-11}	Atkinson and Arey (2003)
1,3,5-trimethylbenzene	$1.32\times10^{-11}\times\exp(450/T)$	Bohn and Zetzsch (2012)
1,2,3-trimethylbenzene	$3.61\times10^{-12}\times\exp(620/T)$	Bohn and Zetzsch (2012)
1,2,4-trimethylbenzene	$2.73\times10^{-12}\times\exp(730/T)$	Bohn and Zetzsch (2012)
3-Ethyltoluene	1.2×10^{-11}	Atkinson and Arey (2003)
4-Ethyltoluene	1.2×10^{-11}	Atkinson and Arey (2003)
S/IVOCs		

S/IVOC	2×10^{-11}	Ma et al. (2017)
Biogenics		
Isoprene	$2.7\times10^{-11}\times\exp(390/T)$	Atkinson et al. (2006)
α-pinene	$1.2\times10^{-11}\times\exp(440/T)$	Atkinson et al. (2006)
β-pinene	$1.55\times10^{-11}\times\exp(467/T)$	Atkinson and Arey (2003)
Radicals		
$NO + RO_2$	$2.8\times10^{-12}\times\exp(300/T)$	Sander et al. (2011)
$HO_2 + RO_2$	$4.1\times10^{-13}\times\exp(750/T)$	Sander et al. (2011)
$RO_2 + RO_2$	$9.5\times10^{-14}\times\exp(390/T)$	Sander et al. (2011)

[a]Showing the rate constant at 298 K, 1013 hPa. However, for this study, we used the temperature and pressure dependent formulation listed in each respective reference.
[b]This is the average of m-xylene and p-xylene rate constants.

SI 6. Potential SOA Calculations

To determine the amount of SOA produced from the observed precursors, Eq. S3 was used, where *Y* is the stoichiometric aerosol yield for each hydrocarbon (RH) species *i,* similar to other studies (e.g., Zhao et al., 2014). The updated yields from Ma et al. (2017) were used, which incorporate a correction for the gas-phase partitioning of semi-volatile compounds to chamber walls (Krechmer et al., 2016). Since there were no direct measurements of S/IVOC concentrations, an estimated (Robinson et al., 2007; Dzepina et al., 2009) relationship between the amount of gas-phase S/IVOC co-emitted with POA at the typical temperatures (~20°C) and OA mass concentrations (~10 μg sm^{-3}) observed over Seoul were used. The POA is taken from Figure 5b and is within the range of values observed in other urban environments (Zhang et al., 2005; Hayes et al., 2013; Ait-Helal et al., 2014; Kim et al., 2018) (13 μg sm^{-3} $ppmv^{-1}$ in Seoul versus 4.5 – 28.8 μg sm^{-3} $ppmv^{-1}$ in other studies).

$$P(OA) = \sum_i Y_i \times \Delta RH_i \quad \text{(S3)}$$

$$\Delta RH = \frac{RH(t)}{e^{(-k[OH]t)}} - RH(t) \quad \text{(S4)}$$

The hydrocarbons measured on the DC-8 were the concentrations at time, *t*; thus, Eq. SS4 was used, which takes into account the amount of OH that oxidized the hydrocarbon (OH_{exp} =

[OH]t) between emissions and measurement, and k is the OH rate constant for each specific hydrocarbon (SI Table 3).

Finally, to determine the fate of the RO_2 radical in the reactions over Seoul (high/low NO_x regime), and thus, what aerosol yields to use, the RO_2 lifetime with reaction of NO, HO_2, and RO_2 versus photochemical age was calculated (SI Figure 22). The measured NO and HO_2 was used in the calculations, we assumed RO_2 was approximately the same concentration as HO_2 in this calculation (Thornton et al., 2002), and the rate constants in SI Table 3 were used to calculated the lifetime and fractional fate of RO_2. The fate of RO_2 with autoxidation is not included as the rate is still uncertain (Crounse et al., 2013) and it should be less important in highly polluted environments such as Seoul, especially at the lower photochemical ages (< 0.5 eq. days) where most SOA is observed to be formed. The dominant sink of RO_2 over Seoul during KORUS-AQ is the reaction with NO, suggesting that the SOA yields for “high NO” conditions should be used to describe the production of SOA.

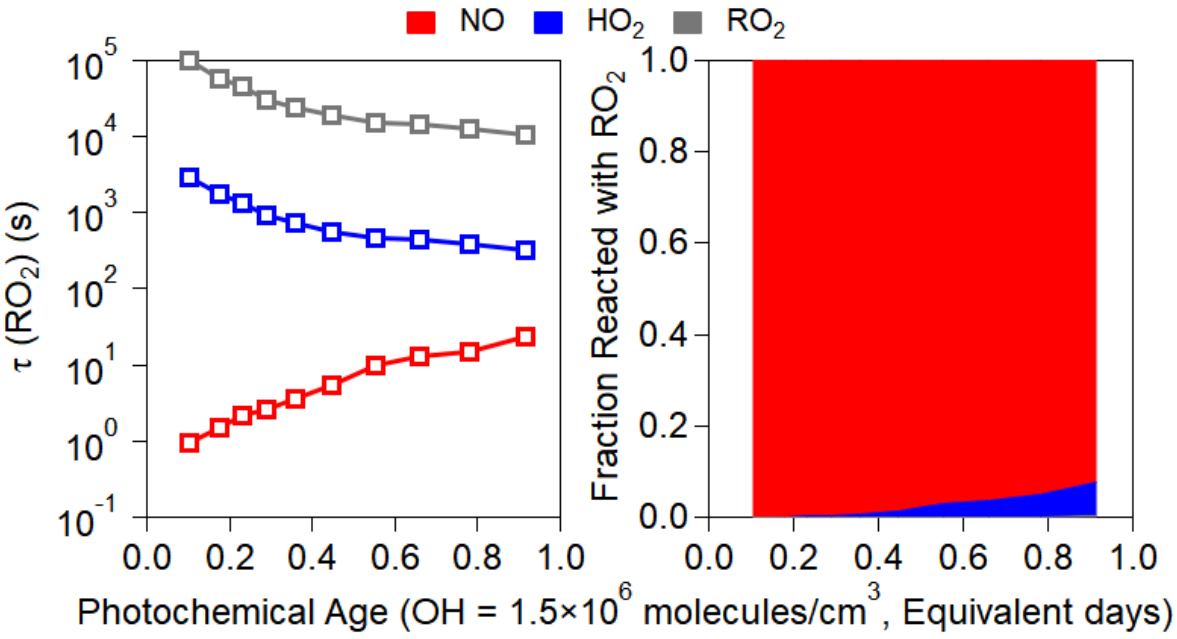

SI Figure 22. (left) Lifetime of RO_2 due to reactions with NO (red), HO_2 (blue), and RO_2 (grey) versus NO_x photochemical clock, normalized by OH = 1.5×10^6 molecules/cm^3. (right) Fraction of RO_2 reacting with NO (red), HO_2 (blue), or RO_2 (red) versus NO_x photochemical clock, normalized by OH = 1.5×10^6 molecules/cm^3. Values are calculated using observations over Seoul, South Korea, during KORUS-AQ, and RO_2 is assumed to be approximately equal to HO_2 (Thornton et al., 2002).

SI 7. FLEXPART Source Analysis

Source contributions have been estimated using Lagrangian backtrajectory calculations with the FLEXPART-WRF model (Brioude et al., 2013) in version 3.3.1, driven by meteorological output from NCEP GFS (NCEP) analyses downscaled to 5 km horizontal resolution using the Weather Research and Forecasting (WRF) model (Skamarock et al., 2008) in combination with the CREATE emission inventory (Woo et al., 2013). Approximately 20,000 parcels are released in 1 min intervals from the then-current location of the DC-8 during its research flights and parcel trajectories are followed back in time for 24 hours. The total time parcels spent in the lowermost 100 m—as surrogate for air having contact with an emission source at the ground—is recorded (residence time, [s kg^{-1} m^3]) and then folded with the emission fluxes ([kg m^{-2} s^{-1}]) given by the CREATE inventory for different compounds and source regions. This delivers an estimate of the source contribution (as increment in volume mixing ratio at the receptor, i.e., the DC-8 location) of the emissions of a given compound from a given region, assuming a perfect transport simulation and an inert compound.

SI 8. Intercomparisons of CU-AMS with Other Measurements on the NASA DC-8

We evaluate the measurement comparisons of the CU-AMS versus other aerosol measurements on-board the DC-8 during KORUS-AQ. We start with the mist chamber / ion chromatograph instrument (MC/IC), which has a comparable size cut as the AMS. The comparisons for SO_4 show good correlation ($R^2 = 0.76$) and slope close to 1 (0.95) (SI Figure 23). The higher scatter for the MC/IC is thought to arise from the lag and smearing in the measurements that has been observed in prior studies (TAbMET, 2009). For example, the correlation between instruments without lag and smearing have R^2 of 0.87 – 0.91 (CU-AMS versus extinction and CU-AMS vs K-AMS for certain RFs). If the MC/IC and CU-AMS SO_4 measurements are averaged to the sampling frequency of the University of New Hampshire filters (not shown), the R^2 improves (0.82) with no impact on the slope.

The comparison between the UNH filters and CU-AMS SO_4 shows higher R^2 (0.86) but lower slope (0.80), compared to MC/IC vs. CU-AMS. The higher R^2 is likely due to longer averaging time and lack of smearing that occurred with the MC/IC. As a comparison, the R^2 between MC/IC and filters are 0.84. The lower slope for the filters than the MC/IC is thought to be due to the different size cut-offs for the two measurements. For the filters, the upper size cut-off is ~4 μm (McNaughton et al., 2007); whereas, the upper size cut-off for the MC/IC is comparable to the AMS aerosol size cut-off (~ 1 μm aerodynamic). This means that the filter samples may include SO_4^{2-} from sea salt (sodium and calcium) and dust (calcium) (Heo et al., 2009; Kim et al., 2016; Heim et al., 2018). This is shown in SI Figure 24 and described in detail in Heim et al. (2018). Heim et al. (2018) found that dust dominated supermicron aerosol for approximately half of the campaign, and during these periods, supermicron SO_4^{2-} accounted for ~50% of the total SO_4^{2-} (sub plus supermicron). Taken together, the comparisons of SO_4 mass

concentrations from the CU-AMS from these two different methods (filter and MC/IC) indicate that the CU-AMS quantitatively captures the concentrations of SO_4.

Next, we compare the non-refractory species concentrations measured by the CU- and K-AMS. Intercomparisons between these two measurements for a few flights have been presented in prior publications (Hu et al., 2018a, 2018b). The K-AMS used a capture vaporizer, which leads to CE of ~1 for all ambient species (Hu et al., 2017a, 2017b; Xu et al., 2017). Here, we investigate the entire campaign. As shown in SI Figure 25, $R^2 > 0.80$ for all five species, and all slopes fall within ±20% of unity, which is within the combined uncertainty of both AMSs (~27%). However, at high concentrations (greater than ~5 – 10 μg sm^{-3}), the scatter between the two measurements increases, and for some species (e.g., SO_4), there is a slight curvature in the comparisons, where CU-AMS is greater than K-AMS. We believe this discrepancy originated from differences in transmission vs. particle size through the aerosol inlet and focusing lens (SI Figure 26). In-field calibrations showed that The K-AMS had 50% transmission at 615 nm (vacuum aerodynamic diameter; DeCarlo et al. (2004)), compared to the CU-AMS 50% transmission occurring at 900 nm. The reasons for the smaller transmission of the K-AMS are likely related to the PCI design (Bahreini et al., 2008, 2009) or possibly an underperforming aerodynamic lens in K-AMS (Liu et al., 2007). It was found that, in general, the RFs could be split between RFs generally below the K-AMS size cut-off (RFs 1 – 9, 11, 15, and 19) and above the size cut-off (RFs 10, 12 – 14, 16 – 18, 20) (SI Figure 27). The slopes and R^2 greatly improves for the observations below the K-AMS cut-off versus above (for slopes, 1.02 versus 0.84 and for R^2, 0.91 versus 0.82).

Finally, the ratios of the total AMS PM_1 masses measured by CU-AMS and K-AMS remain nearly constant about one (within ±11%) for the entire campaign and show no trend with estimated CE (for the standard vaporizer only) using the Middlebrook et al. (2012) algorithm (SI Figure 28).

Thus, when accounting for transmission effects, the two AMSs agree to within 10%, and the CU-AMS agrees to within 20% with the other co-located aerosol mass concentration measurements (filters and MC/IC) on the DC-8. This provides overall confidence in the calculated CE for the standard vaporizer (Middlebrook et al., 2012), RIE, and transmission of PM_1 for the CU-AMS measurements.

Besides directly comparing species mass, another well-established method to investigate aerosol instrument quantification is to compare the measured PM_1 mass (CU-AMS plus BC from SP2) versus the submicron extinction measured using methods described in Section 2.3.2 (nephlometer for scattering and absorption by PSAP) (e.g., DeCarlo et al., 2008). During KORUS-AQ, the slope between mass and extinction is 6.00 $m^2\ g^{-1}$ (SI Figure 29) with an R^2 of 0.87. The high correlation and similar slope compared to prior comparisons (Hand and Malm, 2007; DeCarlo et al., 2008; Dunlea et al., 2009; Shinozuka et al., 2009; Liu et al., 2017) indicates that the CU-AMS was not substantially impacted by the aerosol transmission effects discussed above. Also, the strong correlation ($R^2 = 0.87$) between the two instruments, which both have comparable, very high time resolution, indicate that the CU-AMS did not experience any plume recovery artifacts that were observed with the MC/IC or artifacts in measuring highly concentrated plumes.

Finally, we compare the PM_1 volume concentrations estimated from the LAS PM_1 versus the CU-AMS plus SP2. For this comparison, we use the calibrated AMS transmission curve during this campaign (SI Figure 30), which is consistent with those from recent studies (Knote et al., 2011; Hu et al., 2017b), to correct for particle transmission differences between the instruments. The LAS diameters were corrected by a factor of 1.115 from the PSL-calibrated values, to account for the lower refractive index of ambient particles, similar to Liu et al. (2017). To estimate the volume concentration from the combined AMS and BC measurements, we assume additive species

volumes (DeCarlo et al., 2004). Species densities of 1.78 g cm^{-3} for NH_4, pNO_3, and SO_4 (Lide, 1991; Salcedo et al., 2006), 1.52 g cm^{-3} for Chl (Lide, 1991; Salcedo et al., 2006), 1.77 g cm^{-3} for BC (Park et al., 2004), and the OA density is estimated from the CU-AMS O/C and H/C ratios of OA using the parameterization of Kuwata et al. (2012). The comparison between total PM_1 volume estimated from the CU-AMS plus BC vs. versus LAS shows a correlation (R^2) of 0.86. However, the volume from AMS plus SP2 is higher (slope of 1.56) when comparing all of KORUS-AQ. We hypothesize that this may be due to saturation of the LAS detector at high particle concentrations that were frequently observed in this campaign (greater than 1800 particles cm^{-3} or total CU-AMS plus SP2 mass greater than 40 μg sm^{-3}), as has been observed in prior comparisons (Liu et al., 2017), or a change in the refractive index when OA becomes dominant at these high concentrations (Moise et al., 2015). Different filters are tested and shown in SI Figure 30 and SI ***Figure 31***, using both values reported in literature and values that represent a stable ratio between LAS and calculated CU-AMS plus SP2 volume. If we filter for data when there is less than 20 μg sm^{-3}, the slope drops to 1.00, showing agreement between within the combined uncertainties (R^2 = 0.79), and providing strong evidence that LAS saturation at higher concentrations is the main reason for the apparent disagreement when analyzing the entire campaign.

We further investigate (SI Figure 31) whether the slope could be due to LAS saturation or a bias in RIE_{OA}, or in CE, vs. the values used in our analyses (Jimenez et al., 2016; Xu et al., 2018). There is a slight increase in the ratio of AMS plus SP2 to LAS volumes versus OA/total CU-AMS mass at high fractions of OA, although still within the combined measurement uncertainties. With filtered data (less than 1600 particles cm^{-3} or total CU-AMS mass less than 20 μg sm^{-3}), the volume ratios remain nearly flat, even at high *f*(OA). This confirms that LAS saturation is the most likely cause for the differences. Finally, a recent study (Xu et al., 2018) has reported new laboratory

measurements of RIE_{OA} = 1.6±0.5, although these authors indicated that it was unclear whether this value was applicable to ambient particles, and the value of RIE_{OA} = 1.4 used in this study is well within their reported uncertainty. When using RIE_{OA} = 1.6 in our analysis (not shown) the slope for the entire dataset decrease by only 6% (1.56 to 1.47), indicating that RIE uncertainties cannot explain the bulk of the observed difference.

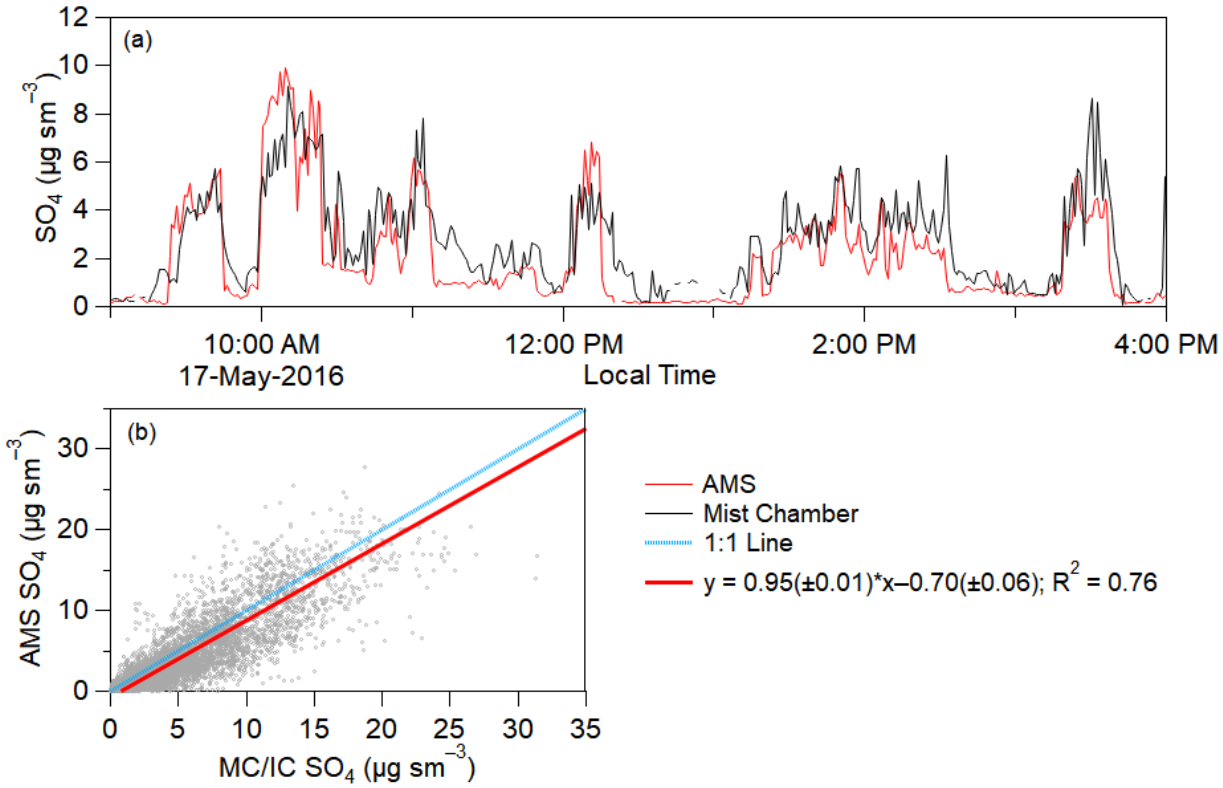

SI Figure 23. (top) Time series of mist-chamber (dark red line) and CU-AMS (red line) SO_4 for one flight (RF17). (bottom) Scatter plot of CU-AMS SO_4 versus mist-chamber ion-chromatograph (MC/IC) SO_4 for entire KORUS-AQ campaign.

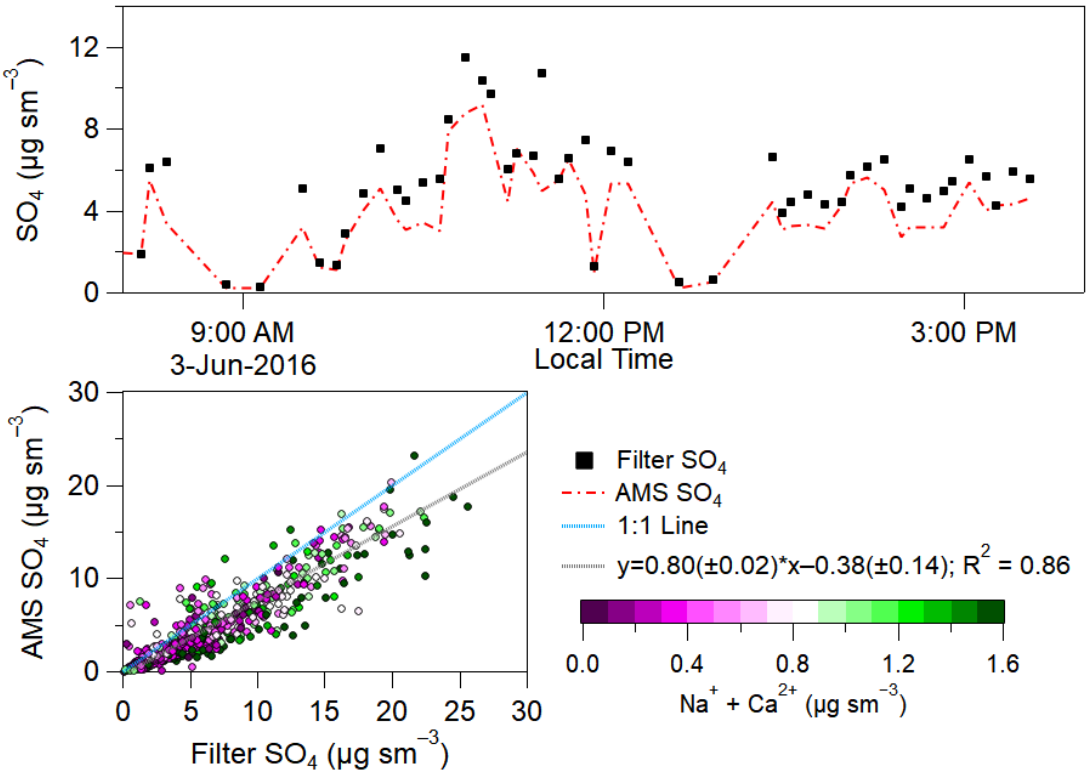

SI Figure 24. (top) Time series of filter (black squares) and CU-AMS (red line) SO_4 for one flight (RF17). The CU-AMS data has been averaged to the filter sampling time. (bottom) Scatter plot of CU-AMS SO_4 versus filter SO_4 for entire KORUS-AQ campaign. The points are colored by the total sodium (Na^+) and calcium (Ca^{2+}) measured by the filters, as indicators of sea salt and dust, respectively.

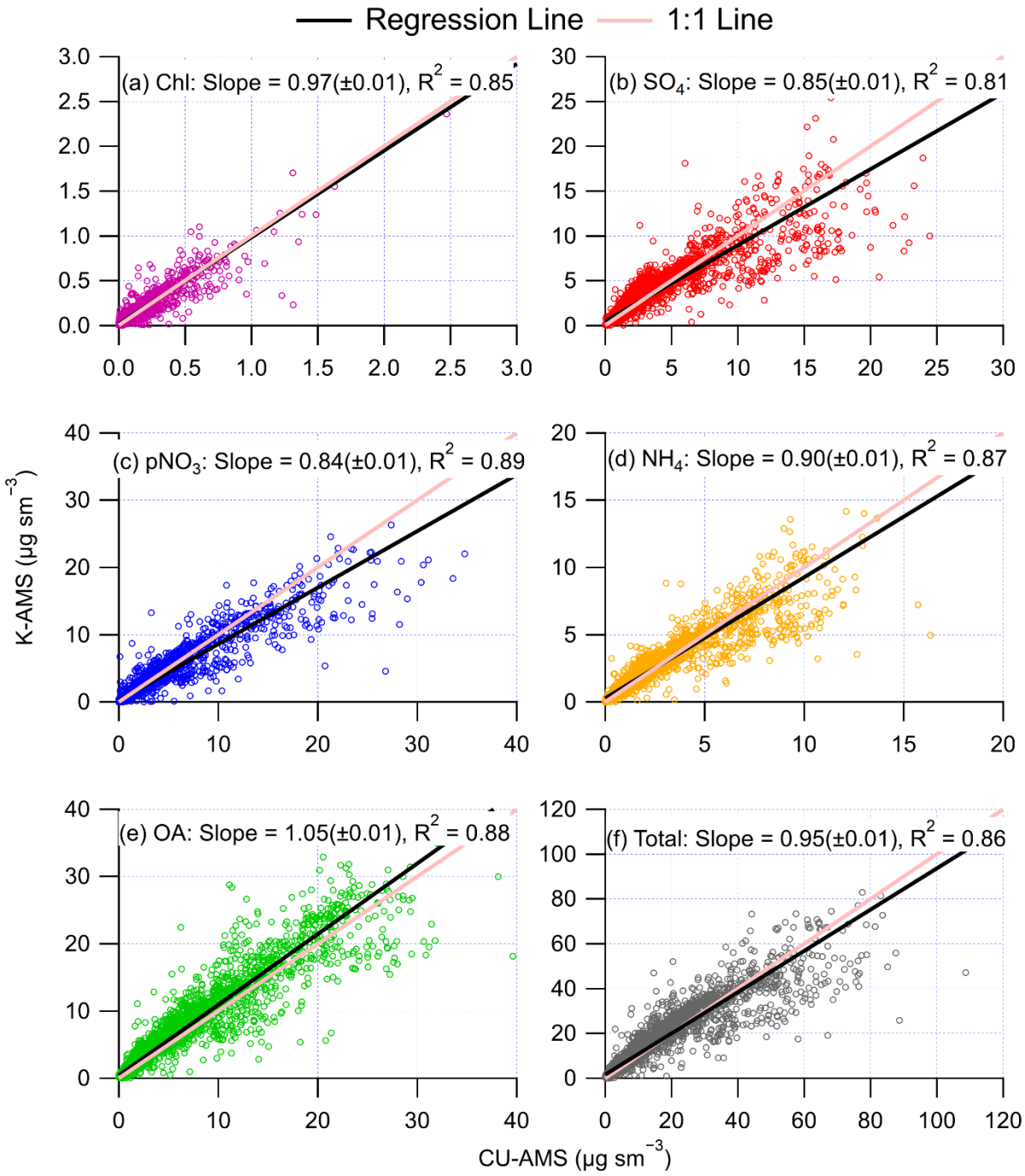

SI Figure 25. Scatter plot of not transmission corrected K-AMS versus CU-AMS mass concentrations for all of KORUS-AQ for (a) Chl, (b) SO_4, (c) pNO_3, (d) NH_4, (e) OA, and (f) total AMS mass. The slopes and R^2 for all comparisons are shown in each scatter plot.

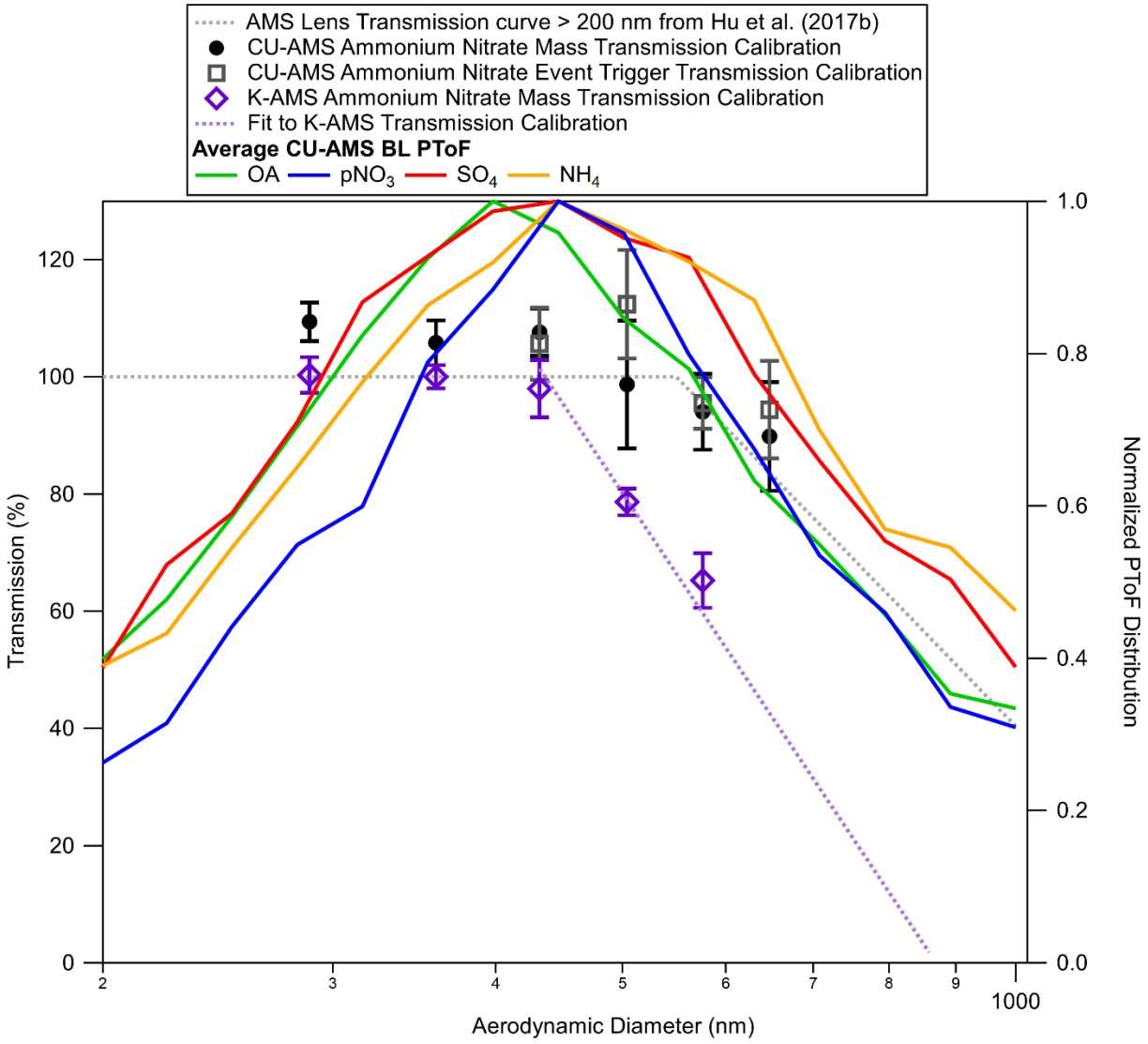

SI Figure 26. (left axis) Transmission curve for CU-AMS (black circle and dark grey square) and K-AMS (purple diamond). The curve from literature (Knote et al., 2011; Hu et al., 2017b), which describes the CU-AMS, is shown (grey dotted line). The fit for K-AMS transmission is shown with the purple dotted line. (right axis) Average mass distributions for OA (green), pNO_3 (blue), SO_4 (red), and NH_4 (orange) measured by CU-AMS in the boundary layer during KORUS-AQ. Note that some of the apparent signal at larger particle sizes is caused by the limited time response of the AMS detection system.

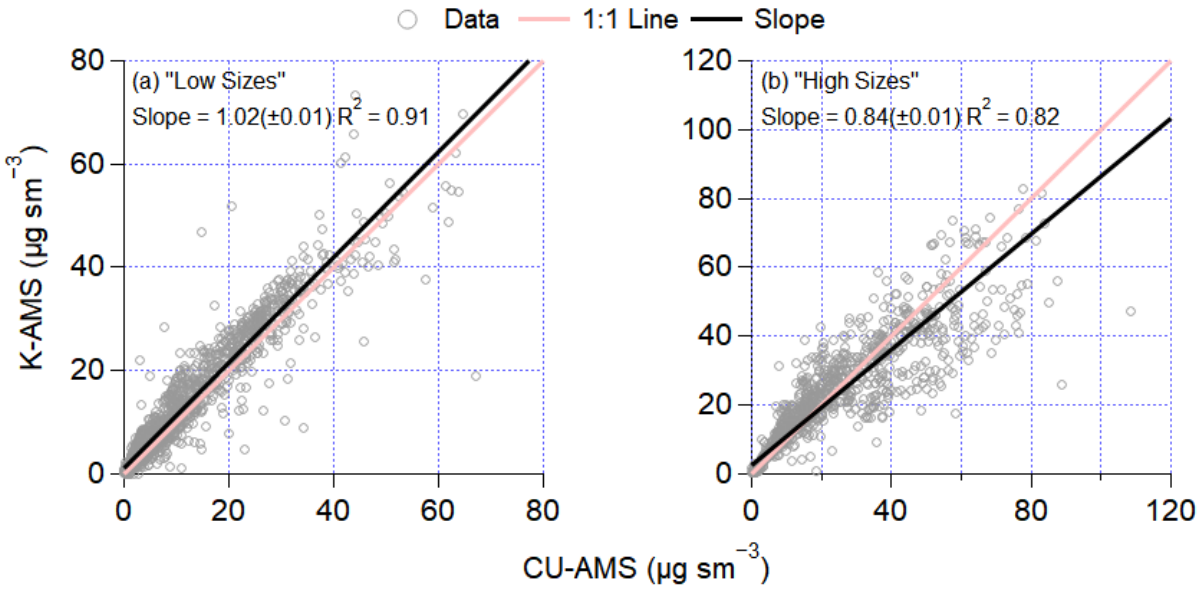

SI Figure 27. Scatter plot of K-AMS versus CU-AMS total mass concentrations (a) RFs 1 – 9, 11, 15, and 19 and (b) RFs 10, 12 – 14, 16 – 18, and 20. These are flights where the average sizes were found below (a) and above (b) the K-AMS size cut-off (SI Figure 26). The slopes and R^2 for all comparisons are shown in each scatter plot.

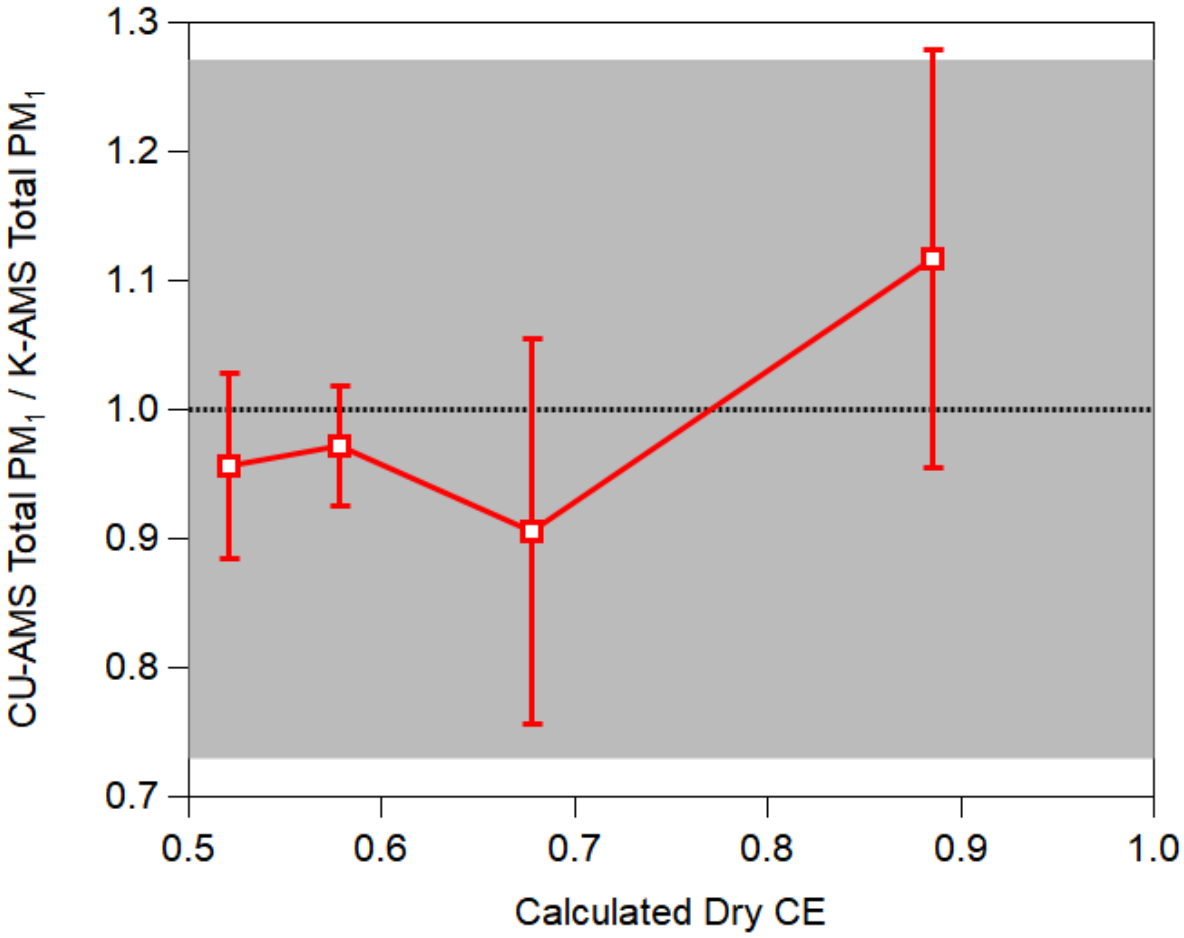

SI Figure 28. Binned total PM_1 AMS mass ratios, normalized by the average ratio, versus the calculated CE used for the CU-AMS measurements. The error bars are the standard error about the mean, and the shaded grey area is the combined uncertainty of the two AMS measurements (±27%). The data is only for flights where the PM_1 sizes were typically below the K-AMS size cut-off (RFs 1 – 9, 11, 15, and 19).

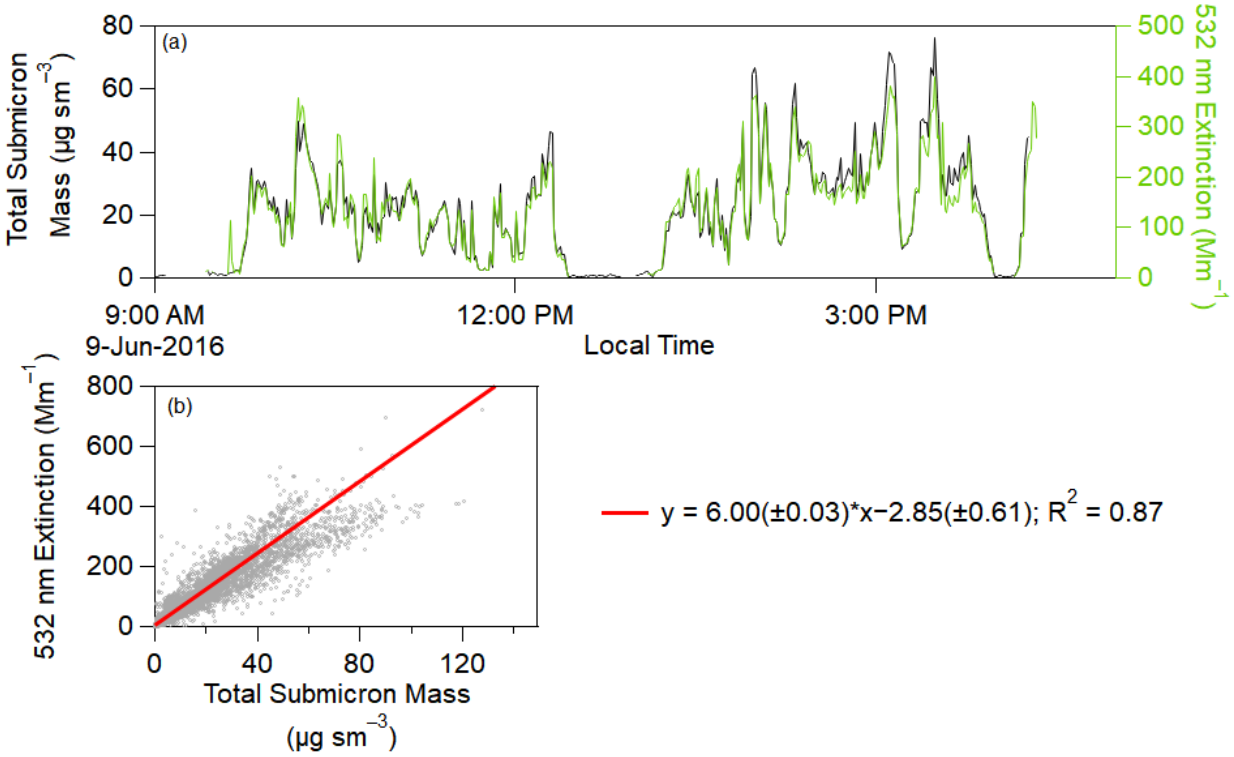

SI Figure 29. (top) Time series of total submicron mass (black, left axis) and 532 nm extinction (green, right axis) for one flight (RF19). (bottom) Scatter plot of 532 nm extinction versus total submicron mass (black carbon + CU-AMS species) for the entire KORUS-AQ campaign.

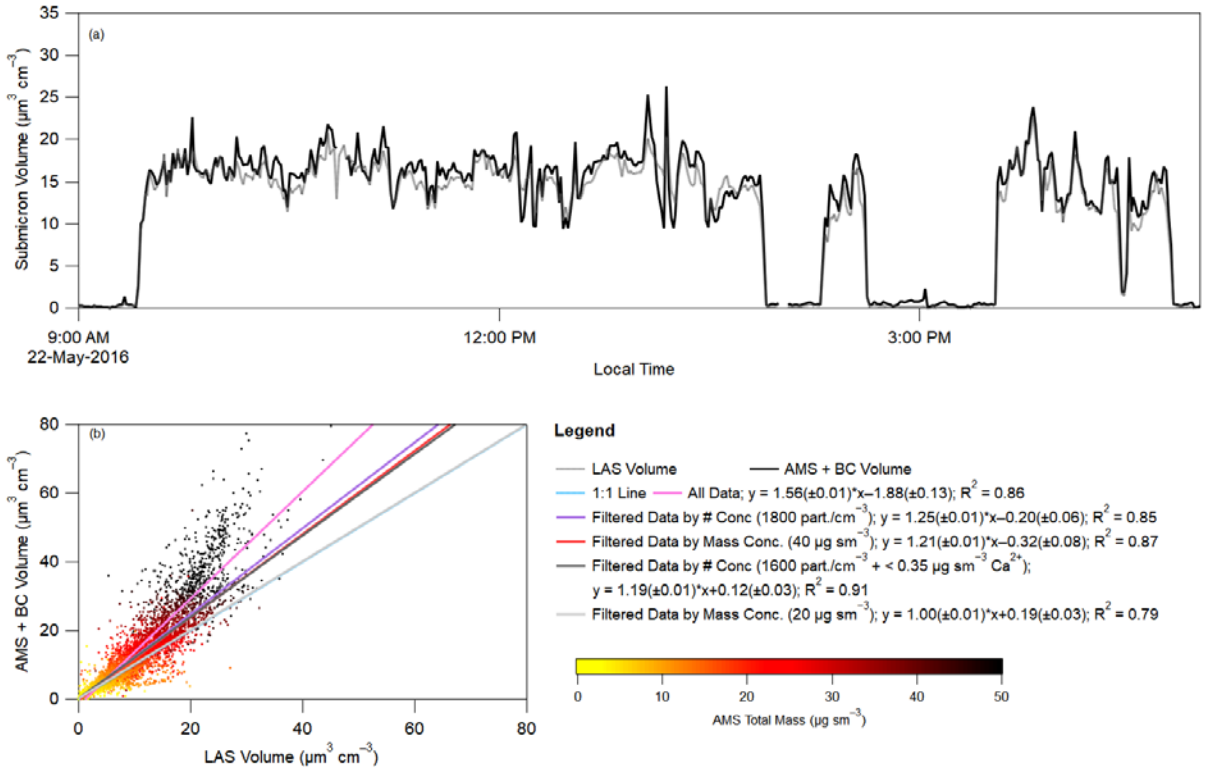

SI Figure 30. (top) Time series of total submicron volume from LAS (grey dashed line) and CU-AMS plus black carbon (black) for one flight (RF11). (bottom) Scatter plot of total submicron volume (black carbon + CU-AMS species) versus LAS volume for entire KORUS-AQ campaign. The data is colored by total CU-AMS mass. Pink line is a fit to all data, the purple line is a fit to data where the particle number concentration is less than 1800 particles scm^{-3}. The red line is a fit to the data where the CU-AMS plus SP2 total mass is less than 40 μg sm^{-3}. The black line is a fit to the data where the particle number concentration is less than 1600 particles scm^{-3} and Ca^{2+} concentration is less than 0.35 μg sm^{-3}. Finally, the grey line is a fit to the data where the CU-AMS plus BC total mass is less than 20 μg sm^{-3}.

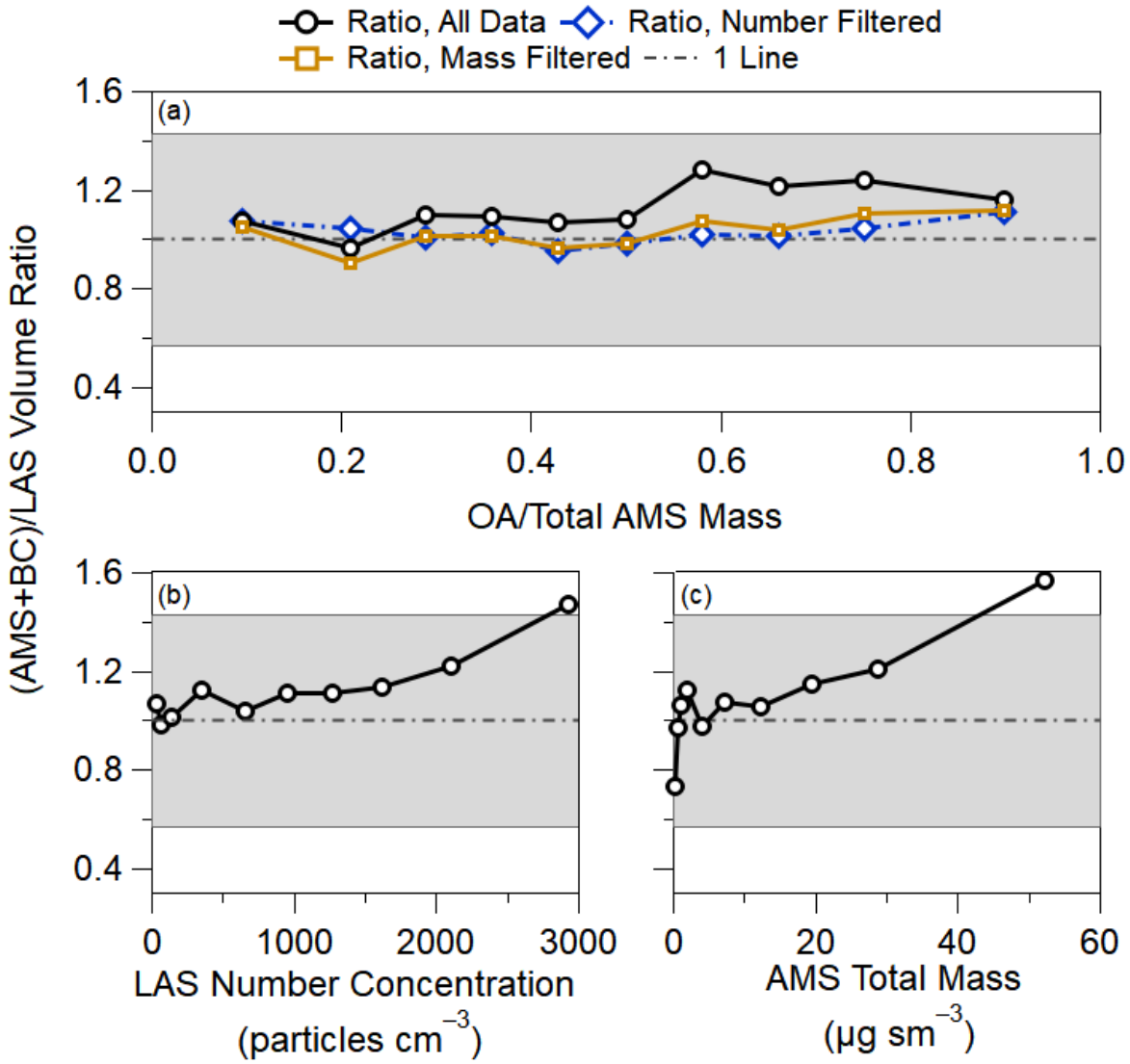

SI Figure 31. (a) Binned volume ratio (CU-AMS plus black carbon volume/LAS Volume) versus fraction of organic aerosol (OA) to total CU-AMS mass. (b) Binned volume ratio versus LAS particle number concentration. (c) Binned volume ratio versus CU-AMS total mass. In all figures, the black data is for all data whereas the blue data is for the volume ratio where the particle number concentration is less than 1600 particles cm^{-3} and the orange data is for the volume ratio where the CU-AMS total mass concentration is less than 20 µg sm^{-3}. Also, the shaded area represents the combined uncertainty in both measurements (Bahreini et al., 2009).

SI 9. Fractional PM_1 Contribution to Vertical Profile

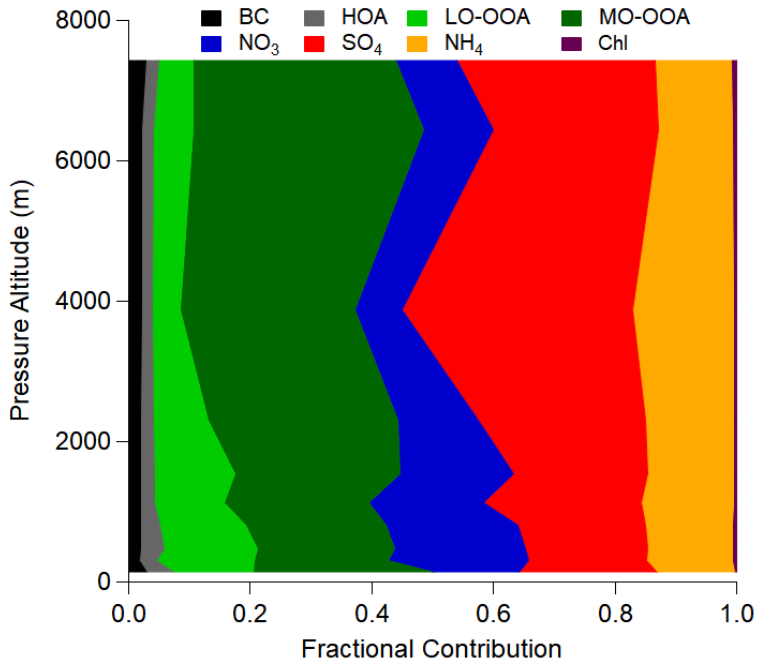

SI Figure 32. Fractional contribution of PM_1 contribution vertical profile for all of KORUS-AQ.

SI 10. Observed Aerosol Production over Seoul, South Korea

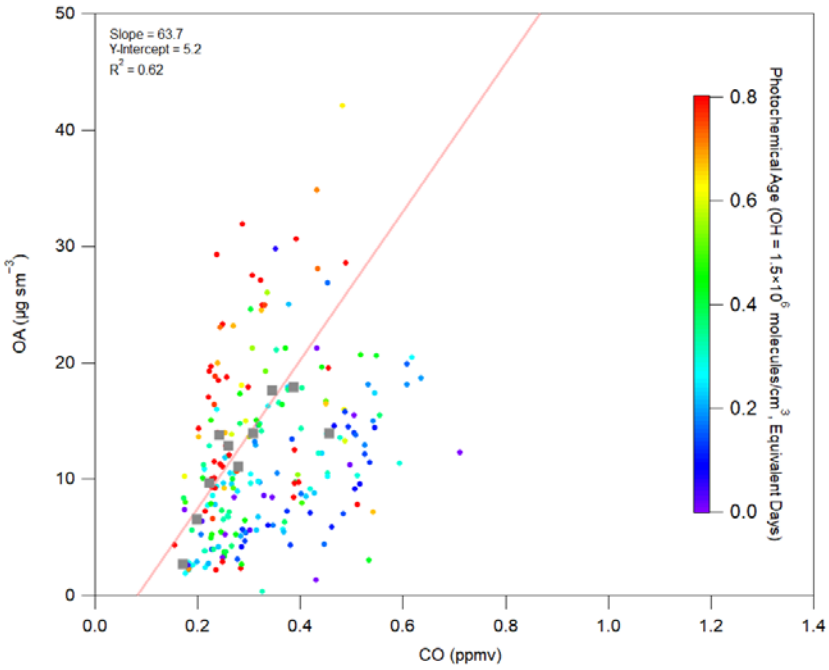

SI Figure 33. Scatter plot of OA versus CO, observed over Seoul, during KORUS-AQ. The points are colored by the NO_x photochemical clock. The fit is for the decile binned data.

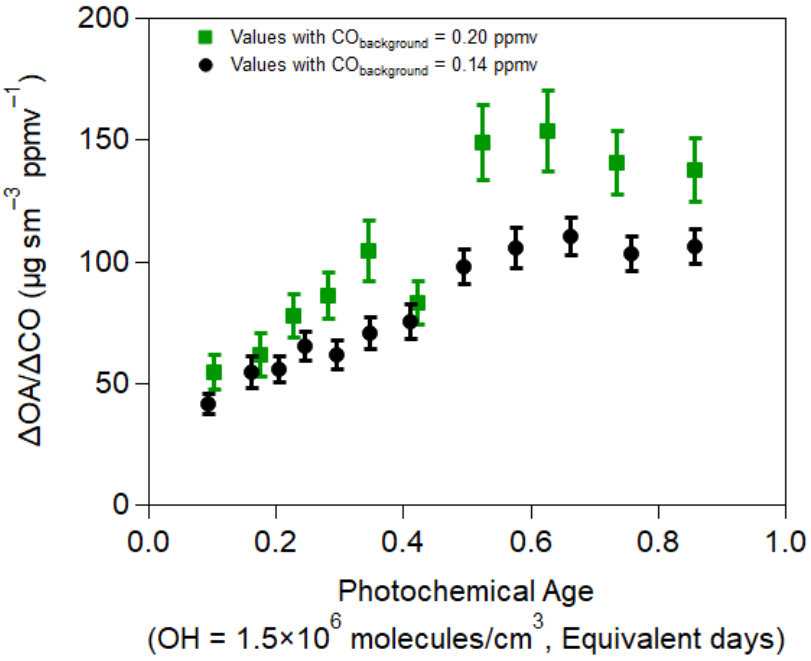

SI Figure 34. Comparison of ΔOA/ΔCO observed over Seoul with different CO backgrounds.

SI Table 4. Compilation of slopes used to convert from ΔOA/ΔCO to ΔOA/ΔCO$_2$ used in this study.

Location	*Slope (ppmv CO/ppmv CO$_2$)*	*Study*
Mexico City	0.045	Vay et al. (2009)
Los Angeles	0.009	Peischl et al., (2013)
Beijing	0.02	Wang et al. (2010)
		Silva et al. (2013)
		Tohjima et al. (2014)
Outflow China	0.02	Wang et al. (2010)
		Silva et al. (2013)
		Tohjima et al. (2014)
Seoul	0.01	Silva et al. (2013)
		Tang et al. (2018)

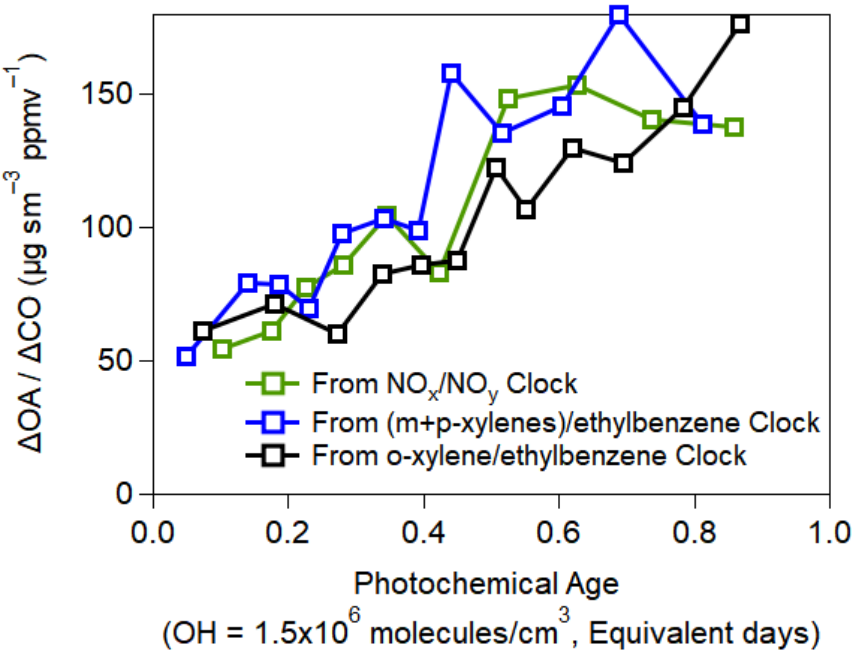

SI Figure 35. Same as **Figure 4**(a), but comparing results using three different photochemical clocks (SI Figure 21).

SI 11. Oxidation of OA

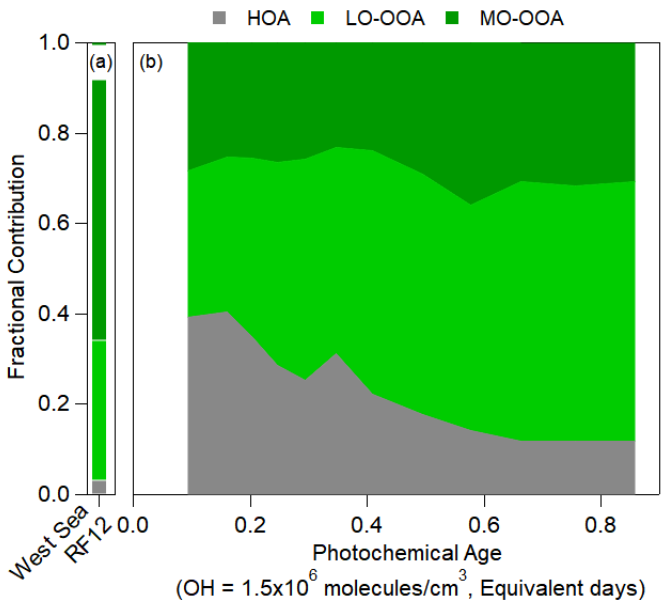

SI Figure 36. Same as **Figure 6**b, but speciated for MO-OOA, LO-OOA, and HOA. (a) is over the West Sea (RF12) and (b) is over Seoul.

First, we briefly discuss how the AMS OA source tracers typically used to investigate OA chemistry evolved over Seoul (SI Figure 37). During KORUS-AQ, there was no appreciable influence from isoprene production of IEPOX-SOA (Hu et al., 2015), as the ion indicative of isoprene IEPOX-SOA ($C_5H_6O^+$) remained at background values typical of air without isoprene SOA influence.

Similarly, biomass burning OA (BBOA) appeared to be present but dilute in its contribution to OA. Most of the OA had $f_{C_2H_4O_2}$, an ion indicative of biomass burning and levoglucosan (Schneider et al., 2006; Aiken et al., 2010), below 0.1 over Seoul, and the PMF factors fall near the limit of detection for BBOA (Cubison et al., 2011) and lower than the values that typically indicate ambient and laboratory BBOA emissions at various stages of chemical evolution (Cubison et al., 2011; Ortega et al., 2013). We speculate that the limited BBOA is highly

mixed into the OA from the numerous, small agricultural fires that were observed during the campaign and have been observed during this time period, during other years, in South Korea (Kang et al., 2006). However, the amount of fresher BBOA was not high enough, nor as strong of a feature as observed in prior studies (Aiken et al., 2010; DeCarlo et al., 2010; Cubison et al., 2011; Hu et al., 2016), to reliably resolve a separate BBOA PMF factor. As shown in SI Figure 11, typical gas-phase biomass burning tracers (CO, NO_x, acetonitrile, HCN, and black carbon) do not show a consistent strong correlation with any of the PMF factors, further suggesting that BBOA is not a major contributor, and any BBOA present is highly mixed with HOA and the oxidized OA. Consistent with our results, Kim et al. (2017) did not resolve a BBOA factor from a ground site in Seoul during the KORUS campaign.

Similar to other studies over urban areas or for chamber studies oxidizing urban VOCs (e.g., benzene, xylenes, etc.) (Ng et al., 2010; Freney et al., 2014a; Ortega et al., 2016), marked chemical evolution was observed as tracked by the $C_2H_3O^+$ and CO_2^+ ions. The evolution of these two ions, as a fraction of total OA, fall in the same space as has been observed in these prior studies, indicating consistent photochemical evolution of SOA over urban locations.

Finally, unlike Kim et al. (2017), we did not observe clear indication for cooking organic aerosol (COA) in our PMF results. The COA was at a minimum (less than 1 $\mu g\ m^{-3}$) at the surface in Seoul during the times the DC-8 overpassed (Kim et al., 2018); thus, we speculate the amount of COA sampled was a small fraction of OA and was mostly lumped into the HOA factor. This does not affect our characterization of HOA as POA, since COA is also a primary aerosol emission.

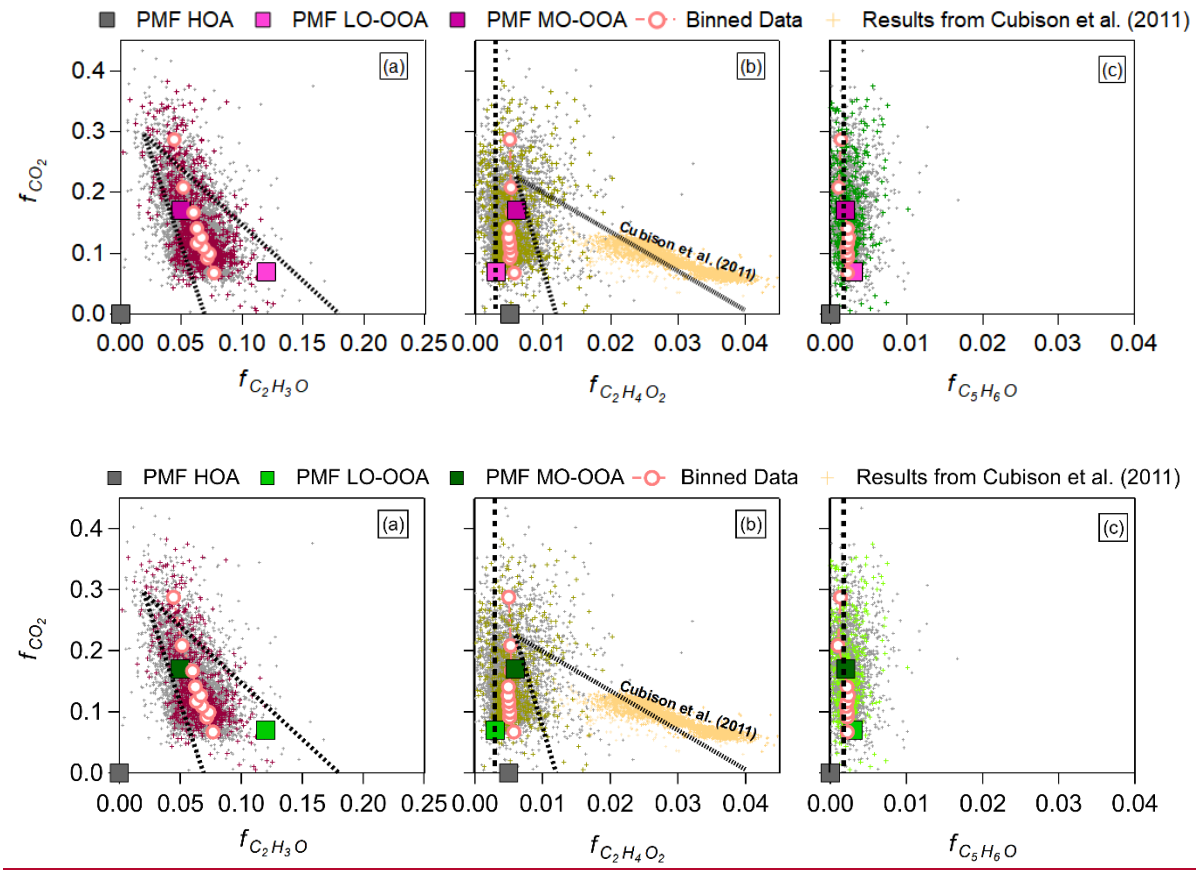

SI Figure 37. Plots of (a) f_{CO_2} versus $f_{C_2H_3O}$, (b) f_{CO_2} versus $f_{C_2H_4O_2}$, and (c) f_{CO_2} versus $f_{C_5H_6O}$. Points highlighted in color refer to observations over Seoul, South Korea, during KORUS-AQ. In (a), the triangle is from Ng et al. (2010); in (b), the triangle is from Cubison et al. (2011), and the vertical line is the typical "background" values for $f_{C_2H_4O_2}$ from Cubison et al. (2011); and, in (c), the vertical line is the typical "background" values for $f_{C_5H_6O}$ from Hu et al. (2015). The PMF results for each triangle plot are shown in squares, where grey is HOA, light ~~pink~~green is LO-OOA, and dark ~~pink~~green is MO-OOA. The light orange dots in (b) are the observations from ARCTAS forest fires (Cubison et al., 2011), as an example for data strongly impacted by biomass burning. The ~~binned~~ quantile average values (averaged the x variables according to quantiles of the y variables) for each comparison are shown in light red circles~~crosses~~.

S12. Particle organic nitrates

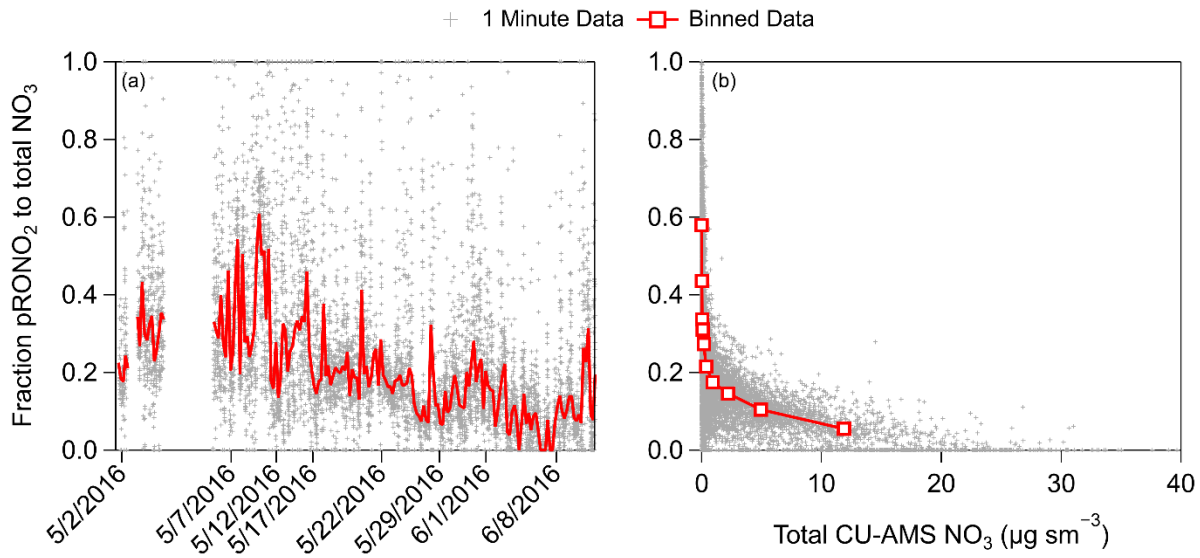

SI Figure 38. Time series of the fractional contribution of organic nitrates ($pRONO_2$) to the total pNO_3 signal during KORUS-AQ. (b) Fractional contribution of organic nitrates versus pNO_3 during KORUS-AQ.

References

Aiken, A. C., Salcedo, D., Cubison, M. J., Huffman, J. A., DeCarlo, P. F., Ulbrich, I. M., Docherty, K. S., Sueper, D., Kimmel, J. R., Worsnop, D. R., Trimborn, A., Northway, M., Stone, E. A., Schauer, J. J., Volkamer, R. M., Fortner, E., de Foy, B., Wang, J., Laskin, A., Shutthanandan, V., Zheng, J., Zhang, R., Gaffney, J., Marley, N. A., Paredes-Miranda, G., Arnott, W. P., Molina, L. T., Sosa, G. and Jimenez, J. L.: Mexico City aerosol analysis during MILAGRO using high resolution aerosol mass spectrometry at the urban supersite (T0) – Part 1: Fine particle composition and organic source apportionment, Atmos. Chem. Phys, 9(9), 6633–6653, doi:10.5194/acpd-9-8377-2009, 2009.

Aiken, A. C., de Foy, B., Wiedinmyer, C., DeCarlo, P. F., Ulbrich, I. M., Wehrli, M. N., Szidat, S., Prévôt, A. S. H., Noda, J., Wacker, L., Volkamer, R., Fortner, E., Wang, J., Laskin, A., Shutthanandan, V., Zheng, J., Zhang, R., Paredes-Miranda, G., Arnott, W. P., Molina, L. T., Sosa, G., Querol, X. and Jimenez, J. L.: Mexico City aerosol analysis during MILAGRO using high resolution aerosol mass spectrometry at the urban supersite (T0)-Part 2: Analysis of the biomass burning contribution and the non-fossil carbon fraction, Atmos. Chem. Phys., 10(12), 5315–5341, doi:10.5194/acp-10-5315-2010, 2010.

Ait-Helal, W., Borbon, A., Sauvage, S., De Gouw, J. A., Colomb, A., Gros, V., Freutel, F., Crippa, M., Afif, C., Baltensperger, U., Beekmann, M., Doussin, J.-F. F., Durand-Jolibois, R., Fronval, I., Grand, N., Leonardis, T., Lopez, M., Michoud, V., Miet, K., Perrier, S., Prévôt, A. S. H., Schneider, J., Siour, G., Zapf, P. and Locoge, N.: Volatile and intermediate volatility organic compounds in suburban Paris: Variability, origin and importance for SOA formation, Atmos. Chem. Phys., 14(19), 10439–10464, doi:10.5194/acp-14-10439-2014, 2014.

Akagi, S. K., Craven, J. S., Taylor, J. W., Mcmeeking, G. R., Yokelson, R. J., Burling, I. R., Urbanski, S. P., Wold, C. E., Seinfeld, J. H., Coe, H., Alvarado, M. J. and Weise, D. R.: Evolution of trace gases and particles emitted by a chaparral fire in California, Atmos. Chem. Phys., 12, 1397–1421, doi:10.5194/acp-12-1397-2012, 2012.

Aknan, A. and Chen, G.: KORUS-AQ DC-8 Aircraft Dataset, [online] Available from: https://www-air.larc.nasa.gov/cgi-bin/ArcView/korusaq (Accessed 6 December 2018), 2018.

Al-Saadi, J., Carmichael, G., Crawford, J., Emmons, L., Korean, S. K., Group, S., Song, C.-K., Chang, L.-S., Lee, G., Kim, J. and Park, R.: NASA Contributions to KORUS-AQ: An International Cooperative Air Quality Field Study in Korea, 2015.

Anderson, T. L. and Ogren, J. A.: Determining Aerosol Radiative Properties Using the TSI 3563 Integrating Nephelometer, Aerosol Sci. Technol., 29(1), 57–69, doi:10.1080/02786829808965551, 1998.

Arnold, S. R., Methven, J., Evans, M. J., Chipperfield, M. P., Lewis, A. C., Hopkins, J. R., Mcquaid, J. B., Watson, N., Purvis, R. M., Lee, J. D., Atlas, E. L., Blake, D. R. and Rappenglück, B.: Statistical inference of OH concentrations and air mass dilution rates from successive observations of nonmethane hydrocarbons in single air masses, J. Geophys. Res. Atmos., 112, D10S40, doi:10.1029/2006JD007594, 2007.

Atkinson, R.: Kinetics of the gas-phase reactions of OH radicals with alkanes and cycloalkanes, Atmos. Chem. Phys., 3(6), 2233–2307, doi:10.5194/acp-3-2233-2003, 2003.

Atkinson, R. and Arey, J.: Atmospheric Degradation of Volatile Organic Compounds, Chem. Rev.,

103, 4605–4638, doi:10.1021/CR0206420, 2003.

Atkinson, R., Baulch, D. L., Cox, R. A., Crowley, J. N., Hampson, R. F., Hynes, R. G., Jenkin, M. E., Rossi, M. J. and Troe, J.: Evaluated kinetic and photochemical data for atmospheric chemistry: Volume I - gas phase reactions of Ox, HO_x , NO_x and SO_x species, Atmos. Chem. Phys., 4(6), 1461–1738, doi:10.5194/acp-4-1461-2004, 2004.

Atkinson, R., Baulch, D. L., Cox, R. A., Crowley, J. N., Hampson, R. F., Hynes, R. G., Jenkin, M. E., Rossi, M. J., Troe, J. and IUPAC Subcommittee: Evaluated kinetic and photochemical data for atmospheric chemistry: Volume II - gas phase reactions of organic species, Atmos. Chem. Phys., 6(11), 3625–4055, doi:10.5194/acp-6-3625-2006, 2006.

Bahreini, R., Dunlea, E. J., Matthew, B. M., Simons, C., Docherty, K. S., DeCarlo, P. F., Jimenez, J. L., Brock, C. A. and Middlebrook, A. M.: Design and Operation of a Pressure-Controlled Inlet for Airborne Sampling with an Aerodynamic Aerosol Lens, Aerosol Sci. Technol., 42(6), 465–471, doi:10.1080/02786820802178514, 2008.

Bahreini, R., Ervens, B., Middlebrook, A. M., Warneke, C., de Gouw, J. A., DeCarlo, P. F., Jimenez, J. L., Brock, C. A., Neuman, J. A., Ryerson, T. B., Stark, H., Atlas, E., Brioude, J., Fried, A., Holloway, J. S., Peischl, J., Richter, D., Walega, J., Weibring, P., Wollny, A. G. and Fehsenfeid, F. C.: Organic aerosol formation in urban and industrial plumes near Houston and Dallas, Texas, J. Geophys. Res., 114(16), D00F16, doi:10.1029/2008JD011493, 2009.

Baklanov, A., Molina, L. T. and Gauss, M.: Megacities, Air Quality and Climate, Atmos. Environ., 126, 235–249, doi:10.1016/j.atmosenv.2015.11.059, 2016.

Blake, N. J., Blake, D. R., Sive, B. C., Katzenstein, A. S., Meinardi, S., Wingenter, O. W., Atlas, E. L., Flocke, F., Ridley, B. A. and Rowland, F. S.: The seasonal evolution of NMHC's and light alkyl nitrates at middle to northern latitudes during TOPSE, J. Geophys. Res., 108(D4), 8359, 2003.

Bohn, B. and Zetzsch, C.: Kinetics and mechanism of the reaction of OH with the trimethylbenzenes – experimental evidence for the formation of adduct isomers, Phys. Chem. Chem. Phys., 14(40), 13933, doi:10.1039/c2cp42434g, 2012.

Brioude, J., Arnold, D., Stohl, A., Cassiani, M., Morton, D., Seibert, P., Angevine, W., Evan, S., Dingwell, A., Fast, J. D., Easter, R. C., Pisso, I., Burkhart, J. and Wotawa, G.: The Lagrangian particle dispersion model FLEXPART-WRF version 3.1, Geosci. Model Dev., 6(6), 1889–1904, doi:10.5194/gmd-6-1889-2013, 2013.

Campuzano-Jost, P., Day, D. A., Nault, B. A., Schroder, J. C. and Jimenez, J. L.: Temporal Variability of the Pieber Effect and Some Notes on AMS Dection Limits, in 17th AMS Users' Meeting, Portland. [online] Available from: http://cires1.colorado.edu/jimenez-group/UsrMtgs/UsersMtg17/10-14-2016_PCJ_AMSUsersMtg_Prez.pdf (Accessed 5 April 2018), 2016.

Canagaratna, M. R., Jayne, J. T., Jimenez, J. L., Allan, J. D., Alfarra, M. R., Zhang, Q., Onasch, T. B., Drewnick, F., Coe, H., Middlebrook, A. M., Delia, A., Williams, L. R., Trimborn, A. M., Northway, M. J., DeCarlo, P. F., Kolb, C. E., Davidovits, P. and Worsnop, D. R.: Chemical and microphysical characterization of ambient aerosols with the Aerodyne Aerosol Mass Spectrometer, Mass Spectrom. Rev., 26(2), 185–222, doi:10.1002/mas, 2007.

Canagaratna, M. R., Jimenez, J. L., Kroll, J. H., Chen, Q., Kessler, S. H., Massoli, P., Hildebrandt

Ruiz, L., Fortner, E., Williams, L. R., Wilson, K. R., Surratt, J. D., Donahue, N. M., Jayne, J. T. and Worsnop, D. R.: Elemental ratio measurements of organic compounds using aerosol mass spectrometry: characterization, improved calibration, and implications, Atmos. Chem. Phys., 15(1), 253–272, doi:10.5194/acp-15-253-2015, 2015.

Cappa, C. D. and Jimenez, J. L.: Quantitative estimates of the volatility of ambient organic aerosol, Atmos. Chem. Phys., 10(12), 5409–5424, doi:10.5194/acp-10-5409-2010, 2010.

Cappa, C. D., Jathar, S. H., Kleeman, M. J., Docherty, K. S., Jimenez, J. L., Seinfeld, J. H. and Wexler, A. S.: Simulating secondary organic aerosol in a regional air quality model using the statistical oxidation model – Part 2: Assessing the influence of vapor wall losses, Atmos. Chem. Phys., 16(5), 3041–3059, doi:10.5194/acp-16-3041-2016, 2016.

Chen, Q., Heald, C. L., Jimenez, J. L., Canagaratna, M. R., He, L., Huang, X.-F., Campuzano-Jost, P., Palm, B. B., Poulain, L., Kuwata, M., Martin, S. T., Abbatt, J. P. D., Lee, A. K. Y., Liggio, J., Zhang, Q., He, L. and Huang, X.-F.: Elemental composition of organic aerosol: The gap between ambient and laboratory measurements, Geophys. Res. Lett., 42(10), 4182–4189, doi:10.1002/2015GL063693, 2015.

Choi, J. K., Heo, J. B., Ban, S. J., Yi, S. M. and Zoh, K. D.: Chemical characteristics of PM2.5 aerosol in Incheon, Korea, Atmos. Environ., 60, 583–592, doi:10.1016/j.atmosenv.2012.06.078, 2012.

Collier, S., Zhou, S., Onasch, T. B., Jaffe, D. A., Kleinman, L., Sedlacek, A. J., Briggs, N. L., Hee, J., Fortner, E., Shilling, J. E., Worsnop, D., Yokelson, R. J., Parworth, C., Ge, X., Xu, J., Butterfield, Z., Chand, D., Dubey, M. K., Pekour, M. S., Springston, S. and Zhang, Q.: Regional Influence of Aerosol Emissions from Wildfires Driven by Combustion Efficiency: Insights from the BBOP Campaign, Environ. Sci. Technol., 50(16), 8613–8622, doi:10.1021/acs.est.6b01617, 2016.

Craven, J. S., Metcalf, A. R., Bahreini, R., Middlebrook, A., Hayes, P. L., Duong, H. T., Sorooshian, A., Jimenez, J. L., Flagan, R. C. and Seinfeld, J. H.: Los Angeles Basin airborne organic aerosol characterization during CalNex, J. Geophys. Res. Atmos., 118(19), 11,453-11,467, doi:10.1002/jgrd.50853, 2013.

Crippa, M., Canonaco, F., Lanz, V. A., Äijälä, M., Allan, J. D., Carbone, S., Capes, G., Ceburnis, D., Dall'Osto, M., Day, D. A., DeCarlo, P. F., Ehn, M., Eriksson, A., Freney, E., Hildebrandt Ruiz, L. H., Hillamo, R., Jimenez, J. L., Junninen, H., Kiendler-Scharr, A., Kortelainen, A.-M., Kulmala, M., Laaksonen, A., Mensah, A. A., Mohr, C., Nemitz, E., O'Dowd, C., Ovadnevaite, J., Pandis, S. N., Petäjä, T., Poulain, L., Saarikoski, S., Sellegri, K., Swietlicki, E., Tiitta, P., Worsnop, D. R., Baltensperger, U. and Prévôt, A. S. H.: Organic aerosol components derived from 25 AMS data sets across Europe using a consistent ME-2 based source apportionment approach, Atmos. Chem. Phys., 14(12), 6159–6176, doi:10.5194/acp-14-6159-2014, 2014.

Crounse, J., McKinney, K. A., Kwan, A. J. and Wennberg, P. O.: Measurement of gas-phase hydroperoxides by chemical ionization mass spectrometry, Anal. Chem., 78(19), 6726–6732, doi:doi:10.1021/ac0604235, 2006.

Crounse, J. D., Nielsen, L. B., Jørgensen, S., Kjaergaard, H. G. and Wennberg, P. O.: Autoxidation of Organic Compounds in the Atmosphere, J. Phys. Chem. Lett., 4(20), 3513–3520, doi:10.1021/jz4019207, 2013.

Cubison, M. J., Ortega, A. M., Hayes, P. L., Farmer, D. K., Day, D. A., Lechner, M. J., Brune, W. H., Apel, E., Diskin, G. S., Fisher, J. A., Fuelberg, H. E., Hecobian, A., Knapp, D. J., Mikoviny, T., Riemer, D., Sachse, G. W., Sessions, W., Weber, R. J., Weinheimer, A. J., Wisthaler, A. and Jimenez, J. L.: Effects of aging on organic aerosol from open biomass burning smoke in aircraft and laboratory studies, Atmos. Chem. Phys., 11(23), 12049–12064, doi:10.5194/acp-11-12049-2011, 2011.

Day, D. A., Wooldridge, P. J., Dillon, M. B., Thornton, J. A. and Cohen, R. C.: A thermal dissociation laser-induced fluorescence instrument for in situ detection of NO_2, peroxy nitrates, alkyl nitrates, and HNO_3, J. Geophys. Res., 107(D5-6), 4046, doi:10.1029/2001JD000779, 2002.

DeCarlo, P. F., Slowik, J. G., Worsnop, D. R., Davidovits, P., Jimenez, J. L., Stainken, K., Williams, L., Jayne, J., Kolb, C. and Rudich, Y.: Particle Morphology and Density Characterization by Combined Mobility and Aerodynamic Diameter Measurements. Part 1: Theory, Aerosol Sci. Technol., 38(12), 1185–1205, doi:10.1080/027868290903907, 2004.

DeCarlo, P. F., Kimmel, J. R., Trimborn, A., Northway, M. J., Jayne, J. T., Aiken, A. C., Gonin, M., Fuhrer, K., Horvath, T., Docherty, K. S., Worsnop, D. R. and Jimenez, J. L.: Field-Deployable, High-Resolution, Time-of-Flight Aerosol Mass Spectrometer, Anal. Chem., 78(24), 8281–8289, doi:10.1021/ac061249n, 2006.

DeCarlo, P. F., Dunlea, E. J., Kimmel, J. R., Aiken, A. C., Sueper, D., Crounse, J., Wennberg, P. O., Emmons, L., Shinozuka, Y., Clarke, A., Zhou, J., Tomlinson, J., Collins, D. R., Knapp, D., Weinheimer, A. J., Montzka, D. D., Campos, T. and Jimenez, J. L.: Fast airborne aerosol size and chemistry measurements above Mexico City and Central Mexico during the MILAGRO campaign, Atmos. Chem. Phys., 8(14), 4027–4048, doi:10.5194/acp-8-4027-2008, 2008.

DeCarlo, P. F., Ulbrich, I. M., Crounse, J., de Foy, B., Dunlea, E. J., Aiken, A. C., Knapp, D., Weinheimer, A. J., Campos, T., Wennberg, P. O. and Jimenez, J. L.: Investigation of the sources and processing of organic aerosol over the Central Mexican Plateau from aircraft measurements during MILAGRO, Atmos. Chem. Phys., 10(12), 5257–5280, doi:10.5194/acp-10-5257-2010, 2010.

Deming, B., Pagonis, D., Liu, X., Talukdar, R. K., Roberts, J. M., Veres, P. R., Krechmer, J. E., de Gouw, J. A., Jimenez, J. L. and Zieman, P. J.: Measurements of Delays of Gas-Phase Compounds in a Wide Variety of Tubing Materials due to Gas-Wall Partitioning, Atmos. Meas. Tech., In Prep., 2018.

Dibb, J. E., Talbot, R. W., Scheuer, E. M., Seid, G., Avery, M. A. and Singh, H. B.: Aerosol chemical composition in Asian continental outflow during the TRACE-P campaign: Comparison with PEM-West B, J. Geophys. Res., 108(D21), 8815, doi:10.1029/2002JD003111, 2003.

Diskin, G. S., Podolske, J. R., Sachse, G. W. and Slate, T. A.: Open-path airborne tunable diode laser hygrometer, vol. 4817, edited by A. Fried, p. 196, International Society for Optics and Photonics., 2002.

Docherty, K. S., Aiken, A. C., Huffman, J. A., Ulbrich, I. M., DeCarlo, P. F., Sueper, D., Worsnop, D. R., Snyder, D. C., Peltier, R. E., Weber, R. J., Grover, B. D., Eatough, D. J., Williams, B. J., Goldstein, A. H., Ziemann, P. J. and Jimenez, J. L.: The 2005 Study of Organic Aerosols at Riverside (SOAR-1): instrumental intercomparisons and fine particle composition, Atmos. Chem. Phys., 11(23), 12387–12420, doi:DOI 10.5194/acp-11-12387-2011, 2011.

Drewnick, F., Hings, S. S., Alfarra, M. R., Prevot, A. S. H. and Borrmann, S.: Aerosol quantification with the Aerodyne Aerosol Mass Spectrometer: detection limits and ionizer background effects, Atmos. Meas. Tech., 2(1), 33–46, doi:10.5194/amt-2-33-2009, 2009.

Dunlea, E. J., DeCarlo, P. F., Aiken, A. C., Kimmel, J. R., Peltier, R. E., Weber, R. J., Tomlison, J., Collins, D. R., Shinozuka, Y., McNaugthon, C. S., Howell, S. G., Clarke, A. D., Emmons, L. K., Apel, E. C., Pfister, G. G., van Donkelaar, A., Martin, R. V., Millett, D. B., Heald, C. L. and Jimenez, J. L.: Evolution of Asian aerosols during transpacific transport in INTEX-B, Atmos. Chem. Phys., 9(19), 7257–7287, doi:10.5194/acp-9-7257-2009, 2009.

Dzepina, K., Volkamer, R. M. R., Madronich, S., Tulet, P., Ulbrich, I. M., Zhang, Q., Cappa, C. D., Ziemann, P. J. and Jimenez, J. L.: Evaluation of recently-proposed secondary organic aerosol models for a case study in Mexico City, Atmos. Chem. Phys., 9(15), 5681–5709, doi:10.5194/acp-9-5681-2009, 2009.

Dzepina, K., Cappa, C. D., Volkamer, R. M., Madronich, S., DeCarlo, P. F., Zaveri, R. A. and Jimenez, J. L.: Modeling the Multiday Evolution and Aging of Secondary Organic Aerosol During MILAGRO 2006, Environ. Sci. Technol., 45(8), 3496–3503, doi:10.1021/es103186, 2011.

Faloona, I. C., Tan, D., Lesher, R. L., Hazen, N. L., Frame, C. L., Simpas, J. B., Harder, H., Martinez, M., Di Carlo, P., Ren, X. and Brune, W. H.: A Laser-induced Fluorescence Instrument for Detecting Tropospheric OH and HO_2 : Characteristics and Calibration, J. Atmos. Chem., 47(2), 139–167, doi:10.1023/B:JOCH.0000021036.53185.0e, 2004.

Farmer, D. K., Matsunaga, A., Docherty, K. S., Surratt, J. D., Seinfeld, J. H., Ziemann, P. J. and Jimenez, J. L.: Response of an aerosol mass spectrometer to organonitrates and organosulfates and implications for atmospheric chemistry, Proc. Natl. Acad. Sci. U. S. A., 107(15), 6670–6675, doi:10.1073/pnas.0912340107, 2010.

Freney, E. J., Sellegri, K., Canonaco, F., Colomb, A., Borbon, A., Michoud, V., Doussin, J.-F., Crumeyrolle, S., Amarouche, N., Pichon, J.-M., Bourianne, T., Gomes, L., Prevot, A. S. H., Beekmann, M. and Schwarzenböeck, A.: Characterizing the impact of urban emissions on regional aerosol particles: airborne measurements during the MEGAPOLI experiment, Atmos. Chem. Phys., 14(3), 1397–1412, doi:10.5194/acp-14-1397-2014, 2014a.

Freney, E. J., Sellegri, K., Canonaco, F., Colomb, A., Borbon, A., Michoud, V., Crumeyrolle, S., Amarouche, N., Bourianne, T., Gomes, L., Prevot, A. S. H., Beekmann, M. and Schwarzenböeck, A.: Characterizing the impact of urban emissions on regional aerosol particles: Airborne measurements during the MEGAPOLI experiment, Atmos. Chem. Phys., 14(3), 1397–1412, doi:10.5194/acp-14-1397-2014, 2014b.

Fried, A., Cantrell, C., Olson, J., Crawford, J. H., Weibring, P., Walega, J., Richter, D., Junkermann, W., Volkamer, R., Sinreich, R., Heikes, B. G., O'Sullivan, D., Blake, D. R., Blake, N., Meinardi, S., Apel, E., Weinheimer, A., Knapp, D., Perring, A., Cohen, R. C., Fuelberg, H., Shetter, R. E., Hall, S. R., Ullmann, K., Brune, W. H., Mao, J., Ren, X., Huey, L. G., Singh, H. B., Hair, J. W., Riemer, D., Diskin, G. and Sachse, G.: Detailed comparisons of airborne formaldehyde measurements with box models during the 2006 INTEX-B and MILAGRO campaigns: Potential evidence for significant impacts of unmeasured and multi-generation volatile organic carbon compounds, Atmos. Chem. Phys., 11(22), 11867–11894, doi:10.5194/acp-11-11867-2011, 2011.

Fry, J. L., Draper, D. C., Zarzana, K. J., Campuzano-Jost, P., Day, D. A., Jimenez, J. L., Brown, S. S., Cohen, R. C., Kaser, L., Hansel, A., Cappellin, L., Karl, T., Hodzic Roux, A., Turnipseed,

A., Cantrell, C., Lefer, B. L. and Grossberg, N.: Observations of gas- and aerosol-phase organic nitrates at BEACHON-RoMBAS 2011, Atmos. Chem. Phys., 13(17), 8585–8605, doi:10.5194/acp-13-8585-2013, 2013.

Ge, X., Setyan, A., Sun, Y. and Zhang, Q.: Primary and secondary organic aerosols in Fresno, California during wintertime: Results from high resolution aerosol mass spectrometry, J. Geophys. Res. Atmos., 117(D19), n/a-n/a, doi:10.1029/2012JD018026, 2012.

George, I. J., Slowik, J. and Abbatt, J. P. D.: Chemical aging of ambient organic aerosol from heterogeneous reaction with hydroxyl radicals, Geophys. Res. Lett., 35(13), L13811, doi:10.1029/2008GL033884, 2008.

Goldberg, D. L., Vinciguerra, T. P., Hosley, K. M., Loughner, C. P., Canty, T. C., Salawitch, R. . and Dickerson, R. R.: Evidence for an increase in the ozone photochemical lifetime in the eastern United States using a regional air quality model, J. Geophys. Res. Atmos., 120, 12,778-12,793, doi:10.1002/2015JD02390, 2015.

Gordon, T. D., Tkacik, D. S., Presto, A. A., Zhang, M., Jathar, S. H., Nguyen, N. T., Massetti, J., Truong, T., Cicero-Fernandez, P., Maddox, C., Rieger, P., Chattopadhyay, S., Maldonado, H., Maricq, M. M. and Robinson, A. L.: Primary Gas- and Particle-Phase Emissions and Secondary Organic Aerosol Production from Gasoline and Diesel Off-Road Engines, Environ. Sci. Technol., 47(24), 14137–14146, doi:10.1021/es403556e, 2013.

de Gouw, J. A., Middlebrook, A. M., Warneke, C., Goldan, P. D., Kuster, W. C., Roberts, J. M., Fehsenfeld, F. C., Worsnop, D. R., Canagaratna, M. R., Pszenny, A. A. P., Keene, W. C., Marchewka, M. L., Bertman, S. B. and Bates, T. S.: Budget of organic carbon in a polluted atmosphere: Results from the New England Air Quality Study in 2002, J. Geophys. Res., 110(16), D16305, doi:10.1029/2004JD005623, 2005.

de Gouw, J. A., Brock, C. A., Atlas, E. L., Bates, T. S., Fehsenfeld, F. C., Goldan, P. D., Holloway, J. S., Kuster, W. C., Lerner, B. M., Matthew, B. M., Middlebrook, A. M., Onasch, T. B., Peltier, R. E., Quinn, P. K., Senff, C. J., Stohl, A., Sullivan, A. P., Trainer, M., Warneke, C., Weber, R. J. and Williams, E. J.: Sources of particulate matter in the northeastern United States in summer: 1. Direct emissions and secondary formation of organic matter in urban plumes, J. Geophys. Res., 113(8), D08301, doi:10.1029/2007JD009243, 2008.

de Gouw, J. A., Welsh-Bon, D., Warneke, C., Kuster, W. C., Alexander, L., Baker, A. K., Beyersdorf, A. J., Blake, D. R., Canagaratna, M., Celada, a. T., Huey, L. G., Junkermann, W., Onasch, T. B., Salcido, A., Sjostedt, S. J., Sullivan, A. P., Tanner, D. J., Vargas, O., Weber, R. J., Worsnop, D. R., Yu, X. Y. and Zaveri, R.: Emission and chemistry of organic carbon in the gas and aerosol phase at a sub-urban site near Mexico City in March 2006 during the MILAGRO study, Atmos. Chem. Phys., 9(10), 3425–3442, doi:10.5194/acp-9-3425-2009, 2009.

de Gouw, J. A., Gilman, J. B., Kim, S.-W., Lerner, B. M., Isaacman-VanWertz, G., McDonald, B. C., Warneke, C., Kuster, W. C., Lefer, B. L., Griffith, S. M., Dusanter, S., Stevens, P. S. and Stutz, J.: Chemistry of Volatile Organic Compounds in the Los Angeles basin: Nighttime Removal of Alkenes and Determination of Emission Ratios, J. Geophys. Res., 122(21), 11,843-11,861, doi:10.1002/2017JD027459, 2017.

Grieshop, A. P., Miracolo, M. A., Donahue, N. M. and Robinson, A. L.: Constraining the Volatility Distribution and Gas-Particle Partitioning of Combustion Aerosols Using Isothermal Dilution and Thermodenuder Measurements, Environ. Sci. Technol., 43(13), 4750–4756,

doi:10.1021/Es8032378, 2009.

Griffin, R. J., Chen, J., Carmody, K., Vutukuru, S. and Dabdub, D.: Contribution of gas phase oxidation of volatile organic compounds to atmospheric carbon monoxide levels in two areas of the United States, J. Geophys. Res. Atmos., 112(D10), doi:10.1029/2006JD007602, 2007.

Hallquist, M., Wenger, J. C., Baltensperger, U., Rudich, Y., Simpson, D., Claeys, M., Dommen, J., Donahue, N. M., George, C., Goldstein, A. H., Hamilton, J. F., Herrmann, H., Hoffmann, T., Iinuma, Y., Jang, M., Jenkin, M. E., Jimenez, J. L., Kiendler-Scharr, A., Maenhaut, W., McFiggans, G., Mentel, T. F., Monod, A., Prévôt, A. S. H., Seinfeld, J. H., Surratt, J. D., Szmigielski, R. and Wildt, J.: The formation, properties and impact of secondary organic aerosol: current and emerging issues, Atmos. Chem. Phys., 9(14), 5155–5236, doi:10.5194/acp-9-5155-2009, 2009.

Hand, J. L. and Malm, W. C.: Review of aerosol mass scattering efficiencies from ground-based measurements since 1990, J. Geophys. Res., 112(D16), D16203, doi:10.1029/2007JD008484, 2007.

Hayes, P. L., Ortega, A. M., Cubison, M. J., Froyd, K. D., Zhao, Y., Cliff, S. S., Hu, W. W., Toohey, D. W., Flynn, J. H., Lefer, B. L., Grossberg, N., Alvarez, S., Rappenglück, B., Taylor, J. W., Allan, J. D., Holloway, J. S., Gilman, J. B., Kuster, W. C., de Gouw, J. A., Massoli, P., Zhang, X., Liu, J., Weber, R. J., Corrigan, A. L., Russell, L. M., Isaacman, G., Worton, D. R., Kreisberg, N. M., Goldstein, A. H., Thalman, R., Waxman, E. M., Volkamer, R., Lin, Y. H., Surratt, J. D., Kleindienst, T. E., Offenberg, J. H., Dusanter, S., Griffith, S., Stevens, P. S., Brioude, J., Angevine, W. M. and Jimenez, J. L.: Organic aerosol composition and sources in Pasadena, California, during the 2010 CalNex campaign, J. Geophys. Res., 118(16), 9233–9257, doi:10.1002/jgrd.50530, 2013.

Hayes, P. L., Carlton, A. G., Baker, K. R., Ahmadov, R., Washenfelder, R. A., Alvarez, S., Rappenglück, B., Gilman, J. B., Kuster, W. C., de Gouw, J. A., Zotter, P., Prévôt, A. S. H., Szidat, S., Kleindienst, T. E., Ma, P. K. and Jimenez, J. L.: Modeling the formation and aging of secondary organic aerosols in Los Angeles during CalNex 2010, Atmos. Chem. Phys., 15(10), 5773–5801, doi:10.5194/acp-15-5773-2015, 2015.

Heald, C. L., Kroll, J. H., Jimenez, J. L., Docherty, K. S., Decarlo, P. F., Aiken, A. C., Chen, Q., Martin, S. T., Farmer, D. K. and Artaxo, P.: A simplified description of the evolution of organic aerosol composition in the atmosphere, Geophys. Res. Lett., 37(8), L08803, doi:10.1029/2010GL042737, 2010.

Heim, E., Dibb, J., Scheuer, E., Campuzano-Jost, P., Nault, B. A., Jimenez, J. L., Peterson, D., Knote, C., Fenn, M., Hair, J., Beyersdorf, A. J. and Anderson, B. E.: Asian Dust Observed during KORUS-AQ Facilitates the Uptake and Incorporation of Soluble Pollutants during Transport to South Korea: The Hwangsa Anthropogenic Model, J. Geophys. Res. Atmos., submitted, 2018.

Hennigan, C. J., Sullivan, A. P., Fountoukis, C. I., Nenes, A., Hecobian, A., Vargas, O., Peltier, R. E., Hanks, A. T. C., Huey, L. G., Lefer, B. L., Russell, A. G. and Weber, R. J.: On the volatility and production mechanisms of newly formed nitrate and water soluble organic aerosol in Mexico City, Atmos. Chem. Phys., 8(14), 3761–3768, doi:10.5194/acp-8-3761-2008, 2008.

Heo, J.-B., Hopke, P. K. and Yi, S.-M.: Source apportionment of PM2.5 in Seoul, Korea, Atmos. Chem. Phys., 9(14), 4957–4971, doi:10.5194/acp-9-4957-2009, 2009.

Herndon, S. C., Onasch, T. B., Wood, E. C., Kroll, J. H., Canagaratna, M. R., Jayne, J. T., Zavala,

M. A., Knighton, W. B., Mazzoleni, C., Dubey, M. K., Ulbrich, I. M., Jimenez, J. L., Seila, R., de Gouw, J. A., de Foy, B., Fast, J., Molina, L. T., Kolb, C. E. and Worsnop, D. R.: Correlation of secondary organic aerosol with odd oxygen in Mexico City, Geophys. Res. Lett., 35(15), doi:10.1029/2008GL034058, 2008.

Hersey, S. P., Craven, J. S., Metcalf, A. R., Lin, J., Lathem, T., Suski, K. J., Cahill, J. F., Duong, H. T., Sorooshian, A., Jonsson, H. H., Shiraiwa, M., Zuend, A., Nenes, A., Prather, K. A., Flagan, R. C. and Seinfeld, J. H.: Composition and hygroscopicity of the Los Angeles Aerosol: CalNex, J. Geophys. Res. Atmos., 118(7), 3016–3036, doi:10.1002/jgrd.50307, 2013.

Hildebrandt Ruiz, L., Paciga, A. L., Cerully, K. M., Nenes, A., Donahue, N. M. and Pandis, S. N.: Formation and aging of secondary organic aerosol from toluene: changes in chemical composition, volatility, and hygroscopicity, Atmos. Chem. Phys., 15(14), 8301–8313, doi:10.5194/acp-15-8301-2015, 2015.

Hodzic, A. and Jimenez, J. L.: Modeling anthropogenically controlled secondary organic aerosols in a megacity: A simplified framework for global and climate models, Geosci. Model Dev., 4(4), 901–917, doi:10.5194/gmd-4-901-2011, 2011.

Hodzic, A., Jimenez, J. L., Madronich, S., Canagaratna, M. R., DeCarlo, P. F., Kleinman, L. and Fast, J.: Modeling organic aerosols in a megacity: Potential contribution of semi-volatile and intermediate volatility primary organic compounds to secondary organic aerosol formation, Atmos. Chem. Phys., 10(12), 5491–5514, doi:10.5194/acp-10-5491-2010, 2010.

Hodzic, A., Madronich, S., Kasibhatla, P. S., Tyndall, G., Aumont, B., Jimenez, J. L., Lee-Taylor, J. and Orlando, J.: Organic photolysis reactions in tropospheric aerosols: effect on secondary organic aerosol formation and lifetime, Atmos. Chem. Phys., 15(16), 9253–9269, doi:10.5194/acp-15-9253-2015, 2015.

Hong, J.-W. and Hong, J.: Changes in the Seoul Metropolitan Area Urban Heat Environment with Residential Redevelopment, J. Appl. Meteorol. Climatol., 55, 1091–1106, doi:10.1175/JAMC-D-15-0321.1, 2016.

Hu, W., Hu, M., Hu, W., Jimenez, J. L., Yuan, B., Chen, W., Wang, M., Wu, Y., Chen, C., Wang, Z., Peng, J., Zeng, L. and Shao, M.: Chemical composition, sources and aging process of sub-micron aerosols in Beijing: contrast between summer and winter, J. Geophys. Res. Atmos., doi:10.1002/2015JD024020, 2016.

Hu, W., Campuzano-Jost, P., Day, D. A., Croteau, P., Canagaratna, M. R., Jayne, J. T., Worsnop, D. R. and Jimenez, J. L.: Evaluation of the new capture vaporizer for aerosol mass spectrometers (AMS) through field studies of inorganic species, , doi:10.1080/02786826.2017.1296104, 2017a.

Hu, W., Campuzano-Jost, P., Day, D. A., Croteau, P., Canagaratna, M. R., Jayne, J. T., Worsnop, D. R. and Jimenez, J. L.: Evaluation of the new capture vapourizer for aerosol mass spectrometers (AMS) through laboratory studies of inorganic species, Atmos. Meas. Tech., 10(6), 2897–2921, doi:10.5194/amt-10-2897-2017, 2017b.

Hu, W., Day, D. A., Campuzano-Jost, P., Nault, B. A., Park, T., Lee, T., Croteau, P., Canagaratna, M. R., Jayne, J. T., Worsnop, D. R. and Jimenez, J. L.: Evaluation of the new capture vaporizer for Aerosol Mass Spectrometers: Characterization of organic aerosol mass spectra, Aerosol Sci. Technol., 52(7), 752–739, doi:10.1080/02786826.2018.1454584, 2018a.

Hu, W., Day, D. A., Campuzano-Jost, P., Nault, B. A., Park, T., Lee, T., Croteau, P., Canagaratna,

M. R., Jayne, J. T., Worsnop, D. R. and Jimenez, J. L.: Evaluation of the New Capture Vaporizer for Aerosol Mass Spectrometers (AMS): Elemental Composition and Source Apportionment of Organic Aerosols (OA), ACS Earth Sp. Chem., 2(4), 410–421, doi:10.1021/acsearthspacechem.8b00002, 2018b.

Hu, W. W., Hu, M., Yuan, B., Jimenez, J. L., Tang, Q., Peng, J. F., Hu, W., Shao, M., Wang, M., Zeng, L. M., Wu, Y. S., Gong, Z. H., Huang, X. F. and He, L. Y.: Insights on organic aerosol aging and the influence of coal combustion at a regional receptor site of central eastern China, Atmos. Chem. Phys., 13(19), 10095–10112, doi:10.5194/acp-13-10095-2013, 2013.

Hu, W. W., Campuzano-Jost, P., Palm, B. B., Day, D. A., Ortega, A. M., Hayes, P. L., Krechmer, J. E., Chen, Q., Kuwata, M., Liu, Y. J., de Sá, S. S., McKinney, K., Martin, S. T., Hu, M., Budisulistiorini, S. H., Riva, M., Surratt, J. D., St. Clair, J. M., Isaacman-Van Wertz, G., Yee, L. D., Goldstein, A. H., Carbone, S., Brito, J., Artaxo, P., de Gouw, J. A., Koss, A., Wisthaler, A., Mikoviny, T., Karl, T., Kaser, L., Jud, W., Hansel, A., Docherty, K. S., Alexander, M. L., Robinson, N. H., Coe, H., Allan, J. D., Canagaratna, M. R., Paulot, F. and Jimenez, J. L.: Characterization of a real-time tracer for Isoprene Epoxydiols-derived Secondary Organic Aerosol (IEPOX-SOA) from aerosol mass spectrometer measurements, Atmos. Chem. Phys., 15(8), 11807–11833, doi:10.5194/acp-15-11807-2015, 2015.

Huang, C., Wang, H. L., Li, L., Wang, Q., Lu, Q., de Gouw, J. A., Zhou, M., Jing, S. A., Lu, J. and Chen, C. H.: VOC species and emission inventory from vehicles and their SOA formation potentials estimation in Shanghai, China, Atmos. Chem. Phys., 15(19), 11081–11096, doi:10.5194/acp-15-11081-2015, 2015.

Huey, L. G., Tanner, D. J., Slusher, D. L., Dibb, J. E., Arimoto, R., Chen, G., Davis, D., Buhr, M. P., Nowak, J. B., Mauldin III, R. L., Eisele, F. L. and Kosciuch, E.: CIMS measurements of HNO_3 and SO_2 at the South Pole during ISCAT 2000, Atmos. Environ., 38(32), 5411–5421, doi:10.1016/J.ATMOSENV.2004.04.037, 2004.

Huffman, J. A., Docherty, K. S., Aiken, A. C., Cubison, M. J., Ulbrich, I. M., DeCarlo, P. F., Sueper, D., Jayne, J. T., Worsnop, D. R., Ziemann, P. J. and Jimenez, J. L.: Chemically-resolved aerosol volatility measurements from two megacity field studies, Atmos. Chem. Phys., 9(1), 7161–7182, doi:doi:10.5194/acp-9-7161-2009, 2009.

Hunter, J. F., Day, D. A., Palm, B. B., Yatavelli, R. L. N., Chan, A. W. H., Kaser, L., Cappellin, L., Hayes, P. L., Cross, E. S., Carrasquillo, A. J., Campuzano-Jost, P., Stark, H., Zhao, Y., Hohaus, T., Smith, J. N., Hansel, A., Karl, T., Goldstein, A. H., Guenther, A., Worsnop, D. R., Thornton, J. A., Heald, C. L., Jimenez, J. L. and Kroll, J. H.: Comprehensive characterization of atmospheric organic carbon at a forested site, Nat. Geosci., 10(10), 748–753, doi:10.1038/ngeo3018, 2017.

Jacob, D. J.: Heterogeneous chemistry and tropospheric ozone, Atmos. Environ., 34, 2131–2159, doi:10.1016/S1352-2310(99)00462-8, 2000.

Janssen, R. H. H., Tsimpidi, A. P., Karydis, V. A., Pozzer, A., Lelieveld, J., Crippa, M., Prévôt, A. S. H., Ait-Helal, W., Borbon, A., Sauvage, S. and Locoge, N.: Influence of local production and vertical transport on the organic aerosol budget over Paris, J. Geophys. Res. Atmos., 1–21, doi:10.1002/2016JD026402, 2017.

Jathar, S. H., Miracolo, M. A., Tkacik, D. S., Donahue, N. M., Adams, P. J. and Robinson, A. L.: Secondary Organic Aerosol Formation from Photo-Oxidation of Unburned Fuel: Experimental Results and Implications for Aerosol Formation from Combustion Emissions, Environ. Sci.

Technol., 47(22), 12886–12893, doi:10.1021/es403445q, 2013.

Jathar, S. H., Gordon, T. D., Hennigan, C. J., Pye, H. O. T., Pouliot, G., Adams, P. J., Donahue, N. M. and Robinson, A. L.: Unspeciated organic emissions from combustion sources and their influence on the secondary organic aerosol budget in the United States., Proc. Natl. Acad. Sci. U. S. A., 111(29), 10473–10478, doi:10.1073/pnas.1323740111, 2014.

Jayne, J. T. and Worsnop, D. R.: Particle Capture Device Aerodyne Research, 2015.

Jeong, U., Kim, J., Lee, H. and Lee, Y. G.: Assessing the effect of long-range pollutant transportation on air quality in Seoul using the conditional potential source contribution function method, Atmos. Environ., 150, 33–44, doi:10.1016/j.atmosenv.2016.11.017, 2017.

Jimenez, J. L., Canagaratna, M. R., Donahue, N. M., Prevot, A. S. H., Zhang, Q., Kroll, J. H., DeCarlo, P. F., Allan, J. D., Coe, H., Ng, N. L., Aiken, A. C., Docherty, K. S., Ulbrich, I. M., Grieshop, A. P., Robinson, A. L., Duplissy, J., Smith, J. D., Wilson, K. R., Lanz, V. A., Hueglin, C., Sun, Y. L., Tian, J., Laaksonen, A., Raatikainen, T., Rautiainen, J., Vaattovaara, P., Ehn, M., Kulmala, M., Tomlinson, J. M., Collins, D. R., Cubison, M. J., Dunlea, E. J., Huffman, J. A., Onasch, T. B., Alfarra, M. R., Williams, P. I., Bower, K., Kondo, Y., Schneider, J., Drewnick, F., Borrmann, S., Weimer, S., Demerjian, K., Salcedo, D., Cottrell, L., Griffin, R., Takami, A., Miyoshi, T., Hatakeyama, S., Shimono, A., Sun, J. Y., Zhang, Y. M., Dzepina, K., Kimmel, J. R., Sueper, D., Jayne, J. T., Herndon, S. C., Trimborn, A. M., Williams, L. R., Wood, E. C., Middlebrook, A. M., Kolb, C. E., Baltensperger, U., Worsnop, D. R. and Worsnop, D. R.: Evolution of organic aerosols in the atmosphere., Science, 326(5959), 1525–1529, doi:10.1126/science.1180353, 2009.

Jimenez, J. L., Canagaratna, M. R., Donahue, N. M., Prévôt, A. S. H., Zhang, Q., Kroll, J. H., DeCarlo, P. F., Allan, J. D., Coe, H., Ng, N. L., Aiken, A. C., Docherty, K. S., Ulbrich, I. M., Grieshop, A. P., Robinson, A. L., Duplissy, J., Smith, J. D., Wilson, K. R., Lanz, V. A., Hueglin, C., Sun, Y. L., Tian, J., Laaksonen, A., Raatikainen, T., Rautiainen, J., Vaattovaara, P., Ehn, M., Kulmala, M., Tomlinson, J. M., Collins, D. R., Cubison, M. J., Dunlea, E. J., Huffman, J. A., Onasch, T. B., Alfarra, M. R., Williams, P. I., Bower, K., Kondo, Y., Schneider, J., Drewnick, F., Borrmann, S., Weimer, S., Demerjian, K., Salcedo, D., Cottrell, L., Griffin, R., Takami, A., Miyoshi, T., Hatakeyama, S., Shimono, A., Sun, J. Y., Zhang, Y. M., Dzepina, K., Kimmel, J. R., Sueper, D., Jayne, J. T., Herndon, S. C., Trimborn, A. M., Williams, L. R., Wood, E. C., Middlebrook, A. M., Kolb, C. E., Baltensperger, U. and Worsnop, D. R.: Evolution of Organic Aerosols in the Atmosphere, Science (80-.)., 326(5959), 1525–1529, doi:10.1126/science.1180353, 2009.

Jimenez, J. L., Canagaratna, M. R., Drewnick, F., Allan, J. D., Alfarra, M. R., Middlebrook, A. M., Slowik, J. G., Zhang, Q., Coe, H., Jayne, J. T. and Worsnop, D. R.: Comment on “The effects of molecular weight and thermal decomposition on the sensitivity of a thermal desorption aerosol mass spectrometer,” Aerosol Sci. Technol., 50(9), i–xv, doi:10.1080/02786826.2016.1205728, 2016.

Jimenez, J. L., Campuzano-Jost, P., Day, D. A., Nault, B. A., Schroder, J. C. and Cubison, M. J.: Frequently AMS Questions for AMS Data Users, [online] Available from: http://cires.colorado.edu/jimenez-group/wiki/index.php?title=FAQ_for_AMS_Data_Users, accessed month-year (Accessed 6 December 2018), 2018.

Kang, C. M., Kang, B. W. and Lee, H. S.: Source identification and trends in concentrations of

gaseous and fine particulate principal species in Seoul, South Korea, J. Air Waste Manag. Assoc., 56(7), 911–921, doi:10.1080/10473289.2006.10464506, 2006.

Kang, E., Root, M. J., Toohey, D. W. and Brune, W. H.: Introducing the concept of Potential Aerosol Mass (PAM), Atmos. Chem. Phys., 7(22), 5727–5744, doi:10.5194/acp-7-5727-2007, 2007.

Kang, E., Lee, M., Brune, W. H., Lee, T., Park, T., Ahn, J. and Shang, X.: Photochemical aging of aerosol particles in different air masses arriving at Baengnyeong Island, Korea, Atmos. Chem. Phys., 18(9), 6661–6677, doi:10.5194/acp-18-6661-2018, 2018.

Khare, P. and Gentner, D. R.: Considering the future of anthropogenic gas-phase organic compound emissions and the increasing influence of non-combustion sources on urban air quality, Atmos. Chem. Phys., 18(8), 5391–5413, doi:10.5194/acp-18-5391-2018, 2018.

Kim, B. M., Seo, J., Kim, J. Y., Lee, J. Y. and Kim, Y.: Transported vs. local contributions from secondary and biomass burning sources to PM2.5, Atmos. Environ., 144, 24–36, doi:10.1016/j.atmosenv.2016.08.072, 2016.

Kim, H., Zhang, Q., Bae, G.-N., Kim, J. Y. and Lee, S. B.: Sources and atmospheric processing of wintertime aerosols in Seoul, Korea: Insights from real-time measurements using a high-resolution aerosol mass spectrometer, Atmos. Chem. Phys. Discuss., 17(3), 2009–2003, doi:10.5194/acp-17-2009-2017, 2017.

Kim, H., Zhang, Q. and Heo, J.: Influence of Intense secondary aerosol formation and long-range transport on aerosol chemistry and properties in the Seoul Metropolitan Area during spring time : Results from KORUS-AQ, Atmos. Chem. Phys., 18, 7149–7168, doi:10.51944/acp-2017-947, 2018.

Kim, H. C., Kim, E. H., Kim, B. U. and Kim, S.: Regional Contributions to the Particulate Matter Concentration in the Seoul Metropolitan Area, Korea: Seasonal Variation and Sensitivity to Meteorology, Atmos. Chem. Phys, 17(17), 10315–10332, doi:10.5194/acp-17-10315-2017, 2017.

Kim, H. S., Huh, J. B., Hopke, P. K., Holsen, T. M. and Yi, S. M.: Characteristics of the major chemical constituents of PM2.5 and smog events in Seoul, Korea in 2003 and 2004, Atmos. Environ., 41(32), 6762–6770, doi:10.1016/j.atmosenv.2007.04.060, 2007.

Kim, S., Huey, L. G., Stickel, R. E., Tanner, D. J., Crawford, J. H., Olson, J. R., Chen, G., Brune, W. H., Ren, X., Lesher, R., Wooldridge, P. J., Bertram, T. H., Perring, A., Cohen, R. C., Lefer, B. L., Shetter, R. E., Avery, M., Diskin, G. and Sokolik, I.: Measurement of HO_2NO_2 in the free troposphere during the Intercontinental Chemical Transport Experiment–North America 2004, J. Geophys. Res., 112, D12S01, doi:10.1029/2006JD007676, 2007.

Kim, Y. J., Woo, J. H., Ma, Y. Il, Kim, S., Nam, J. S., Sung, H., Choi, K. C., Seo, J., Kim, J. S., Kang, C. H., Lee, G., Ro, C. U., Chang, D. and Sunwoo, Y.: Chemical characteristics of long-range transport aerosol at background sites in Korea, Atmos. Environ., 43(34), 5556–5566, doi:10.1016/j.atmosenv.2009.03.062, 2009.

Kimmel, J. R., Farmer, D. K., Cubison, M. J., Sueper, D., Tanner, C., Nemitz, E., Worsnop, D. R., Gonin, M. and Jimenez, J. L.: Real-time aerosol mass spectrometry with millisecond resolution, Int. J. Mass Spectrom., 303(1), 15–26, doi:10.1016/j.ijms.2010.12.004, 2011.

Kleinman, L., Kuang, C., Sedlacek, A., Senum, G., Springston, S., Wang, J., Zhang, Q., Jayne, J.,

Fast, J., Hubbe, J., Shilling, J. and Zaveri, R.: What do correlations tell us about anthropogenic-biogenic interactions and SOA formation in the Sacramento plume during CARES?, Atmos. Chem. Phys., 16(3), 1729–1746, doi:10.5194/acp-16-1729-2016, 2016.

Kleinman, L. I., Daum, P. H., Lee, Y.-N., Senum, G. I., Springston, S. R., Wang, J., Berkowitz, C., Hubbe, J., Zaveri, R. A., Brechtel, F. J., Jayne, J., Onasch, T. B. and Worsnop, D.: Aircraft observations of aerosol composition and ageing in New England and Mid-Atlantic States during the summer 2002 New England Air Quality Study field campaign, J. Geophys. Res., 112(D9), D09310, doi:10.1029/2006JD007786, 2007.

Kleinman, L. I., Springston, S. R., Daum, P. H., Lee, Y.-N., Nunnermacker, L. J., Senum, G. I., Wang, J., Weinstein-Lloyd, J., Alexander, M. L., Hubbe, J., Ortega, J., Canagaratna, M. R. and Jayne, J.: The time evolution of aerosol composition over the Mexico City plateau, Atmos. Chem. Phys., 8(6), 1559–1575, doi:10.5194/acp-8-1559-2008, 2008.

Kleinman, L. I., Springston, S. R., Wang, J., Daum, P. H., Lee, Y.-N. N., Nunnermacker, L. J., Senum, G. I., Weinstein-Lloyd, J., Alexander, M. L., Hubbe, J., Ortega, J., Zaveri, R. A., Canagaratna, M. R. and Jayne, J.: The time evolution of aerosol size distribution over the Mexico City plateau, Atmos. Chem. Phys., 9(13), 4261–4278, doi:10.5194/acpd-9-1621-2009, 2009.

Knote, C., Brunner, D., Vogel, H., Allan, J., Asmi, A., Äijälä, M., Carbone, S., van der Gon, H. D., Jimenez, J. L., Kiendler-Scharr, A., Mohr, C., Poulain, L., Prévôt, A. S. H., Swietlicki, E. and Vogel, B.: Towards an online-coupled chemistry-climate model: evaluation of trace gases and aerosols in COSMO-ART, Geosci. Model Dev., 4(4), 1077–1102, doi:10.5194/gmd-4-1077-2011, 2011.

Knote, C., Hodzic, A., Jimenez, J. L., Volkamer, R., Orlando, J. J., Baidar, S., Brioude, J., Fast, J., Gentner, D. R., Goldstein, A. H., Hayes, P. L., Knighton, W. B., Oetjen, H., Setyan, A., Stark, H., Thalman, R., Tyndall, G., Washenfelder, R., Waxman, E. and Zhang, Q.: Simulation of semi-explicit mechanisms of SOA formation from glyoxal in aerosol in a 3-D model, Atmos. Chem. Phys., 14(12), 6213–6239, doi:10.5194/acp-14-6213-2014, 2014.

Krechmer, J. E., Pagonis, D., Ziemann, P. J. and Jimenez, J. L.: Quantification of Gas-Wall Partitioning in Teflon Environmental Chambers Using Rapid Bursts of Low-Volatility Oxidized Species Generated in Situ, Environ. Sci. Technol., 50(11), 5757–5765, doi:10.1021/acs.est.6b00606, 2016.

Krechmer, J. E., Day, D. A., Ziemann, P. J. and Jimenez, J. L.: Direct Measurements of Gas/Particle Partitioning and Mass Accommodation Coefficients in Environmental Chambers, Environ. Sci. Technol., 51(20), 11867–11875, doi:10.1021/acs.est.7b02144, 2017.

Kroll, J. H. and Seinfeld, J. H.: Chemistry of secondary organic aerosol: Formation and evolution of low-volatility organics in the atmosphere, Atmos. Environ., 42(16), 3593–3624, doi:10.1016/J.ATMOSENV.2008.01.003, 2008.

Kroll, J. H., Donahue, N. M., Jimenez, J. L., Kessler, S. H., Canagaratna, M. R., Wilson, K. R., Altieri, K. E., Mazzoleni, L. R., Wozniak, A. S., Bluhm, H., Mysak, E. R., Smith, J. D., Kolb, C. E. and Worsnop, D. R.: Carbon oxidation state as a metric for describing the chemistry of atmospheric organic aerosol., Nat. Chem., 3(2), 133–139, doi:10.1038/nchem.948, 2011.

Kuwata, M., Zorn, S. R. and Martin, S. T.: Using Elemental Ratios to Predict the Density of Organic Material Composed of Carbon, Hydrogen, and Oxygen, Environ. Sci. Technol., 46(2),

787–794, doi:10.1021/es202525q, 2012.

Lambe, A. T., Ahern, A. T., Williams, L. R., Slowik, J. G., Wong, J. P. S., Abbatt, J. P. D., Brune, W. H., Ng, N. L., Wright, J. P., Croasdale, D. R., Worsnop, D. R., Davidovits, P. and Onasch, T. B.: Characterization of aerosol photooxidation flow reactors: heterogeneous oxidation, secondary organic aerosol formation and cloud condensation nuclei activity measurements, Atmos. Meas. Tech., 4(3), 445–461, doi:10.5194/amt-4-445-2011, 2011.

Lambe, A. T., Onasch, T. B., Croasdale, D. R., Wright, J. P., Martin, A. T., Franklin, J. P., Massoli, P., Kroll, J. H., Canagaratna, M. R., Brune, W. H., Worsnop, D. R. and Davidovits, P.: Transitions from Functionalization to Fragmentation Reactions of Laboratory Secondary Organic Aerosol (SOA) Generated from the OH Oxidation of Alkane Precursors, Environ. Sci. Technol., 46(10), 5430–5437, doi:10.1021/Es300274t, 2012.

Landrigan, P. J., Fuller, R., Acosta, N. J. R., Adeyi, O., Arnold, R., Basu, N., Baldé, A. B., Bertollini, R., Bose-O'Reilly, S., Boufford, J. I., Breysse, P. N., Chiles, T., Mahidol, C., Coll-Seck, A. M., Cropper, M. L., Fobil, J., Fuster, V., Greenstone, M., Haines, A., Hanrahan, D., Hunter, D., Khare, M., Krupnick, A., Lanphear, B., Lohani, B., Martin, K., Mathiasen, K. V, McTeer, M. A., Murray, C. J. L., Ndahimananjara, J. D., Perera, F., Potočnik, J., Preker, A. S., Ramesh, J., Rockström, J., Salinas, C., Samson, L. D., Sandilya, K., Sly, P. D., Smith, K. R., Steiner, A., Stewart, R. B., Suk, W. A., van Schayck, O. C. P., Yadama, G. N., Yumkella, K. and Zhong, M.: The Lancet Commission on pollution and health, Lancet, 391(10119), 462–512, doi:10.1016/S0140-6736(17)32345-0, 2018.

Lee, G., Choi, H. S., Lee, T., Choi, J., Park, J. S. and Ahn, J. Y.: Variations of regional background peroxyacetyl nitrate in marine boundary layer over Baengyeong Island, South Korea, Atmos. Environ., 61, 533–541, doi:10.1016/j.atmosenv.2012.07.075, 2012.

Lee, H. M., Park, R. J., Henze, D. K., Lee, S., Shim, C., Shin, H. J., Moon, K. J. and Woo, J. H.: PM2.5 source attribution for Seoul in May from 2009 to 2013 using GEOS-Chem and its adjoint model, Environ. Pollut., 221, 377–384, doi:10.1016/j.envpol.2016.11.088, 2017.

Lee, S., Ho, C.-H., Lee, Y. G., Choi, H.-J. and Song, C.-K.: Influence of transboundary air pollutants from China on the high-PM10 episode in Seoul, Korea for the period October 16–20, 2008, Atmos. Environ., 77, 430–439, doi:10.1016/J.ATMOSENV.2013.05.006, 2013.

Lee, T., Choi, J., Lee, G., Ahn, J., Park, J. S., Atwood, S. A., Schurman, M., Choi, Y., Chung, Y. and Collett, J. L.: Characterization of aerosol composition, concentrations, and sources at Baengnyeong Island, Korea using an aerosol mass spectrometer, Atmos. Environ., 120, 297–306, doi:10.1016/j.atmosenv.2015.08.038, 2015.

Lelieveld, J., Evans, J. S., Fnais, M., Giannadaki, D. and Pozzer, A.: The contribution of outdoor air pollution sources to premature mortality on a global scale, Nature, 525(7569), 367–371, doi:10.1038/nature15371, 2015.

Li, R., Palm, B. B., Ortega, A. M., Hlywiak, J., Hu, W., Peng, Z., Day, D. A., Knote, C., Brune, W. H., de Gouw, J. A. and Jimenez, J. L.: Modeling the radical chemistry in an oxidation flow reactor: radical formation and recycling, sensitivities, and the OH exposure estimation equation., J. Phys. Chem. A, 119(19), 4418–4432, doi:10.1021/jp509534k, 2015.

Lide, D. R.: CRC Handbook of Chemistry and Physics, CRC Press Inc., USA., 1991.

Liu, P. S. K., Deng, R., Smith, K. A., Williams, L. R., Jayne, J. T., Canagaratna, M. R., Moore,

K., Onasch, T. B., Worsnop, D. R. and Deshler, T.: Transmission Efficiency of an Aerodynamic Focusing Lens System: Comparison of Model Calculations and Laboratory Measurements for the Aerodyne Aerosol Mass Spectrometer, Aerosol Sci. Technol., 41(8), 721–733, doi:10.1080/02786820701422278, 2007.

Liu, T., Wang, X., Deng, W., Hu, Q., Ding, X., Zhang, Y., He, Q., Zhang, Z., Lü, S., Bi, X., Chen, J. and Yu, J.: Secondary organic aerosol formation from photochemical aging of light-duty gasoline vehicle exhausts in a smog chamber, Atmos. Chem. Phys., 15(15), 9049–9062, doi:10.5194/acp-15-9049-2015, 2015.

Liu, X., Huey, L. G., Yokelson, R. J., Selimovic, V., Simpson, I. J., Müller, M., Jimenez, J. L., Campuzano-Jost, P., Beyersdorf, A. J., Blake, D. R., Butterfield, Z., Choi, Y., Crounse, J. D., Day, D. A., Diskin, G. S., Dubey, M. K., Fortner, E., Hanisco, T. F., Hu, W., King, L. E., Kleinman, L., Meinardi, S., Mikoviny, T., Onasch, T. B., Palm, B. B., Peischl, J., Pollack, I. B., Ryerson, T. B., Sachse, G. W., Sedlacek, A. J., Shilling, J. E., Springston, S., St. Clair, J. M., Tanner, D. J., Teng, A. P., Wennberg, P. O., Wisthaler, A. and Wolfe, G. M.: Airborne measurements of western U.S. wildfire emissions: Comparison with prescribed burning and air quality implications, J. Geophys. Res., 122(11), 6108–6129, doi:10.1002/2016JD026315, 2017.

Ma, P. K., Zhao, Y., Robinson, A. L., Worton, D. R., Goldstein, A. H., Ortega, A. M., Jimenez, J.-L., Zotter, P., Prévôt, A. S. H., Szidat, S. and Hayes, P. L.: Evaluating the impact of new observational constraints on P-S/IVOC emissions, multi-generation oxidation, and chamber wall losses on SOA modeling for Los Angeles, CA, Atmos. Chem. Phys., 17(15), 9237–9259, doi:10.5194/acp-17-9237-2017, 2017.

Mao, J., Ren, X., Brune, W. H., Olson, J. R., Crawford, J. H., Fried, a., Huey, L. G., Cohen, R. C., Heikes, B., Singh, H. B., Blake, D. R., Sachse, G. W., Diskin, G. S., Hall, S. R. and Shetter, R. E.: Airborne measurement of OH reactivity during INTEX-B, Atmos. Chem. Phys., 9(1), 163–173, doi:10.5194/acp-9-163-2009, 2009.

Matsunaga, A. and Ziemann, P. J.: Gas-Wall Partitioning of Organic Compounds in a Teflon Film Chamber and Potential Effects on Reaction Product and Aerosol Yield Measurements, Aerosol Sci. Technol., 44(10), 881–892, doi:10.1080/02786826.2010.501044, 2010.

McDonald, B. C., de Gouw, J. A., Gilman, J. B., Jathar, S. H., Akherati, A., Cappa, C. D., Jimenez, J. L., Lee-Taylor, J., Hayes, P. L., McKeen, S. A., Cui, Y. Y., Kim, S.-W., Gentner, D. R., Isaacman-VanWertz, G., Goldstein, A. H., Harley, R. A., Frost, G. J., Roberts, J. M., Ryerson, T. B. and Trainer, M.: Volatile chemical products emerging as largest petrochemical source of urban organic emissions., Science, 359(6377), 760–764, doi:10.1126/science.aaq0524, 2018.

McKeen, S. A., Liu, S. C., Hsie, E.-Y., Lin, X., Bradshaw, J. D., Smyth, S., Gregory, G. L. and Blake, D. R.: Hydrocarbon ratios during PEM-WEST A: A model perspective, J. Geophys. Res. Atmos., 101(D1), 2087–2109, doi:10.1029/95JD02733, 1996.

McMeeking, G. R., Bart, M., Chazette, P., Haywood, J. M., Hopkins, J. R., McQuaid, J. B., Morgan, W. T., Raut, J.-C., Ryder, C. L., Savage, N., Turnbull, K. and Coe, H.: Airborne measurements of trace gases and aerosols over the London metropolitan region, Atmos. Chem. Phys., 12(11), 5163–5187, doi:10.5194/acp-12-5163-2012, 2012.

McNaughton, C. S., Clarke, A. D., Howell, S. G., Pinkerton, M., Anderson, B., Thornhill, L., Hudgins, C., Winstead, E., Dibb, J. E., Scheuer, E. and Maring, H.: Results from the DC-8 Inlet Characterization Experiment (DICE): Airborne versus surface sampling of mineral dust and sea

salt aerosols, Aerosol Sci. Technol., 41(2), 136–159, doi:10.1080/02786820601118406, 2007.

Middlebrook, A. M., Bahreini, R., Jimenez, J. L. and Canagaratna, M. R.: Evaluation of Composition-Dependent Collection Efficiencies for the Aerodyne Aerosol Mass Spectrometer using Field Data, Aerosol Sci. Technol., 46(3), 258–271, doi:10.1080/02786826.2011.620041, 2012.

Miracolo, M. A., Presto, A. A., Lambe, A. T., Hennigan, C. J., Donahue, N. M., Kroll, J. H., Worsnop, D. R. and Robinson, A. L.: Photo-Oxidation of Low-Volatility Organics Found in Motor Vehicle Emissions: Production and Chemical Evolution of Organic Aerosol Mass, Environ. Sci. Technol., 44(5), 1638–1643, doi:10.1021/es902635c, 2010.

Mitroo, D., Sun, Y., Combest, D. P., Kumar, P. and Williams, B. J.: Assessing the degree of plug flow in oxidation flow reactors (OFRs): a study on a potential aerosol mass (PAM) reactor, Atmos. Meas. Tech, 11, 1741–1756, doi:10.5194/amt-11-1741-2018, 2018.

Moise, T., Flores, J. M. and Rudich, Y.: Optical Properties of Secondary Organic Aerosols and Their Changes by Chemical Processes, Chem. Rev., 115(10), 4400–4439, doi:10.1021/cr5005259, 2015.

Mollner, A. K., Valluvadasan, S., Feng, L., Sprague, M. K., Okumura, M., Milligan, D. B., Bloss, W. J., Sander, S. P., Martien, P. T., Harley, R. a, McCoy, A. B. and Carter, W. P. L.: Rate of Gas Phase Association of Hydroxyl Radical and Nitrogen Dioxide, Science (80-.)., 330(6004), 646–9, doi:10.1126/science.1193030, 2010.

Monks, P. S., Granier, C., Fuzzi, S., Stohl, A., Williams, M. L., Akimoto, H., Amann, M., Baklanov, A., Baltensperger, U., Bey, I., Blake, N., Blake, R. S., Carslaw, K., Cooper, O. R., Dentener, F., Fowler, D., Fragkou, E., Frost, G. J., Generoso, S., Ginoux, P., Grewe, V., Guenther, A., Hansson, H. C., Henne, S., Hjorth, J., Hofzumahaus, A., Huntrieser, H., Isaksen, I. S. A., Jenkin, M. E., Kaiser, J., Kanakidou, M., Klimont, Z., Kulmala, M., Laj, P., Lawrence, M. G., Lee, J. D., Liousse, C., Maione, M., McFiggans, G., Metzger, A., Mieville, A., Moussiopoulos, N., Orlando, J. J., O'Dowd, C. D., Palmer, P. I. I., Parrish, D. D., Petzold, A., Platt, U., Pöschl, U., Prévôt, A. S. H., Reeves, C. E., Reimann, S., Rudich, Y., Sellegri, K., Steinbrecher, R., Simpson, D., ten Brink, H., Theloke, J., van der Werf, G. R., Vautard, R., Vestreng, V., Vlachokostas, C. and von Glasow, R.: Atmospheric composition change - global and regional air quality, Atmos. Environ., 43(33), 5268–5350, doi:10.1016/j.atmosenv.2009.08.021, 2009.

Morino, Y., Tanabe, K., Sato, K. and Ohara, T.: Secondary organic aerosol model intercomparison based on secondary organic aerosol to odd oxygen ratio in Tokyo, J. Geophys. Res. Atmos., 119(23), 13,489-13,505, doi:10.1002/2014JD021937, 2014.

Müller, M., Mikoviny, T., Feil, S., Haidacher, S., Hanel, G., Hartungen, E., Jordan, A., Märk, L., Mutschlechner, P., Schottkowsky, R., Sulzer, P., Crawford, J. H. and Wisthaler, A.: A compact PTR-ToF-MS instrument for airborne measurements of volatile organic compounds at high spatiotemporal resolution, Atmos. Meas. Tech., 7(11), 3763–3772, doi:10.5194/amt-7-3763-2014, 2014.

Murphy, B. N., Donahue, N. M., Fountoukis, C. and Pandis, S. N.: Simulating the oxygen content of ambient organic aerosol with the 2D volatility basis set, Atmos. Chem. Phys., 11(15), 7859–7873, doi:10.5194/acp-11-7859-2011, 2011.

Murphy, B. N., Woody, M. C., Jimenez, J. L., Carlton, A. M. G., Hayes, P. L., Liu, S., Ng, N. L.,

Russell, L. M., Setyan, A., Xu, L., Young, J., Zaveri, R. A., Zhang, Q. and Pye, H. O. T.: Semivolatile POA and parameterized total combustion SOA in CMAQv5.2: impacts on source strength and partitioning, Atmos. Chem. Phys., 17(18), 11107–11133, doi:10.5194/acp-17-11107-2017, 2017.

Murphy, D. M.: The effects of molecular weight and thermal decomposition on the sensitivity of a thermal desorption aerosol mass spectrometer, Aerosol Sci. Technol., 50(2), 118–125, doi:10.1080/02786826.2015.1136403, 2016.

Myhre, G., Shindell, D., Bréon, F.-M., Collins, W., Fuglestvedt, J., Huang, J., Koch, D., Lamarque, J.-F., Lee, D., Mendoza, B., Nakajima, T., Robock, A., Stephens, G., Takemura, T. and Zhang, H.: Anthropogenic and Natural Radiative Forcing, in Climate Change 2013: The Physical Science Basis. Contribution of Working Group I to the Fifth Assessment Report of the Intergovernmental Panel on Climate Change, edited by T. F. Stocker, D. Qin, G.-K. Plattner, M. Tignor, S. K. Allen, J. Boschung, A. Nauels, Y. Xia, V. Bex, and P. M. Midgley, p. 659, Cambridge University Press, Cambridge, United Kingdom and New York, NY, USA, United Kingdom and New York, NY, USA. [online] Available from: https://www.ipcc.ch/report/ar5/wg1/, 2013.

Nault, B. A., Campuzano-Jost, P., Schroder, J. C., Sueper, D. and Jimenez, J. L.: Using Event Trigger Panel for IE/AB and Transmission Curve Calibrations, in 17th AMS Users' Meeting, Portland. [online] Available from: http://cires1.colorado.edu/jimenez-group/wiki/index.php/AMSUsrMtgs#17th_AMS_Users_Meeting.2C_Portland.2C_Oregon, 2016.

NCEP: National Centers for Environmental Prediction, [online] Available from: http://www.emc.ncep.noaa.gov/GFS/doc.php (Accessed 16 November 2017), n.d.

Neuman, J. A., Parrish, D. D., Ryerson, T. B., Brock, C. A., Wiedinmyer, C., Frost, G. J., Holloway, J. S. and Fehsenfeld, F. C.: Nitric acid loss rates measured in power plant plumes, J. Geophys. Res., 109(23), 1–13, doi:10.1029/2004JD005092, 2004.

Ng, N. L., Canagaratna, M. R., Zhang, Q., Jimenez, J. L., Tian, J., Ulbrich, I. M., Kroll, J. H., Docherty, K. S., Chhabra, P. S., Bahreini, R., Murphy, S. M., Seinfeld, J. H., Hildebrandt, L., Donahue, N. M., Decarlo, P. F., Lanz, V. A., Prévôt, A. S. H., Dinar, E., Rudich, Y. and Worsnop, D. R.: Organic aerosol components observed in Northern Hemispheric datasets from Aerosol Mass Spectrometry, Atmos. Chem. Phys., 10(10), 4625–4641, doi:10.5194/acp-10-4625-2010, 2010.

Nguyen, T. B., Crounse, J. D., Teng, A. P., St. Clair, J. M., Paulot, F., Wolfe, G. M. and Wennberg, P. O.: Rapid deposition of oxidized biogenic compounds to a temperate forest, Proc. Natl. Acad. Sci., 112(5), E392–E401, doi:10.1073/pnas.1418702112, 2015.

Novelli, P. C., Crotwell, A., Lang, P. M. and Mund, J.: Atmospheric Carbon Monoxide Dry Air Mole Fractions from the NOAA ESRL Carbon Cycle Cooperative Global Air Sampling Network, 1988-2016, Version: 2017-07-28, [online] Available from: ftp://aftp.cmdl.noaa.gov/data/trace_gases/co/flask/surface/, 2017.

OECD: Exposure to PM2.5 in countries and regions : Exposure to PM2.5 in macroregions, [online] Available from: https://stats.oecd.org/index.aspx?queryid=72722 (Accessed 1 August 2018), 2018.

Ortega, A. M., Day, D. A., Cubison, M. J., Brune, W. H., Bon, D., de Gouw, J. A. and Jimenez, J. L.: Secondary organic aerosol formation and primary organic aerosol oxidation from biomass-

burning smoke in a flow reactor during FLAME-3, Atmos. Chem. Phys., 13(22), 11551–11571, doi:10.5194/acp-13-11551-2013, 2013.

Ortega, A. M., Hayes, P. L., Peng, Z., Palm, B. B., Hu, W., Day, D. A., Li, R., Cubison, M. J., Brune, W. H., Graus, M., Warneke, C., Gilman, J. B., Kuster, W. C., de Gouw, J. A., Gutiérrez-Montes, C. and Jimenez, J. L.: Real-time measurements of secondary organic aerosol formation and aging from ambient air in an oxidation flow reactor in the Los Angeles area, Atmos. Chem. Phys., 16(11), 7411–7433, doi:10.5194/acp-16-7411-2016, 2016.

Ots, R., Vieno, M., Allan, J. D., Reis, S., Nemitz, E., Young, D. E., Coe, H., Di Marco, C., Detournay, A., Mackenzie, I. A., Green, D. C. and Heal, M. R.: Model simulations of cooking organic aerosol (COA) over the UK using estimates of emissions based on measurements at two sites in London, Atmos. Chem. Phys., 16(21), 13773–13789, doi:10.5194/acp-16-13773-2016, 2016.

Pagonis, D., Krechmer, J. E., de Gouw, J., Jimenez, J. L. and Ziemann, P. J.: Effects of gas–wall partitioning in Teflon tubing and instrumentation on time-resolved measurements of gas-phase organic compounds, Atmos. Meas. Tech., 10(12), 4687–4696, doi:10.5194/amt-10-4687-2017, 2017.

Palm, B. B., Campuzano-Jost, P., Ortega, A. M., Day, D. A., Kaser, L., Jud, W., Karl, T., Hansel, A., Hunter, J. F., Cross, E. S., Kroll, J. H., Peng, Z., Brune, W. H. and Jimenez, J. L.: In situ secondary organic aerosol formation from ambient pine forest air using an oxidation flow reactor, Atmos. Chem. Phys., 16(5), 2943–2970, doi:10.5194/acp-16-2943-2016, 2016.

Palm, B. B., Campuzano-Jost, P., Day, D. A., Ortega, A. M., Fry, J. L., Brown, S. S., Zarzana, K. J., Dube, W., Wagner, N. L., Draper, D. C., Kaser, L., Jud, W., Karl, T., Hansel, A., Gutiérrez-Montes, C. and Jimenez, J. L.: Secondary organic aerosol formation from in situ OH, O3, and NO3 oxidation of ambient forest air in an oxidation flow reactor, Atmos. Chem. Phys., 17(8), 5331–5354, doi:10.5194/acp-17-5331-2017, 2017.

Palm, B. B., de Sá, S. S., Day, D. A., Campuzano-Jost, P., Hu, W., Seco, R., Sjostedt, S. J., Park, J.-H., Guenther, A. B., Kim, S., Brito, J., Wurm, F., Artaxo, P., Thalman, R., Wang, J., Yee, L. D., Wernis, R., Isaacman-VanWertz, G., Goldstein, A. H., Liu, Y., Springston, S. R., Souza, R., Newburn, M. K., Alexander, M. L., Martin, S. T. and Jimenez, J. L.: Secondary organic aerosol formation from ambient air in an oxidation flow reactor in central Amazonia, Atmos. Chem. Phys., 18(1), 467–493, doi:10.5194/acp-18-467-2018, 2018.

Park, K., Kittelson, D. B., Zachariah, M. R. and McMurry, P. H.: Measurement of Inherent Material Density of Nanoparticle Agglomerates, J. Nanoparticle Res., 6(2/3), 267–272, doi:10.1023/B:NANO.0000034657.71309.e6, 2004.

Park, M.-S., Park, S.-H., Chae, J.-H., Choi, M.-H., Song, Y., Kang, M. and Roh, J.-W.: High-resolution urban observation network for user-specific meteorological information service in the Seoul Metropolitan Area, South Korea, Atmos. Meas. Tech, 10, 1575–1594, doi:10.5194/amt-10-1575-2017, 2017.

Park, M. E., Song, C. H., Park, R. S., Lee, J., Kim, J., Lee, S., Woo, J.-H., Carmichael, G. R., Eck, T. F., Holben, B. N., Lee, S.-S., Song, C. K. and Hong, Y. D.: New approach to monitor transboundary particulate pollution over Northeast Asia, Atmos. Chem. Phys, 14, 659–674, doi:10.5194/acp-14-659-2014, 2014.

Park, S. S., Kim, J.-H. and Jeong, J.-U.: Abundance and sources of hydrophilic and hydrophobic water-soluble organic carbon at an urban site in Korea in summer., J. Environ. Monit., 14(1), 224–32, doi:10.1039/c1em10617a, 2012.

Parrish, D. D., Stohl, A., Forster, C., Atlas, E. L., Blake, D. R., Goldan, P. D., Kuster, W. C. and de Gouw, J. A.: Effects of mixing on evolution of hydrocarbon ratios in the troposphere, J. Geophys. Res., 112(D10), D10S34, doi:10.1029/2006JD007583, 2007.

Parrish, D. D., Ryerson, T. B., Mellqvist, J., Johansson, J., Fried, A., Richter, D., Walega, J. G., Washenfelder, R. A., de Gouw, J. A., Peischl, J., Aikin, K. C., McKeen, S. A., Frost, G. J., Fehsenfeld, F. C. and Herndon, S. C.: Primary and secondary sources of formaldehyde in urban atmospheres: Houston Texas region, Atmos. Chem. Phys., 12(7), 3273–3288, doi:10.5194/acp-12-3273-2012, 2012.

Peischl, J., Ryerson, T. B., Brioude, J., Aikin, K. C., Andrews, A. E., Atlas, E., Blake, D., Daube, B. C., de Gouw, J. A., Dlugokencky, E., Frost, G. J., Gentner, D. R., Gilman, J. B., Goldstein, A. H., Harley, R. A., Holloway, J. S., Kofler, J., Kuster, W. C., Lang, P. M., Novelli, P. C., Santoni, G. W., Trainer, M., Wofsy, S. C. and Parrish, D. D.: Quantifying sources of methane using light alkanes in the Los Angeles basin, California, J. Geophys. Res. Atmos., 118(10), 4974–4990, doi:10.1002/jgrd.50413, 2013.

Peng, J. F., Hu, M., Wang, Z. B., Huang, X. F., Kumar, P., Wu, Z. J., Guo, S., Yue, D. L., Shang, D. J., Zheng, Z. and He, L. Y.: Submicron aerosols at thirteen diversified sites in China: size distribution, new particle formation and corresponding contribution to cloud condensation nuclei production, Atmos. Chem. Phys., 14(18), 10249–10265, doi:10.5194/acp-14-10249-2014, 2014.

Peng, Z., Day, D. A., Stark, H., Li, R., Lee-Taylor, J., Palm, B. B., Brune, W. H. and Jimenez, J. L.: HO_x radical chemistry in oxidation flow reactors with low-pressure mercury lamps systematically examined by modeling, Atmos. Meas. Tech., 8(11), 4863–4890, doi:10.5194/amt-8-4863-2015, 2015.

Peng, Z., Day, D. A., Ortega, A. M., Palm, B. B., Hu, W., Stark, H., Li, R., Tsigaridis, K., Brune, W. H. and Jimenez, J. L.: Non-OH chemistry in oxidation flow reactors for the study of atmospheric chemistry systematically examined by modeling, Atmos. Chem. Phys., 16(7), 4283–4305, doi:10.5194/acp-16-4283-2016, 2016.

Perring, A. E., Bertram, T. H., Farmer, D. K., Wooldridge, P. J., Dibb, J., Blake, N. J., Blake, D. R., Singh, H. B., Fuelberg, H., Diskin, G., Sachse, G. and Cohen, R. C.: The production and persistence of $\Sigma RONO_2$ in the Mexico City plume, Atmos. Chem. Phys., 10(15), 7215–7229, doi:10.5194/acp-10-7215-2010, 2010.

Pieber, S. M., El Haddad, I., Slowik, J. G., Canagaratna, M. R., Jayne, J. T., Platt, S. M., Bozzetti, C., Daellenbach, K. R., Fröhlich, R., Vlachou, A., Klein, F., Dommen, J., Miljevic, B., Jiménez, J. L., Worsnop, D. R., Baltensperger, U. and Prévôt, A. S. H.: Inorganic Salt Interference on CO2+ in Aerodyne AMS and ACSM Organic Aerosol Composition Studies, Environ. Sci. Technol., 50(19), 10494–10503, doi:10.1021/acs.est.6b01035, 2016.

Platt, S. M., El Haddad, I., Zardini, A. A., Clairotte, M., Astorga, C., Wolf, R., Slowik, J. G., Temime-Roussel, B., Marchand, N., Ježek, I., Drinovec, L., Močnik, G., Möhler, O., Richter, R., Barmet, P., Bianchi, F., Baltensperger, U. and Prévôt, A. S. H.: Secondary organic aerosol formation from gasoline vehicle emissions in a new mobile environmental reaction chamber, Atmos. Chem. Phys., 13(18), 9141–9158, doi:10.5194/acp-13-9141-2013, 2013.

Platt, S. M., El Haddad, I., Pieber, S. M., Zardini, A. A., Suarez-Bertoa, R., Clairotte, M., Daellenbach, K. R., Huang, R.-J., Slowik, J. G., Hellebust, S., Temime-Roussel, B., Marchand, N., de Gouw, J., Jimenez, J. L., Hayes, P. L., Robinson, A. L., Baltensperger, U., Astorga, C. and Prévôt, A. S. H.: Gasoline cars produce more carbonaceous particulate matter than modern filter-equipped diesel cars, Sci. Rep., 7(1), 4926, doi:10.1038/s41598-017-03714-9, 2017.

Presto, A. A., Gordon, T. D. and Robinson, A. L.: Primary to secondary organic aerosol: Evolution of organic emissions from mobile combustion sources, Atmos. Chem. Phys., 14(10), 5015–5036, doi:10.5194/acp-14-5015-2014, 2014.

Price, H. U., Jaffe, D. A., Cooper, O. R. and Doskey, P. V: Photochemistry, ozone production, and dilution during long-range transport episodes from Eurasia to the northwest United States, J. Geophys. Res. Atmos., 109, D23S13, doi:10.1029/2003JD004400, 2004.

Pye, H. O. T. and Seinfeld, J. H.: A global perspective on aerosol from low-volatility organic compounds, Atmos. Chem. Phys. Atmos. Chem. Phys., 10(9), 4377–4401, doi:10.5194/acp-10-4377-2010, 2010.

Richter, D., Weibring, P., Walega, J. G., Fried, A., Spuler, S. M. and Taubman, M. S.: Compact highly sensitive multi-species airborne mid-IR spectrometer, Appl. Phys. B, 119(1), 119–131, doi:10.1007/s00340-015-6038-8, 2015.

Robinson, A. L., Donahue, N. M., Shrivastava, M. K., Weitkamp, E. A., Sage, A. M., Grieshop, A. P., Lane, T. E., Pierce, J. R. and Pandis, S. N.: Rethinking Organic Aerosols: Semivolatile Emissions and Photochemical Aging, Science (80-.)., 315(5816), 1259–1262, doi:10.1126/science.1133061, 2007.

Romer, P. S., Duffey, K. C., Wooldridge, P. J., Allen, H. M., Ayres, B. R., Brown, S. S., Brune, W. H., Crounse, J. D., de Gouw, J., Draper, D. C., Feiner, P. A., Fry, J. L., Goldstein, A. H., Koss, A., Misztal, P. K., Nguyen, T. B., Olson, K., Teng, A. P., Wennberg, P. O., Wild, R. J., Zhang, L. and Cohen, R. C.: The lifetime of nitrogen oxides in an isoprene-dominated forest, Atmos. Chem. Phys., 16(12), 7623–7637, doi:10.5194/acp-16-7623-2016, 2016.

Sachse, G. W., Hill, G. F., Wade, L. O. and Perry, M. G.: Fast-Response, High-Precision Carbon Monoxide Sensor using a Tunable Diode Laser Absorption Technique, J. Geophys. Res., 92(D2), 2071–2081, doi:doi:10.1029/JD092iD02p02071, 1987.

Salcedo, D., Onasch, T. B., Dzepina, K., Canagaratna, M. R., Zhang, Q., Huffman, J. A., Decarlo, P. F., Jayne, J. T., Mortimer, P., Worsnop, D. R., Kolb, C. E., Johnson, K. S., Zuberi, B., Marr, L. C., Volkamer, R., Molina, L. T., Molina, M. J., Cardenas, B., Bernabe, R. M., Marquez, C., Gaffney, J. S., Marley, N. A., Laskin, A., Shutthanandan, V., Xie, Y., Brune, W., Lesher, R., Shirley, T. and Jimenez, J. L.: Characterization of ambient aerosols in Mexico City during the MCMA-2003 campaign with Aerosol Mass Spectrometry: results from the CENICA Supersite, Atmos. Chem. Phys., 6(4), 925–946, doi:10.5194/acp-6-925-2006, 2006.

Sander, S. P., Abbatt, J. P. D., Barker, J. R., Burkholder, J. B., Friedl, R. R., Golden, D. M., Huie, R. E., Kolb, C. E., Kurylo, M. J., Moortgat, G. K., Orkin, V. L. and Wine, P. H.: Chemical Kinetics and Photochemical Data for Use in Atmospheric Studies, Evaluation No. 17, JPL Publ. 10-6, Jet Propuls. Lab. Pasadena, 2011.

Sato, K., Nakashima, Y., Morino, Y., Imamura, T., Kurokawa, J. and Kajii, Y.: Total OH reactivity measurements for the OH-initiated oxidation of aromatic hydrocarbons in the presence of NO_x,

Atmos. Environ., 171, 272–278, doi:10.1016/j.atmosenv.2017.10.036, 2017.

Schneider, J., Hings, S. S., Nele Hock, B., Weimer, S., Borrmann, S., Fiebig, M., Petzold, A., Busen, R. and Kärcher, B.: Aircraft-based operation of an aerosol mass spectrometer: Measurements of tropospheric aerosol composition, J. Aerosol Sci., 37(7), 839–857, doi:10.1016/j.jaerosci.2005.07.002, 2006.

Schroder, J. C., Campuzano-Jost, P., Day, D. A., Shah, V., Larson, K., Sommers, J. M., Sullivan, A. P., Campos, T., Reeves, J. M., Hills, A., Hornbrook, R. S., Blake, N. J., Scheuer, E., Guo, H., Fibiger, D. L., McDuffie, E. E., Hayes, P. L., Weber, R. J., Dibb, J. E., Apel, E. C., Jaeglé, L., Brown, S. S., Thronton, J. A. and Jimenez, J. L.: Sources and Secondary Production of Organic Aerosols in the Northeastern US during WINTER, J. Geophys. Res. Atmos., doi:10.1029/2018JD028475, 2018.

Schwantes, R. H., Schilling, K. A., McVay, R. C., Lignell, H., Coggon, M. M., Zhang, X., Wennberg, P. O. and Seinfeld, J. H.: Formation of Highly Oxygenated Low-Volatility Products from Cresol Oxidation, Atmos. Chem. Phys., 7(5), 3453–3474, doi:10.5194/acp-17-3453-2017, 2017.

Schwarz, J. P., Samset, B. H., Perring, A. E., Spackman, J. R., Gao, R. S., Stier, P., Schulz, M., Moore, F. L., Ray, E. A. and Fahey, D. W.: Global-scale seasonally resolved black carbon vertical profiles over the Pacific, Geophys. Res. Lett., 40(20), 5542–5547, doi:10.1002/2013GL057775, 2013.

Seo, J., Kim, J. Y., Youn, D., Lee, J. Y., Kim, H., Lim, Y. Bin, Kim, Y. and Jin, H. C.: On the multi-day haze in the Asian continental outflow: An important role of synoptic condition combined with regional and local sources, Atmos. Chem. Phys., 17(15), 9311–9332, doi:10.5194/acp-17-9311-2017, 2017.

Shinozuka, Y., Clarke, A. D., DeCarlo, P. F., Jimenez, J. L., Dunlea, E. J., Roberts, G. C., Tomlinson, J. M., Collins, D. R., Howell, S. G., Kapustin, V. N., McNaughton, C. S. and Zhou, J.: Aerosol optical properties relevant to regional remote sensing of CCN activity and links to their organic mass fraction: airborne observations over Central Mexico and the US West Coast during MILAGRO/INTEX-B, Atmos. Chem. Phys., 9(18), 6727–6742, 2009.

Shrivastava, M., Cappa, C. D., Fan, J., Goldstein, A. H., Guenther, A. B., Jimenez, J. L., Kuang, C., Laskin, A., Martin, S. T., Ng, N. L., Petaja, T., Pierce, J. R., Rasch, P. J., Roldin, P., Seinfeld, J. H., Shilling, J., Smith, J. N., Thornton, J. A., Volkamer, R., Wang, J., Worsnop, D. R., Zaveri, R. A., Zelenyuk, A. and Zhang, Q.: Recent advances in understanding secondary organic aerosol: Implications for global climate forcing, Rev. Geophys., 55(2), 509–559, doi:10.1002/2016RG000540, 2017.

Shrivastava, M. K., Lane, T. E., Donahue, N. M., Pandis, S. N. and Robinson, A. L.: Effects of gas particle partitioning and aging of primary emissions on urban and regional organic aerosol concentrations, J. Geophys. Res., 113(D18), D18301, doi:10.1029/2007JD009735, 2008.

Silva, S. J., Arellano, A. F. and Worden, H. M.: Toward anthropogenic combustion emission constraints from space-based analysis of urban CO_2/CO sensitivity, Geophys. Res. Lett., 40(18), 4971–4976, doi:10.1002/grl.50954, 2013.

Skamarock, C., Klemp, B., Dudhia, J., Gill, O., Barker, D., Duda, G., Huang, X., Wang, W. and Powers, G.: A Description of the Advanced Research WRF Version 3, , doi:10.5065/D68S4MVH,

2008.

Slusher, D. L., Huey, L. G., Tanner, D. J., Flocke, F. M. and Roberts, J. M.: A thermal dissociation–chemical ionization mass spectrometry (TD-CIMS) technique for the simultaneous measurement of peroxyacyl nitrates and dinitrogen pentoxide, J. Geophys. Res., 109(D19), D19315, doi:10.1029/2004JD004670, 2004.

Sprengnether, M. M., Demerjian, K. L., Dransfield, T. J., Clarke, J. S., Anderson, J. G. and Donahue, N. M.: Rate Constants of Nine C6-C9 Alkanes with OH from 230 to 379 K: Chemical Tracers for [OH], J. Phys. Chem. A2, 113, 5030–5038, doi:10.1021/jp810412m, 2009.

Stith, J. L., Ramanathan, V., Cooper, W. A., Roberts, G. C., DeMott, P. J., Carmichael, G., Hatch, C. D., Adhikary, B., Twohy, C. H., Rogers, D. C., Baumgardner, D., Prenni, A. J., Campos, T., Gao, R., Anderson, J. and Feng, Y.: An overview of aircraft observations from the Pacific Dust Experiment campaign, J. Geophys. Res., 114(D5), D05207, doi:10.1029/2008JD010924, 2009.

Sueper, D.: ToF-AMS Data Analysis Software Webpage, [online] Available from: http://cires1.colorado.edu/jimenez-group/wiki/index.php/ToF-AMS_Analysis_Software (Accessed 4 January 2017), 2018.

TAbMET: TAbMEP Assessment: POLARCAT HNO3 Summary, in TAbMEP POLARCAT/ICARTT Analysis, edited by G. Chen, https://www-air.larc.nasa.gov/TAbMEP2_polarcat.html, Boulder., 2009.

Talbot, R. W., Dibb, J. E., Lefer, B. L., Scheuer, E. M., Bradshaw, J. D., Sandholm, S. T., Smyth, S., Blake, D. R., Blake, N. J., Sachse, G. W., Collins, J. E. and Gregory, G. L.: Large-scale distributions of tropospheric nitric, formic, and acetic acids over the western Pacific basin during wintertime, J. Geophys. Res., 102(D23), 28303–28313, 1997.

Tang, W., Arellano, A. F., DiGangi, J. P., Choi, Y., Diskin, G. S., Agustí-Panareda, A., Parrington, M., Massart, S., Gaubert, B., Lee, Y., Kim, D., Jung, J., Hong, J., Hong, J.-W., Kanaya, Y., Lee, M., Stauffer, R. M., Thompson, A. M., Flynn, J. H. and Woo, J.-H.: Evaluating High-Resolution Forecasts of Atmospheric CO and CO_2 from a Global Prediction System during KORUS-AQ Field Campaign, Atmos. Chem. Phys. Discuss., 1–41, doi:10.5194/acp-2018-71, 2018.

Thornton, J. A., Wooldridge, P. J., Cohen, R. C., Martinez, M., Harder, H., Brune, W. H., Williams, E. J. J., Roberts, J. M. M., Fehsenfeld, F. C., Hall, S. R., Shetter, R. E. E., Wert, B. P. and Fried, A.: Ozone production rates as a function of NO_x abundances and HO_x production rates in the Nashville urban plume, J. Geophys. Res., 107(D12), 1–17, doi:10.1029/2001JD000932, 2002.

Tkacik, D. S., Lambe, A. T., Jathar, S., Li, X., Presto, A. A., Zhao, Y., Blake, D., Meinardi, S., Jayne, J. T., Croteau, P. L. and Robinson, A. L.: Secondary Organic Aerosol Formation from in-Use Motor Vehicle Emissions Using a Potential Aerosol Mass Reactor., Environ. Sci. Technol., 48(19), 11235–42, doi:10.1021/es502239v, 2014.

Tohjima, Y., Kubo, M., Minejima, C., Mukai, H., Tanimoto, H., Ganshin, A., Maksyutov, S., Katsumata, K., Machida, T. and Kita, K.: Temporal changes in the emissions of CH4 and CO from China estimated from CH4 / CO2 and CO / CO2 correlations observed at Hateruma Island, Atmos. Chem. Phys., 14(3), 1663–1677, doi:10.5194/acp-14-1663-2014, 2014.

Tritscher, T., Dommen, J., DeCarlo, P. F., Gysel, M., Barmet, P. B., Praplan, A. P., Weingartner, E., Prévôt, A. S. H., Riipinen, I., Donahue, N. M. and Baltensperger, U.: Volatility and

hygroscopicity of aging secondary organic aerosol in a smog chamber, Atmos. Chem. Phys., 11(22), 11477–11496, doi:10.5194/acp-11-11477-2011, 2011.

Tsimpidi, A. P., Karydis, V. A., Zavala, M., Lei, W., Molina, L., Ulbrich, I. M., Jimenez, J. L. and Pandis, S. N.: Evaluation of the volatility basis-set approach for the simulation of organic aerosol formation in the Mexico City metropolitan area, Atmos. Chem. Phys., 10(2), 525–546, doi:10.5194/acp-10-525-2010, 2010.

Tsimpidi, A. P., Karydis, V. A., Pandis, S. N. and Lelieveld, J.: Global-scale combustion sources of organic aerosols: sensitivity to formation and removal mechanisms, Atmos. Chem. Phys., 17(12), 7345–7364, doi:10.5194/acp-17-7345-2017, 2017.

Ulbrich, I. M., Canagaratna, M. R., Zhang, Q., Worsnop, D. R. and Jimenez, J. L.: Interpretation of organic components from Positive Matrix Factorization of aerosol mass spectrometric data, Atmos. Chem. Phys., 9(9), 2891–2918, doi:10.5194/acp-9-2891-2009, 2009.

UNDESA, P. D.: World Urbanization Prospects: The 2014 Revision., 2015.

Vay, S. A., Tyler, S. C., Choi, Y., Blake, D. R., Blake, N. J., Sachse, G. W., Diskin, G. S. and Singh, H. B.: Sources and transport of Δ14C in CO 2 within the Mexico City Basin and vicinity, Atmos. Chem. Phys., 9, 4973–4985, doi:10.159/acp-9-4973-2009, 2009.

Virkkula, A.: Correction of the Calibration of the 3-wavelength Particle Soot Absorption Photometer (3λ PSAP), Aerosol Sci. Technol., 44, 706–712, doi:10.1080/02786826.2010.482110, 2010.

Volkamer, R., Jimenez, J. L., San Martini, F., Dzepina, K., Zhang, Q., Salcedo, D., Molina, L. T., Worsnop, D. R. and Molina, M. J.: Secondary organic aerosol formation from anthropogenic air pollution: Rapid and higher than expected, Geophys. Res. Lett., 33(17), L17811, doi:10.1029/2006GL026899, 2006.

Wang, Y., Munger, J. W., Xu, S., McElroy, M. B., Hao, J., Nielsen, C. P. and Ma, H.: CO_2 and its correlation with CO at a rural site near Beijing: implications for combustion efficiency in China, Atmos. Chem. Phys., 10(18), 8881–8897, doi:10.5194/acp-10-8881-2010, 2010.

Weibring, P., Richter, D., Walega, J. G., Rippe, L. and Fried, A.: Difference frequency generation spectrometer for simultaneous multispecies detection, Opt. Express, 18(26), 27670, doi:10.1364/OE.18.027670, 2010.

Weinheimer, A. J., Walega, J. G., Ridley, B. A., Gary, B. L., Blake, D. R., Blake, N. J., Rowland, F. S., Sachse, G. W., Anderson, B. E. and Collins, J. E.: Meridional distributions of NOx , NOy , and other species in the lower stratosphere and upper troposphere during AASE II, Geophys. Res. Lett., 21(23), 2583–2586, doi:10.1029/94GL01897, 1994.

WHO: Ambient air pollution: A global assessment of exposure and burden of disease, World Health Organization., 2016.

Williams, L.: What is My Vaporizer Temperature? Vaporizer Temperature Power Curve for Several Systems, [online] Available from: http://cires1.colorado.edu/jimenez-group/UsrMtgs/UsersMtg11/WilliamsAMSUsersMtg_2010_VapT.pdf (Accessed 12 March 2018), 2010.

Wisthaler, A., Hansel, A., Dickerson, R. R. and Crutzen, P. J.: Organic trace gas measurements by PTR-MS during INDOEX 1999, J. Geophys. Res., 107(D19), 8024, doi:10.1029/2001JD000576,

2002.

Woo, J.-H., An, S.-M., Kim, D.-Y., Kim, H.-K., Choi, K.-C. and Kim, Y.-H.: Development of the Asia Emission Inventory in Support of Integrated Modeling of Climate and Air Quality (III), Incheon, Korea., 2013.

Wood, E. C., Canagaratna, M. R., Herndon, S. C., Onasch, T. B., Kolb, C. E., Worsnop, D. R., Kroll, J. H., Knighton, W. B., Seila, R., Zavala, M., Molina, L. T., DeCarlo, P. F., Jimenez, J. L., Weinheimer, A. J., Knapp, D. J., Jobson, B. T., Stutz, J., Kuster, W. C. and Williams, E. J.: Investigation of the correlation between odd oxygen and secondary organic aerosol in Mexico City and Houston, Atmos. Chem. Phys., 10(18), 8947–8968, doi:DOI 10.5194/acp-10-8947-2010, 2010.

Woody, M. C., Baker, K. R., Hayes, P. L., Jimenez, J. L., Koo, B. and Pye, H. O. T.: Understanding sources of organic aerosol during CalNex-2010 using the CMAQ-VBS, Atmos. Chem. Phys., 16(6), 4081–4100, doi:10.5194/acp-16-4081-2016, 2016.

Wooldridge, P. J., Perring, A. E., Bertram, T. H., Flocke, F. M., Roberts, J. M., Singh, H. B., Huey, L. G., Thornton, J. A., Wolfe, G. M., Murphy, J. G., Fry, J. L., Rollins, A. W., LaFranchi, B. W. and Cohen, R. C.: Total Peroxy Nitrates (ΣPNs) in the atmosphere: the Thermal Dissociation-Laser Induced Fluorescence (TD-LIF) technique and comparisons to speciated PAN measurements, Atmos. Meas. Tech., 3(3), 593–607, doi:DOI 10.5194/amt-3-593-2010, 2010.

Wu, W., Zhao, B., Wang, S. and Hao, J.: Ozone and secondary organic aerosol formation potential from anthropogenic volatile organic compounds emissions in China, J. Environ. Sci., 53, doi:10.1016/j.jes.2016.03.025, 2016.

Xu, W., Croteau, P., Williams, L., Canagaratna, M., Onasch, T., Cross, E., Zhang, X., Robinson, W., Worsnop, D. and Jayne, J.: Laboratory characterization of an aerosol chemical speciation monitor with $PM_{2.5}$ measurement capability, Aerosol Sci. Technol., 51(1), 69–83, doi:10.1080/02786826.2016.1241859, 2017.

Xu, W., Lambe, A., Silva, P., Hu, W., Onasch, T., Williams, L., Croteau, P., Zhang, X., Renbaum-Wolff, L., Fortner, E., Jimenez, J. L., Jayne, J., Worsnop, D. and Canagaratna, M.: Laboratory evaluation of species-dependent relative ionization efficiencies in the Aerodyne Aerosol Mass Spectrometer, Aerosol Sci. Technol., 1–16, doi:10.1080/02786826.2018.1439570, 2018.

Yuan, B., Hu, W. W., Shao, M., Wang, M., Chen, W. T., Lu, S. H., Zeng, L. M. and Hu, M.: VOC emissions, evolutions and contributions to SOA formation at a receptor site in eastern China, Atmos. Chem. Phys., 13(17), 8815–8832, doi:10.5194/acp-13-8815-2013, 2013.

Zhang, Q., Stanier, C. O., Canagaratna, M. R., Jayne, J. T., Worsnop, D. R., Pandis, S. N. and Jimenez, J. L.: Insights into the chemistry of new particle formation and growth events in Pittsburgh based on aerosol mass spectrometry, Environ. Sci. Technol., 38(18), 4797–4809, doi:Doi 10.1021/Es035417u, 2004.

Zhang, Q., Alfarra, M. R., Worsnop, D. R., James, D., Coe, H., Canagaratna, M. R. and Jimenez, J. L.: Deconvolution and Quantification of Hydrocarbon-like and Oxygenated Organic Aerosols Based on Aerosol Mass Spectrometry Deconvolution and Quantification of Hydrocarbon-like and Oxygenated Organic Aerosols Based on Aerosol Mass Spectrometry, Environ. Sci. Technol., 39(13), 4938–4952, doi:10.1021/es048568l, 2005.

Zhang, Q., Jimenez, J. L., Canagaratna, M. R., Allan, J. D., Coe, H., Ulbrich, I., Alfarra, M. R.,

Takami, A., Middlebrook, A. M., Sun, Y. L., Dzepina, K., Dunlea, E., Docherty, K., DeCarlo, P. F., Salcedo, D., Onasch, T., Jayne, J. T., Miyoshi, T., Shimono, A., Hatakeyama, S., Takegawa, N., Kondo, Y., Schneider, J., Drewnick, F., Borrmann, S., Weimer, S., Demerjian, K., Williams, P., Bower, K., Bahreini, R., Cottrell, L., Griffin, R. J., Rautiainen, J., Sun, J. Y., Zhang, Y. M. and Worsnop, D. R.: Ubiquity and dominance of oxygenated species in organic aerosols in anthropogenically-influenced Northern Hemisphere midlatitudes, Geophys. Res. Lett., 34(13), L13801, doi:10.1029/2007gl029979, 2007.

Zhang, Q. J., Beekmann, M., Freney, E., Sellegri, K., Pichon, J. M., Schwarzenboeck, A., Colomb, A., Bourrianne, T., Michoud, V. and Borbon, A.: Formation of secondary organic aerosol in the Paris pollution plume and its impact on surrounding regions, Atmos. Chem. Phys., 15(24), 13973–13992, doi:10.5194/acp-15-13973-2015, 2015.

Zhang, X., Smith, K. A., Worsnop, D. R., Jimenez, J., Jayne, J. T. and Kolb, C. E.: A Numerical Characterization of Particle Beam Collimation by an Aerodynamic Lens-Nozzle System: Part I. An Individual Lens or Nozzle, Aerosol Sci. Technol., 36, 617–631, doi:10.1080/02786820252883856, 2002.

Zhang, X., Smith, K. A., Worsnop, D. R., Jimenez, J. L., Jayne, J. T., Kolb, C. E., Morris, J. and Davidovits, P.: Numerical Characterization of Particle Beam Collimation: Part II Integrated Aerodynamic-Lens–Nozzle System, Aerosol Sci. Technol., 38, 619–638, doi:10.1080/02786820490479833, 2004.

Zhang, X., Cappa, C. D., Jathar, S. H., McVay, R. C., Ensberg, J. J., Kleeman, M. J., Seinfeld, J. H. and Christopher D. Cappa: Influence of vapor wall loss in laboratory chambers on yields of secondary organic aerosol., Proc. Natl. Acad. Sci. U. S. A., 111(16), 1–6, doi:10.1073/pnas.1404727111, 2014.

Zhao, Y., Hennigan, C. J., May, A. A., Tkacik, D. S., de Gouw, J. A., Gilman, J. B., Kuster, W. C., Borbon, A. and Robinson, A. L.: Intermediate-volatility organic compounds: a large source of secondary organic aerosol, Environ. Sci. Technol., 48(23), 13743–50, doi:10.1021/es5035188, 2014.

Zhao, Y., Nguyen, N. T., Presto, A. A., Hennigan, C. J., May, A. A. and Robinson, A. L.: Intermediate Volatility Organic Compound Emissions from On-Road Gasoline Vehicles and Small Off-Road Gasoline Engines, Environ. Sci. Technol., 50(8), 4554–4563, doi:10.1021/acs.est.5b06247, 2016.

Ziemba, L. D., Lee Thornhill, K., Ferrare, R., Barrick, J., Beyersdorf, A. J., Chen, G., Crumeyrolle, S. N., Hair, J., Hostetler, C., Hudgins, C., Obland, M., Rogers, R., Scarino, A. J., Winstead, E. L. and Anderson, B. E.: Airborne observations of aerosol extinction by in situ and remote-sensing techniques: Evaluation of particle hygroscopicity, Geophys. Res. Lett., 40(2), 417–422, doi:10.1029/2012GL054428, 2013.